UNIVERSITY OF CALGARY

P-wave seismic imaging through dipping transversely isotropic media.

by

Jennifer M. Leslie

A THESIS

SUBMITTED TO THE FACULTY OF GRADUATE STUDIES

IN PARTIAL FULFILMENT OF THE REQUIREMENTS FOR THE

DEGREE OF DOCTOR OF PHILOSOPHY

DEPARTMENT OF GEOLOGY AND GEOPHYSICS

CALGARY, ALBERTA

OCTOBER, 1999

ABSTRACT

P-wave seismic anisotropy is of growing concern to the exploration industry. The transmissional effects through dipping anisotropic strata, such as shales, cause substantial depth and lateral positioning errors when imaging subsurface targets. Using anisotropic physical models the limitations of conventional isotropic migration routines were determined to be significant. In addition, these models were used to validate both anisotropic depth migration routines and an anisotropic, numerical raytracer.

In order to include anisotropy in these processes, one must be able to quantify the anisotropy using two parameters, ε and δ. These parameters were determined from headwave velocity measurements on anisotropic strata, in the parallel-, perpendicular- and 45°-to-bedding directions. This new method was developed using refraction seismic techniques to measure the necessary velocities in the Wapiabi Formation shales, the Brazeau Group interbedded sandstones and shales, the Cardium Formation sandstones and the Palliser Formation limestones. The Wapiabi Formation and Brazeau Group rocks were determined to be anisotropic with ε=0.23±0.05, δ=-0.05±0.07 and ε=0.11±0.04, δ=0.42±0.06, respectively. The sandstones and limestones of the Cardium and Palliser formations were both determined to be isotropic, in these studies.

In a complementary experiment, a new procedure using vertical seismic profiling (VSP) techniques was developed to measure the anisotropic headwave velocities. Using a multi-offset source configuration on an appropriately dipping, uniform panel of anisotropic strata, the required velocities were measured directly and modelled. In this study, the geologic model was modelled using an anisotropic raytracer, developed for the experiment. The anisotropy was successfully modelled using anisotropic parameters based on the refraction seismic results.

With a firm idea of the anisotropic parameters from the aforementioned studies, these parameters were then used in the anisotropic depth migration of a real dataset from the Alberta Foothills. The final anisotropic section demonstrated several improvements over

the isotropic section. This anisotropic section is considered to be more accurate, in terms of depth and lateral position of reflectors, and thus a more complete solution than the isotropic result.

In conclusion, seismic velocity anisotropy can seriously affect the imaging of subsurface play targets and every effort should be made to take these effects into account using anisotropic processing routines.

ACKNOWLEDGEMENTS

Many thanks to all the people involved in this project. In particular, I would like to thank my supervisor, Dr. Don C. Lawton, for without his faith, insight, support, guidance and encouragement, this project would not have existed in this form. Thanks to Drs. Deb Spratt, Gary Margrave, Larry Lines, Art Limbird and Doug Schmitt for their comments and suggestions; thereby, making this project more intelligible and coherent.

I would like to thank Amoco Canada and Kelman Technologies Inc. for the use of their pre-stack depth migration algorithms used in this thesis. Specifically, Mr. Tom Dickson, Dr. John Varsek and Mr. Sam Gray of Amoco Canada, as well as Mssers. Ron Schmid, Rick Steele and Rob Vestrum of Kelman Technologies Inc. for their technical assistance and insight into the pre-stack depth migration sections of this thesis. Thanks especially to Mr. Eric Gallant who built the physical models used in this study and who also acquired the ultrasonic data over these models.

I thank the staff and students of the University of Calgary 1996 and 1998 Geophysics Field Schools and the staff of both the FRP and CREWES consortia for their assistance in acquiring the refraction data. Thanks especially to Mssers. Malcolm Bertram, Eric Gallant and Henry Bland for their assistance in organizing and executing the acquisition of the refraction survey data and their infinite wisdom regarding ProMAX. Thanks, also, to the landowners that graciously allowed us to use their property for the acquisition of this data.

I gratefully acknowledge the financial support for the VSP experiment provided by Petro-Canada Resources and Shell Canada, in participation with the Natural Sciences and Engineering Research Council (NSERC) of Canada Industrial Post-Graduate Scholarship. I also acknowledge Schlumberger Canada for their advice and assistance in acquiring the data for the VSP survey. I would like to particularly thank Dr. Charles Boyer of Petro-Canada for his technical assistance in interpreting the experimental data.

Thanks also to the anonymous donor of the seismic data from the Alberta Foothills. Without their generosity Chapter 6 would not have been possible. In addition, the general financial support from the sponsors of the Foothills Research Project as well as personal support from SEG, CSEG and Conwest scholarships is also acknowledged.

Last, but not least, I thank my family and all my friends who gave me the support and encouragement I needed to finish this degree and to make my time here enjoyable. It wasn't easy, but it was all worthwhile.

To My Parents

TABLE OF CONTENTS

LIST OF TABLES

LIST OF FIGURES

CHAPTER 1 INTRODUCTION

1.1 Introduction

Seismic anisotropy is the variation of the velocity of seismic waves, with direction, through a medium. This is true for both compressional (P-waves) as well as shear (S-waves). This dissertation is primarily concerned with P-wave anisotropy. It is known that the main causes of seismic anisotropy are due to aligned mineral grains, aligned cracks, aligned crystals and periodic thin layering [Helbig, 1994]. The simplest form of anisotropy is referred to as transverse isotropy (TI) where all directions perpendicular to the axis of symmetry are equivalent or isotropic [Helbig, 1994]. When the axis of symmetry is normal to the free surface, the material is considered to have vertical transverse isotropy (VTI) [Crampin, 1986]. It is known that the majority of sedimentary basins are composed, primarily, of shales and are also the main location of hydrocarbon reserves [Schoenberg, 1994; Sayers, 1994; Hornby et al., 1994]. Hence, the anisotropy due to the periodic thin layering of shales is very important and needs to be studied. Seismic anisotropy will affect time-to-depth conversions of seismic data which, in turn, will result in incorrect images of subsurface structures. This misrepresentation can seriously alter the location of interpreted exploration targets. Therefore, by studying seismic anisotropy, one can better assess a play target, thereby reducing the risks and costs involved.

Banik (1984) discovered a strong correlation between the presence of shales and measured velocity anisotropy. It has since been shown that shales exhibit TI, with a symmetry axis perpendicular-to-bedding, when probed with wavelengths that are longer than the thickness of the layers [Postma, 1955; Backus, 1962; Levin, 1979; Schoenberg, 1994; Johnston and Christensen, 1995]. Hence, shales exhibit an intrinsic anisotropy, resulting from the fine layering of the minerals, and the difference between the fast and slow velocities can be as much as 30% [Backus, 1962; Berryman, 1979; Levin, 1979; Jones and Wang, 1981; Banik, 1984; Gaiser, 1990; Sayers, 1994; Hornby et al., 1994; Kebaili and Schmitt, 1996]. Extrinsic anisotropy is a result of alternating layers of

isotropic or anisotropic media, with the layering of these materials being less than the wavelength of the probing seismic wave. Both intrinsic and extrinsic anisotropy is considered to exist in interbedded shales and sandstones in the Rocky Mountain Foothills, where folding and thrusting further compound the problem. No longer are the stratigraphic horizons horizontal, but are thrusted, often at steep angles, to the surface. These dipping layers are expected to induce changes in slowness and result in velocity anomalies in seismic data [Crampin, 1977; Gaiser, 1990]. The difference between the perpendicular-to- and parallel-to-bedding, hence the respective fast and slow, velocities is significant, increasing with the degree of anisotropy. This variation in velocity is assumed to have a significant effect on the traveltimes to the horizons below dipping clastic sequences, resulting in an apparent velocity anomaly in the seismic data.

1.2 Anisotropic P-wave Propagation

In order to understand and model geometric *P*-wave raypaths through any 2-D model, in the presence of elliptical and anelliptical anisotropy, some general theory must be established. Snell's law and both phase and group angles need to be considered across each interface [Crampin, 1977; Chapman and Pratt, 1992, Pratt and Chapman, 1992; Keith and Crampin, 1977a; Berryman, 1979; Gaiser, 1990; Dellinger and Vernik, 1994; Vestrum, 1994; Slawinski, 1995]. Computation of both reflection and transmission coefficients at anisotropic boundaries has previously been considered; however, none has considered interfaces that were not normal to the interface [Daley and Hron, 1977, Keith and Crampin, 1977a,b; Levin, 1978; Byun, 1982; Gaiser, 1990; Slawinski et al., 1995]. An elliptical wavefront solution, the simplest anisotropy assumption, was first considered to determine whether a complete, general anisotropic solution could be obtained for all ray angles. Also a solution that allows the major and minor axes of the ellipse to be oriented arbitrarily in 2-D space with respect to the interface, was developed.

1.2.1 Elliptical Anisotropy Solution

In this section, the relationship between the phase, $v(\theta)$, and group, $V(\phi)$, velocities are derived, as well as the critical angle, under the assumption of elliptical anisotropy and a

general rotation of the symmetry axis of the incident and refracted media. The basis of the elliptical solution was a combination of equations derived by Levin (1978) and Byun (1982) for an elliptically anisotropic medium. In this type of medium, a wavefront will be elliptical, and the equation of the phase velocity surface is given by [Byun, 1982],

$$v^2(\theta) = v_v^2 \cos^2(\theta) + v_h^2 \sin^2(\theta) \qquad (1.1)$$

where, v_v is the vertical or perpendicular-to-bedding velocity, v_h is the horizontal or parallel-to-bedding velocity and the phase angle, θ, is measured from the slow velocity axis. In this thesis, the terms v_{slow} and v_{fast} are sometimes used to describe v_v and v_h, respectively, in order to generalize the theory for dipping TI media. The phase velocity, $v(\theta)$, refers to the velocity of the seismic wavefront in a direction parallel to the wavefront normal. In contrast, the group or ray velocity, $V(\phi)$, is the velocity of the wave surface, in a direction radially outward from a point source in the anisotropic medium (Figure 1.1) [Winterstein, 1990; Thomsen, 1986].

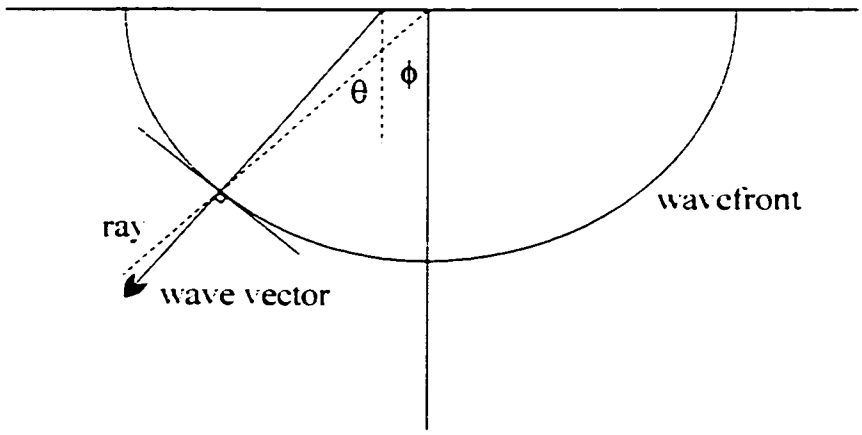

Figure 1.1. Diagram illustrating the difference between phase angle (θ) and group or ray angle (ϕ) for the VTI case [adapted from Thomsen (1986)].

The relationship between phase and group velocity is given by [Byun, 1982],

$$\frac{v(\theta)}{V(\phi)} = \cos(\phi - \theta) \qquad (1.2)$$

where $V(\phi)$ and ϕ relate to the group velocity surface and $v(\theta)$ and θ relate to the phase velocity surface.

Also given by Byun (1982) is,

$$\tan(\phi) = \left({}^{v_h}\!/_{v_v} \right)^2 \tan(\theta) . \qquad (1.3)$$

The group velocity surface is derived by the following procedure. Squaring equation (1.2) gives,

$$v^2(\theta) = V^2(\phi)\cos^2(\phi - \theta) = V^2(\phi)\left[\cos(\phi)\cos(\theta) + \sin(\phi)\sin(\theta)\right]^2 \qquad (1.2')$$

Equating equations (1.1) and (1.2'),

$$V^2(\phi)\left[\cos^2(\phi)\cos^2(\theta) + 2\cos(\phi)\cos(\theta)\sin(\phi)\sin(\theta) + \sin^2(\phi)\sin^2(\theta)\right] = v_v^2\cos^2(\theta) + v_h^2\sin^2(\theta)$$

Multiplication by $\left({}^{1}\!/_{\cos^2(\theta)} \right)$ yields,

$$V^2(\phi)\left[\cos^2(\phi) + 2\sin(\phi)\cos(\phi)\tan(\theta) + \sin^2(\phi)\tan^2(\theta)\right] = v_v^2 + v_h^2\tan^2(\theta)$$

Substituting for $\tan(\theta)$ from equation (1.3) results in,

$$V^2(\phi)\left[\cos^2(\phi) + 2\sin(\phi)\cos(\phi)\left\{\frac{v_v^2\sin(\phi)}{v_h^2\cos(\phi)}\right\} + \sin^2(\phi)\left\{\frac{v_v^4\sin^2(\phi)}{v_h^4\cos^2(\phi)}\right\}\right] = v_v^2 + v_h^2\left\{\frac{v_v^4\sin^2(\phi)}{v_h^4\cos^2(\phi)}\right\}$$

Multiplication by $\left(v_h^4\cos^2(\phi)\right)$ yields,

$$V^2(\phi)\left[v_h^4\cos^4(\phi) + 2v_v^2v_h^2\sin^2(\phi)\cos^2(\phi) + v_v^4\sin^4(\phi)\right] = v_v^2v_h^4\cos^2(\phi) + v_h^2v_v^4\sin^2(\phi)$$

Rearranging gives,

$$V^2(\phi)\left[v_h^2\cos^2(\phi) + v_v^2\sin^2(\phi)\right]^2 = v_v^2v_h^2\left[v_h^2\cos^2(\phi) + v_v^2\sin^2(\phi)\right]$$

Therefore,

$$V^2(\phi) = \frac{v_v^2 v_h^2}{\left[v_h^2 \cos^2(\phi) + v_v^2 \sin^2(\phi)\right]}$$

or,

$$\frac{1}{V^2(\phi)} = \frac{\sin^2(\phi)}{v_h^2} + \frac{\cos^2(\phi)}{v_v^2} \tag{1.4}$$

which is the equation for the group velocity surface.

Figure 1.2 illustrates a ray being transmitted through an interface. All angles are measured counterclockwise positive and angle direction is important. Angles ϕ and θ are the ray (group) and phase angles, respectively, and are measured from the slow velocity axis of the ellipse, v_{slow}, or, in other words, the axis of symmetry of the medium. If the axis of symmetry is rotated from the normal of the interface, the rotated angle γ, is measured from the interface normal. When $\gamma \neq 0$, the interface is not parallel to the fast velocity axis, or shale laminations, which is often the case in folded and faulted environments. This allows for a general elliptical solution to be obtained.

In order to develop the general elliptical numerical raytracer described in Chapter 2, the following relationships must be established. Note that all equations are valid in both the incident and refracted media and the angle definitions for each medium is given in Figure 1.2.

In the incident medium, the ray incident propagation angle, α, and rotation angle of the symmetry axis, γ, are known. Hence, from Figure 1.2, the ray incident and refracted propagation angles are described by:

$$\alpha = \phi + \gamma. \tag{1.5}$$

The horizontal slowness, or ray parameter p, which is conserved across an interface according to Snell's Law, is defined as,

$$p = \frac{\sin(\theta)}{v} \tag{1.6}$$

for the isotropic case (i.e. $\theta = \phi$, and $\gamma = 0$). This becomes,

$$p = \frac{\sin(\theta + \gamma)}{v(\theta)} \tag{1.7}$$

for the anisotropic case. Note that the phase velocity is dependent upon θ and the rotation angle of the symmetry axis (γ) is also included.

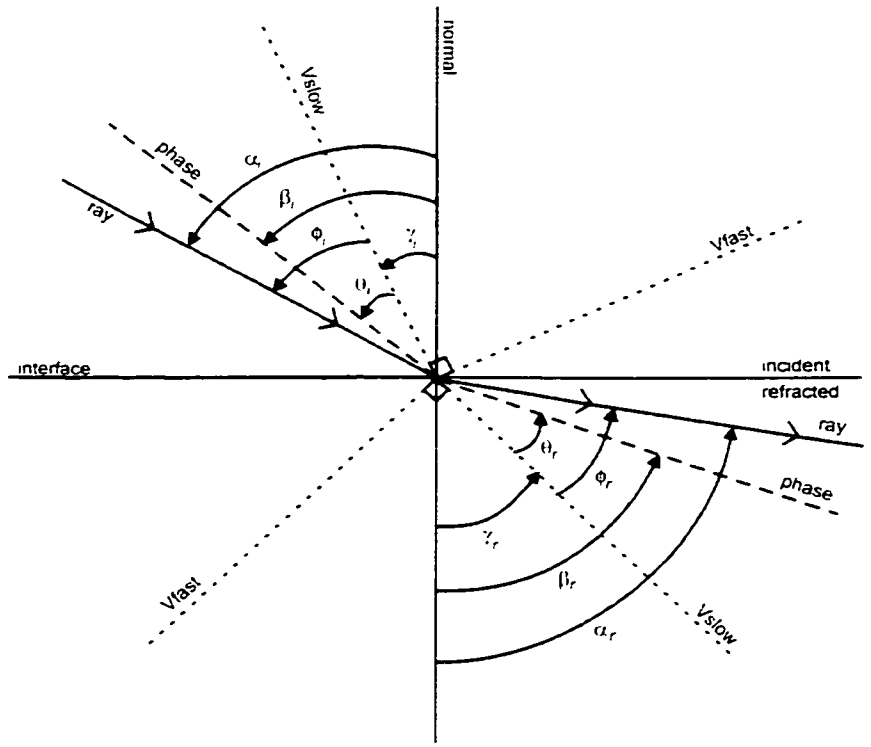

Figure 1.2. Generalized angle definition for a ray being transmitted through an interface.

Now, by expanding equation (1.7), the ray parameter may then be expressed as a function of vertical and horizontal velocities, v_v and v_h respectively, phase velocity, θ, and axis rotation angle, γ,

$$p = \frac{\sin(\theta)\cos(\gamma) + \cos(\theta)\sin(\gamma)}{\sqrt{v_v^2 \cos^2(\theta) + v_h^2 \sin^2(\theta)}}.$$

Multiplying the numerator and denominator of the previous equation by $\left(1/\cos(\theta)\right)$ yields,

$$p = \frac{\sin(\gamma) + \cos(\gamma)\tan(\theta)}{\sqrt{v_v^2 + v_h^2 \tan^2(\theta)}} \tag{1.8}$$

which is the ray parameter in terms of v_v, v_h, axis rotation angle, γ and phase angle, θ.

Substituting for $\tan(\theta)$ from equation (1.3) yields,

$$p = \frac{\sin(\gamma) + \cos(\gamma)\left[\frac{v_v^2}{v_h^2}\tan(\phi)\right]}{\sqrt{v_v^2 + v_h^2\left[\frac{v_v^4}{v_h^4}\tan^2(\phi)\right]}}$$

Multiplying the numerator and denominator by $1/v_v^2$, gives,

$$p = \frac{v_v^{-2}\sin(\gamma) + v_h^{-2}\cos(\gamma)\tan(\phi)}{\sqrt{v_v^{-2} + v_h^{-2}\tan^2(\phi)}} \tag{1.9}$$

which is the ray parameter in terms of v_v, v_h, axis rotation angle, γ and ray angle, ϕ. This allows for the calculation of the ray parameter in the incident medium, directly from given information.

Since the ray parameter is conserved across the interface, it is necessary to obtain the refracted ray angle, ϕ, in terms of the ray parameter, p, in order to calculate the refracted ray propagation angle, α. Rearranging equation (1.4) results in,

$$\frac{1}{V(\phi)\cos(\phi)} = \sqrt{v_v^{-2} + v_h^{-2}\tan^2(\phi)} \qquad (1.4')$$

Substituting equation (1.4') into equation (1.9),

$$p = V(\phi)\left[v_v^{-2}\sin(\gamma)\cos(\phi) + v_h^{-2}\cos(\gamma)\sin(\phi)\right] \qquad (1.10)$$

Squaring equation (1.9),

$$p^2 = \frac{v_v^{-4}\sin^2(\gamma) + 2v_v^{-2}v_h^{-2}\sin(\gamma)\cos(\gamma)\tan(\phi) + v_h^{-4}\cos^2(\gamma)\tan^2(\phi)}{v_v^{-2} + v_h^{-2}\tan^2(\phi)}$$

Cross-multiplying and rearranging yields,

$$p^2v_v^{-2} + p^2v_h^{-2}\tan^2(\phi) = v_v^{-4}\sin^2(\gamma) + 2v_v^{-2}v_h^{-2}\sin(\gamma)\cos(\gamma)\tan(\phi) + v_h^{-4}\cos^2(\gamma)\tan^2(\phi)$$

Hence,

$$\left(p^2v_h^{-2} - v_h^{-4}\cos^2(\gamma)\right)\tan^2(\phi) - \left(2v_v^{-2}v_h^{-2}\sin(\gamma)\cos(\gamma)\right)\tan(\phi) + \left(p^2v_v^{-2} - v_v^{-4}\sin^2(\gamma)\right) = 0$$

Using the quadratic formula to solve for $\tan(\phi)$ yields,

$$\tan(\phi) = \frac{2v_v^{-2}v_h^{-2}\sin(\gamma)\cos(\gamma) \pm \sqrt{4v_v^{-4}v_h^{-4}\sin^2(\gamma)\cos^2(\gamma) - 4\left(p^2v_h^{-2} - v_h^{-4}\cos^2(\gamma)\right)\left(p^2v_v^{-2} - v_v^{-4}\sin^2(\gamma)\right)}}{2\left(p^2v_h^{-2} - v_h^{-4}\cos^2(\gamma)\right)}$$

Multiplying the numerator and denominator by $v_v^2v_h^4$ yields,

$$\tan(\phi) = \frac{v_h^2\sin(\gamma)\cos(\gamma) \pm pv_h^2\sqrt{v_v^2\cos^2(\gamma) + v_h^2\sin^2(\gamma) - (pv_hv_v)^2}}{v_v^2\left(p^2v_h^2 - \cos^2(\gamma)\right)}$$

Therefore,

$$\tan(\phi) = \left(\frac{v_h^2}{v_v^2}\right)\frac{\sin(\gamma)\cos(\gamma) \pm p\sqrt{v_v^2\cos^2(\gamma) + v_h^2\sin^2(\gamma) - (pv_hv_v)^2}}{p^2v_h^2 - \cos^2(\gamma)} \qquad (1.11)$$

which is the ray angle, ϕ, in terms of the ray parameter, p, axis rotation angle, γ, v_v, and v_h. This allows for the calculation of the refracted ray angle, ϕ, and hence the ray refracted propagation angle, α, using the known parameters of the refracted medium.

Note that for a normal ray, p=0, equation (1.11) reduces to,

$$\tan(\phi) = -\left(\frac{v_h^2}{v_v^2}\right)\tan(\gamma).$$

The refracted phase angle, θ, may also be described in terms of the refracted medium's parameters. Squaring equation (1.8) and rearranging gives,

$$p^2v_v^2 + p^2v_h^2\tan^2(\theta) = \sin^2(\gamma) + 2\sin(\gamma)\cos(\gamma)\tan(\theta) + \cos^2(\gamma)\tan^2(\theta)$$

Hence,

$$(p^2v_h^2 - \cos^2(\gamma))\tan^2(\theta) + (-2\sin(\gamma)\cos(\gamma))\tan(\theta) + (p^2v_v^2 - \sin^2(\gamma)) = 0$$

Using the quadratic formula to solve for $\tan(\theta)$ yields,

$$\tan(\theta) = \frac{2\sin(\gamma)\cos(\gamma) \pm \sqrt{4\sin^2(\gamma)\cos^2(\gamma) - 4\left(p^2v_h^2 - \cos^2(\gamma)\right)\left(p^2v_v^2 - \sin^2(\gamma)\right)}}{2\left(p^2v_h^2 - \cos^2(\gamma)\right)}$$

Multiplying and rearranging results in,

$$\tan(\theta) = \frac{\sin(\gamma)\cos(\gamma) \pm p\sqrt{v_v^2\cos^2(\gamma) + v_h^2\sin^2(\gamma) - \left(pv_hv_v\right)^2}}{\left(p^2v_h^2 - \cos^2(\gamma)\right)} \qquad (1.12)$$

which is the phase angle, θ, in terms of the ray parameter, p, axis rotation angle, γ, v_v, and v_h.

Note that substitution of equation (1.12) into equation (1.11) yields,

$$\tan(\phi) = \left(\frac{v_h^2}{v_v^2}\right)\tan(\theta). \tag{1.3}$$

For completeness, the phase incident and refracted propagation angles are defined as,

$$\beta = \theta + \gamma \tag{1.13}$$

as in Figure 1.2.

Note that equation (1.7) becomes,

$$p = \frac{\sin(\beta)}{v(\theta)}. \tag{1.14}$$

for the anisotropic case. Critical refraction must also be considered, which occurs when,

$$\theta_c \geq \sin^{-1}(v_i / v_r) \tag{1.15}$$

for the isotropic case. v_i and v_r refer to the incident and refracted phase velocities, respectively. For the elliptically anisotropic case, critical refraction occurs when,

$$\left[v_h^2 \sin^2(\gamma) + v_v^2 \cos^2(\gamma) - (p v_h v_v)^2\right] < 0. \tag{1.16}$$

1.2.2 Anelliptical Anisotropy Solution

For weakly anisotropic media, the following Thomsen (1986) equations can be used:

$$\varepsilon \equiv \frac{c_{11} - c_{33}}{2c_{33}} = \frac{v_h - v_v}{v_v} \tag{1.17}$$

$$\delta \equiv \frac{(c_{13}+c_{44})^2-(c_{33}-c_{44})^2}{2c_{33}(c_{33}-c_{44})} = 4\left(\frac{v_{45}}{v_v}-1\right)-\left(\frac{v_h}{v_v}-1\right) \qquad (1.18)$$

where c_{ij} are the elastic stiffness coefficients and v_v, v_{45} and v_h are the perpendicular-to-, 45°-to- and parallel-to- bedding phase velocities, respectively. An anisotropic medium is considered weakly anisotropic when the difference between the bedding-normal and bedding-perpendicular velocities is less than 20% [Thomsen, 1986]. Also, for an anisotropic medium to be considered elliptically anisotropic, the parameters ε and δ must be equal [Thomsen, 1986]. However, this is only a mathematical simplification as ε and δ usually differ in actual rock samples [Thomsen, 1986; Tsvankin and Thomsen, 1994].

It is worthy to note that the percentage (%) anisotropy is calculated as follows, throughout this thesis:

$$\%\ \text{anisotropy} = \frac{v_h - v_v}{v_h} \times 100\ \% \qquad (1.19)$$

Using Thomsen (1986) notation, the phase velocity is given by,

$$v(\theta) = \alpha_o(1+\delta\sin^2(\theta)\cos^2(\theta)+\varepsilon\sin^4(\theta)). \qquad (1.20)$$

where $\alpha_o = v_v$. The relationship between the group and phase angles is,

$$\tan(\phi) = \tan(\theta)\left[1+2\delta+4(\varepsilon-\delta)\sin^2(\theta)\right]. \qquad (1.21)$$

The ray velocity can be obtained by,

$$V(\phi) = \alpha_o(1+\delta\sin^2(\phi)\cos^2(\phi)+\varepsilon\sin^4(\phi)). \qquad (1.22)$$

1.3 Measuring ε and δ

In order to use the Thomsen (1986) notation for computing the propagation of P-waves through anisotropic media, one must have knowledge about the values of both ε and δ. Obtaining accurate values for these parameters has been widely investigated, mainly

through the investigation of nonhyperbolic moveout, from surface seismic data, in homogeneous, flat lying layers. Tsvankin and Thomsen (1994) first investigated the relationship between anisotropy and (non)hyperbolic moveout in seismic data. Note also that the hyperbolic moveout equation is strictly valid only for a reflector below an homogeneous isotropic or elliptically anisotropic layer. Tsvankin and Thomsen (1994) determined that the presence of anisotropy resulted in nonhyperbolic moveout, even in an homogeneous layer, and that for P-waves, the relative magnitude of deviations from hyperbolic moveout increases with increasing $|\varepsilon - \delta|$. They also discovered that the short-spread moveout velocity is not equal to the rms velocity, even for horizontal layers, in the presence of anisotropy. Thus the P-wave moveout from horizontal reflectors is insufficient to recover the VTI parameters, even when using long offsets [Tsvankin and Thomsen, 1994; Alkhalifah and Tsvankin, 1995]. As a result, the process of inverting for the anisotropic parameters is complicated using surface seismic data. It was also shown that the vertical S-wave velocity has a minimal effect on the P-wave traveltimes. This allows for the P-wave traveltimes to then be characterized by only three independent parameters: vertical P-wave velocity (v_v), ε and δ [Tsvankin and Thomsen, 1994; Alkhalifah and Tsvankin, 1995; Tsvankin, 1996 and 1997].

Alkhalifah and Tsvankin (1995) have developed an inversion routine, using modified equations from Tsvankin (1995), which provides sufficient information to perform *time* processing steps. These include DMO, pre- and post-stack time migration but not depth migration. The time-to-depth conversion requires an accurate knowledge of the vertical P-wave velocity, which cannot be determined from the P-wave NMO velocities alone [Tsvankin and Thomsen, 1994; Alkhalifah and Tsvankin, 1995]. Unfortunately, this inversion routine is only valid for a homogeneous, TI medium above a moderately dipping reflector (<50-60°). In addition, this process yields only the vertical P-wave NMO velocities and an effective anisotropic parameter η, which is defined by Alkhalifah and Tsvankin (1995) as follows:

$$\eta = \frac{\varepsilon - \delta}{1 - 2\delta} \tag{1.23}$$

This parameter, η, is an indication of the deviation from ellipticity of a material. However, in order to obtain the individual values of v_v, ε and δ, required for depth processing routines, one must have additional external information, such as well logs, cross well information or a check shot survey.

When working in a complexly structured environment, such as the Rocky Mountain Fold and Thrust Belt, one does not encounter flat-lying structures very often. Generally, the rocks are often folded and thrusted to steep dip angles, which may or may not outcrop at surface. With this in mind, the process of obtaining the anisotropic parameters from surface seismic data is not feasible, particularly when the wavelength of structures is significantly less than the seismic recording aperture. An additional problem is that the rock formations in the Southern Alberta Foothills may possess varying degrees of anisotropy, as a result of both intrinsic (e.g. Wapiabi and Blackstone shales) and extrinsic (e.g. Lower Brazeau/Belly River interbedded shales and sandstones) properties. See Figure 1.3 for stratigraphic column of the southern Rocky Mountain Foothills. This may result in lateral inhomogeneity in anisotropic parameters as well as velocity in the subsurface, especially when these formations are folded and thrusted. In these environments, the optimal approach to subsurface imaging is pre-stack depth migration, but this process requires prior knowledge of the anisotropic parameters of various formations.

1.4 Structure and Objectives of Thesis

The majority of work published to date does not adequately address the problem of reflection seismic imaging in anisotropic media with a tilted symmetry axis. Most of the examples published-to-date describe horizontally layered media with a vertical symmetry axis (VTI), or vertically aligned cracks with a horizontal symmetry axis (HTI), and virtually nothing with intermediate dip angles [for example, Tsvankin, 1997]. Thus the focus of this dissertation is to address the tilted symmetry axis problem of the complexly structured environment, in the pre-stack depth migration domain. This includes the development of both refraction seismic and VSP field techniques to determine the

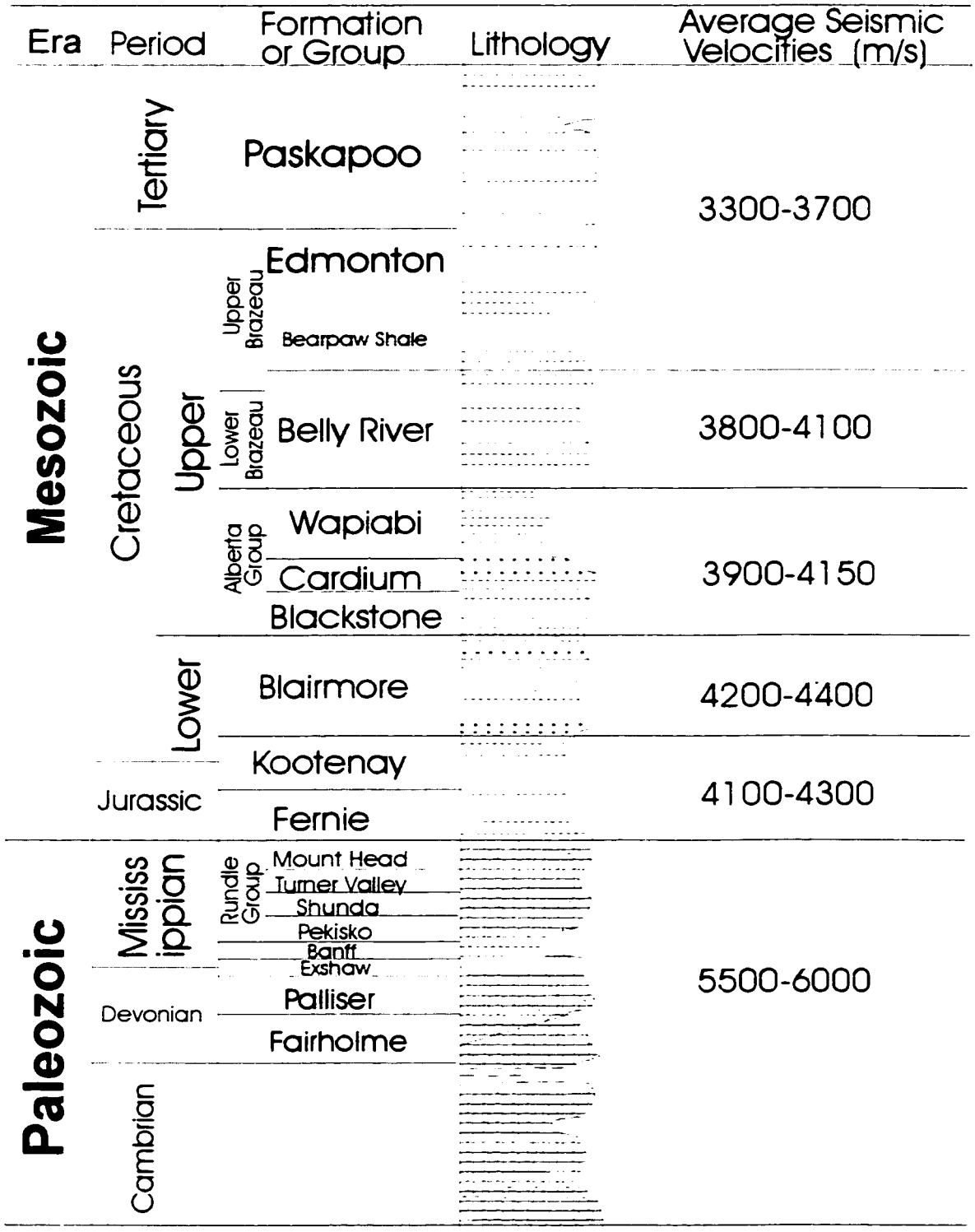

Figure 1.3. **Stratigraphic column from the Southern Alberta Foothills [adapted from Slotboom, 1992].**

individual anisotropic parameters necessary for the depth migration process. These experimental techniques have not been previously employed for the determination of anisotropic parameters of rocks at a seismic wavelength scale.

Two physical models, representative of structures found in the foothills of central Alberta and incorporating anisotropic material were used to demonstrate the 'pull-up' effects of anisotropy due to steeply dipping shales. These physical models are extremely useful for assessing the effects of anisotropy on seismic images since the velocities, anisotropic parameters, dip angles, and the exact location and geometry of the thrust sheets are known *a priori*. The objective of the experiments with physical models was to determine if the effects of anisotropy, particularly transverse isotropy, would significantly affect isotropic migration results. Initially, numerical analysis was undertaken on these model data, described in Chapter 2, to assess the magnitude of the anisotropic effects of dipping strata, which can affect traveltimes significantly.

Pre-stack depth migration was then performed on both physical model datasets, and these results are described in Chapter 3 using both isotropic and anisotropic velocity models. The first physical model dataset was examined using the isotropic, pre-stack depth migration (PSDM) routine at Amoco Canada, in the summer of 1996. This was done to assess the limitations of the isotropic PSDM. To evaluate the differences between isotropic and anisotropic PSDM, both physical model datasets were subsequently analyzed using the software provided by Kelman Technologies Inc., in the spring of 1998.

Current methods of time-to-depth conversion of P-wave seismic data do not address the traveltime and velocity distortions caused by seismic anisotropy, especially in areas of complex geological structure. The first step in addressing this problem is to know which rock units are anisotropic and to quantify their anisotropic parameters. This quantification can be done using laboratory studies on core and outcrop samples; however, this can be very difficult, particularly when examining the notoriously anisotropic rock type of shales. Also, it is difficult to mimic the *in situ* conditions in the

laboratory and, secondly, the friable shale samples also tend to break apart under the saturated conditions necessary to determine their anisotropic parameters. Hence, *in situ* measurements of the rocks are preferred since they give a more robust characterization of their properties. In this thesis, refraction seismic techniques have been developed, in Chapter 4, to measure anisotropic parameters of shales and other clastic sequences, *in situ*. By laying out seismic lines parallel, perpendicular and at 45° to the local strike directions, the Thomsen (1986) anisotropic parameters, ε and δ have been determined from the bedding-parallel, bedding-perpendicular and intermediate (45° azimuth) velocities. These refraction techniques were developed and applied in seven different field experiments, measuring the velocity variations in the Wapiabi, Cardium and Palliser formations as well as rocks of the Brazeau Group (Figure 1.3).

VSP technology has been previously considered for the determination of velocity anisotropy in rocks; however, these methods are limited to dips less than 5° [Kebaili and Schmitt, 1996; Sayers, 1997; MacBeth, 1998]. Therefore, with this limitation, these applications are not appropriate in moderate to steep dip environments, such as in the Foothills of the Rocky Mountain Fold and Thrust Belt. In Chapter 5, a new approach to using VSP technology to determine the anisotropic parameters is developed and tested in an Alberta Foothills well. To calculate the anisotropic parameters, ε and δ, in the presence of moderate to steep dips, accurate determinations of the bedding-normal, bedding-perpendicular and 45° velocities are required. Using multi-offset VSP technology, these velocities were determined from the first arrival information through a thick homogeneous, moderately dipping (30-60°), uniformly dipping panel of rocks and a multi-offset source configuration.

In Chapter 6, the migration of an Alberta Foothills surface seismic dataset is described and processed using anisotropic pre-stack depth migration. This required a geologically controlled velocity model, and the anisotropic parameters determined from the refraction (Chapter 4) and VSP (Chapter 5) surveys. Anisotropic depth migration was used to provide an optimally imaged depth section.

1.5 Geology and Study Areas

This thesis involved several field sites in southern Alberta where experiments were undertaken. A stratigraphic column of formations in the foothills of southern Alberta is shown in Figure 1.3. The main geologic formations of interest belong to the Devonian, Mississippian and Upper Cretaceous periods. The Mississippian rocks are the oldest and deepest rocks involved in structural deformation in the areas studied, most of which were in the Triangle Zone, a structural feature at the leading edge of the fold and thrust belt [Lawton et al., 1994; Gordy et al., 1977]. The top of the Paleozoic strata, which are comprised mainly of carbonate rocks, is a major marker of interest in seismic data as this is the boundary between the overlying clastic rocks and the underlying carbonate rocks. It is in this seismic reflector that the effects of anisotropy in the overlying sediments are evident. The Mississippian rocks overlie the Devonian Exshaw and Palliser Formations and Fairholme Group. The Exshaw Formation is a black shale which is often a major glide horizon in the southern Alberta foothills [Slotboom, 1992]. The Palliser Formation and Fairholme Group are mainly composed of carbonate rocks. In strata of Mesozoic age, Alberta Group rocks, comprising the Wapiabi, Cardium and Blackstone formations, are of greatest interest in this study. The Blackstone and Wapiabi formations are marine shales and are both important detachment horizons [Slotboom, 1992]. They range in thickness from 300-450 m and exhibit intrinsic anisotropic properties. Between these formations lies the Cardium Formation, which is composed mainly of sandstones and conglomerates [Slotboom, 1992]. Above the Alberta Group lie the interbedded sandstones and shales of the Belly River Formation of the Brazeau Group (Figure 1.3). This formation is also of interest due to the extrinsic anisotropic properties of the interbedded layers.

The locations of the various surveys are shown on a map of Alberta, Canada, shown in Figure 1.4. Refraction seismic surveys were undertaken at sites near Jumpingpound Creek, Longview, Seebe, and Exshaw. The VSP survey was performed at Wildcat Hills.

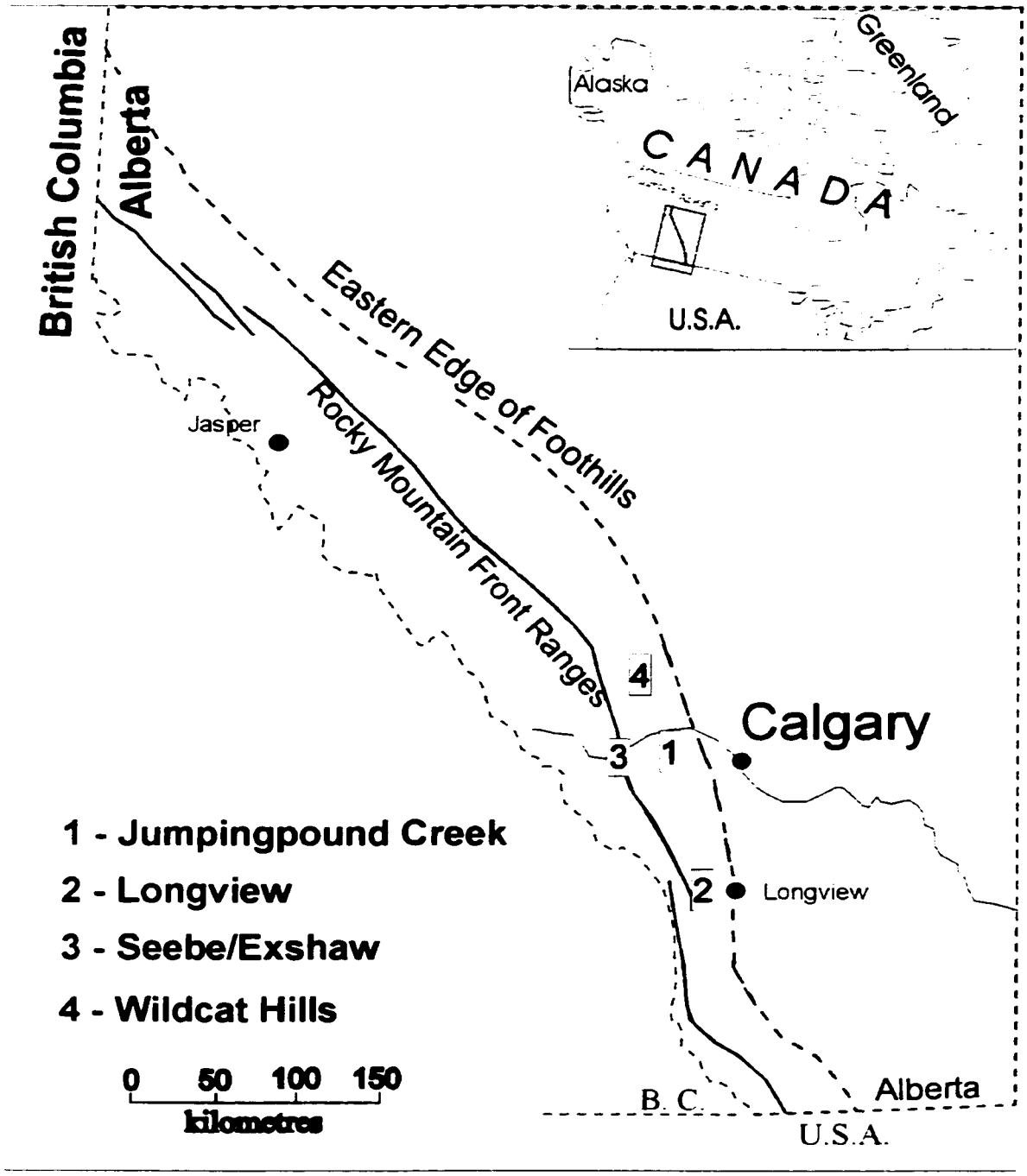

Figure 1.4. Map of Alberta indicating the field survey areas examined in this dissertation. Seven refraction surveys were performed in various locations near Jumpingpound Creek, Longview and Seebe/Exshaw. The VSP survey was performed at Wildcat Hills.

CHAPTER 2 PHYSICAL AND NUMERICAL MODELLING THROUGH ANISOTROPIC MEDIA

2.1 Introduction

Physical models, representative of structures found in the foothills of central Alberta and incorporating anisotropic material, e.g. phenolic laminate, were used to demonstrate the pull-up effects of anisotropy due to steeply dipping shales. These physical models are extremely useful for assessing effects of anisotropy on seismic reflectors below dipping strata since the velocities, anisotropic parameters, dip angles, and the exact location and geometry of the thrust sheets are known *a priori*. By studying physical models, it is also easier to predict and understand the results obtained in the field. Also, this allowed for the determination of the effects of anisotropy, particularly transverse isotropy, and whether they significantly affect isotropic migration results.

Initial work involved the development of a numerical raytracer to predict the traveltimes of primary waves, or *P*-waves, through these physical models. The purpose of this work was to numerically model geometric *P*-wave raypaths though any 2-D model, in the presence of elliptical or anelliptical anisotropy. The raytracing program was then tested by two different physical models, to determine the stability of the subroutine written for the general elliptically anisotropic case with a variable symmetry axis.

2.2 Principles of the Traveltime Raytracing Program

The numerical raytracer was modified to calculate traveltimes from reflectors within an arbitrary 2D model, incorporating non-vertical symmetry axes. To run the raytracing program, a model file is required, which contains all of the reflector and interface information, including all rotational angles, or γ's, for each interface between media, either or both of which may be anisotropic. Another file, containing the acquisition geometry information of the sources and receivers, is also needed. Once these files have been created, the raytracing program then begins with the starting shot, as defined by the geometry file. A fan of rays is emitted into the model, each of which honours anisotropic

Snell's law across each interface and calculates the group velocity through each layer. At this point, the starting receiver is activated, searching for rays that straddle it. An iterative process is used to determine the ray, which emerges within the capture radius of this receiver. The traveltime for the ray, or rays, is calculated and the process continues for the following receiver. This process is repeated for each receiver defined in the geometry file, after which, the next shot is considered. Once all of the shots have been completed, an output file of the traveltimes is generated. The raytracer was developed to initially model elliptically anisotropic media and later extended to raytrace through anelliptic TI media.

2.3 Testing the Elliptical Anisotropy Subroutine

A Fortran subroutine was written to compute the raypath, the associated velocities and the traveltimes through general anisotropic media. Refer to Figure 1.2 for all angle definitions. This subroutine computes the incoming ray angle (ϕ_i) upon an interface from the ray incident propagation angle (α_i), (equation 1.5) and uses the ray parameter and equation 1.9 to calculate the refracted angle (ϕ_r) from equation 1.11. The refracted propagation angle (α_r) and associated ray velocities were then calculated using equations 1.5 and 1.4, respectively. The rotational angles of the axis of symmetry, γ's, must be defined, for each anisotropic interface of the model, before the calculations can be made. Note that the rotational angle of an isotropic medium is zero. Initially, the elliptical anisotropy code was tested alone using user-defined input angles, after which it was inserted, as a subroutine, into the raytracing program. The code for this subroutine is presented in Appendix I.

The following conditions, to constrain all of the required angles, were found to be sufficient for a general solution of rays impinging on an interface: $|\alpha_i| \le 90^o ; \phi_i \le 90^o ;$ β_i and $\beta_r < 0$ or, β_i and $\beta_r > 0$; and, $|\alpha_r| \le 90^o$. Since the phase angle, θ, is always less than the ray angle, in elliptically anisotropic media the condition that $-90^o < \phi_i < 90^o$

was sufficient to constrain θ_i. The fact that θ_r and ϕ_r are calculated via an arctangent function, results in, θ_r and ϕ_r, also being constrained to $\pm 90°$. However, a constraint on α_r is still needed since it must be between $\pm 90°$ for the ray to be physically valid.

Sometimes α_r was refracted towards the interface normal and, for other cases, away from it. This is one of the important reasons for using the elliptical anisotropy equations, since, the isotropic models do not result in this phenomenon. This minor change in the angles can have a significant effect on the raypaths and traveltimes through the models. It is also noted that the phase angles were always closer to the slow velocity axis than the ray angles. In some models the phase angles are very different from the ray angles, which can have a significant affect on the *P*-wave traveltimes, compared with isotropic raytracing programs, in which both the phase and the ray angles are always equal. One solution that was non-intuitive was that a negative α_i resulted in a positive α_r (Figure 2.1). In this particular case, with a moderately large γ_i and a small negative ray incident propagation angle (α_i), resulted in a slightly positive phase incident propagation angle (β_i). As it is the phase angle that is refracted according to Snell's law, both the phase and ray refracted angles are also positive. Thus it looks as though the propagating ray refracts back onto itself in the refracted medium, hence on the same side of the interface normal, which is counterintuitive.

2.4 Development of the Anelliptical Anisotropy Subroutine

There are two main problems with the anelliptical solution. Firstly, the phase incident angle, θ_i, cannot be determined explicitly from the ray incident angle, ϕ_i, using equation 1.21; thereby, complicating the calculation of the ray parameter, p, at the first interface. By assuming a thin isotropic layer at the top of the model, such that θ and ϕ are equal, this non-explicit conversion may be eliminated. Secondly, once the ray parameter has been calculated at the interface from the incident parameters, the refracted phase angle, θ_r, cannot be explicitly determined from the calculated ray parameter, p, using equation 1.7. Hence, the refracted phase angle values have to be determined iteratively. Initially

this was achieved by a spreadsheet, which calculated all the possible ray parameters, between 0 and 90°, using equation (1.7), incorporating all possible γ_r's. Thus, from the incident medium ray parameter, the refracted phase propagation angle, β_r and associated velocity could be determined from the corresponding ray parameter, calculated in the spreadsheet. From this value the refracted phase angle, θ_r, ray angle (ϕ_r) and velocity could be calculated. At which time the refracted ray propagation angle, α_r, could be determined from equation (1.5).

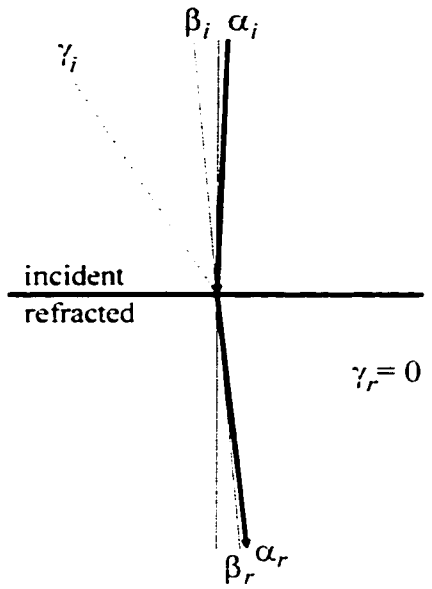

Figure 2.1. Diagram depicting a ray, propagating at an angle (α), impinging on an interface in the incident medium and being refracted back towards the direction of origin in the refracted medium.

It is important to note that all angles were measured with respect to the slow axis of the assumed pseudo-ellipse: the direction perpendicular to the laminations of the phenolic. Hence ϕ and θ are measured with respect to the slow velocity axis of the pseudo-ellipse and γ is measured from the interface normal, counterclockwise positive, as shown in Figure 1.1. Also note that the phase angles and velocities were calculated across the interfaces where the ray angles and velocities were then calculated. This procedure was also incorporated into the raytracing code.

2.5 Physical Modelling

P-wave transducers, vertically polarized with respect to the horizontal plane, were used as both sources and receivers in the acquisition of the two physical model datasets. The transducers are flat-faced and cylindrical, with an active element 12.6 mm in diameter [Cheadle et al., 1991]. When acquiring the data, the contact faces are coupled to the models. The source transducer is driven with a square wave tuned to produce a broadband wavelet with a central frequency of 300 kHz [Cheadle et al., 1991]. The transducers are moved across the model and traces are recorded sequentially and stored on disk, in SEG-Y format. The models are built from materials, such as solid laminates and Plexiglass, which are glued together. Distance and time scaling factors of 1:10 000 are typically used. The details of each model survey are presented in the sections below.

A consideration as to whether group or phase velocities were measured, also had to be taken into account [Keith and Crampin, 1977a; Berryman, 1979; Gaiser, 1990; Dellinger and Vernik, 1994; Vestrum, 1994; Slawinski et al., 1995]. It was determined that the group velocity was measured in these models since the ray length is very much greater than the diameter of the transducers (20cm vs. 1cm).

2.6 Physical Model 1

A 1:10 000 scale model of an anisotropic thrust sheet was constructed in the physical modelling lab of the Department of Geology and Geophysics at the University of Calgary. The model mimics structures found in the central Alberta Foothills (Figure 2.2). Phenolic laminate, consisting of layers of cloth which have been glued together with epoxy, was used as the anisotropic material because it has well understood elastic properties [Cheadle et al., 1991]. A simulated thrust sheet was constructed from the laminate, with corresponding slow and fast velocities of V_{slow} = 2925 m/s and V_{fast} = 3365 m/s, and the Thomsen (1986) anisotropic parameters were δ = 0.081 and ε = 0.150 [Cheadle et al., 1991]. The geometry is a good representation of structures found in the Southern Alberta Foothills. The surrounding isotropic medium was made of Plexiglass, which has a measured velocity of 2740 m/s. The marker of interest was the reflection from the

horizontal, aluminum base of the model, at approximately 2 km depth (scaled), below the thrust sheet. The scaled line length is 5160 m.

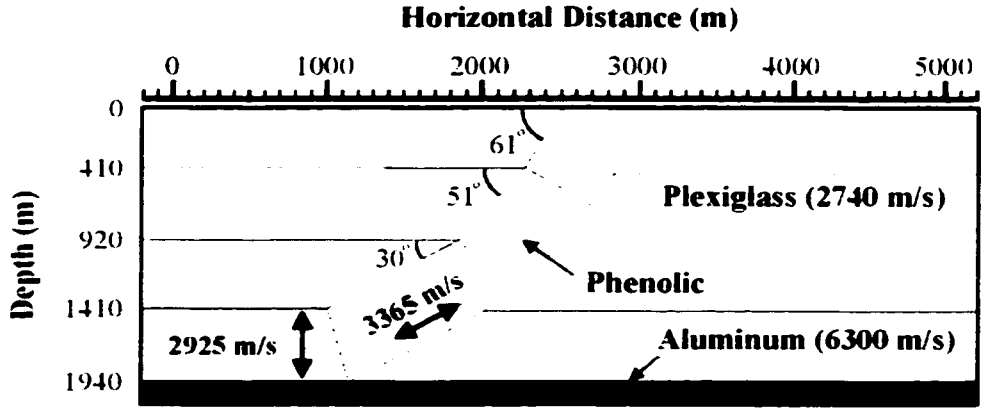

Figure 2.2. Diagram of first physical model built for the FRP. The reflector of interest is the flat aluminum base of the model at 1940 m (scaled).

The results of the 2-D, zero-offset, ultrasonic survey across the model show an apparent structure in this basal reflector, with an amplitude of approximately 100 ms (Figure 2.3). The trace spacing of the zero-offset data is 10 m. By modelling the data, isotropically, using the slow velocity of the phenolic material, the effects of the larger volume of faster material in the thrust sheet, in comparison to the slower velocity of the Plexiglass, could be determined. It was decided that half of the time anomaly, present in the data, was due to these isotropic effects and that the residual anomaly, due solely to anisotropy, was 50 ms. This represents a residual depth structure of approximately 100 m, in this case, which is the magnitude of structures that are considered prospects in the foothills. Hence the effects of anisotropy due to steeply dipping clastics are represented and significant in the seismic data obtained from the physical model. The data gap in the basal reflector of this model is due to critical refraction of rays along the bottom of the steepest dipping block of phenolic.

The results of using zero-offset raytracing to calculate the traveltimes to the flat, basal reflector from model 1 are shown in Figure 2.4. Calculated traveltimes agreed to within

±10 ms of those observed (scaled) from the physical modelling experiment. As shown in Figure 2.4, the results agree exceptionally well with the seismic data, displaying a 100 ms anomaly in the basal horizon. The gaps in the data from the raytracer correspond to shadow zones where there are no geometric raypaths. Diffractions were not included in the traveltime modelling.

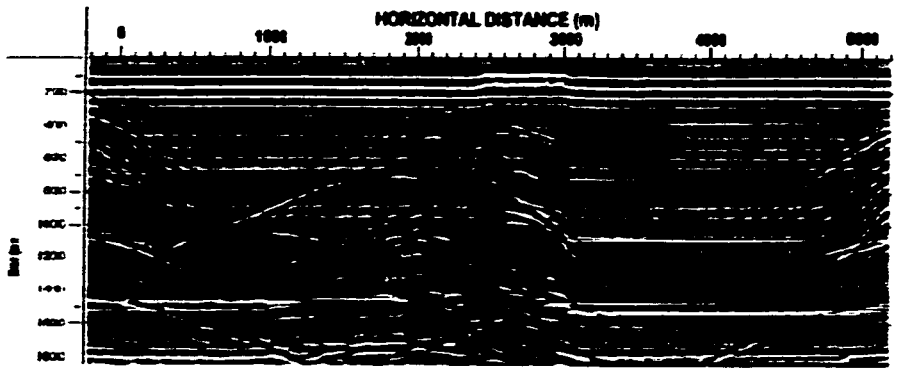

Figure 2.3. Zero-offset data from the ultrasonic survey performed on the first physical model. Note the pull-up (~100 ms) in the basal reflector located at approximately 1400 ms.

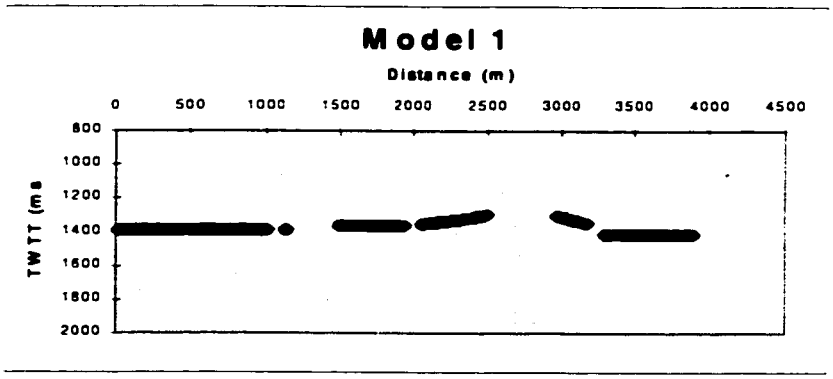

Figure 2.4. Results of raytracing of model 1. Note the 100ms velocity anomaly predicted, which is the same as that in the raw data. Note that the horizontal scale is slightly different from the raw data, as the origin for the raytracing was taken at a slightly different location than the recorded data.

Multi-offset data were also collected over this model and records were combined from forward and reverse passes over the model into 86 shot gathers, at 60 m intervals. The

source-receiver offsets were 200–2000 m and the receiver interval was 20 m. The processing of these data is discussed in Chapter 3.

2.7 Physical Model 2

Another 1:10 000 scale model of an anisotropic thrust sheet was constructed in the physical modeling laboratory (Figure 2.5). The model is comprised completely of phenolic laminate, with alternating layers of linen, such that traveltime anomalies from reflectors at the base of the model could be attributed solely to the anisotropic effects of the variably dipping layers in the model. The velocities of this material were assumed to be V_{slow} = 2925 m/s and V_{fast} = 3365 m/s, respectively, and δ = 0.081 and ε = 0.150, similar to those of model 1 [Cheadle et al., 1991; Thomsen, 1986]. The resulting percentage anisotropy (equation 1.19) is then 13%. The phenolic hanging wall thrust sheet consists of four segments of increasing dip, from 0° to 67.5°. The footwall, flat layers are also made of the same material. The marker of interest was again the reflection from the horizontal base of the model, at approximately 2 km depth (scaled), below the thrust sheet. This model did not have an aluminum base to it. The scaled line length is 5320 m.

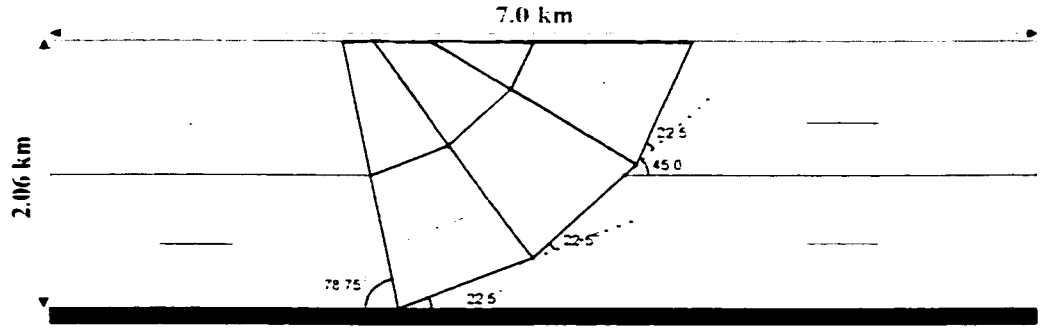

Figure 2.5. Diagram of second physical model built for the FRP. The reflector of interest is the base of the model at 2050 m (scaled).

The 2-D, zero-offset, ultrasonic survey data are shown in Figure 2.6. The trace spacing of the zero-offset data is 10 m. The amount of pull-up is less than 100 ms since the

surrounding isotropic material had been replaced with the higher velocity phenolic laminate, compared with lower velocity Plexiglass in model 1. Hence the velocity contrast is less compared to the first model, resulting in a smaller velocity anomaly, but one which is caused entirely by velocity anisotropy.

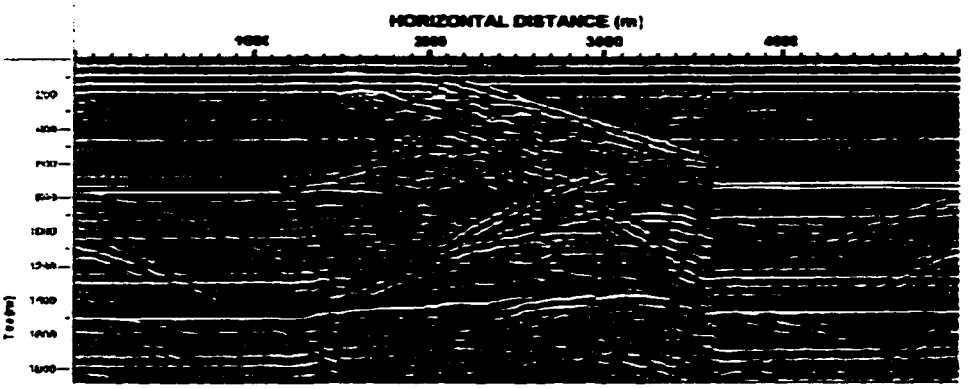

Figure 2.6. Resultant data from the ultrasonic survey performed on the second physical model. Note the pull-up (~50 ms) in the basal reflector located at approximately 1450 ms.

Figure 2.7, shows the results from model 2. The predicted results of this model are as expected, considering the results from model 1, and match observed values within ±10 ms. The amount of pull-up is less than 100 ms since the surrounding isotropic material had been replaced with the higher velocity phenolic laminate. Hence the average ray velocity contrast is less, resulting in a smaller velocity anomaly.

Again multi-offset data were combined from forward and reverse passes over the model into 134 shot gathers, at 40 m intervals. Source-receiver offsets were 200–2000 m with a receiver interval of 20 m. These data are also discussed in Chapter 3.

2.8 Discussion

By assuming elliptical anisotropy in this study, the first order issues arising from the anisotropy could be addressed, simply and easily. This allowed for a simple application to a complicated problem and, thus, a good starting place for the analysis of anisotropy in

seismic data. Also, with the use of zero-offset data, the problem of moveout due to varying ε and δ values, is eliminated. Hence, the elliptical solution is considered valid, for first-order effects, in this situation. This is not the case, such as in the following chapters, where multi-channel data were used.

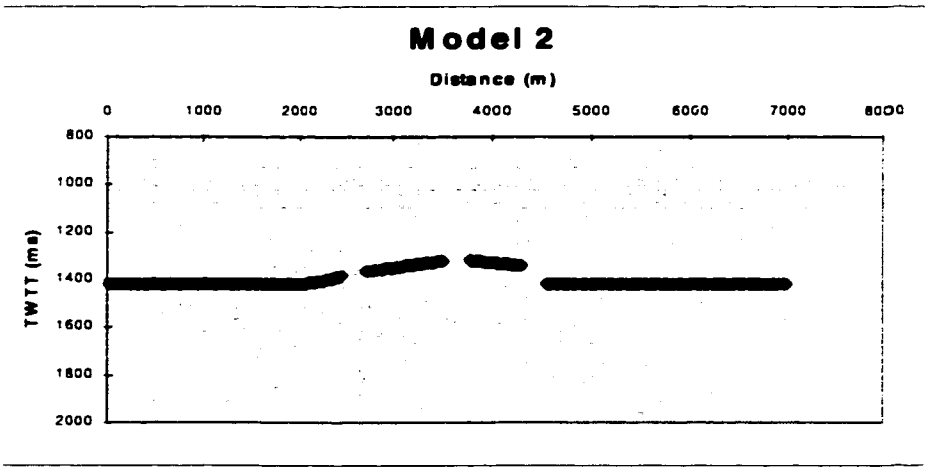

Figure 2.7. Results of the elliptical raytracing on model 2. Note the similarity to the results from model 1, except with a smaller velocity anomaly. Again the horizontal scale is different from the raw data due to a shift in the origin from the recorded data.

The raytracing code was well constrained and the numerical modelling results indicate that a general, elliptical, raytracing solution had been found. The results for each comparison model were as expected and the correlation to the actual data was exceptionally good, within ±10 ms. Thus the elliptical assumption was a reasonable solution for the zero-offset data.

CHAPTER 3 DEPTH MIGRATION OF PHYSICAL MODEL DATA

3.1 Introduction

Pre-stack depth migration was undertaken on multi-channel data collected over the two physical models, as described in Chapter 2, using both isotropic and anisotropic velocity models. The isotropic solution was examined at Amoco Canada as a summer project in 1996, using their in-house pre-stack depth migration code. A good understanding of the limitations of isotropic migration code ensued. The anisotropic solution was then pursued in conjunction with Kelman Technologies Inc. in the spring of 1998. The difference between isotropic and anisotropic migrations is that the traveltime generator for the anisotropic, Kirchhoff, pre-stack depth migration was developed such that anisotropic group velocities were used to propagate the wavefronts for traveltime computation [Vestrum et al., 1999]. In the isotropic case, a point on the wavefront propagates normal to the wavefront using the local velocity. In the anisotropic case, a point on the wavefront propagates radially outwards from the sourcepoint at the group velocity, which may be oblique to the wavefront normal [Vestrum et al., 1999].

One of the methods used, in this dissertation, to determine the validity of migration velocities was to look at the common image gathers (CIGs). A CIG is a display of pre-stack migration traces versus the source-receiver offset corresponding to a fixed reflector point [Zhu et al., 1998]. The migration moveout effects are prominent on CIGs and allow for effective velocity analysis, as a result. Zhu et al. (1998) give a detailed analysis of the mathematical relationships between high and low migration velocities and the pre- and post-stack migrated seismic section. Essentially, a high migration velocity, with respect to the 'true' velocity, will produce a 'frown' on the CIG and the migrated depth of the event will be too large. Whereas, a low migration velocity, with respect to the 'true' velocity, will produce a 'smile' on the CIG and the migration depth will be too shallow. If the migration velocity is equal to the true velocity, the image will be at the correct depth and event on the CIG will show no residual moveout.

3.2 Amoco Pre-Stack Depth Migration – Model 1

Data from model 1 (Figures 2.1 and 2.2) were pre-stack depth migrated using code made available by Amoco Canada. The model data were initially processed with a spiking deconvolution and a 500 ms AGC. The data were then migrated to determine if the anomaly present in the basal aluminum marker could be eliminated using isotropic velocities only. Hence, the objective was to determine whether assigning appropriate isotropic velocities could minimize the depth anomaly caused by anisotropic components of the model. Several velocity models were tested and two are discussed here. The best solution was considered to be the one that gave the closest representation of the physical model in terms of reflector image and location in depth. Figure 3.1 shows the result of using only the fast velocity for the anisotropic thrust sheet. The depth anomaly has been eliminated from the basal reflector, but the reflector is located 100 m too deep under the thrust sheet, as known from the physical model. Also, the CIGs are over-corrected (i.e. smiling) under the thrust sheet, indicating that this migration velocity is too low and that it should be higher (Figure 3.2). Nevertheless, this would further compound the migration error if higher velocities were used.

The second isotropic depth migration is a result of using a vertical velocity gradient within the thrust sheet, decreasing from the fast velocity to the slow velocity of the phenolic at the bottom of the thrust sheet. This is designed to approximate the anisotropy in the phenolic material, through use of isotropic velocities, with faster velocities at the top of the thrust sheet where the beds are almost vertical, decreasing in velocity to where the beds are flat lying at the base of the thrust sheet. The result of isotropic depth migration using this velocity model is shown in Figure 3.3. This section shows that the depth anomaly has been eliminated, for the most part, while maintaining the correct depth to the reflector. However, again the gathers indicate that the migration velocity of the thrust sheet is too low (Figure 3.4), since the events are over-corrected. Hence, the discrepancies in reflector location and gather shape indicate that anisotropy cannot be properly accounted for using the isotropic, pre-stack depth migration.

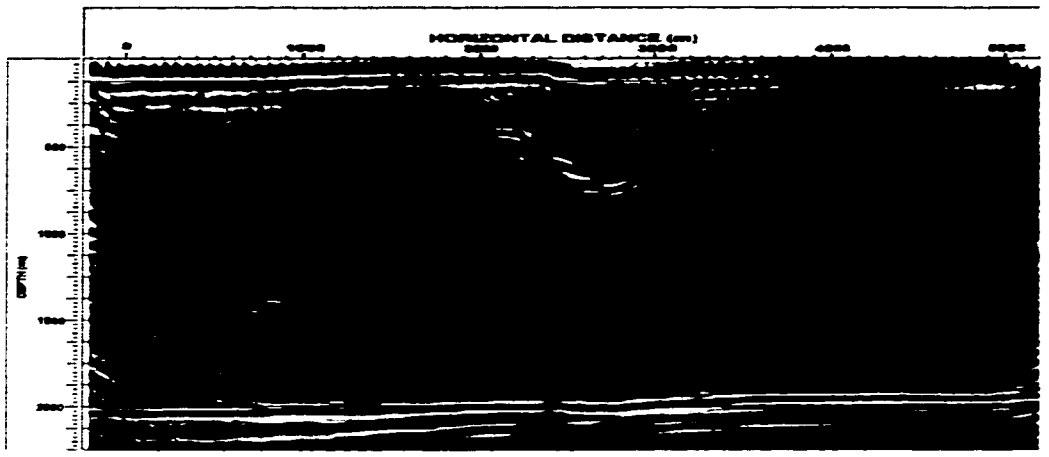

Figure 3.1. Isotropic, pre-stack depth migrated section of model 1 using a constant, fast velocity in the thrust sheet. Note that the basal reflector is located too deep under the thrust sheet (Amoco software).

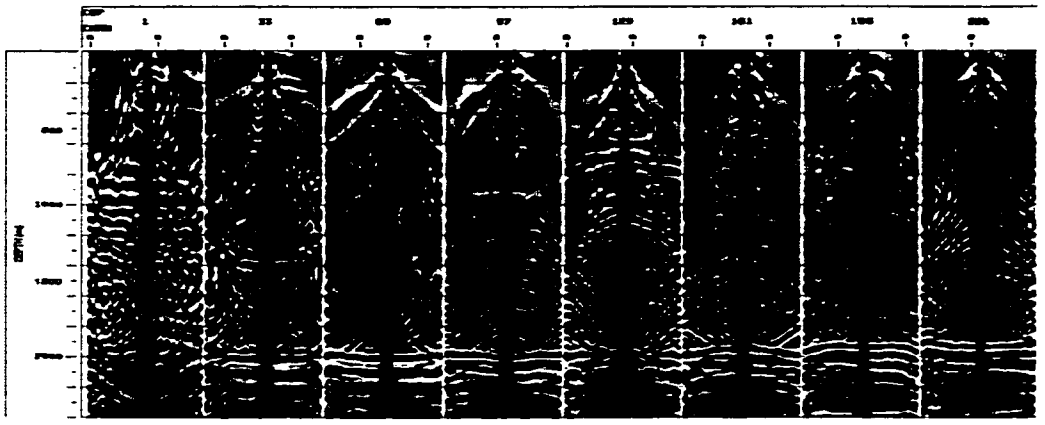

Figure 3.2. A sampling of depth gathers, evenly distributed across the model, resulting from the migration in Figure 3.1. Note that the gathers indicate that the migration velocities used are too low under the thrust sheet (third from left) and too high in the Plexiglass section (second and third from right).

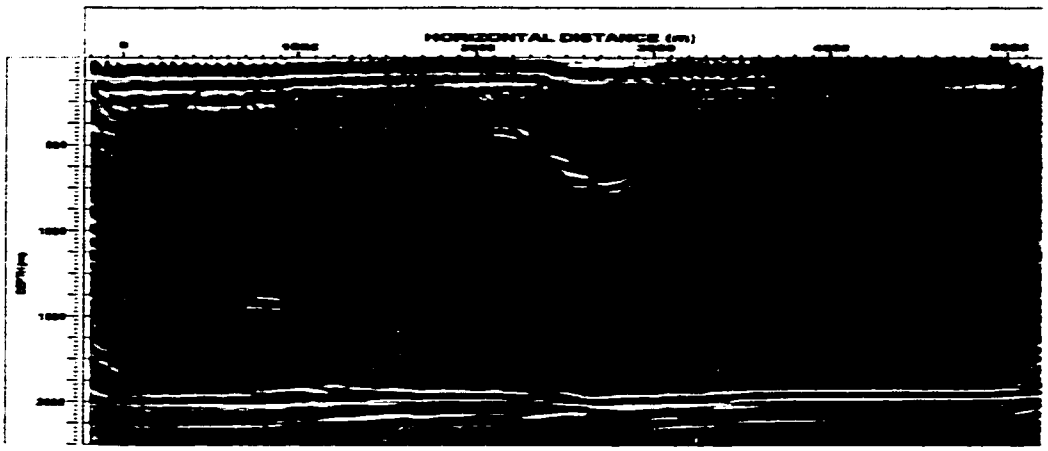

Figure 3.3. Isotropic, pre-stack depth migrated section of model 1 using a vertical velocity gradient in the thrust sheet. Note that the basal reflector is located at the correct depth under the thrust sheet; however, some residual structure is present in this reflector (Amoco software).

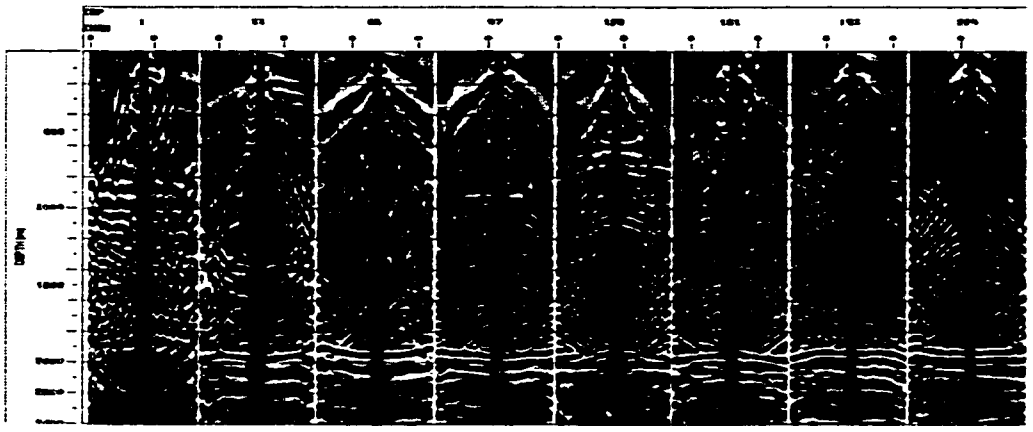

Figure 3.4. A sampling of depth gathers, evenly distributed across the model, resulting from the migration in Figure 3.3. Note the distorted nature of the gathers, especially under the thrust sheet (second, third and fourth gathers from left), which indicate that the migration velocity used was too low. Again the second and third gathers from the right demonstrate that the migration velocity in the Plexiglass was too fast.

3.3 Kelman Pre-Stack Depth Migration - Model 1

The purpose of this part of the study was to duplicate the results of the Amoco experiment and then to use the model data to test the anisotropic depth migration code. The physical model 1 data were processed as follows: mute; pre-stack depth migration (isotropic and anisotropic); scale; and filter (bandpass Ormsby 8-12, 50-60 Hz). The data were first migrated isotropically, with a velocity model built using the constant fast velocity of the thrust sheet and its actual spatial location for the migration, similar to that done for the Amoco study. As before, the objective was to eliminate the anomaly in the basal reflector and to obtain the correct depth image of the reflector. The results of this migration are shown in Figure 3.5 and the associated CIGs in Figure 3.6 (near offsets on the right and far offsets on the left of each CIG). The continuity of the basal reflector is good; however, again it is located too far in depth under the thrust sheet, compared to Figures 3.1 and 3.2. In addition, the gathers in this location indicate that the migration velocity is too low, due to the 'smiling' image on the CIGs, and should be increased. In doing so, the reflector would be pushed even farther in depth, which is incorrect. This result is the same as was determined in the Amoco study.

The second isotropic velocity model used a horizontal velocity gradient in the thrust sheet, grading from the fast velocity of the phenolic in the top right corner of the thrust to the slow velocity in the flat lying phenolic in the bottom left. This was done in attempt to account for the anisotropy of the phenolic material. Note that this model is slightly different from the Amoco study in that this velocity model used a horizontal velocity gradient and the Amoco model used a vertical velocity gradient. The result is a correctly placed reflector, under the thrust sheet, but the continuity of the reflector is somewhat compromised (Figure 3.7). This is a similar result to that found in the Amoco study (Figure 3.3). Again, events in the CIGs are smiling, which indicates that, although the reflector is correctly located in depth, a higher migration velocity should have been used to correctly migrate the data (Figure 3.8, compared with Figure 3.4). This would also be incorrect, according to the known physical model. Again, the results of the Kelman study

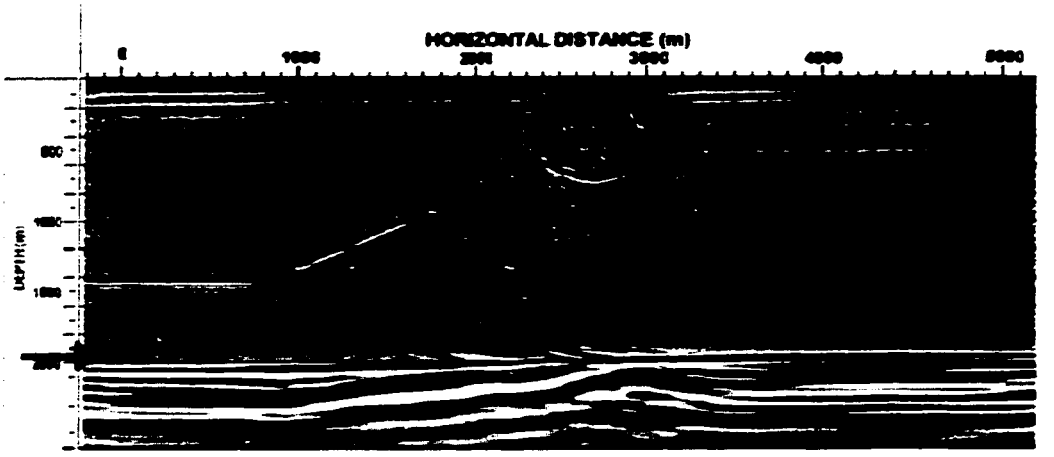

Figure 3.5. Isotropic, pre-stack depth migrated section of model 1 using a constant, fast velocity in the thrust sheet. The arrow indicates the true depth position of the basal reflector. Note that the basal reflector is located too deep under the thrust sheet (Kelman software).

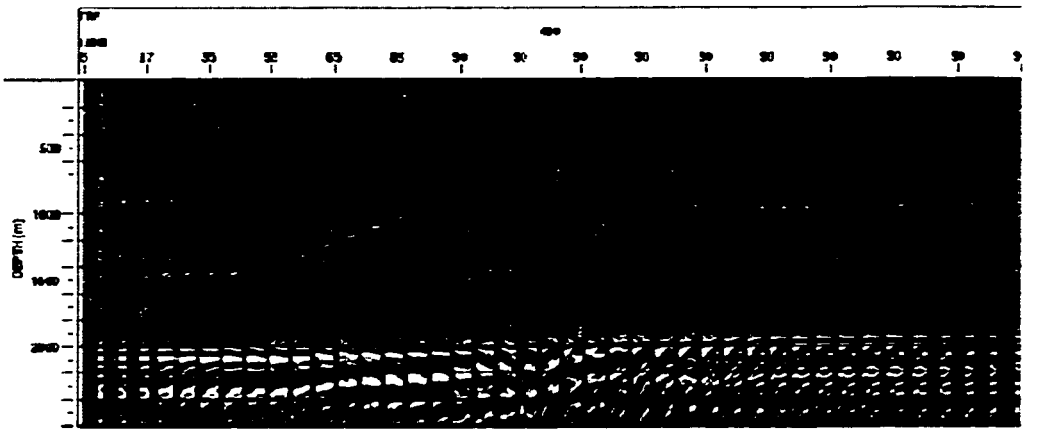

Figure 3.6. A sampling of depth gathers, evenly distributed across the model, resulting from the migration in Figure 3.5. Note that the near offsets are at the right side of each gather and the far offsets at the left. The basal reflector gathers located under the thrust sheet are over-corrected, demonstrating the need for a faster migration velocity.

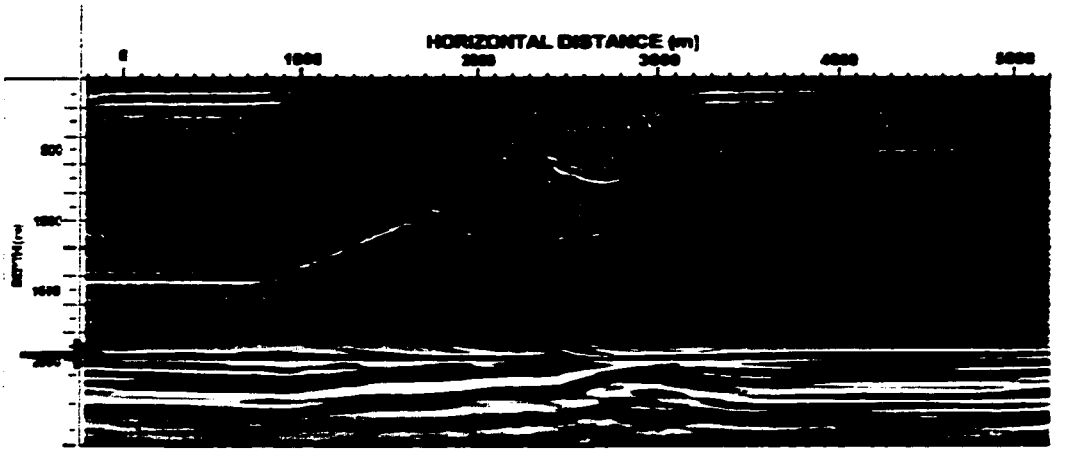

Figure 3.7. Isotropic, pre-stack depth migrated section of model 1 using a horizontal velocity gradient in the thrust sheet. Note that the basal reflector, at arrow, is located at the correct depth beneath the thrust sheet; however, some residual structure is present in this reflector (Kelman software).

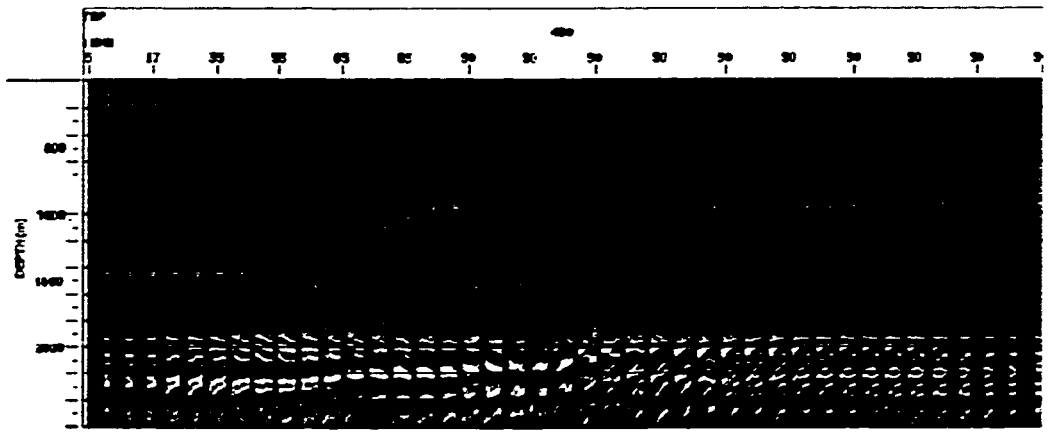

Figure 3.8. A sampling of depth gathers, evenly distributed across the model, resulting from the migration in Figure 3.7. Note the distorted nature of the basal reflector in the gathers, especially under the thrust sheet, which indicate that the migration velocity used was too low.

were successful in duplicating the results of the Amoco study, further indicating that isotropic velocities are insufficient to migrate data collected over an anisotropic model.

The only way to eliminate the discrepancy between correct depth and residual moveout on image gathers is to use anisotropic pre-stack depth migration. By using the correct velocity model, and all the correct parameters (ε, δ and dip) from the physical model, one obtains a correct depth image of the original model (Figure 3.9) which is supported by the associated CIGs (Figure 3.10). Reflector continuity is maintained, it is correctly located in depth and events within the CIG are flattened. Hence, all the discrepancies from the isotropic depth migration process have been eliminated. It should be noted that the small amount of residual moveout in the CIG is associated with the velocity model building process. The migration velocity model is built in time. However, the structural geometry of the model, is measured in depth, and the conversion from depth to time in the velocity model building process introduces small irregularities into the velocity model and, subsequently, in the migration. In conventional migration, the depth model is not known, thus the velocity model must be built deterministically.

3.4 Kelman Pre-Stack Depth Migration - Model 2

Data from physical model 2 (Figures 2.4 and 2.5) were processed using a mute, pre-stack depth migration (isotropic and anisotropic), scale and filter (bandpass Ormsby 8-12, 50-60 Hz). Again, for comparison purposes this model dataset was first processed isotropically, using a gradient velocity model, in order to attempt to eliminate the anomaly in the reflector from the base of the model. The base of the thrust was defined and a horizontal velocity gradient was applied to the dipping part of the thrust: grading from the fast velocity of the phenolic in the top right corner to the slow velocity of the phenolic in the flat-lying layers, in the bottom left. The resultant isotropic depth migration is comparable to the results of the first model (Figure 3.11). The basal reflector is located correctly in depth, with some minor structure present; however, the CIGs exhibit considerable residual moveout which indicates that a higher velocity should have been used to properly migrate the data (Figure 3.12). It is also interesting to note that the

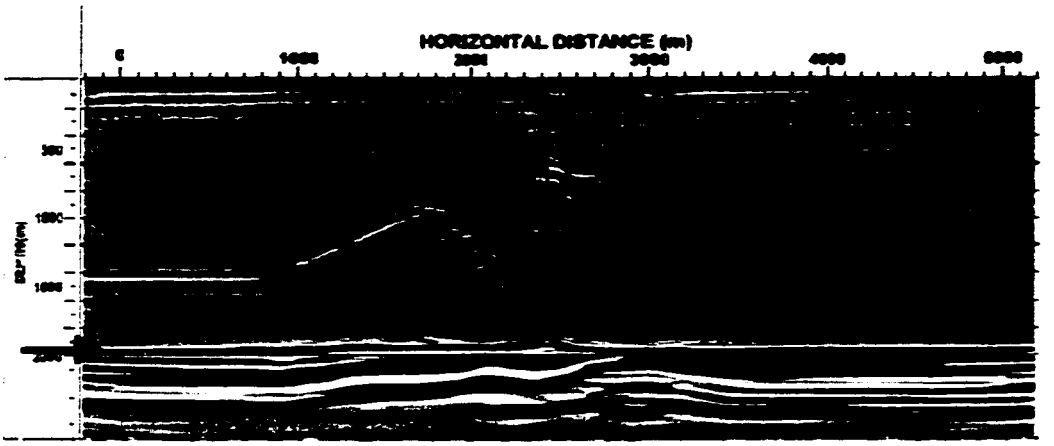

Figure 3.9. Anisotropic, pre-stack depth migrated section of model 1 using the correct parameters of the physical model. Note that the arrowed basal reflector is located at the correct depth beneath the thrust sheet and the residual structure in the reflector of interest has been eliminated (Kelman software).

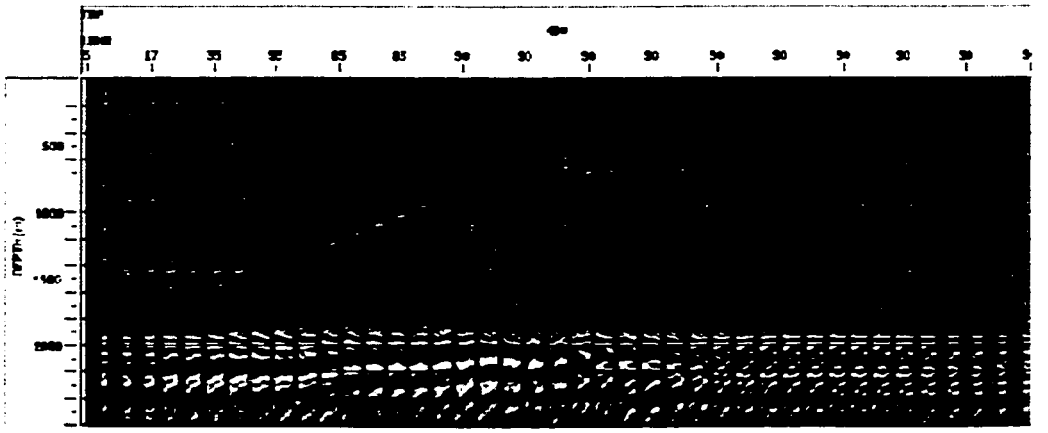

Figure 3.10. A sampling of depth gathers, evenly distributed across the model, resulting from the migration in Figure 3.9. The minor residual moveout present in the basal reflector gathers is attributed to the velocity model building process.

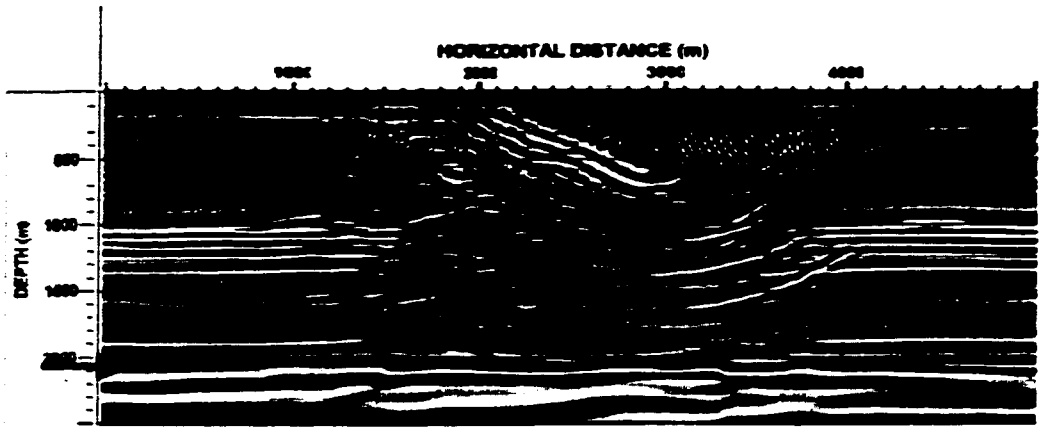

Figure 3.11. Isotropic, pre-stack depth migrated section of model 2 using a horizontal velocity gradient in the thrust sheet. Arrow indicates the true depth location of the basal reflector. Note that the basal reflector (trough) is located at the correct depth beneath the thrust sheet; however, some residual structure is present in this reflector (Kelman software).

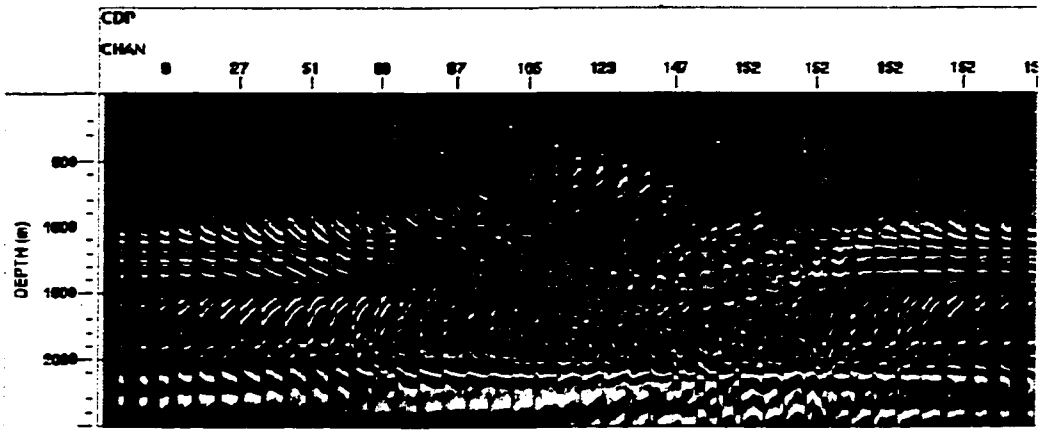

Figure 3.12. A sampling of depth gathers, evenly distributed across the model, resulting from the migration in Figure 3.11. Note the distorted moveout of the basal reflector in the gathers, especially under the thrust sheet, which indicate that the migration velocity used was too low.

CIGs also exhibit considerable moveout in the shallow, flat lying reflectors, on the edges of the model at approximately 1 km scaled depth. The CIGs are also over-corrected in this region, demonstrating that a higher migration velocity is necessary to properly migrate the data. This is incorrect according to the model geometry, which also indicates that the isotropic velocities are insufficient to migrate even the flat lying geology in the anisotropic model.

The continuity of the basal reflector is compromised because model 2 does not have an aluminum base. Since the model is sitting on a tabletop, thus going from a high velocity medium to a slow velocity medium, there is a negative impedance contrast at the base of the model. Also, there is a multiple which destructively interferes with the basal reflector, resulting from the horizontal seam, about halfway down the model, at approximately 1 km scaled depth. Thus the basal reflector is very strong in the middle of the section and weak at the edges (Figure 3.11).

Data from the second model were then migrated incorporating the known anisotropic parameters into the velocity model. This velocity model consisted of the definition of the thrust base, the actual parameters of the model (slow P-wave velocity, ε and δ) and a continuous definition of dip through the thrust sheet and across the model. No distinctions were made between the different blocks of dipping phenolic as the thrust sheet was modelled as having continuous, smooth curvature in the velocity model. After migration, the basal reflector is correctly located in depth, although it is severely distorted (Figure 3.13). The gathers are comparably distorted as well (Figure 3.14). Given that the input velocity model linearly interpolates the dips between defined values, whereas the actual model has distinctly dipping sections, the results are not surprising. This result illustrates the sensitivity of the depth migration to the geometry model.

In the final anisotropic velocity model, each distinct, dipping section of phenolic was correctly located, with appropriate dip as well as all the correct parameters of the physical model. The result, after migration, is a correct depth section with good reflector

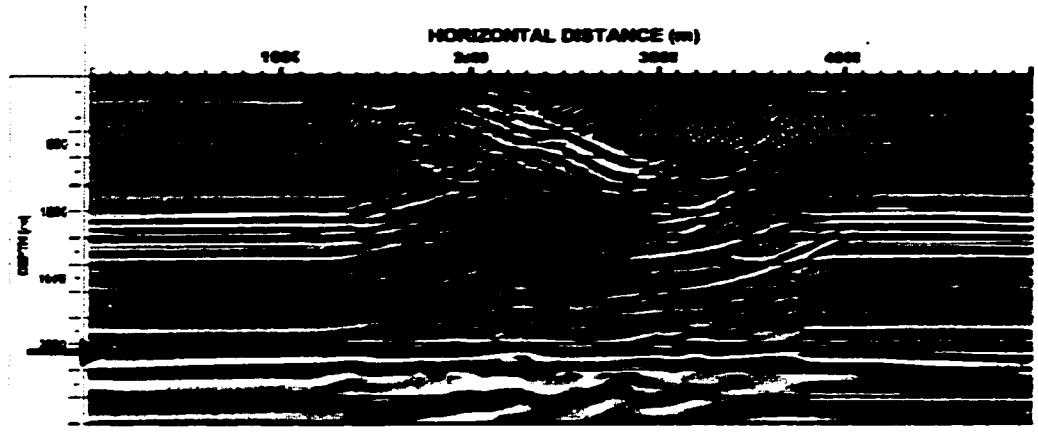

Figure 3.13. Anisotropic, pre-stack depth migrated section of model 2 using a continuous dip definition (no distinctly dipping sections) in the thrust sheet. Note that the arrowed basal reflector is located at the correct depth beneath the thrust sheet; however, there is an excessive amount of residual structure present in the basal reflector (Kelman software).

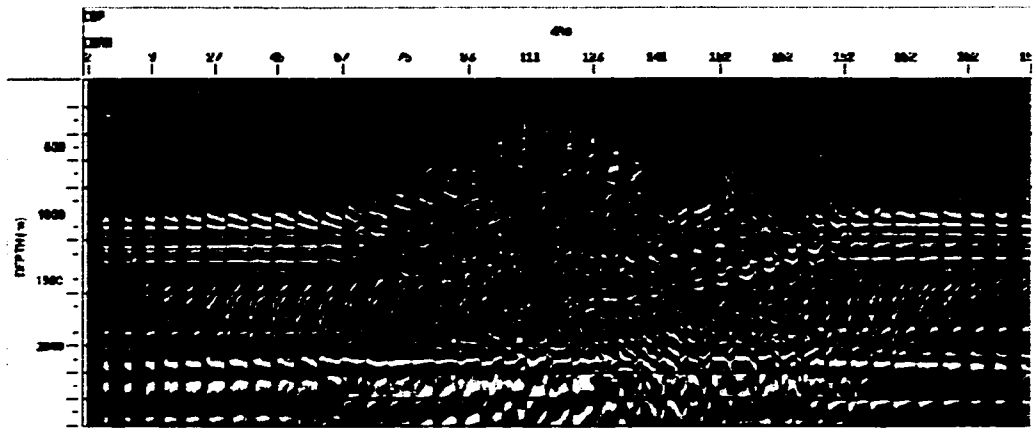

Figure 3.14. A sampling of depth gathers, evenly distributed across the model, resulting from the migration in Figure 3.13. Note the distorted nature of the basal reflector gathers, which indicate that the dips were not assigned accurately.

continuity (Figure 3.15), correct reflector depth and flattened events on the CIGs (Figure 3.16). Again the gathers show some minor residual moveout due to small depth-time conversion errors, as was noted in the results of the first physical model (Figures 3.9 and 3.10). Thus, the same sensitivity to the model building process is also present in the second physical model data.

3.5 Discussion

Physical models are very useful for the study of seismic anisotropy. Since all the necessary parameters of the model can be determined, the seismic data collected over the models are ideal for the testing of processing software, in particular, migration routines. In this study, it has been demonstrated that isotropic, pre-stack depth migration is limited in its ability to correctly migrate seismic data collected over anisotropic physical models, as it leads to discrepancies between the correct reflector depth and the residual moveout in image gathers. The testing completed in this study indicates that conventional pre-stack depth migration is not able to properly compensate for the effects of TI, and the results verify that anisotropic effects cannot be accounted for using isotropic velocities. Therefore, anisotropic, pre-stack depth migration is required to properly process seismic data from these models and, in general, data from foothills environments where anisotropic strata exist.

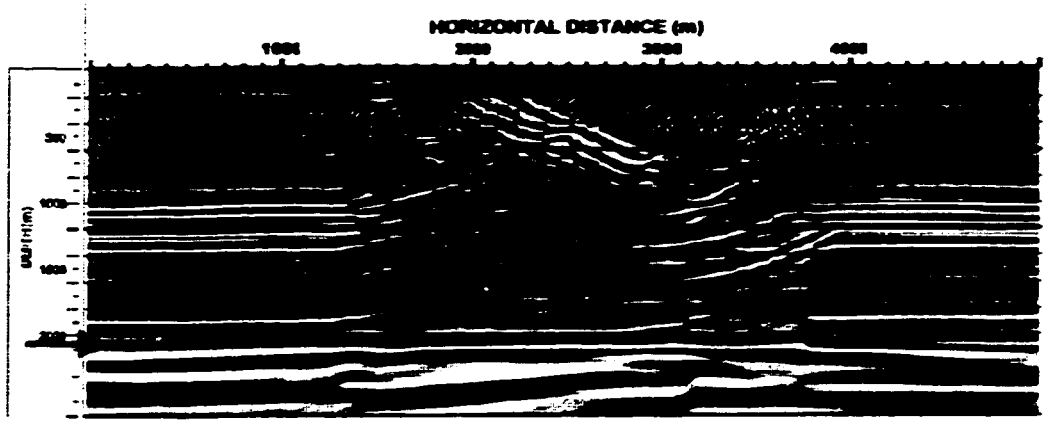

Figure 3.15. Anisotropic, pre-stack depth migrated section of model 2 using distinctly dipping sections in the thrust sheet. Note that the basal reflector, at arrow, is located at the correct depth under the thrust sheet and the residual structure has been eliminated (Kelman software).

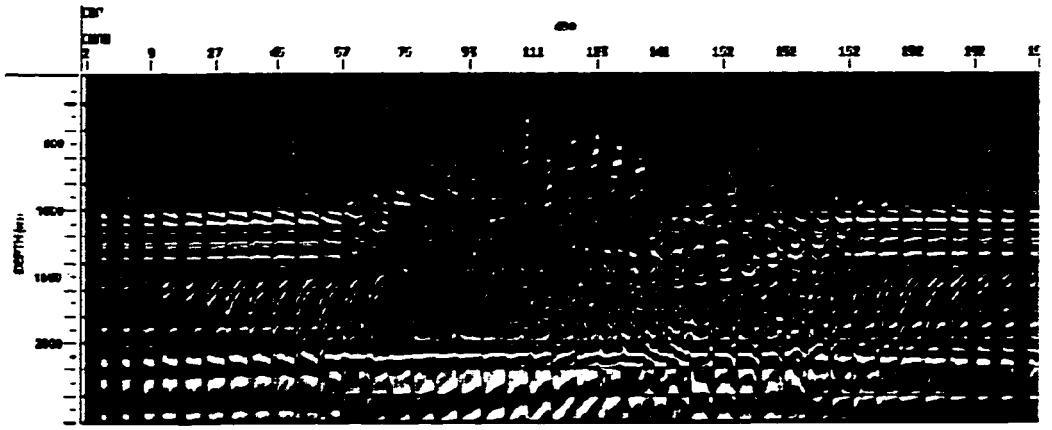

Figure 3.16. A sampling of depth gathers, evenly distributed across the model, resulting from the migration in Figure 3.15. The residual structure present in the basal reflector gathers is attributed to the velocity model building process.

CHAPTER 4 REFRACTION SEISMIC EXPERIMENTS

4.1 Introduction

Clearly, there is a need to determine the anisotropic parameters of rocks in a field experiment, where the bulk response of the rocks can be assessed on the scale of several seismic wavelengths, for direct application to the analysis of reflection seismic data. The approach taken in this study was to undertake a multiazimuth refraction seismic experiment in an area where the rocks of interest outcrop at surface and the strata have a uniform, steep dip, preferably vertical. This structural geometry is relatively common in fold-thrust belts. By laying out seismic lines parallel, perpendicular and at 45° to the local strike directions (Figure 4.1), the Thomsen (1986) anisotropic parameters, ε and δ can be determined using equations 1.17 and 1.18 (Chapter 1). For instance, for vertically dipping strata, the measured velocities along the local dip and strike directions are the bedding-normal and bedding-parallel velocities respectively, equivalent to the vertical and horizontal velocities described by Thomsen (1986) for the VTI case. These parameters were obtained by measurement of headwave velocities along the seismic lines, which were of sufficient length to ensure that the refractor velocities measured are from rocks that are below the near-surface weathered layer. A similar, successful study was undertaken previously by Gendzwill (1993) except that he evaluated anisotropic effects caused by vertical fractures rather than vertical bedding.

Seven multi-azimuthal refraction seismic field studies were performed over a period of three years, 1996-98, on shales of the Wapiabi Formation, interbedded shales and sandstones of the Brazeau Group, Palliser Formation limestones and sandstones of the Cardium Formation. These formations are tabulated in Figure 1.3. These surveys were executed in various locations along the foothills of the Rocky Mountain Fold and Thrust Belt in southern Alberta, Canada (Figure 1.4), after careful consideration of surface geology through the study of both maps and air photos. The Wapiabi shales are strongly suspected of possessing velocity anisotropy, as are the shales and sandstones of the Brazeau Group. Rocks of the Palliser Formation, which are composed primarily of

limestones, are not expected to exhibit intrinsic anisotropy, as do shales, but they may exhibit anisotropy due to fracture orientation. The same is true for the sandstones of the Cardium Formation.

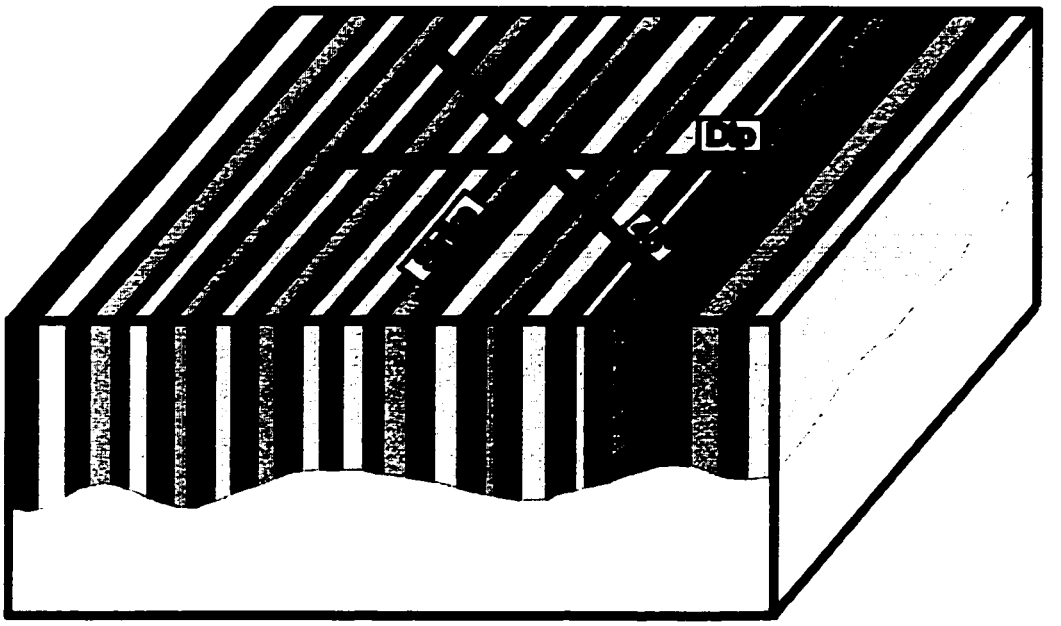

Figure 4.1. Schematic diagram showing the layout of the refraction seismic lines to determine the bedding-parallel, bedding-perpendicular and 45° azimuth velocities.

The first survey was conducted in 1996 at Jumpingpound Creek (Figure 1.4, location 1) with measurements on the steeply dipping shales of the Wapiabi Formation. The second group of surveys incorporated four locations west of Longview (Figure 1.4, location 2), in 1997 and 1998, and measured the anisotropy of the steeply dipping rocks of the Wapiabi Formation, Brazeau Group and Cardium Formation. The third set of experiments investigated the strata of the Palliser and the shallowly dipping Wapiabi formations at two locations near Seebe and Exshaw, respectively (Figure 1.4, location 3), in 1998.

4.2 Data Acquisition

Refraction seismic data were acquired according to the parameters given in Table 4.1. The specific geometries for each location are described in the appropriate sections, later

in this chapter. The source used was a Bison Elastic Wave Generator (EWG Model 3) owned and operated by the University of Calgary and was used in all of the refraction surveys for anisotropic parameter studies in this thesis project. It is a weight drop source, utilizing a 270 kg hammer, which is accelerated onto the ground by gravity, assisted by pre-tensioned elastic bands. An aluminum strike plate laid on the ground below the hammer was necessary to enhance energy coupling and was used in the 1998 surveys. Two different instrument systems were used during the surveys. A 24-bit, 96 channel Bison system operating at 0.25 ms sampling interval and a record length of 0.5 s was used for the 1996-97 surveys and a 24-bit, 60-channel Bison system operating at 0.125 ms sample interval and a record length of 0.25 s was used in the 1998 surveys. A transducer mounted on the EWG sources triggered the instruments for the 1996-97 surveys; however, a more reliable switch closure between the hammer and strike plate was developed and used for the 1998 surveys. The data were recorded directly onto hard disk in SEG-2 format and later copied to either a tape or a high density removable disk. Typically, two to three hammer impacts were summed at each source location to provide optimum signal to noise ratio for the first arrivals. At each shotpoint, the source hammer was offset approximately 1.5-2 m perpendicular to the line direction. Data quality was generally very good with clear first arrivals pickable over the full recording aperture.

4.3 Data Analysis

4.3.1 Geometry

The geometry file for each survey location was built in ProMax establishing the source and receiver locations in Cartesian co-ordinates. The SEG-Y seismic files were imported into ProMax and the following necessary information for each line was set up: number of traces per receiver for each shot; number of shots; and field file number for each shot. The geometry information was also maintained in a spreadsheet in order to produce a basemap, including bearings, at each survey location.

Table 4.1. Survey parameters of refraction seismic lines

Location/ Formation	Line	Azimuth (°)	Length (m)	# Receivers	Receiver Interval (m)	Shot Interval (m)
Jumpingpound Creek '96/ Wapiabi	Strike	157	285	96	3	6
	Dip	67	380	96	4	8
	45°	112	380	96	4	8
Longview '97/ Wapiabi	Strike	161	188	48	4	12
	Dip	71	188	48	4	~12
	45°	116	188	48	4	12
Longview '97/ Brazeau Gp.	Strike	155	284	72	4	18
	Dip	65	284	72	4	18
	45°	110	284	72	4	18
Longview '98/ Brazeau Gp.	Strike	160	236	60	3	48
	Dip	70	236	60	3	48
	45°	25				
Longview '98/ Cardium	Strike	170	236	60	4	48
	Dip	80	236	60	4	48
	45°	35	236	60	4	48
Seebe '98/ Wapiabi	Strike	166	95	20	5	10
	Dip	76	95	20	5	10
	45°	121	95	20	5	10
Exshaw '98/ Palliser	Strike	150				
	Dip	60	95	20	5	10
	45°	105				

4.3.2 First Break Picking

Initially bad traces were removed from each shot record. The first breaks were picked for the first shot record after which the automatic first break picker was initialized. To run the automatic picker in ProMax, a time gate was defined. This was the window within which the neural network picker picked the first breaks. To assess the accuracy of the automatic picker, the first shot record was repicked and the new picks appeared over the original picks. The picks were considered to be precise to ±2 ms and the neural network picker then proceeded to pick the first breaks from all the records within the dataset. Any bad picks were then edited manually. The result was a fairly straight lines of picks, diverging from the shot point. The first break data obtained in ProMax were transferred to a spreadsheet for further analysis.

4.3.3 Velocity Analysis

For inline shots and receivers at each of the survey sites, refractor velocities were generally determined using a 'minus-time' analysis, developed by Hagedoorn (1959) and described, in detail, by Reynolds (1997). In this method, the traveltime data from forward and reverse seismic records are used, hence, requiring a fixed receiver spread with a shot at each end. The minus-time is defined as the time recorded at a receiver from shot A on the forward record (T_{AR}), minus the time recorded at the same receiver from shot B on the reverse record (T_{BR}), minus the total shot-to-shot traveltime of the record (T_{AB}). Hence the minus-time (T^-) can be described, as follows:

$$T^- = T_{AR} - T_{BR} - T_{AB} \qquad (4.1)$$

The minus-time is a mathematical formulation, which eliminates any static effects of both surface and refractor topography from the data. A reliable velocity of the refractor can then be calculated as twice the inverse slope of the minus-time vs. distance graph. At some locations, variations from the minus-time analysis were required and details are provided in the appropriate sections.

4.4 Jumpingpound Creek '96 – Wapiabi Formation

Rocks of the Wapiabi Formation are of Cretaceous age (Alberta Group) and are fine-grained, black, marine shales up to 300m thick, with millimeter scale laminations. The first survey site was at Jumpingpound Creek, approximately 30 km west of Calgary (Figure 4.2). At this location, shales of the Wapiabi Formation dip to the east at a constant angle of about 70° and form part of the eastern flank of the triangle zone in this region [Slotboom et al., 1996]. Here, the regional strike direction is 157°. Figure 4.3 is a photograph of an outcrop of Wapiabi shales immediately along strike from the field survey site. A diagram showing the layout of seismic lines occupied during the survey is given in Figure 4.4. Line lengths were dictated essentially by the available aperture at the site, which was located on a flat floodplain, and generally were longer in the dip direction than in the strike direction (Table 4.1). Each line was recorded by a fixed spread of 96 single, 28 Hz geophones.

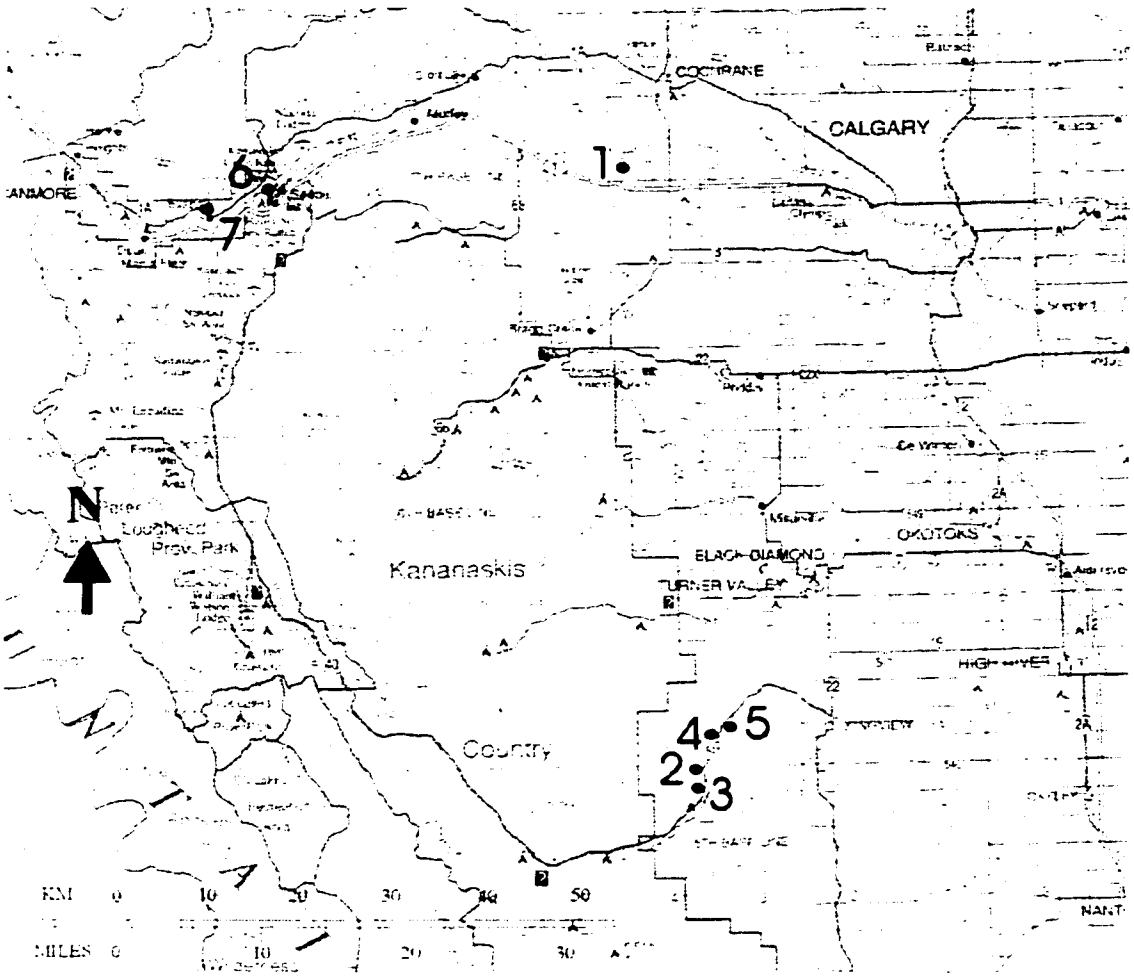

Figure 4.2. Location map of the seven refraction survey experiments, performed in southern Alberta: 1-Jumpingpound Creek '96 (Wapiabi); 2-Longview '97 (Wapiabi); 3-Longview '97 (Brazeau); 4-Longview '98 (Brazeau); 5-Longview '98 (Cardium); 6-Seebe '98 (Wapiabi); 7-Exshaw '98 (Palliser). Base map after Gem Trek Publishing, 1995.

In order to provide data redundancy and allow for detailed static corrections for the surficial weathering layer at the Jumpingpound Creek location, shotpoints were occupied at every second receiver location along the fixed receiver spread for each line. At each shotpoint, the source hammer was skidded 1.5 m perpendicular to the line direction. The program resulted in 49 records being obtained for each line.

Figure 4.3. Photograph of outcropping shales of the Wapiabi Formation at the Jumpingpound Creek location. Note the 60-70° dip of the shales, as indicated by the white horizons in the picture. The refraction survey was performed on the flat floodplain in the foreground.

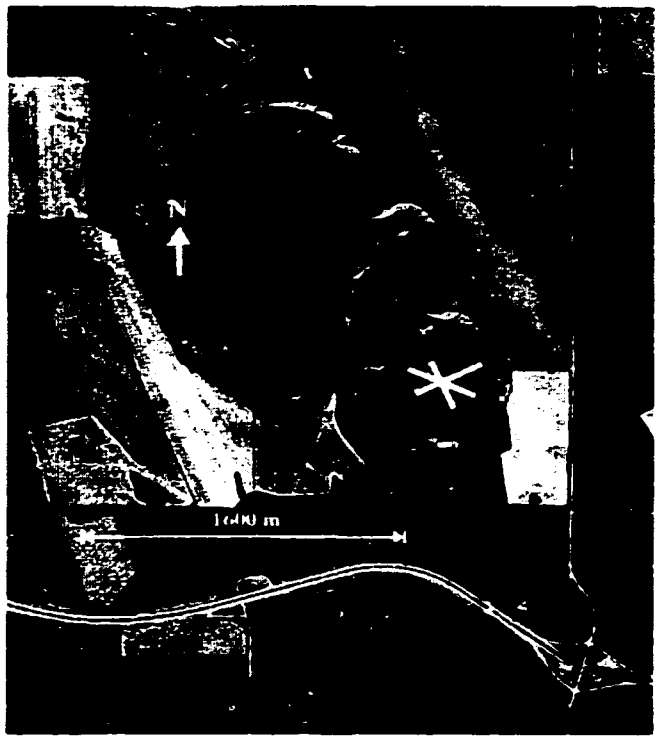

Figure 4.4. Diagram indicating the layout of the refraction seismic survey lines at the Jumpingpound Creek '96, Wapiabi location. Strike line is oriented at 157°.

4.4.1 Refractor Velocity Analysis

Data quality was good with clear first arrivals pickable over the full recording aperture. A plot of the first break picks from the strike line at Jumpingpound Creek is shown in Figure 4.5, with short-wavelength distortions in the curve interpreted to be due to variations in thickness and velocity of the surface layer. This layer is interpreted to be approximately 2 m thick and is composed of reworked glacial sediments and alluvial sands and gravels deposited by Jumpingpound Creek. Traveltimes to the receivers closest to the shot indicate the velocity of this layer at surface is approximately 120 m/s. A minus-time analysis was attempted at this site but the data did not lie on a straight line, indicating turning rays in the shallow depths. In this case, an alternate analysis of the data had to be performed. By applying shot and receiver statics to the data, the low velocity surface layer was effectively reduced from the first break data. Figure 4.6 is a representative first break plot with the static corrections applied. It can be seen from this graph that there were two segments to each record. The segment closest to the shot location is curved, indicating that turning rays needed to be incorporated into the velocity analysis, using a process described by Lawton (1993). By curve-fitting the data and assuming a linear velocity function, $v(z)= v_o+kz$, the velocity gradient, k, was found to be largest in the strike direction with a value of 35 s^{-1}, whereas in the dip direction, the gradient is lower with a value of 20 s^{-1}. The velocity gradient is attributed to weathering of the shales, which extends to a depth of approximately 100 m, as calculated from the raw data plots. At far offsets, the traveltime-distance data became linear with offset, indicating that the base of the weathering layer had been reached. Velocity analysis for anisotropic parameter determination used the data from these longer source-receiver offsets.

4.4.2 Results

As expected, the dip line exhibits a slower velocity than both the strike (fastest) and 45° (intermediate) lines and these velocities are summarized in Table 4.2. The errors in the velocities were determined using the procedure of maximum/minimum slopes. Subsequently, the errors in the anisotropic parameters were determined from the

calculated error in the velocities, using standard error propagation methods for sums and products. The anisotropic parameters for these deeper shales were calculated using the Thomsen (1986) equations from Chapter 1 (equations 1.17 and 1.18) and are summarized in Table 4.2. The bedding-normal and bedding-parallel velocities have been generalized in order to account for the dip of the strata. Note also that the phase and group velocities are equal in both the bedding-normal and bedding-parallel directions. Furthermore, it was determined that the small error in the 45° azimuthal velocity, due to the difference between the phase and group angles, is within the calculated error in δ (Table 4.2).

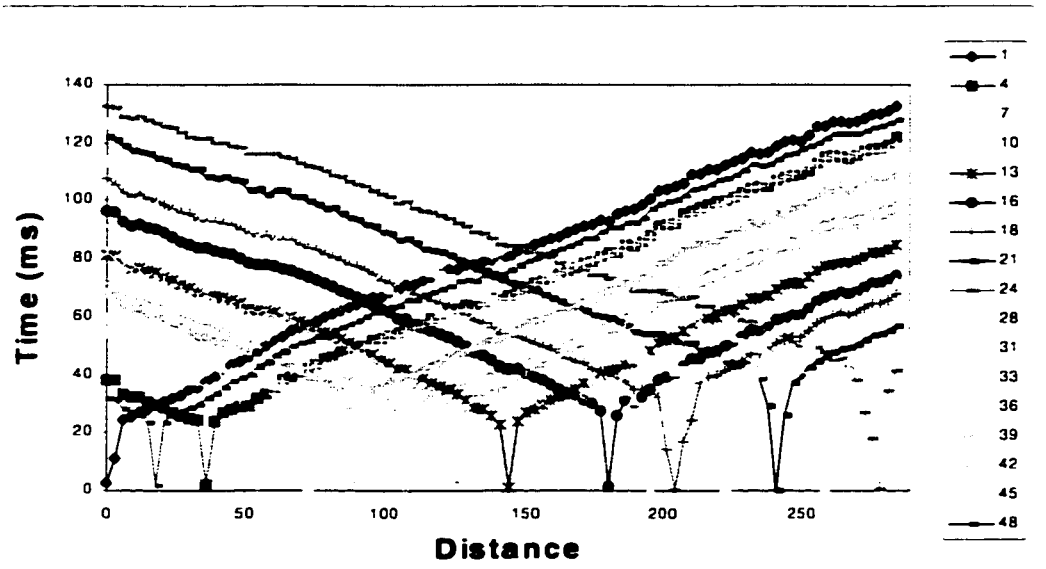

Figure 4.5. Raw first break data for the strike line at Jumpingpound Creek. Only every third record was plotted for clarity.

The calculated velocities for this formation are slightly slower than the sonic velocity values obtained from well logs in the area. This is thought to be a result of weathering of the sediments in this location, perhaps due to the proximity to Jumpingpound Creek. The weathering of these rocks is suspected to cause the curved nature of the minus-time data, implying a near surface velocity gradient, thus requiring a turning ray analysis of the data. Nevertheless, the weathering of the rocks has been consistent in the three velocity directions, thus the calculated anisotropic parameters are expected to be representative of

this formation. The parameter values also lie within the stated limits established by Thomsen (1986).

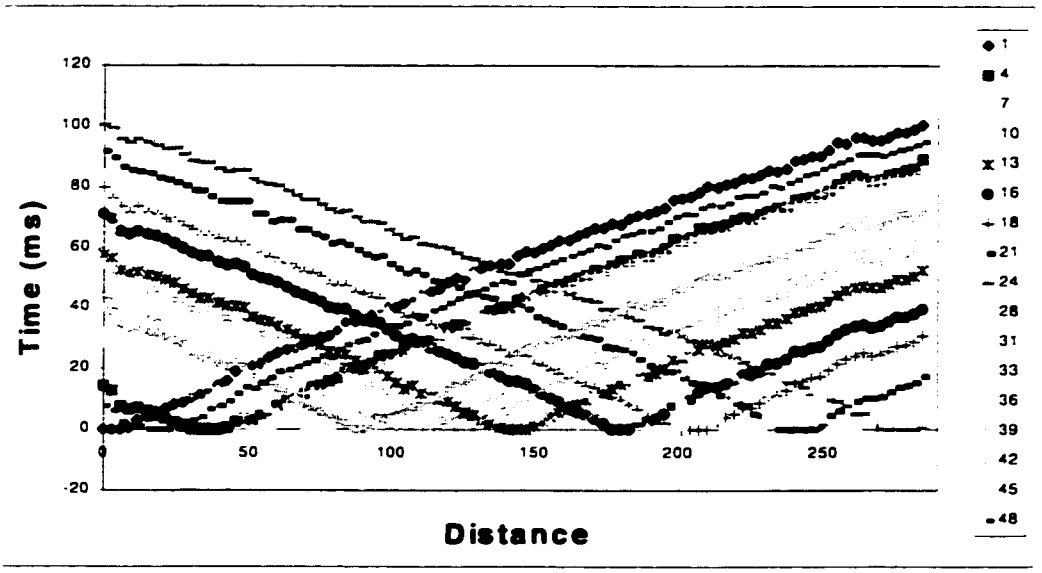

Figure 4.6. First break data for the strike line at Jumpingpound Creek with the source and receiver weathering statics applied. Only every third record was plotted for clarity.

Table 4.2. Summary of velocities calculated from first break data for the shales at the Jumpingpound Creek location.

Location/ Formation	Velocity (±100 m/s)			Anisotropic Parameters	
	Strike	Dip	45°	ε	δ
Jumpingpound Creek '96 /Wapiabi	3200	2800	2900	0.14±0.05	0.00±0.08

4.5 Longview '97 – Wapiabi Formation

The second survey site was located immediately west of highway 541, approximately 20 km west of Longview, Alberta (Figure 4.2). The terrain at this location was variable with one minor creek that cut across the dip line. At this site, the shales of the Wapiabi Formation dip west at a relatively constant angle generally greater than 80°. The regional strike of the shales at this location is 161°. Figure 4.7 is a photograph of the sub-vertical shales of this location, as seen in outcrop in Flat Creek, which is located immediately

adjacent to the survey site. Each line was recorded by a fixed spread of 48 single, 28 Hz geophones with a group interval of 4 m (Table 4.1). Figure 4.8 indicates the seismic line layout for this site. The weathering layer was determined to be considerably thinner (<1m) than at Jumpingpound Creek and 5 records/line were adequate for reliable headwave velocity analysis. At each shotpoint, the source hammer was skidded 2 m perpendicular to the line direction.

Figure 4.7. Photograph of the Wapiabi shale outcrop in Flat Creek, immediately south of the Longview '97 refraction survey site.

4.5.1 Results

At offsets greater than the crossover distance, the first break data plotted on straight lines (Figure 4.9), with some short-wavelength scatter, indicating that there is no vertical velocity gradient in these shales. The approach taken here for velocity analysis was a reciprocal method using 'minus-times' as described by Hagedoorn (1959). Minus-time versus distance graphs for all three lines are given in Figure 4.10. Except for a few noisy data points, the data lay on straight lines indicating that a velocity gradient was not present at this location. The velocities were calculated as twice the inverse slope of each

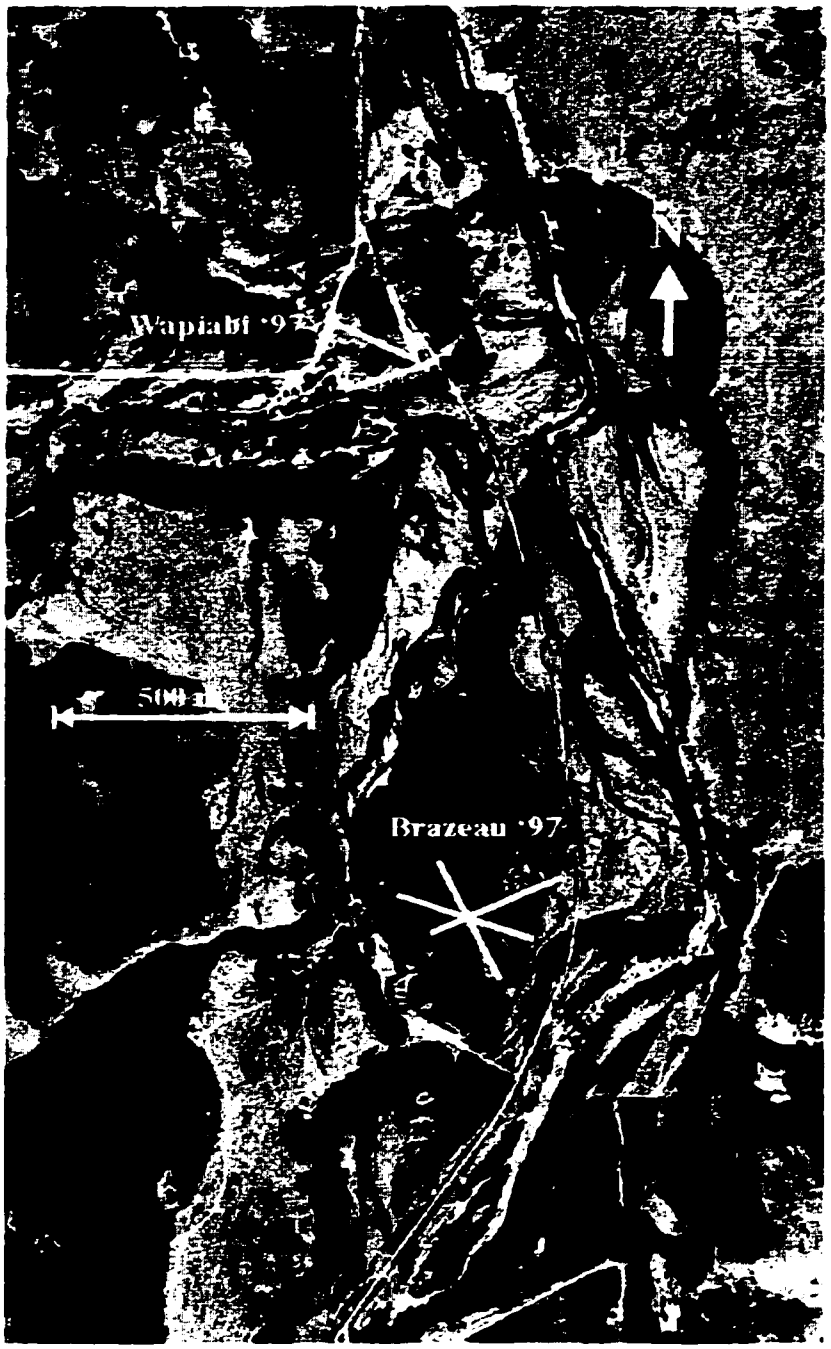

Figure 4.8. Diagram indicating the layout of the Longview '97 refraction seismic surveys.

line and are tabulated in Table 4.3. The anisotropic parameters were calculated using equations 1.17 and 1.18, from Chapter 1, and are also contained in Table 4.3. Again, the errors in the velocities were determined using the procedure of maximum/minimum slopes, as was discussed previously. Subsequently, the errors in the anisotropic parameters were statistically determined from the calculated error in the velocities, again using standard error propagation methods for sums and products. The calculated velocities at this location are close to the values typically recorded on sonic logs through the Wapiabi Formation. Hence, the lack of velocity gradient, combined with the higher velocities and greater degree of anisotropy measured, suggests that the shales at this location are less weathered and possibly less deformed than those shales at the Jumpingpound Creek location. The calculated anisotropic parameters are within the range of values published by Thomsen (1986) and ε is slightly higher than the value at the Jumpingpound Creek location.

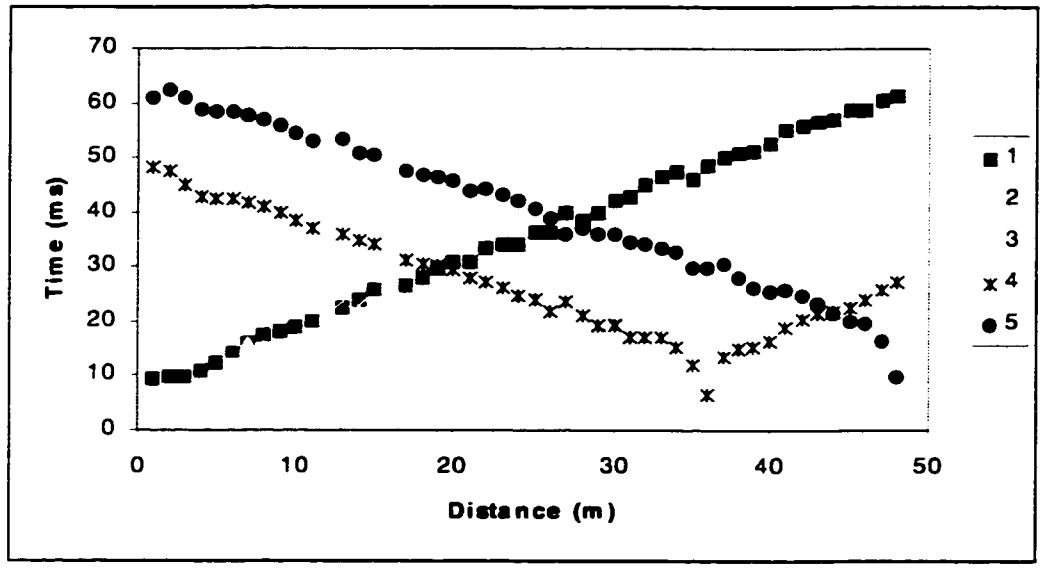

Figure 4.9. Raw first break data of the strike line at the Longview '97, Wapiabi location.

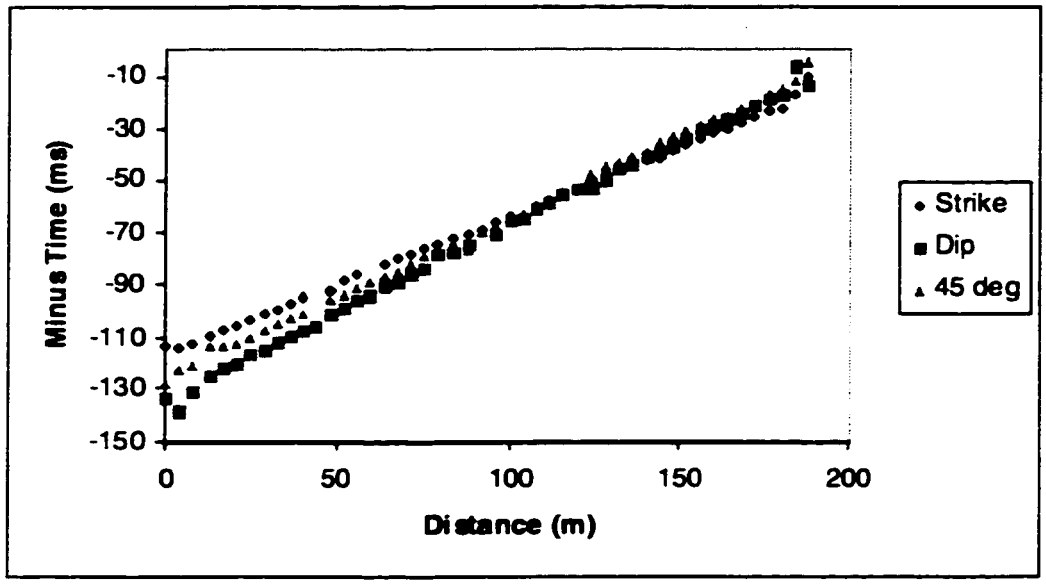

Figure 4.10. Minus-time analysis for the Longview '97, Wapiabi location. Note that the data for each azimuth lie on well-defined straight lines (excluding the endpoints), which have different slopes, allowing for accurate determination of the refractor velocities.

Table 4.3. Summary of velocities calculated from first break data for the shales at the Longview location.

Location/ Formation	Velocity (±100 m/s)			Anisotropic Parameters	
	Strike	Dip	45°	ε	δ
Longview '97 /Wapiabi	3800	3100	3200	0.23±0.05	-0.05±0.07

4.6 Longview '97 – Brazeau Group

The third survey was located west of highway 541, approximately 20 km west of Longview, Alberta (Figure 4.2). The site was an open field, with no significant topography, on the Eadie Ranch, approximately 2 km south of the Flat Creek bridge. In the outcrop along the Highwood River immediately south of this site, rocks of the Belly River Formation dip west at a constant angle of approximately 75°. Figure 4.11 is a photograph of the outcropping Brazeau Group shales and sandstones in the area. The regional strike in this location is 155°. Each line was recorded by a fixed spread of 72

single, 28 Hz geophones with a group interval of 4 m. Figure 4.8 indicates the seismic line layout for this site.

Figure 4.11. Photo of Brazeau Group rocks near the Longview '97 and '98 survey sites, looking southeast.

4.6.1 Results

The first break picks of these data are represented by an example in Figure 4.12. During the minus-time analysis it became apparent that there was a discontinuity in the data (Figure 4.13). The minus-time analysis of the Belly River data reveals a break in the slope of data on both the dip and 45° lines. This has been interpreted as a change in lithology across the refractor, resulting in two different refractor velocities. One possible explanation for this is that the Belly River/Wapiabi contact was not mapped properly on the geologic map of the area. The refraction data show a distinct fast to slow velocity break along the refractor, in the dip direction, 150 m west of where the geologic contact is mapped. This is feasible for wavefronts travelling through the fast Wapiabi Formation to the contact, then through the slower Belly River Formation past the contact. The strike line does not demonstrate a break in slope, indicating that it lies wholly within one

formation. Re-evaluation of the survey confirms that the strike line probably lies within the Belly River Formation but is within 50 m of the contact. The 45° line also shows a break in slope but it is less distinct than on the dip line and is located approximately at the intersection of the strike line. Taking this information into account, the velocities of the Belly River Formation were calculated and the results are tabulated in Table 4.4, although they are considered to be tentative. The percentage anisotropy was calculated to be 18% (equation 1.19) and the anisotropic parameters were calculated to be $\varepsilon = 0.21 \pm 0.05$ and $\delta = 0.50 \pm 0.08$ (equations 1.1.7 and 1.18). The calculated value of δ is considered anomalous, since it is rare to have δ significantly larger than ε [Thomsen, 1986]. It is possible that this experiment was compromised by the change in lithology along the dip line.

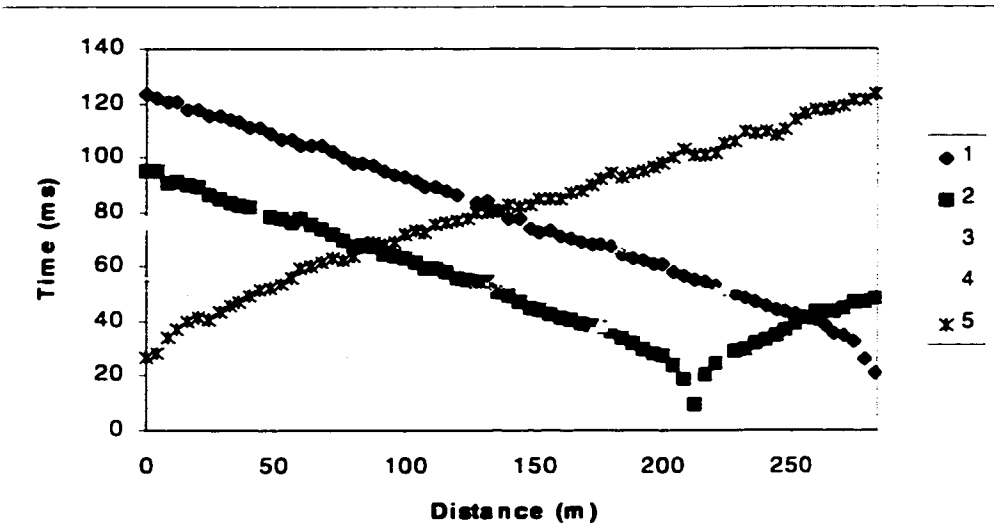

Figure 4.12. Raw first break data of the strike line at the Longview '97, Brazeau Group (Belly River) location.

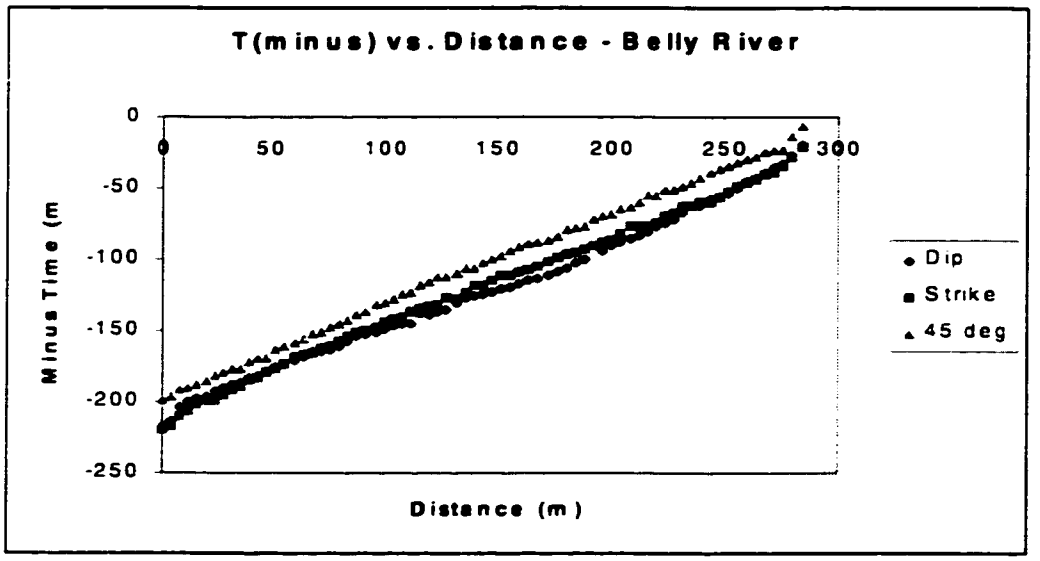

Figure 4.13. Sample minus-time analysis for the Longview '97, Brazeau Group (Belly River) location. Note that the refractor data have a break in slope in the dip line, at approximately 190m, indicating a change in lithology along that line.

Table 4.4. Summary of velocities calculated from first break data for the interbedded shales and sandstones at the Longview location.

Location/ Formation	Velocity (±100 m/s)			Anisotropic Parameters	
	Strike	Dip	45°	ε	δ
Longview '97 /Brazeau Gp.	3200	2600	3100	0.21±0.05	0.50±0.08

4.7 Longview '98 - Brazeau Group

The second Brazeau Group survey was performed immediately west of highway 541, approximately 15 km west of Longview, Alberta (Figure 4.2). The site was an open field on the ranch owned by Mr. Bill Bews, immediately north of the first road south of the Sullivan Creek bridge (Figure 4.14). The field had minor topography and a small, soggy depression in the northwest corner, which affected the last 10 geophones of the strike line. At this location, rocks of the Belly River Formation (Alberta Group) dip west at a constant angle of approximately 70°. The regional strike, at this location, was 160°. The strike and dip lines were recorded by a fixed spread of 60 single, 28 Hz geophones with a group interval of 4 m (Figure 4.14). The 45° velocity was determined by recording four

offline shots into the fixed spread of the dip line (Figure 4.15). Survey parameters for each line are summarized in Table 4.1.

Figure 4.14. Diagram indicating the layout of the Longview '98 refraction seismic surveys. The survey areas are highlighted with rectangles.

4.7.1 Refractor Velocity Analysis

A plot of the raw first break data, for the strike line, are shown in Figure (4.16). The data from both the strike and dip lines were analyzed using a minus-time analysis. The minus-time plots for each line are given in Figure 4.17, from which the strike and dip velocities were computed (Table 4.5). Since a 45° line was not laid out due to physical access limitations, the 45° velocity had to be calculated using a combination of plus and delay times, from the strike and dip lines. As defined by Hagedoorn (1959) the plus time (T^+) is defined as,

$$T^+ = T_{AR} + T_{BR} - T_{AB} \qquad (4.2)$$

where: T_{AR} is the time to a particular receiver on the forward record, from shot A.

T_{BR} is the time to the same receiver on the reverse record, from shot B, and

T_{AB} is the total travel time from shot A to shot B.

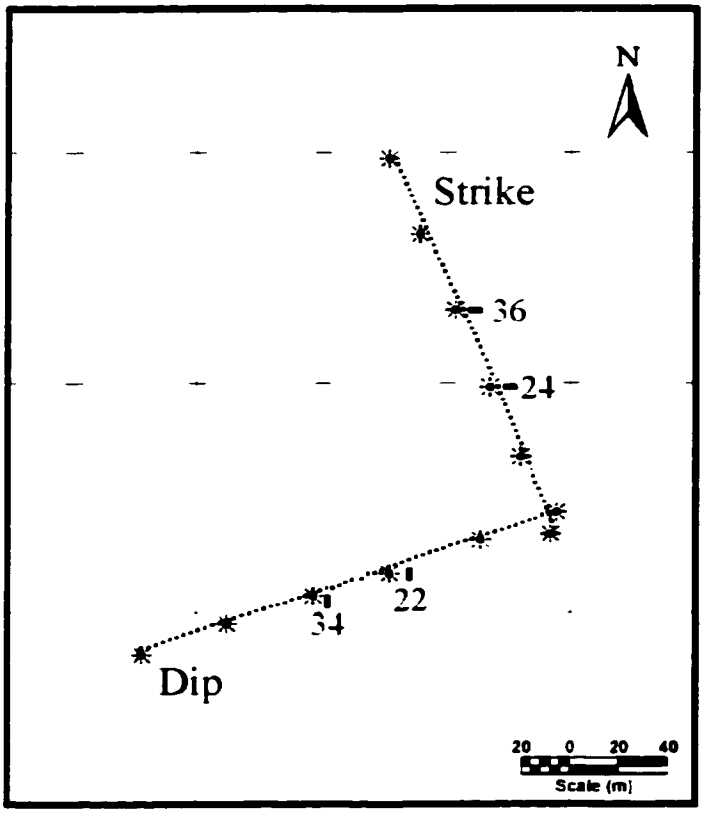

Figure 4.15. Basemap indicating shot and receiver locations for the second Longview '98, Brazeau Group survey.

The delay time of a receiver (δ_r) is defined as,

$$\delta_r = {}^{T_r}\!/_{2} \tag{4.3}$$

For example, consider a shot 60 m from the receiver line (i.e. at receiver 24 on the strike line) and receiver 22 in the dip line (Figure 4.15). The delay time of the shot (δ_s) at 60 m

can then be estimated by the plus-time at the corresponding receiver on the strike line (receiver 24),

$$\delta_{s_{60}} = \frac{1}{2} T_{60}^{+} \tag{4.4}$$

where: T_{60}^{+} is the plus-time at the corresponding receiver located 60 m from the dip line (i.e. receiver 24 on the strike line).

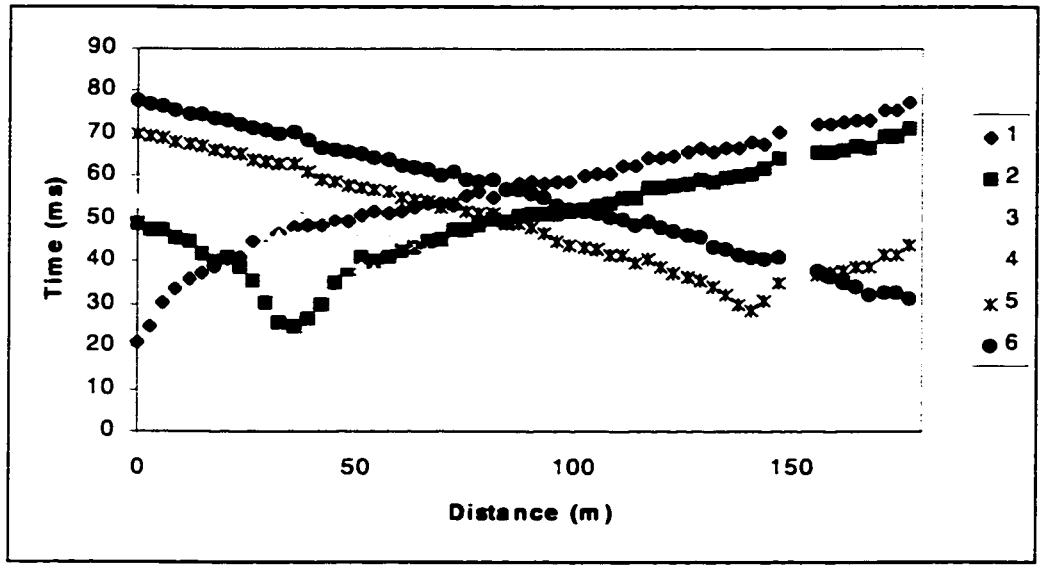

Figure 4.16. Raw shot record from strike line at the Longview '98 survey.

The 45° velocity can then be calculated from,

$$v_{45} = \frac{X_{60-r22}}{\left(T_{r22} - \delta_{s_{60}} - \delta_{r22}\right)} \tag{4.5}$$

where: T_{r22} is the time from the shot at 60 m to receiver 22, and

X_{60-r22} is the distance between the shot at 60 m and receiver 22.

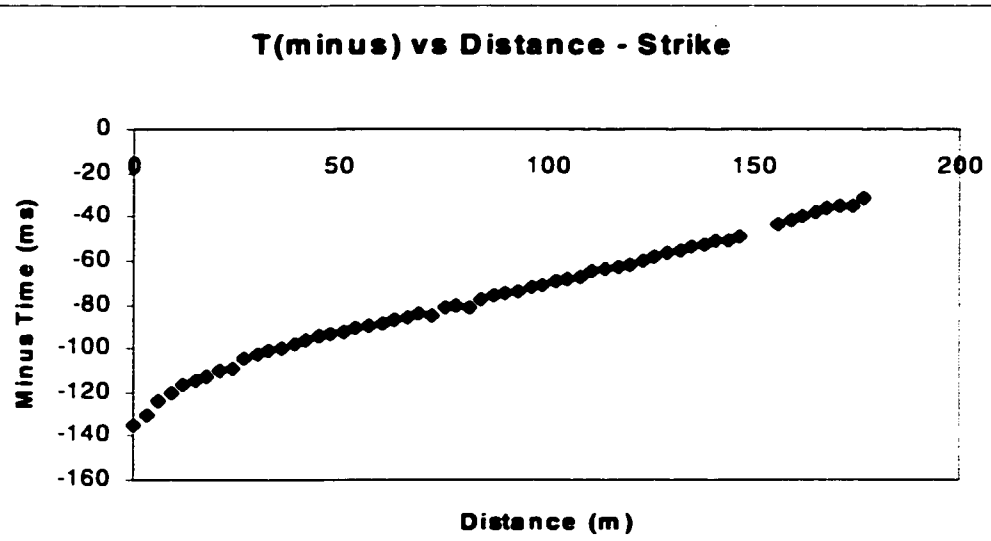

Figure 4.17a. Minus-time results from the strike line at the Longview '98, Brazeau Group location.

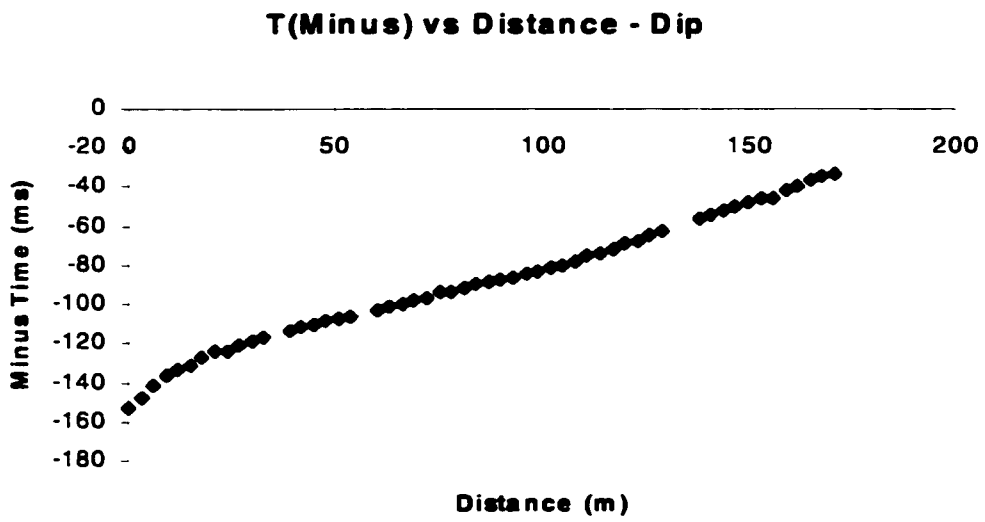

Figure 4.17b. Minus-time results from the dip line at the Longview '98, Brazeau Group location.

The above calculations can be repeated for shot 96m 'north' to receiver 36 to obtain an additional estimate of v_{45}, at this location. The location 132 m 'north' to receiver 48 was

not adequate to provide an accurate estimate of v_{45}, due to the soggy depression in the northwest corner of the field. The average 45° velocity was then calculated between the shot at receiver 24 (strike line) and receiver 22 (dip line) as well as the shot at receiver 36 (strike line) and receiver 34 (dip line). The geometry is displayed in Figure 4.15.

4.7.2 Results

The minus-time analysis was robust for these data (Figure 4.17). Except for a few noisy receivers, all data lay on well-defined line segments. There is a definite break in slope in the minus-time data from the dip line, indicating a transition from a fast velocity medium to a slower velocity medium. This change is interpreted to be the contact between the Brazeau Group and Alberta Group rocks. The azimuthal velocities of the Belly River Formation were calculated and tabulated in Table 4.5. There is a minor surface weathering layer present on the east side of the field. The velocity anisotropy was calculated to be 10% (equation 1.19) and the anisotropic parameters were determined to be $\varepsilon = 0.11$ and $\delta = 0.42$ (equations 1.17 and 1.18). Again these values indicate a large value of δ for this formation, which substantiates the values calculated from the Brazeau '97 survey. These values indicate that the anisotropic wavefronts through the Brazeau Group are very different from those through the Wapiabi Formation. As different as these parameters may be, they are still within the Thomsen (1986) values.

Table 4.5. Summary of velocities calculated from first break data for the Longview - Brazeau Group location.

Location/ Formation	Velocity (±100 m/s)			Anisotropic Parameters	
	Strike	Dip	45°	ε	δ
Longview '98 /Brazeau Gp.	4200	3800	4300	0.11±0.04	0.42±0.06

4.8 Longview '98 - Cardium Formation

This survey was performed immediately east of highway 541, approximately 15 km west of Longview, Alberta (Figure 4.2). The site was an open field on the ranch owned by Mr. Joe Bews, immediately south of the Sullivan Creek bridge (Figure 4.14). No significant

topography was present. At this location, rocks of the Cardium formation (Alberta Group) have near-vertical dips, as indicated by the photograph in Figure 4.18. The regional strike was measured to be 170°. Each line was recorded by a fixed spread of 60 single, 28 Hz geophones with a geophone interval of 4 m (Figure 4.14). Survey parameters for each line are summarized in Table 4.1.

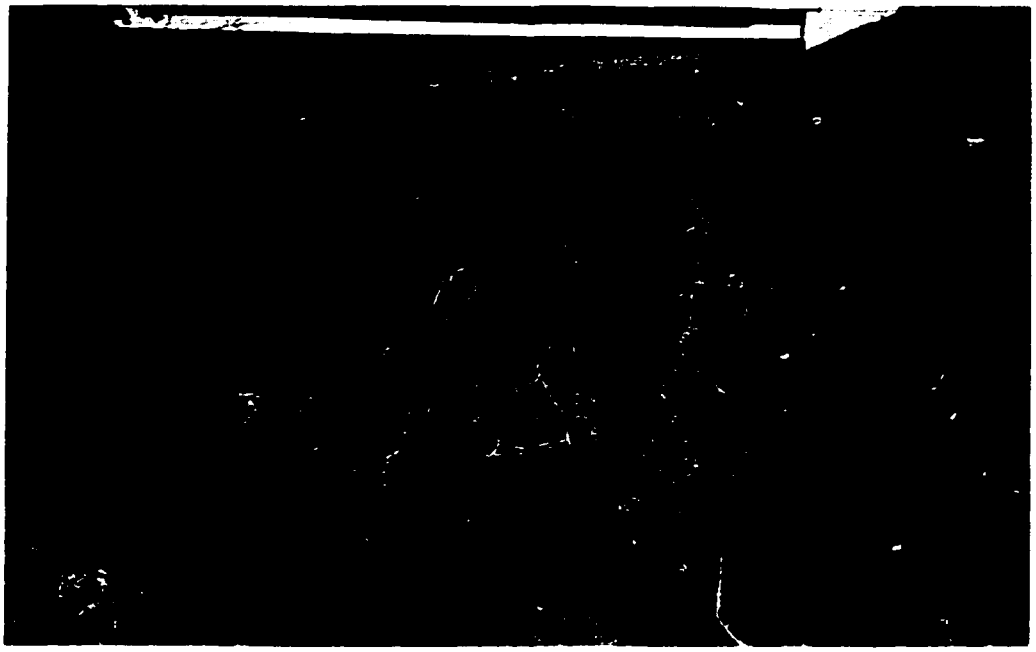

Figure 4.18. Photo of Cardium outcrop at the Sullivan Creek Bridge, Longview, Alberta, looking northwest.

4.8.1 Results

Figure 4.19 represents the raw data for the strike line in this location. The minus-time plots for each line are given in Figures 4.20a,b,c. These data indicate a few noisy receivers and a thick weathering layer in the west side of the field. The velocities were calculated, excluding the weathering layer, and tabulated in Table 4.6. As all three velocities are quite similar, within the error limits, these rocks are interpreted to not exhibit any significant velocity anisotropy.

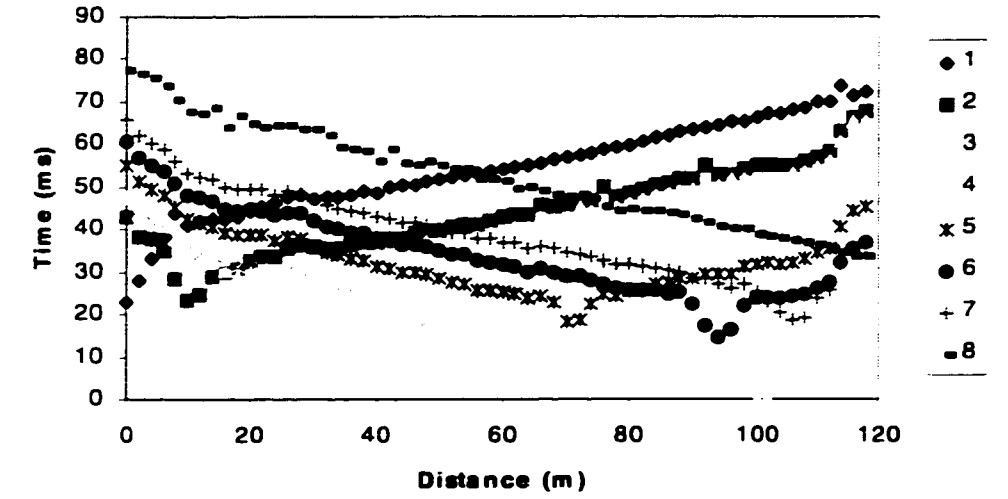

Figure 4.19. Raw shot record for strike line at the Longview '98, Cardium location.

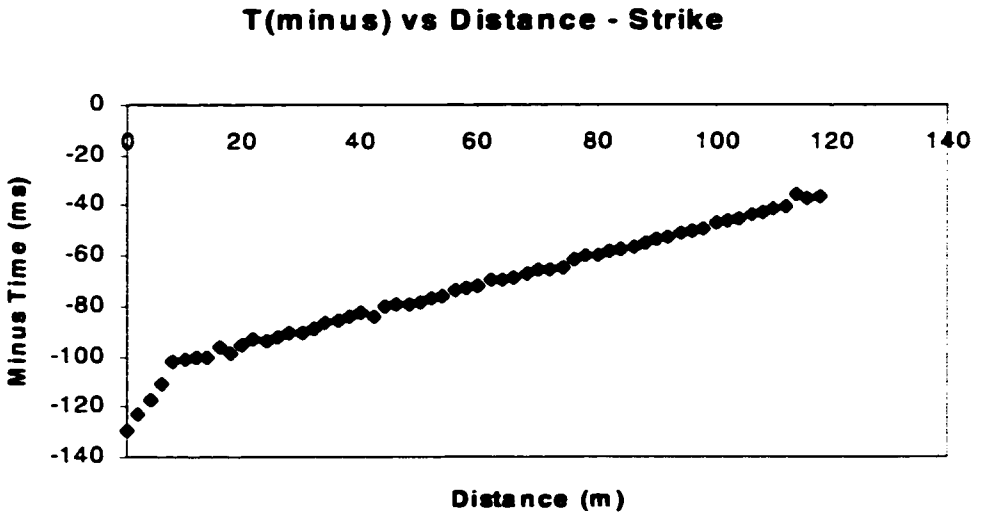

Figure 4.20a. Minus-time results from the strike line at the Cardium location.

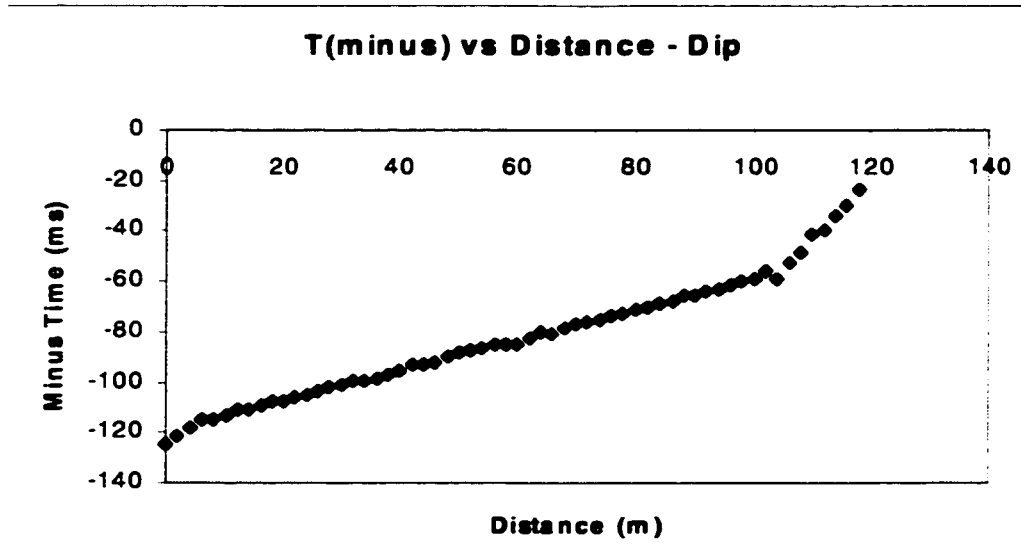

Figure 4.20b. Minus-time results from the dip line at the Cardium location.

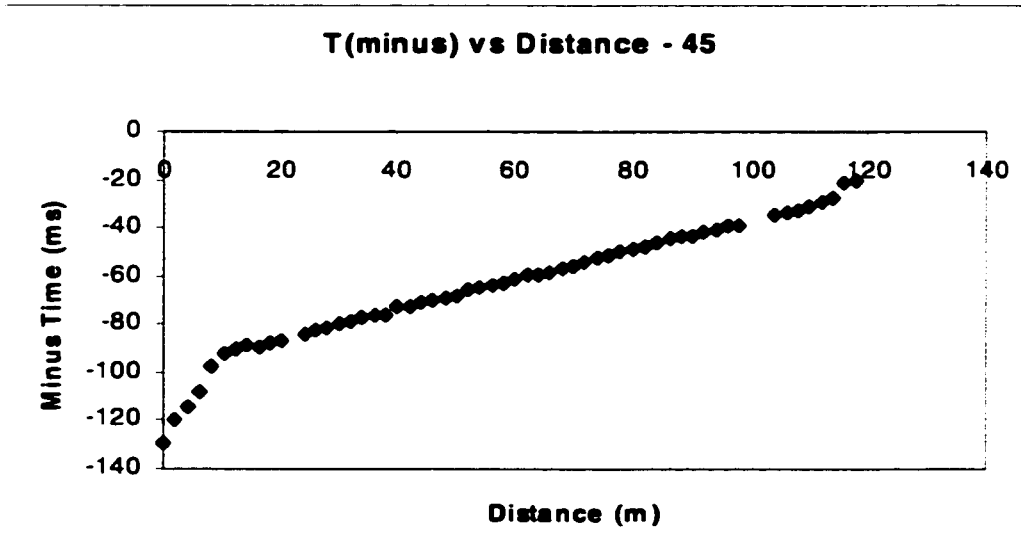

Figure 4.20c. Minus-time results from the 45° azimuth line at the Cardium location.

Table 4.6. Summary of velocities calculated from first break data for the Longview - Cardium Formation location.

Location/ Formation	Velocity (±100 m/s)			Anisotropic Parameters	
	Strike	Dip	45°	ε	δ
Longview '98 /Cardium	3300	3300	3200	0	0

4.9 Seebe '98 - Wapiabi Formation

This survey was performed at the Lafarge Shale Quarry just outside of Seebe, Alberta, approximately 80 km west of Calgary (Figure 4.2). The refraction survey was performed on the floor of the shale quarry, where shales of the Wapiabi Formation (Alberta Group) dip west at a constant angle of approximately 17° (Figure 4.21). The regional strike in this location is 166°. Three lines of data were acquired, in the strike, dip and 45° directions (Figure 4.22). Each line was recorded by a fixed spread of 20, three-component geophones, with a group interval of 5 m. The geophones were also buried, in order to increase coupling and decrease wind noise. Survey parameters for each line are summarized in Table 4.1.

Figure 4.21. Photo of the outcrop in the shale quarry at Seebe, Alberta, looking north.

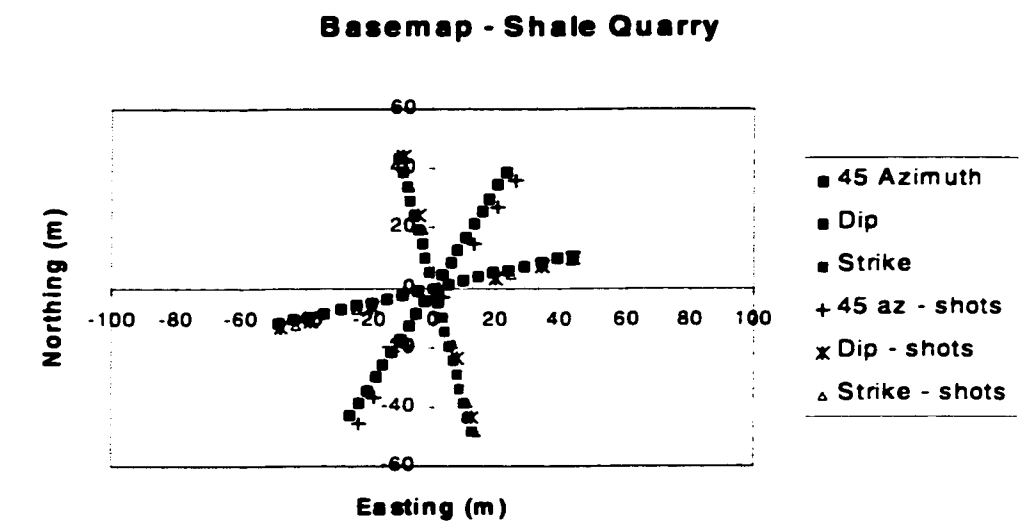

Figure 4.22. Basemap indicating shot and receiver locations for the Seebe '98, Wapiabi shale survey.

4.9.1 Results

The raw data for the strike line are depicted in Figure 4.23. The minus-time plots for each line are given in Figures 4.24a,b,c. Robust velocities were obtained at this site, using this method. Except for a few noisy receivers, the data lay on a straight line and the computed velocities are tabulated in Table 4.7. There is virtually no surface weathering layer present since the survey was undertaken on the recently excavated quarry floor. The velocity anisotropy was calculated to be 19% (equation 1.19). It should be noted that since the dips in this location are rather shallow, an accurate measurement of the slow velocity (i.e. bedding-perpendicular velocity) of the shales is not possible, thus the VTI anisotropic parameters for these shales cannot be calculated. However, since a definite velocity variation with azimuth is measured, at this location, there may be an additional azimuthal anisotropy influence due to an external variable, such as fracturing. Groundwater studies by Lafarge personnel indicate open fractures parallel to strike in the quarry [Lafarge, 1998]. Therefore a combination of both intrinsic and extrinsic anisotropy was being measured. In this case, the calculated anisotropic parameters would not be truly representative of either the intrinsic or extrinsic values of the anisotropy, only

a combination of both influences. Since the two factors cannot be separated, these results cannot be compared with the other Wapiabi Formation results obtained in other surveys.

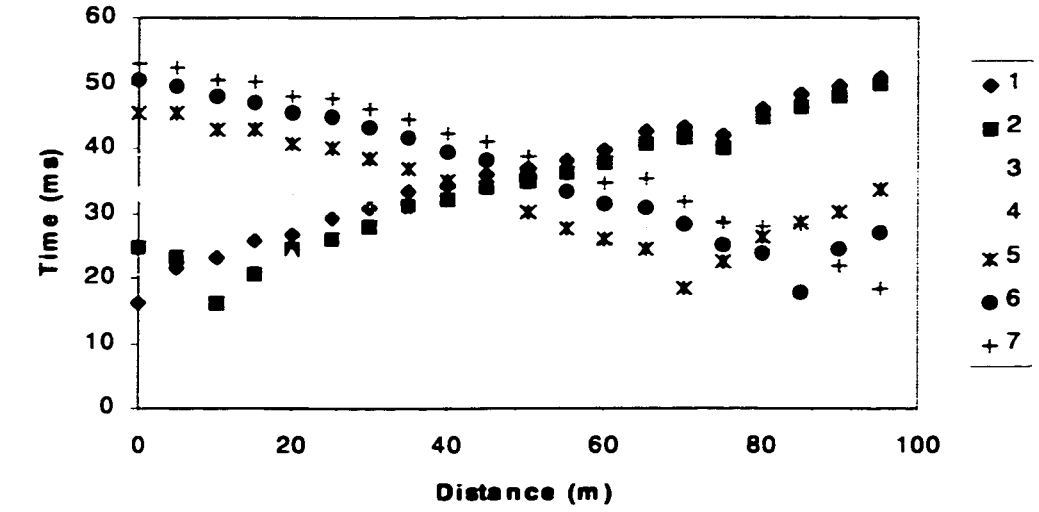

Figure 4.23. Raw shot record from strike line of Seebe '98 survey.

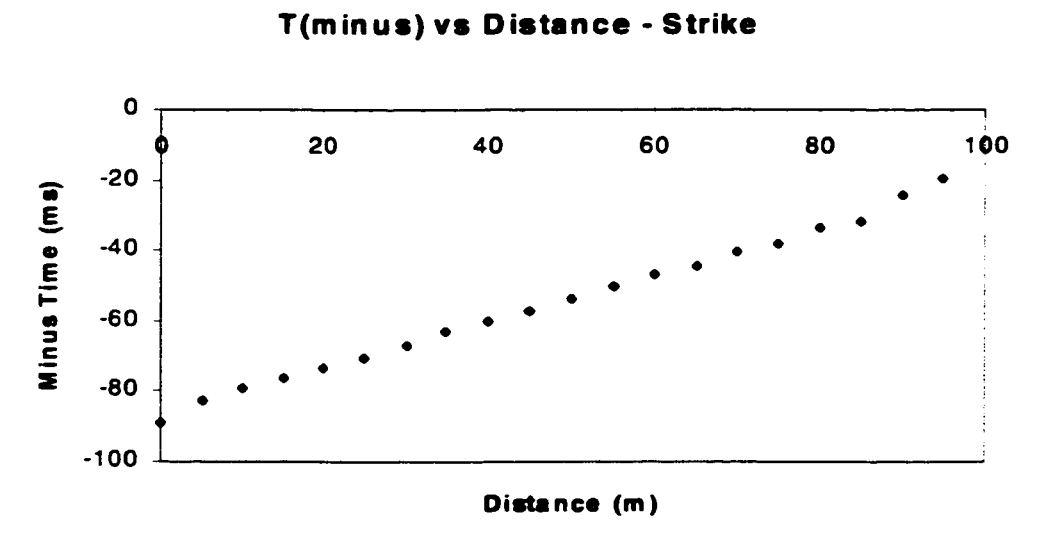

Figure 4.24a. Minus-time results from the strike line at the Seebe '98, Wapiabi shale location.

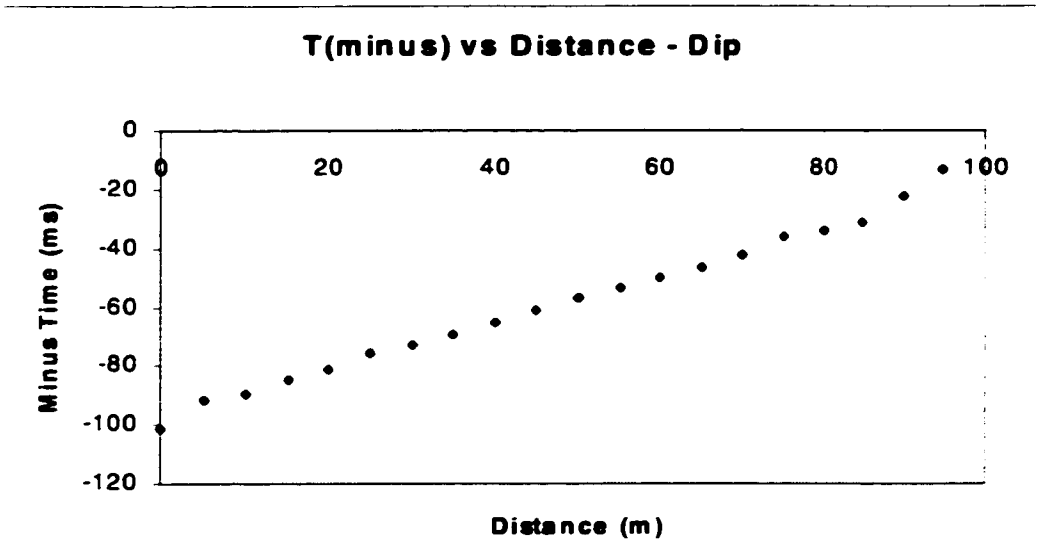

Figure 4.24b. Minus-time results from the dip line at the Seebe '98, Wapiabi shale location.

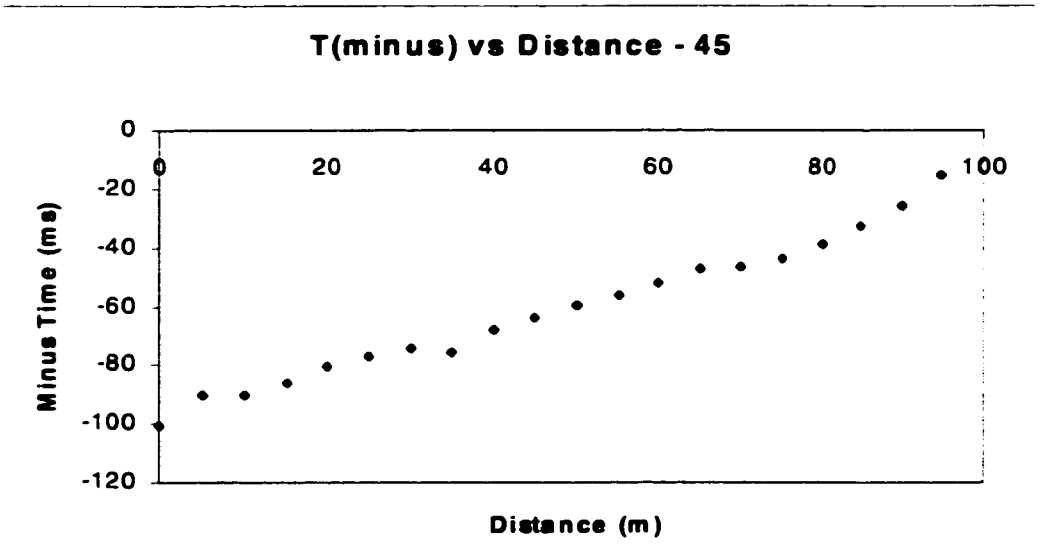

Figure 4.24c. Minus-time results from the 45° azimuth line at the Seebe '98, Wapiabi shale location.

Table 4.7. Summary of velocities calculated from first break data for the Seebe - Wapiabi Formation location.

Location/ Formation	Velocity (±100 m/s)		
	Strike	Dip	45°
Seebe '98 /Wapiabi	3100	2600	2700

A second experiment was undertaken at this location, attempting to estimate the slow velocity of the shales. A hydrophone cable was lowered into two shallow wells, to a maximum of 60 m, in a VSP experiment. The first well was located along the north edge of the shale quarry and the other along the south edge. Data from several offset shots were acquired by the hydrophones but the results were inconclusive, as it was very difficult to determine first arrival traveltimes. Coupling of the hydrophones in the water-filled well appeared to be a problem.

4.10 Exshaw '98 - Palliser Formation

This survey was performed at the Lafarge Limestone Quarry at Exshaw, Alberta, approximately 90 km west of Calgary (Figure 4.2). At this location, limestones of the Palliser Formation (Devonian) dip west at angles generally between 50-55°, with a regional strike of 150° (Figure 4.25). Being that the limestone is resistant and the floor of the quarry is without a surficial layer of loose material, this survey was designed slightly differently than the others. A line of 20, three-component geophones was laid out in the dip direction with a geophone interval of 5 m. The geophones were cemented to the floor of the quarry using lime mud, and were also covered with earth to increase coupling with the limestone and to decrease wind noise. Three-component geophones were used to enable reliable picking of the first breaks. In the absence of a surficial weathering layer, the first arriving P-wave energy was often recorded with greater amplitude on the horizontal components than on the vertical component of the geophone. Data were then recorded into the fixed spread of geophones, with both inline and offline shots, as shown in Figure 4.26. Only one receiver line was established due to the difficulty of coupling the geophones to the cement floor of the quarry.

Figure 4.25. Photo of the Palliser limestone outcrop at the Exshaw quarry, looking north.

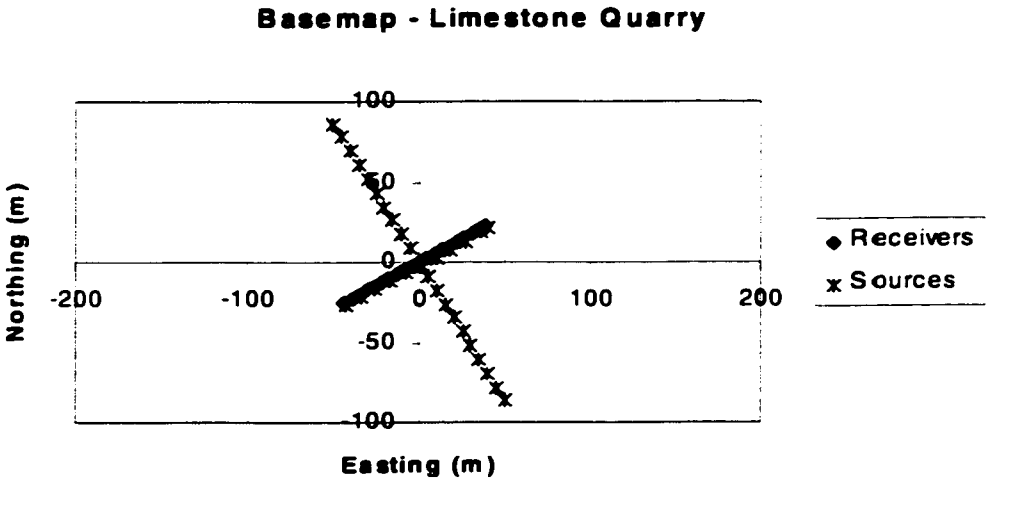

Figure 4.26. Basemap indicating the shot and receiver locations of the Exshaw '98, Palliser Formation survey.

4.10.1 Refractor Velocity Analysis

Raw data from the dip line are shown in Figure 4.27. The minus-time analysis record for the dip line is given in Figure 4.28, and yielded a velocity of 3000±100 m/s. Since the receiver line was not moved from the dip direction, further analysis of the data was necessary to extract the strike and 45° velocities. For the strike velocity, a common receiver gather was assembled, for receiver 11, since the offline shots were located directly crossline with this receiver (Figure 4.26). From this gather, a weighted average strike velocity was directly determined, using inverse slopes, from the first break data from shots both north and south of the dip line (Figure 4.29).

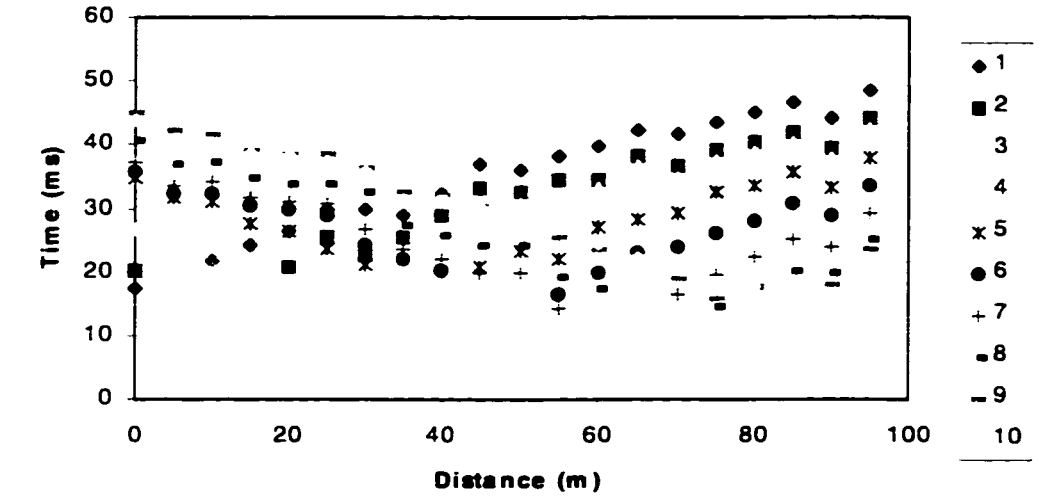

Figure 4.27. Raw shot record for the dip line at the Exshaw '98 survey.

For the 45° azimuth velocity, a combination of plus and delay times was again used (equations 4.2 and 4.3). For example, consider a shot 30 m north of the receiver line and receiver 11 in the strike line, which is 30 m from the shot line, in this location (Figure 4.26). The delay time of the shot (δ_s), at 30 m north, is defined as,

$$\delta_{s_{30N}} = T_{30N} - \delta_{r11} - X_{30N}/v_N \qquad (4.6)$$

where: T_{30N} is the time from the shot at 30 m north to receiver 11.

δ_{r11} is the delay time computed at receiver 11.

X_{30N} is the distance between the shot at 30 m north and receiver 11, and

v_N is the velocity calculated from the CRG, north of the receiver line.

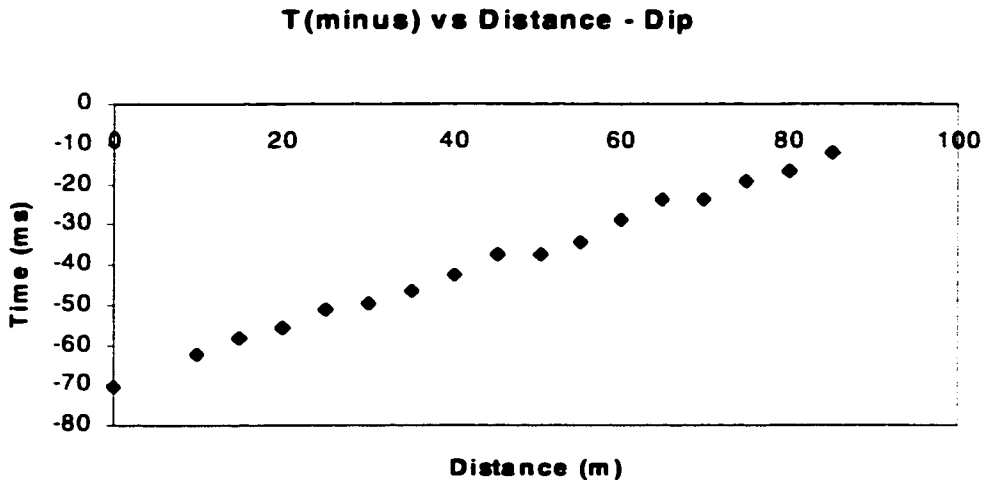

Figure 4.28. Minus-time results from the dip line at the Palliser Formation location.

The 45° velocity can then be calculated from,

$$v_{45} = \frac{X_{30N-r17}}{\left(T_{r17} - \delta_{s_{30N}} - \delta_{r17}\right)} \tag{4.7}$$

where: T_{r17} is the time from the shot at 30 m north to receiver 17.

$X_{30N-r17}$ is the distance between the shot at 30 m north and receiver 17.

The above calculations were also repeated for shot 40N/receiver 3, shot 30S/receiver 17 and shot 40S/receiver 3 to obtain an average estimate of v_{45}, at this location.

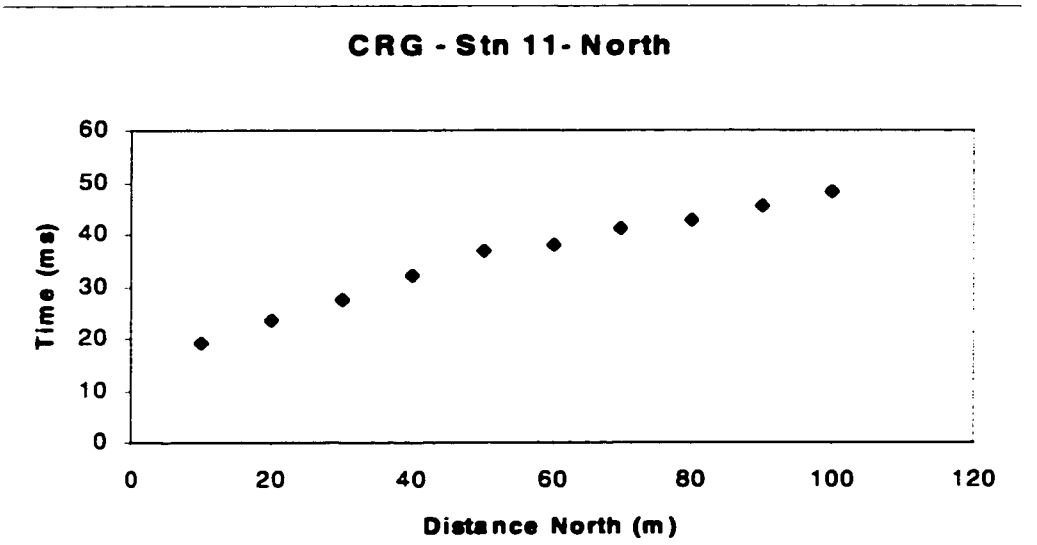

Figure 4.29a. First break traveltimes from a common receiver gather of the shots located north of the receiver line at the Palliser Formation location.

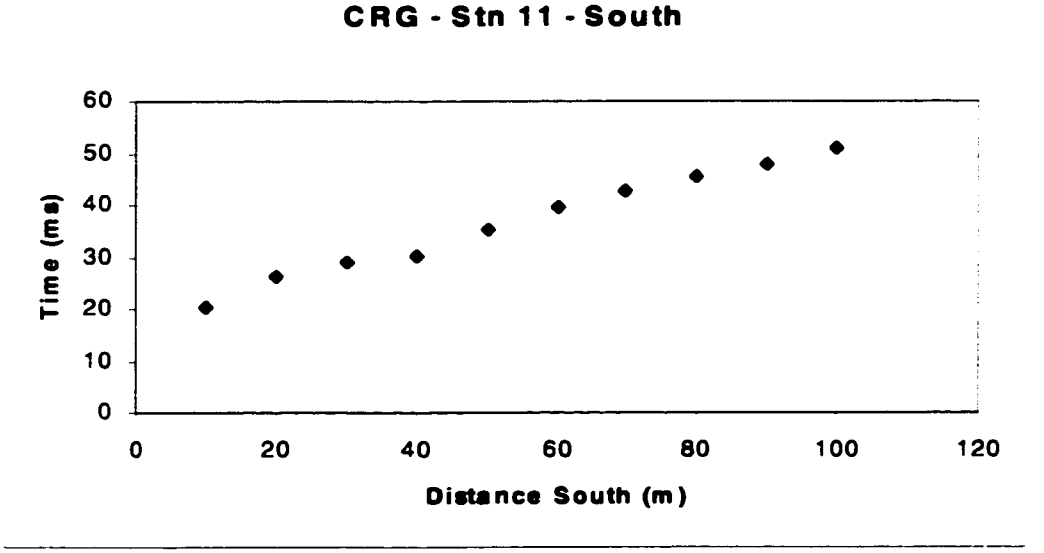

Figure 4.29b. First break traveltimes of a common receiver gather of the shots located south of the receiver line at the Palliser Formation location.

4.10.2 Results

The minus-time analysis worked well for the dip line data (Figure 4.28), as the data lay on a straight line. The dip line velocity was easily calculated and tabulated in Table 4.8. The strike and 45° line velocities were calculated, as above, and are also tabulated in Table 4.8. These velocities show that the same velocity (3000±100 m/s) was calculated along all three directions. There is virtually no surface weathering layer present. As all three velocities are the same, within the error limits, these rocks do not exhibit any velocity anisotropy. The velocities calculated for this limestone are lower than one would expect. These limestones are at surface, thus are not under any overburden or pore pressure, and the low velocities are attributed to extensive fracturing, either natural or induced during quarry blasts. In the quarry outcrops, there appeared to be no consistent fracture direction.

Table 4.8. Summary of velocities calculated from first break data for the Exshaw - Palliser Formation location.

Location/ Formation	**Velocity (±100 m/s)**			**Anisotropic Parameters**	
	Strike	Dip	45°	ε	δ
Exshaw '98 /Palliser	3000	3000	3000	0	0

4.11 Discussion

The results of these surveys indicate conclusively that refraction seismic methods can be used to successfully measure velocity anisotropy, *in situ*, at locations where uniform panels of steeply dipping strata outcrop. The data show that there was a significant surface weathering layer in the Jumpingpound Creek survey location and that turning rays were also present. The other surveys did not show any of these effects. The Longview Wapiabi site shows generally higher velocities and a greater degree of anisotropy, thus a larger ε value, than that found in the Jumpingpound Creek Wapiabi survey. The difference is attributed to a change in the composition of the shales and a greater degree of penetrative strain at the Jumpingpound Creek location, compared with the Longview

location. The δ values calculated from the two surveys are comparable within the calculated errors for the parameters (0.00±0.08 and -0.05±0.07).

The data from the first Longview Brazeau Group site indicate that the Belly River/Wapiabi contact was not located where it is predicted from geologic maps, thereby rendering the results from this particular survey somewhat inconclusive. However, the indication was that the Belly River Formation is anisotropic, similar to the Wapiabi Formation, and that further study of this formation is necessary to properly quantify its anisotropic parameters. The results of the second Brazeau Group survey indicate that these rocks are also anisotropic, which was implied in the first survey. These two surveys both indicate that a δ value higher than ε best describes the wave propagation through this formation. Again the δ values calculated from the two sites are comparable within the errors associated with the parameters (0.50±0.08 and 0.42±0.06). On the other hand, the calculated ε from the Longview '98 Brazeau Group survey (0.21±0.05) was significantly less than the Longview '97 survey (0.11±0.04). The second survey is considered to be more accurate than the first, since the first acquisition survey crossed the Wapiabi/Brazeau Group boundary. Thus the velocities obtained are considered to be more reliable, in the second survey, as are the calculated anisotropic parameters.

This study shows that rocks of the Palliser and the Cardium Formations do not exhibit significant velocity anisotropy. In both surveys, the same velocity was measured along all three azimuths, within the error of the experiment, indicating that the rocks are isotropic. The results from the Wapiabi Formation, shale quarry at Seebe indicate a strong presence of anisotropy; however, without a reliable measurement of the slow velocity, one cannot calculate the exact intrinsic anisotropic parameters. The 20% anisotropy present in these shallow dipping Wapiabi shales, is attributed more to an azimuthal anisotropy arising from aligned fractures in the shales, than to the intrinsic layer induced anisotropy of the shales themselves. Since the fracture orientation was not taken into account when the survey was designed, an accurate measure of the extrinsic anisotropy cannot be

ascertained either. Hence these values cannot be directly compared with the results from the previous Wapiabi Formation surveys at Jumpingpound Creek and Longview.

The anisotropic parameters, particularly δ for the Brazeau Group rocks, appear to be very different from those of the Wapiabi Formation, thus, the P-wave propagation through each formation is quite different, indicating a need to characterize each formation separately. One potential problem arises from the interbedded nature of the Brazeau Group rocks, hindering an accurate assessment of the strike velocity. Due to the layering of the formation, a refraction line in the strike direction could lay entirely in a sandstone or shale layer, not to mention, along a shale/sandstone interface. As such, a representative velocity cannot be obtained without averaging over several values, which was not done in the two refraction experiments on this formation. In addition, the effects of the interbedded nature are more difficult to ascertain in the 45° azimuth velocity as the propagating energy probably travels longer and farther in the faster material (i.e. sandstones), than in the slower (i.e. shales); thereby, skewing the 45° velocity closer to the fast, or strike, velocity of the formation. This is a potential reason for the high δ values calculated in these refraction studies. Nonetheless, the calculated anisotropic parameters for the rocks of the Brazeau Group and the Wapiabi Formation also lie within the range of values for shales as presented by Thomsen (1986) and Vernik and Liu (1997).

CHAPTER 5 VSP EXPERIMENT

5.1 Introduction

Refraction methods were used successfully to measure the anisotropic parameters of rocks in various locations southern Alberta as well as for different rock types (Chapter 4). By laying out seismic lines parallel, perpendicular and at 45° to the local strike directions, the Thomsen (1986) anisotropic parameters, ε and δ were determined from the bedding-parallel, bedding-perpendicular and intermediate (45° azimuth) velocities (Chapter 4).

Vertical Seismic Profiling (VSP) became a popular seismic technique in the early 1980's since it provides a direct relationship between surface seismic data and well information. This relationship helps to remove the ambiguities in interpretations and non-uniqueness in the inverse process. VSP's also give complementary information, such as interval velocity and zero-phase reflectivity [Stewart and Disiena, 1989]. Zero-offset VSP's, or check shot surveys, are used to find the relationship between interval velocity and depth through analysis of the first break data. Multi-offset VSP's use several stationary land shot locations for imaging purposes, using reflected wave information [Gilpatrick and Fouquet, 1989]. Multi-offset surveys are capable of looking ahead of the drill bit, imaging around the borehole, estimating the physical parameters of the rocks, identifying both primary and P-S converted waves, estimating the time-to-depth curve as well as imaging target areas [Cassell, 1984; Slawinski and Parkin, 1996]. This thesis develops a new application of the VSP method by combining zero-offset and multi-offset surveys in an area where the well intersects a uniformly dipping panel of strata. The purpose is to obtain the Thomsen (1986) anisotropic parameters of these rocks at depth.

VSP technology has been considered previously for the determination of velocity anisotropy in rocks; however, these methods are limited to dips less than 5° [Kebaili and Schmitt, 1996; Sayers, 1997; MacBeth, 1998]. Therefore, with this limitation, these applications are not suitable in moderate to steep dip environments, such as in the foothills of the Rocky Mountain Fold and Thrust Belt.

5.2 Design of Experiment

To calculate the anisotropic parameters, ε and δ, in the presence of moderate to steep dips, accurate determinations of the bedding-normal, bedding-perpendicular and 45° velocities were required. Using multi-offset VSP technology, these velocities can be determined from the first arrival information through a moderately dipping (30-60°), uniformly dipping panel of rocks and a multi-offset source configuration, as shown schematically in Figure 5.1. In developing the procedure for this method, the choice of a suitable well had to be made carefully, as there are several factors that had to be considered. The well must penetrate a sufficiently thick, relatively uniform panel of moderately dipping strata (ideally 45°) and it should have no deviation through the rock panel, although minimal deviation in the dip direction is acceptable. To accommodate the need for multiple shot locations, it was required that there be appropriate access, in both the updip and downdip directions from the well, in order to obtain bedding-normal and bedding-parallel velocities to the depths of interest (Figure 5.1). Maximum offset distances of shotpoints from the well should be approximately equal to the well depth.

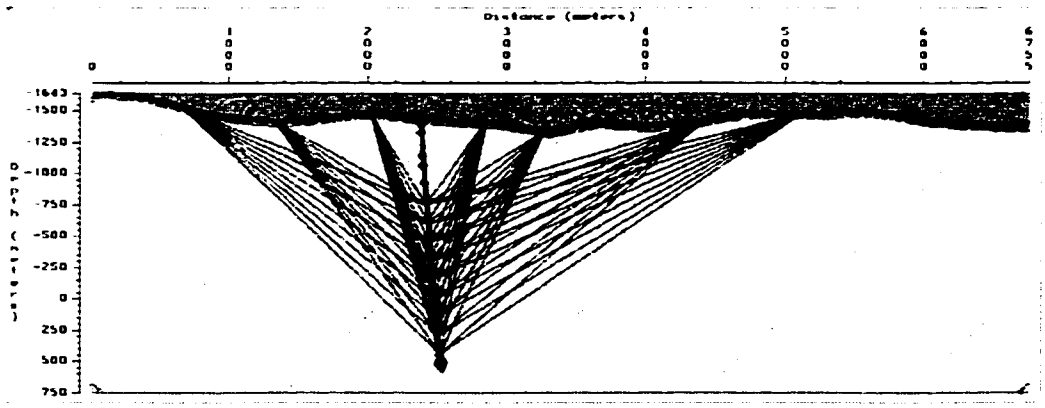

Figure 5.1. Sample design of a multi-offset VSP for a 2km thick package of shales dipping at 45°.

5.3 Location

For this study, Petro-Canada Resources of Calgary, Canada, provided access to a well in which to perform this experiment. The well, 11-10-28-6W5, was located ~80 km

northwest of Calgary, Alberta, in the Wildcat Hills area (Figure 1.4, location 4). The well intersected a 2 km panel of marine shales and some sandstones, dipping at approximately 40° to the southwest, and had only 5° deviation between the surface and the base of the shale panel. The strata are of Cretaceous age.

5.4 Geology

A geologic map of the area encompassing the well is shown in Figure 5.2 and contains clastics of the Brazeau and Alberta Group (Figure 1.3). Surface dips vary from 25° to 50° and three thrust faults were mapped, trending NW-SE, verging eastwards. A geologic cross-section through the well was constructed, based on all available geological and geophysical data. A 3D volume of seismic data was available in the area and was used to constrain the subsurface geology in both the strike and dip directions. Unfortunately, the shallow data were of poor quality and did not yield any additional information to the geologic structure at the well site. However, a high-quality 2D seismic dip line, located approximately 800 m along strike from the well, provided a robust interpretation of the subsurface structural geometry from the near surface to the maximum depth of interest, over the full VSP shot aperture. The seismic section is shown in Figure 5.3. Gamma ray log, sonic log, dip meter (Figure 5.4) and geologic formation top information were available from both the VSP well as well as from a nearby well, located 2 km further to the west (downdip) of the VSP well. A few other wells in the area also provided some geologic information to be considered in the model building process; however, the geologic model was based mainly on the information from the two primary wells, surface geology and the interpreted 2D and 3D seismic data. The final interpreted geologic cross-section through the VSP well is shown in Figure 5.5.

As can be seen by Figure 5.5, the sub-surface geology in this area is more complicated than was initially anticipated. Ideally only a uniform, single panel of shales would dominate the geology; however, this was not the case. The main stratigraphic units identified in the seismic section were; Viking, Blackstone, Cardium, Wapiabi, and Belly River. The Wapiabi and Blackstone formations are known to consist of marine shales

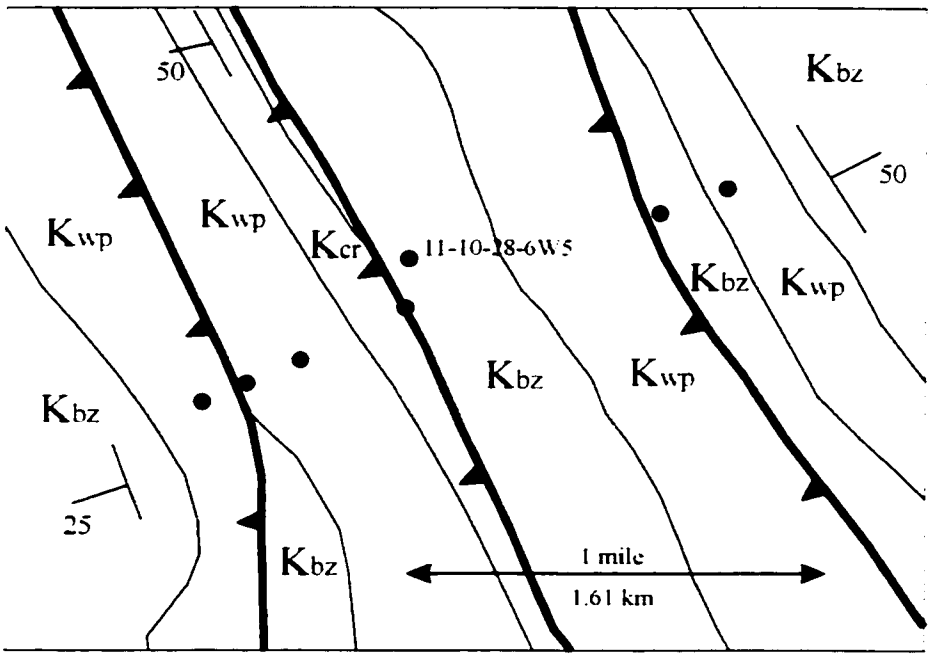

Figure 5.2. Surface geology map of area around the VSP survey (adapted from Ollerenshaw, 1972). The well and shotpoint locations are indicated as well as the Wapiabi (K_{wp}), Cardium (K_{cr}) and Brazeau Group (K_{bz}) Formations.

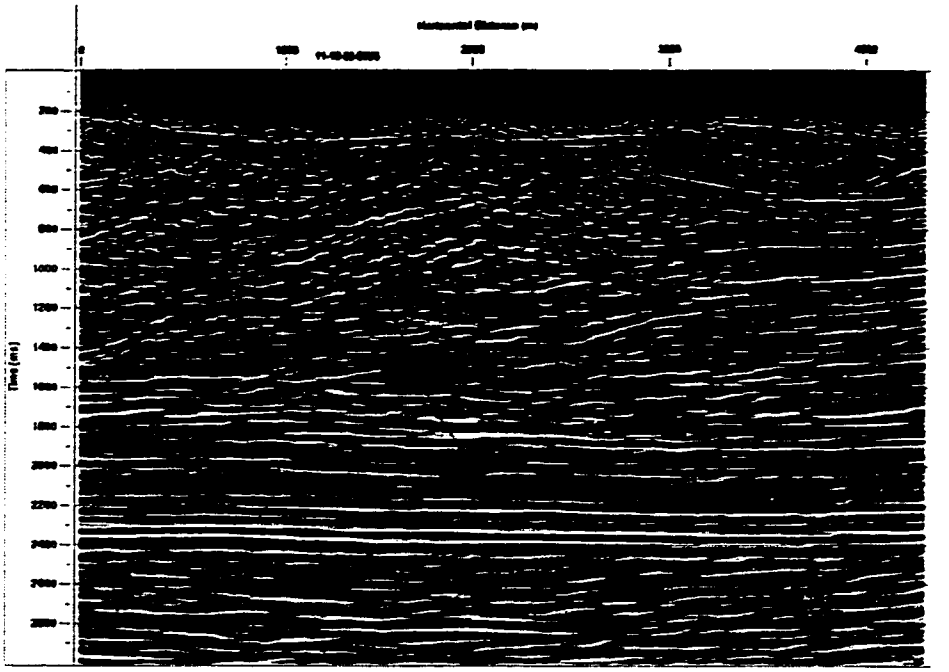

Figure 5.3. 2D seismic section that was interpreted to develop the geologic model for the raytracing analysis. The approximate location of the well is indicated by the black line.

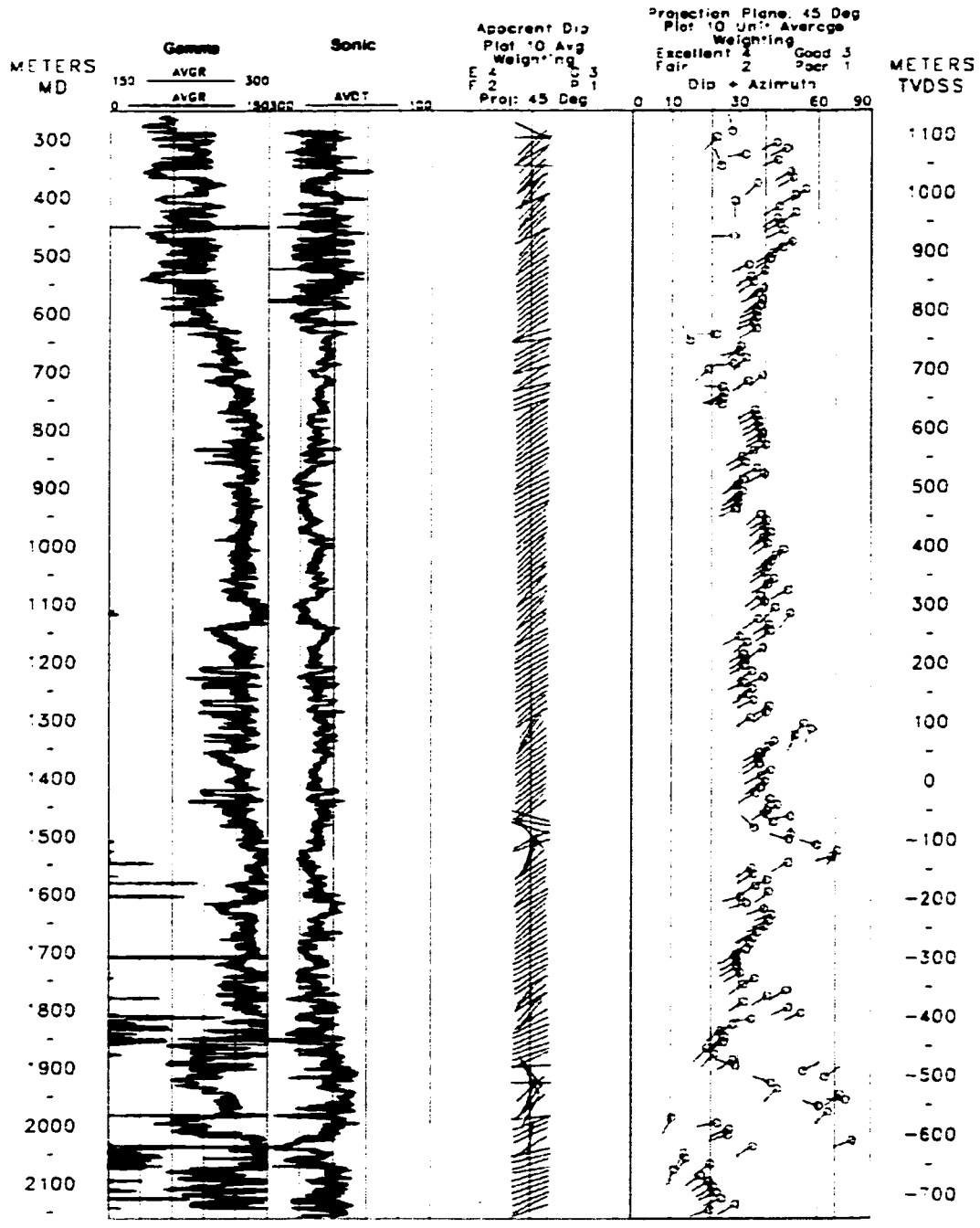

Figure 5.4. Gamma ray, sonic and dip meter logs for the well used in the VSP experiment.

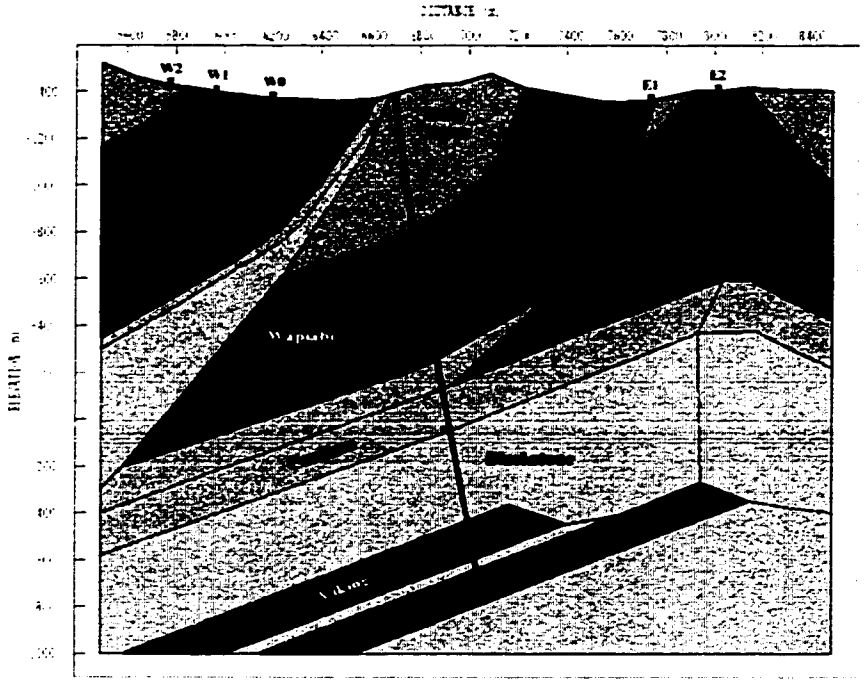

Figure 5.5. Geologic model derived from the interpretation of the 2D seismic data. This interpretation was also constrained by 3D seismic data, surface geology and well information. Five formations are present in the model: Belly River, Wapiabi, Cardium, Blackstone and Viking. The well is indicated by the black line.

and the Belly River Formation is a combination of shales and sandstones. There are three main structural zones in the interpreted section. In the west, a fairly uniform panel of rocks is thrusted to the surface. The main thrust occurs in the Blackstone Formation and a small amount of Blackstone shale is brought to the surface immediately north of the well. This is conformably overlain by the Cardium, Wapiabi and Belly River formations. The dips in this region are approximately 30°, at depth, to 60° at the surface. In the central region, another thrust sheet predominates. This thrust occurs in the Cardium Zone and has many splays associated with it. Consequently, the Cardium Formation is highly deformed, as well as thickened in this region. Above the Cardium Formation lie the Wapiabi and Belly River formations, dipping at angles of 30° to 60°. The eastern region is interpreted to be an anticline that is cored with Wapiabi shales. Small amounts of

Belly River Formation are exposed, at surface, on the flanks of the anticline. The dips on the eastern flank of the anticline, as indicated by the surface geology, are as high as 50°. At depth, it is interpreted that the Cardium Formation follows the general shape of the anticlinal structure, as does the Blackstone Formation. The actual structure at depth cannot be confirmed due to the lack of well data in this region. It is known that at least two thrusts carrying Viking Formation rocks are present at the base of the well, as the top sheet is penetrated by the well. The second sheet is easily identified by the seismic data, located immediately below the first sheet. The significant amount of sandstone present in the section was unanticipated and had to be accounted for in the analysis of the data.

5.5 Data Acquisition

A map view of the well and source points used in the experiment is shown in Figure 5.6. Data from five offset locations were acquired in the dip direction, away from the well, with 3 shotpoints in the downdip direction (W0, W1 and W2 in Figure 5.6) and 2 shotpoints in the updip direction (E1 and E2 in Figure 5.6). The maximum offset of the shotpoints was approximately equal to the depth to the base of the shale formations intersected in the well. A minimum of five shotpoints was determined to provide sufficient data redundancy to estimate the bedding-parallel, bedding-perpendicular and 45°-to-bedding velocities of the 2 km thick clastic package (Figure 5.5). An old seismic line, which traversed the area in the dip direction just south of the well, provided access to the five offset locations (Figure 5.6). Two zero-offset source locations (Zero and E0 in Figure 5.6) were necessary to provide adequate zero-offset imaging. Problems with tube waves arose at the source location immediately adjacent to the wellhead, thus the source had to be offset slightly (E0) to account for this. The source used for the experiment was a single Mertz HD-18 vertical vibrator using an 8 – 80 Hz linear sweep over 12 seconds. Three sweeps were summed at each shotpoint for each tool level. The VSP tool used was Schlumberger's 5-level, 3-component tool with a geophone interval of 15m. Data were collected over tool depths from ~600 m to ~2000 m in the well, with a standard tool interval of 150 m. At shots E1, E2 and W1, the tool interval was reduced to 75 m in order to acquire data for use by Petro-Canada, in part for imaging purposes.

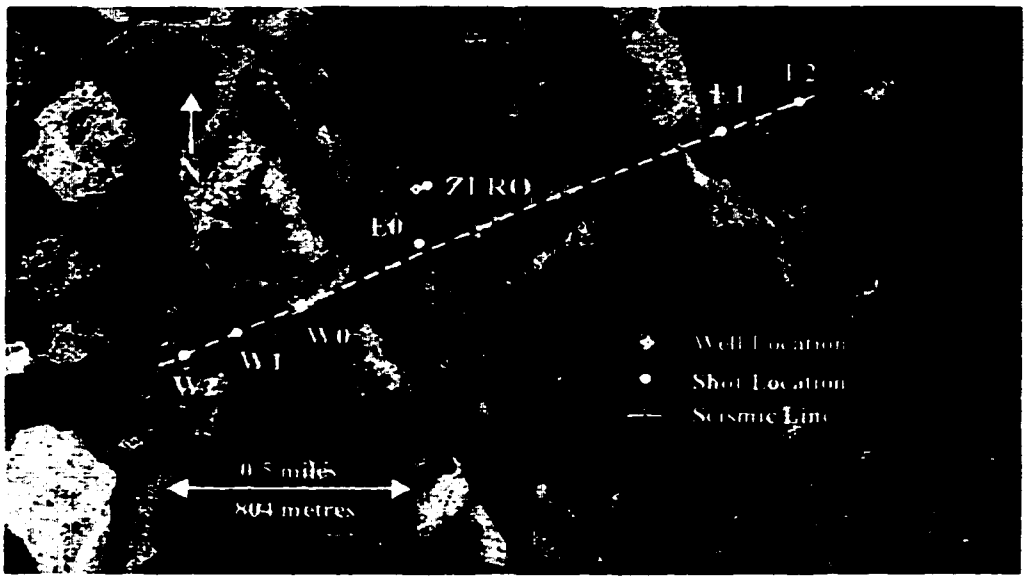

Figure 5.6. Plan view of the VSP survey.

5.6 Data Processing

Preprocessing of the data involved only data rotation into x, y and z coordinates with respect to the acquisition plane. Figures 5.7a-f show the data from the z component, windowed over the direct arrivals, displayed with a 500 ms agc applied. These displays show the high quality of the data from each shot location. The first-break times for each shot location were picked and exported to a spreadsheet, which was used for the main processing of the data. All raw and processed data, from all shot locations, are contained in Appendix II. Firstly the absolute x, y, and z coordinates of all the receiver locations were determined from the deviation survey of the well. The distances from each shot location to each receiver was then calculated as well as the bearing angle (from north) and inclination angle (from surface to receiver). For the five offset shot locations, located both northeast and southwest of the well, the distances and times from the shots to the receivers were projected into the plane of the shots so that a 2-dimensional traveltime analysis could be undertaken. In order to project the well into the line of the VSP shots, several relations need to be developed in order to make the transformation.

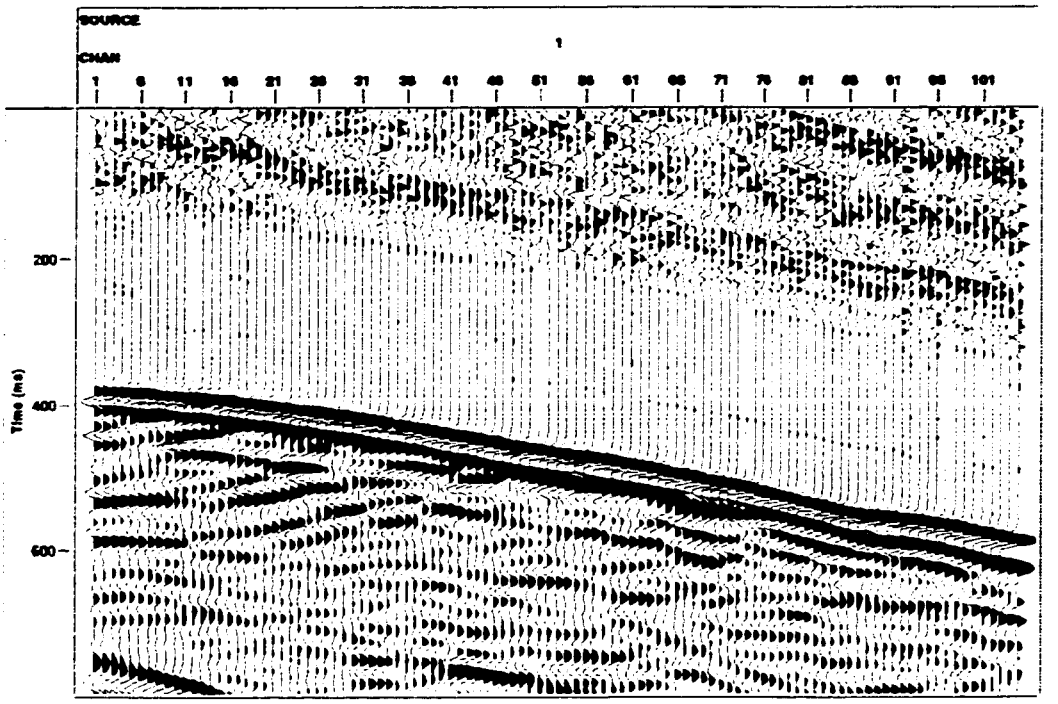

Figure 5.7a. VSP data from shot E2 after rotation.

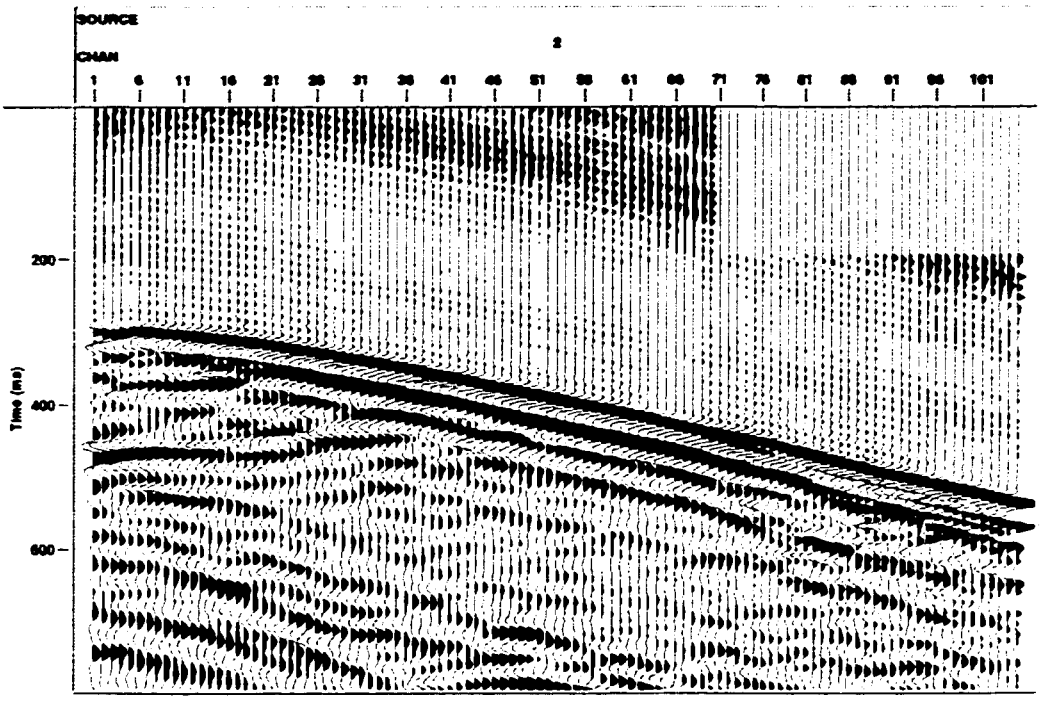

Figure 5.7b. VSP data from shot E1 after rotation.

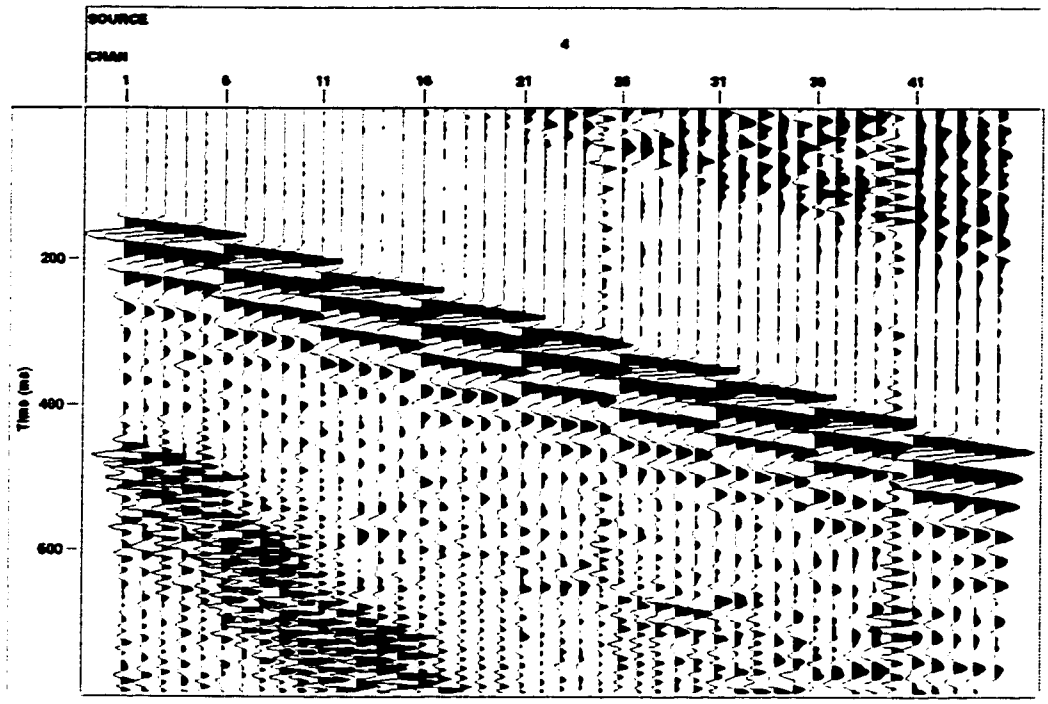

Figure 5.7c. VSP data from shot Zero after rotation.

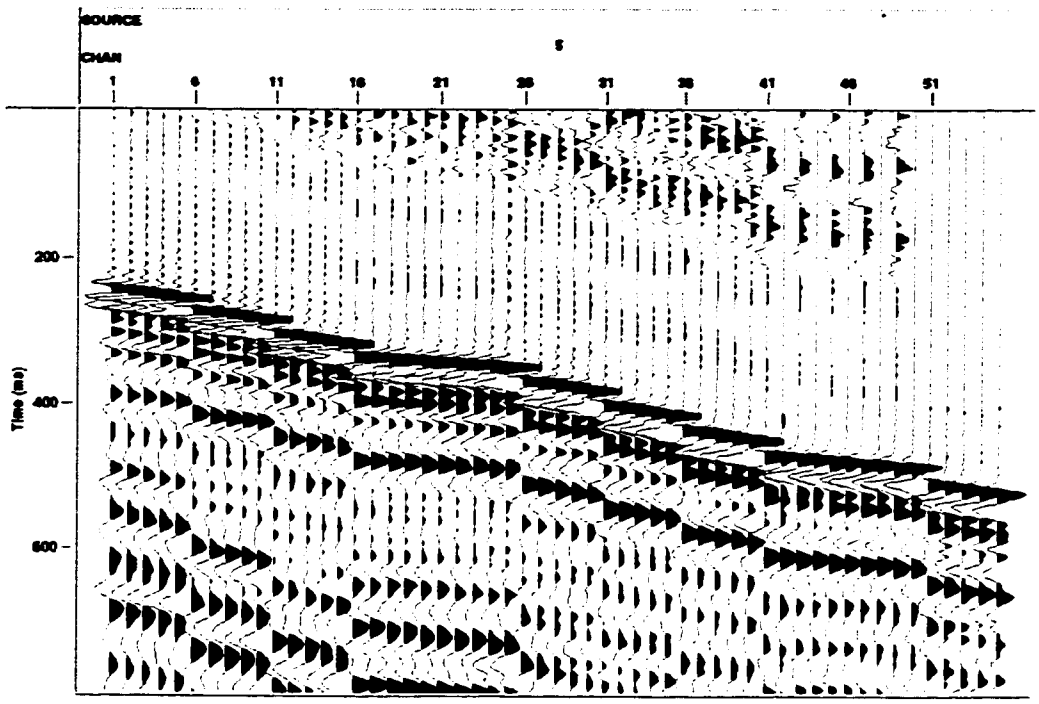

Figure 5.7d. VSP data from shot W0 after rotation.

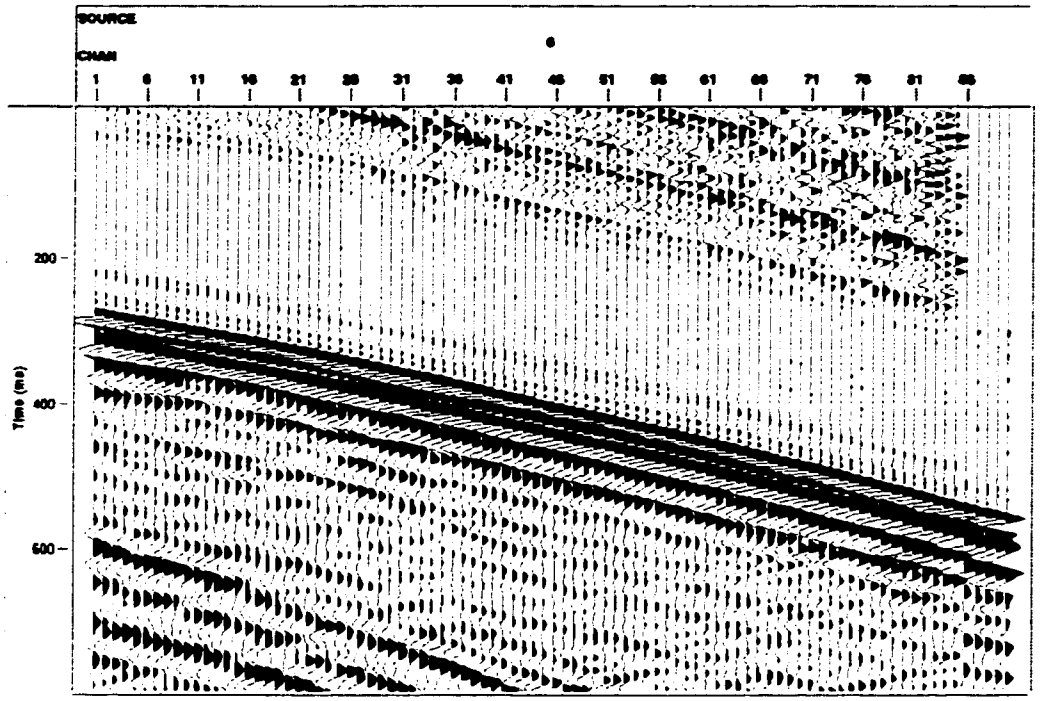

Figure 5.7e. VSP data from shot W1 after rotation.

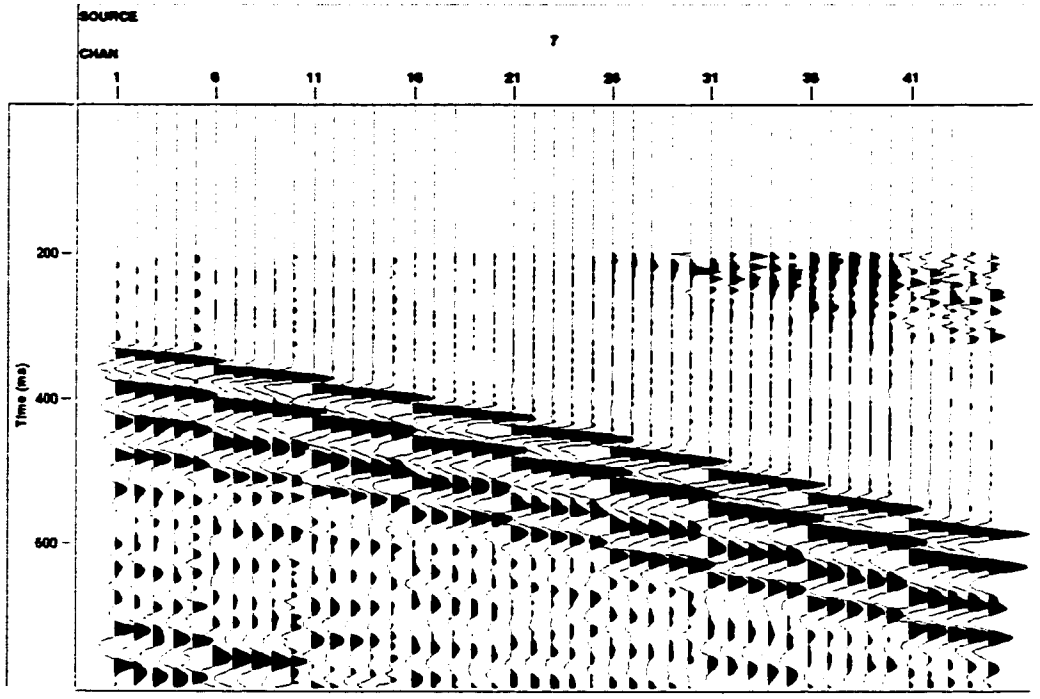

Figure 5.7f. VSP data from shot W2 after rotation.

The required variables are defined as follows and are related in Figure 5.8:

h - is the horizontal distance on the surface from the shotpoint to the well.

h' - is the projected horizontal distance from the shotpoint to the repositioned well.

θ - is the transformation angle between the h and h' planes.

d - is the distance from the shotpoint to the receiver in the well.

d' - is the projected distance from the shotpoint to the repositioned well.

z - is the vertical depth of the receiver in the well. Note that this value is the same in both the actual and transformed planes.

I - is the angle between h and d in the untransformed plane (h).

I' - is the transformed angle between h' and d'.

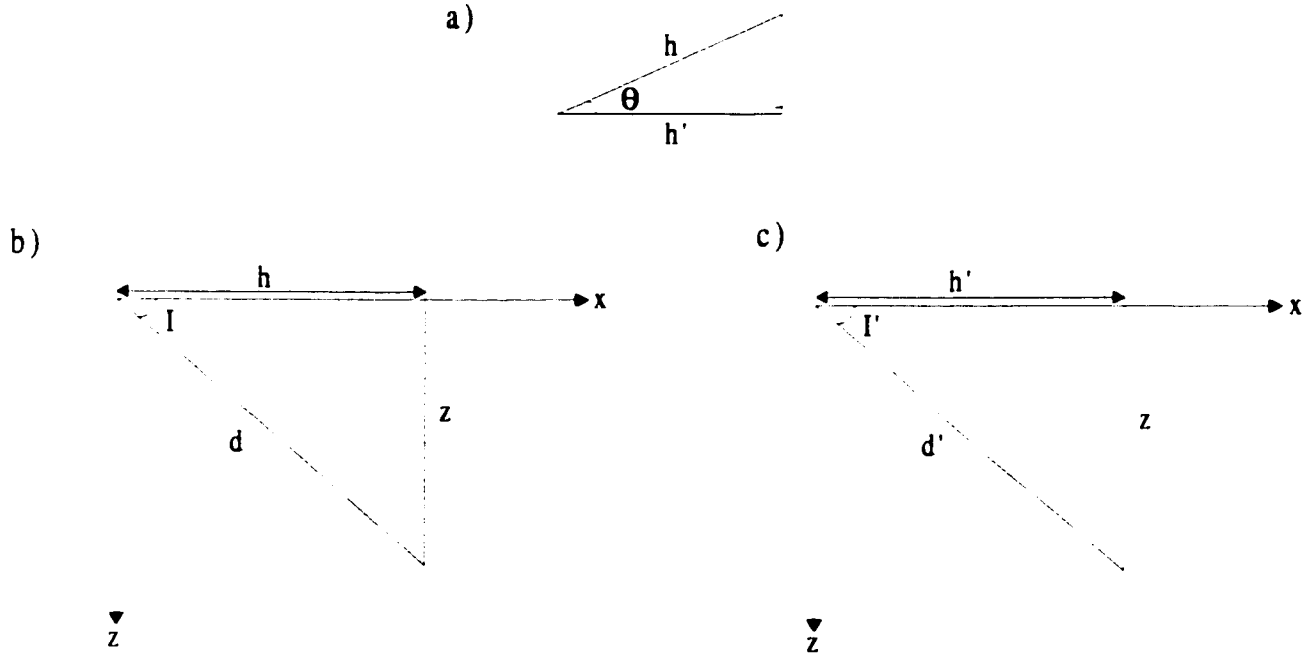

Figure 5.8. For transformation from the a) **h** plane to the **h'** plane (plan view), one must consider the relation between each of the variables in both the b) **h** plane (side view) and c) **h'** plane (side view).

From Figure 5.8a:

$$h' = h\cos\theta \tag{5.1}$$

In the **h** plane (Figure 5.8b):

$$h = d\cos I \tag{5.2}$$

and,

$$z = h\tan I\ . \tag{5.3}$$

In the transformed plane (**h'**) (Figure 5.8c):

$$h' = d'\cos I' \tag{5.4}$$

and,

$$z = h'\tan I'. \tag{5.5}$$

Equating equations 5.3 and 5.5,

$$h\tan I = h'\tan I'$$

Substituting in equation 5.1,

$$h\tan I = h\cos\theta\tan I'$$

Therefore,

$$I' = \tan^{-1}\left(\frac{\tan I}{\cos\theta}\right). \tag{5.6}$$

The projected distance (d') is then, from equations 5.4 and 5.1,

$$d' = \frac{h'}{\cos I'} = \frac{h\cos\theta}{\cos I'}$$

Therefore, substituting in equation 5.2,

$$d' = \frac{d \cos I \cos\theta}{\cos I'} . \qquad (5.7)$$

Similarly, the projected traveltime (t') is,

$$t' = \frac{t \cos I \cos\theta}{\cos I'} . \qquad (5.8)$$

Equations 5.7 and 5.8 were used to calculate the transformed, or projected, distances and traveltimes for the 5 offset shot locations (E2, E1, W0, W1 and W2), in Appendix II. This allowed for the adjustment of the observed traveltimes, such that they could be compared to the 2D forward modelling results.

Source static corrections were evaluated from the 2D seismic line, which intersected all of the VSP offset shotpoints, immediately south of the well (Figure 5.6). Unfortunately, there was a bulk shift applied to the data, which could not be precisely determined due to the age of the data. As such, the exact shot statics could not be applied; however, the variation in source statics was determined to be less than ±10 ms. This was used to quantify the accuracy to which the final modelling could be undertaken.

5.7 Data Analysis

The structural model was digitized and imported into a general TI anisotropic raytracing package that was developed for the analysis (Figure 5.5). This program traced rays through polygons of the model from a shotpoint to each receiver location in the well. Within each polygon, values of bedding-perpendicular velocity (v_o), ε, δ and the bedding dip were specified by the user. These parameters were adjusted iteratively until the modelled ray (group) traveltimes agreed with the observed traveltimes to within ±10 ms. The structural model was not changed during the analysis.

The initial velocity model was constrained using interval velocities, determined from well data, as well as refractor velocities determined through a minus-time analysis [Hagedoorn, 1959]. Interval velocity analysis from the zero-offset source location yielded average velocities of each formation at 40°-to-bedding, as seen in Table 5.1. The 2D seismic line, immediately south of the well, was used to calculate the refractor velocities through a minus-time analysis of first arrival traveltimes. The procedure was similar to that used in the refraction surveys (Chapter 4). The calculated refractor velocities were used to constrain the velocities of the outcropping rock units at each shot location.

Table 5.1. Average interval velocity of each formation, determined at 40°-to-bedding from the zero-offset source location (E0).

Formation	***Average Interval Velocity (m/s)***
Belly River	4100
Wapiabi	4000
Cardium	4100
Blackstone	4000

The starting anisotropic parameters used in the initial model were taken from the refraction survey results, described in Chapter 4. Initially only the Wapiabi and Belly River formations were modelled as being anisotropic, although, eventually the Blackstone Formation was also made anisotropic. The anisotropic parameters for this formation were assumed to be similar to those of the Wapiabi Formation. The dips assigned to these anisotropic bodies were projected from the dip meter data in the well (Figure 5.4). Once the initial model was built, the raytracing was performed. Rays from each of the offset shot locations were used to calculate the traveltime to each receiver location. The zero offset shots were not used directly in the raytracing since their raypaths are intuitively straightforward. The input parameters were adjusted independently, for each iteration of the raytracer, starting with the formation velocities and finishing with the anisotropic parameters. The model parameters were modified iteratively until the computed traveltimes matched the observed values within ± 10 ms, for all records.

5.8 Results

The final anisotropic velocity model is presented in Figure 5.9 and the parameters used are listed in Table 5.2. The average values of ε and δ for each anisotropic formation are typical and within the range defined by Thomsen (1986) and the refraction surveys of Chapter 4. In this case, modelling the Blackstone Formation with a δ value greater than ε, best fit the data, which is not typical of shales [Thomsen, 1986]. This was not expected since this formation is more similar in geology to the Wapiabi Formation than the Belly River Formation. Again this indicates that each anisotropic formation must be quantified individually in order to correctly account for velocity anisotropy in seismic data processing. It is also noted that the Wapiabi velocities, used in the modelling, varied depending on the depth of the Formation. The velocities in the near surface were slightly slower than the velocities at depth, which are attributed to either a weathering gradient at the surface or a compaction gradient at depth.

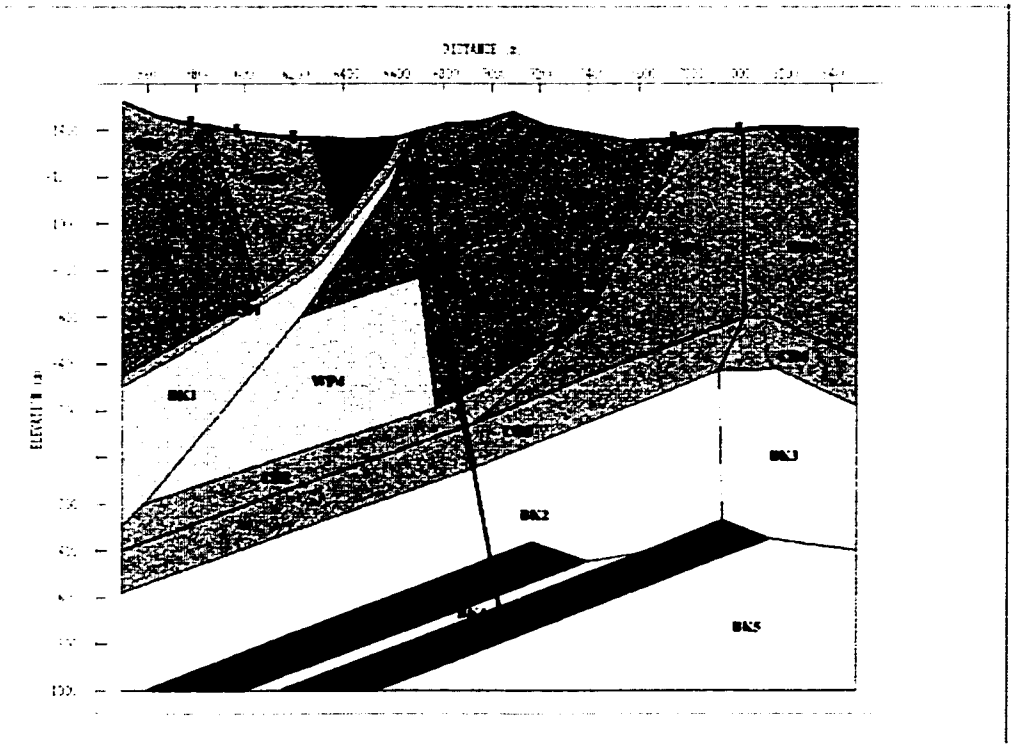

Figure 5.9. This is the final anisotropic velocity model which best fit the observed data during the raytracing procedure. The colours represent velocity, with blue being slowest and red being fastest. The polygon parameters are defined in Table 5.2.

Figure 5.10 depicts a sampling of the rays for each offset shot location. This is not a unique solution, as the input parameters could be altered in many permutations to model the observed data. However, the model shown in Figure 5.9 is an adequate solution given the geologic and geophysical constraints on the data. To complete the study, the anisotropic parameters were set to zero in this model and the traveltimes were recalculated. This provided an isotropic solution to compare with both the observed and anisotropic values.

Table 5.2. Parameters used in the final anisotropic model, applied in the raytracing procedure (Figure 5.9).

Formation	*Velocity (m/s)*	*Dip (°)*	ε	δ
BR1	3600	-30	0.11	0.32
BR2	3700	-45	0.11	0.32
BR3	3500	-40	0.11	0.32
BR4	3700	40	0.11	0.32
WP1	3700	-30	0.10	0.07
WP2	3600	-50	0.10	0.07
WP3	3400	-60	0.10	0.07
WP4	3900	-20	0.10	0.07
WP5	3700	-40	0.10	0.07
WP6	3700	-60	0.10	0.07
WP7	3600	-40	0.10	0.07
WP8	3600	40	0.10	0.07
CD1	4300			
CD2	4300			
CD3	4300			
CD4	4300			
BK1	4000	-45	0.05	0.10
BK2	4100	-40	0.05	0.10
BK3	4100	25	0.05	0.10
BK4	4100	-40	0.05	0.10
BK5	4100	-35	0.05	0.10
VK1	4500			
VK2	4500			

The traveltimes from each shot location, observed, anisotropic and isotropic, were plotted against receiver elevation (Figure 5.10). From these plots, it is evident that the raytracing process successfully modelled the observed traveltimes to within ±10 ms. The eastern

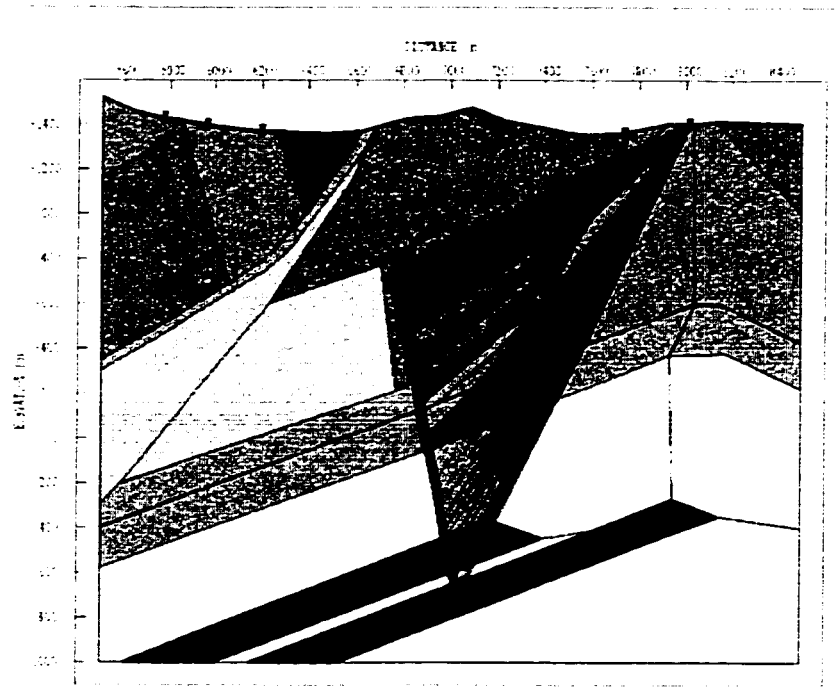

Figure 5.10a. Sample raytracing example from shot E2.

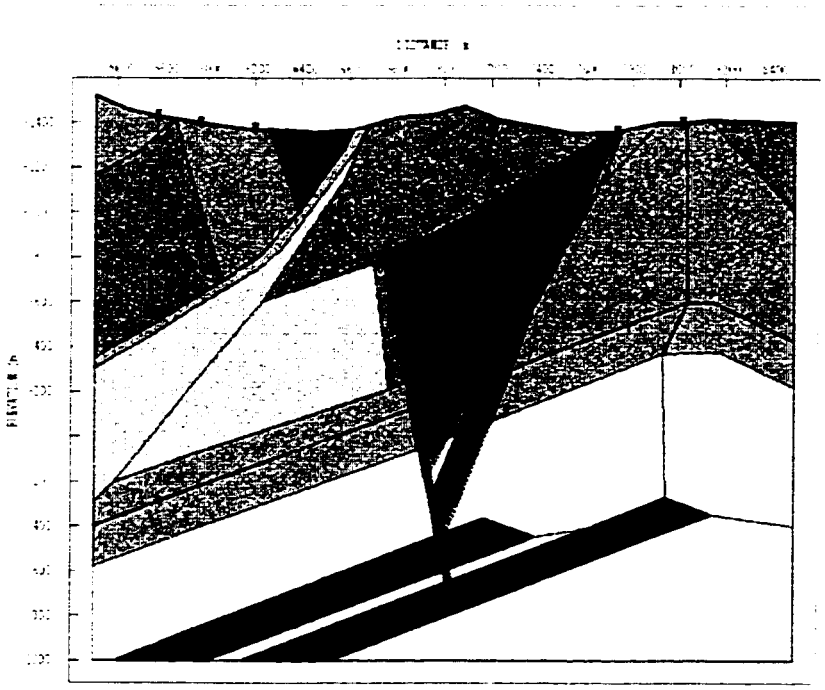

Figure 5.10b. Sample raytracing example from shot E1.

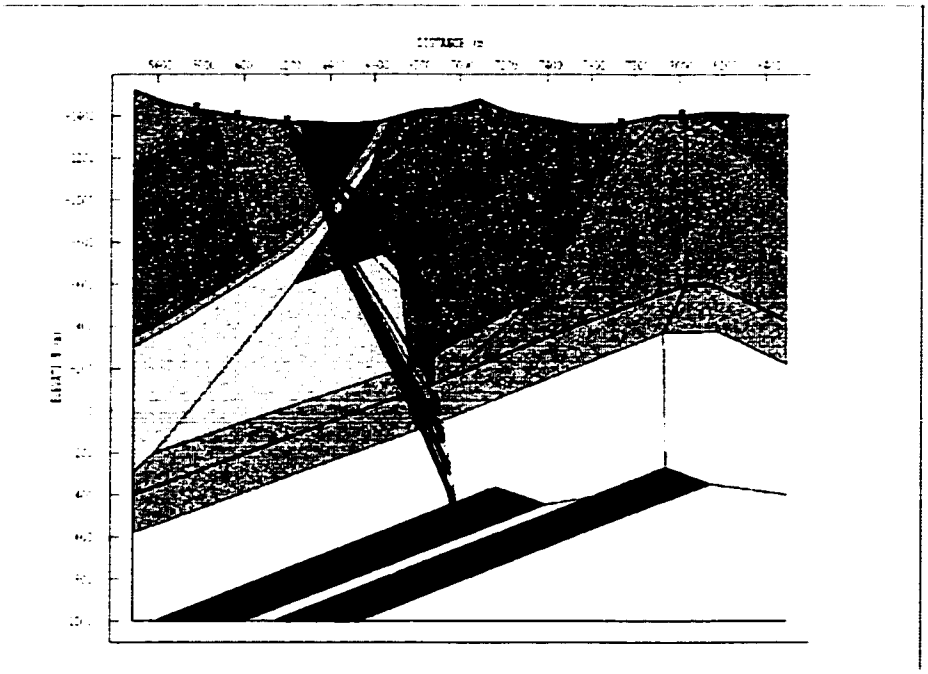

Figure 5.10c. Sample raytracing example from shot W0. Note the shadow zones for the third through sixth receiver locations down the well. This is due to the sharp edges of the polygons as well as the defined parameters therein.

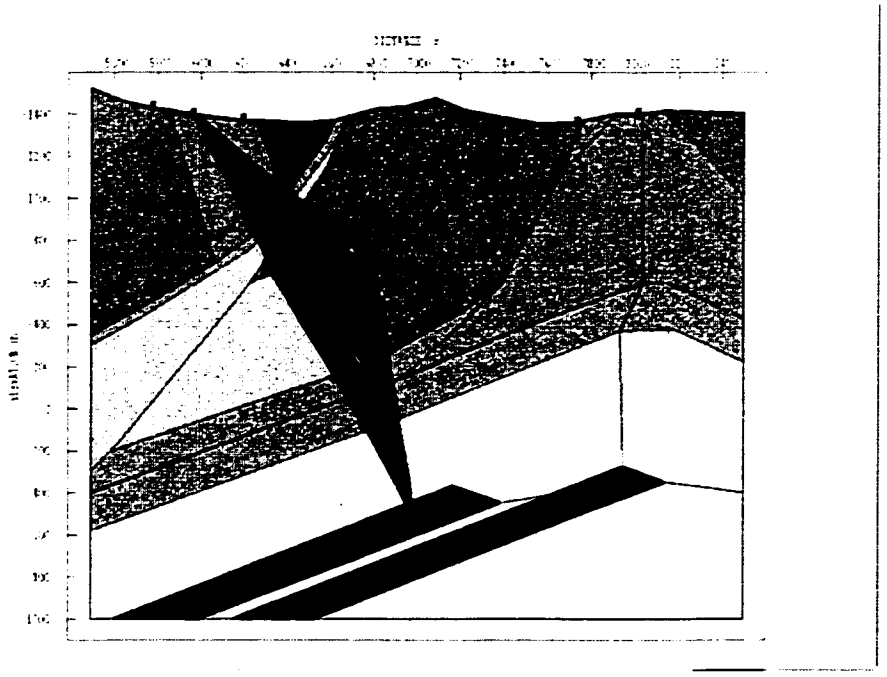

Figure 5.10d. Sample raytracing example from shot W1.

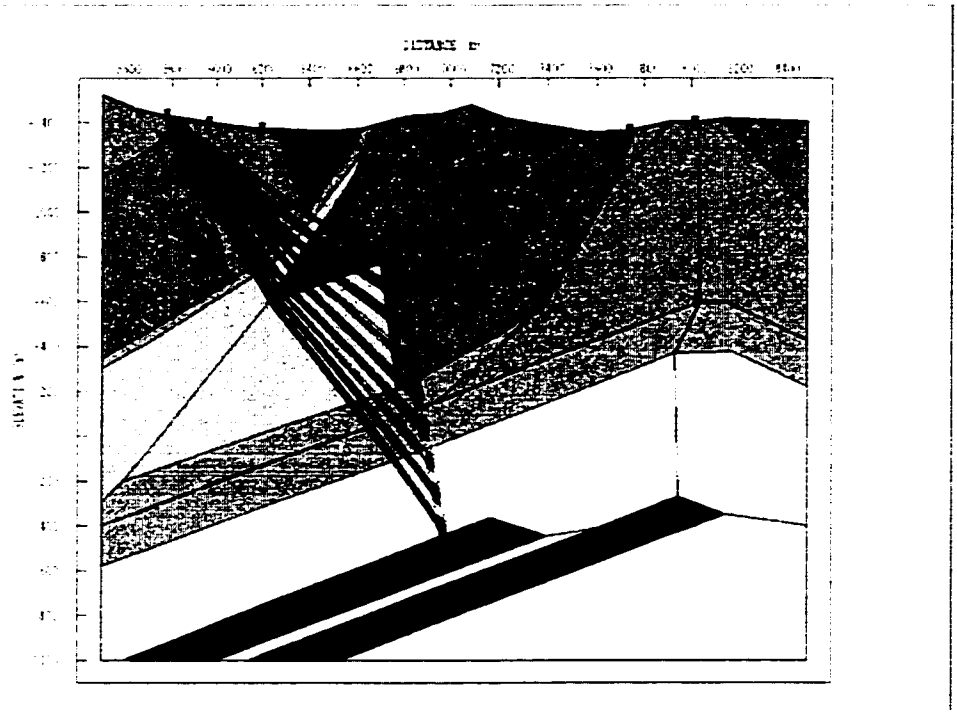

Figure 5.10e. Sample raytracing example from shot W2.

shots were modelled more closely by the anisotropic solution than the isotropic solution, whereas the difference between the solutions for the western shots is considerably less. This is expected since the eastern raypaths are parallel to the bedding of the shales and the western shots are perpendicular-to-bedding. Since the isotropic solution assumes the perpendicular-to-bedding velocity for the formation, the error will be small when the raypaths also tend to be perpendicular-to-bedding. The error will be larger when the raypaths are parallel-to-bedding, as seen in Figures 5.11a and 5.11b.

The computed traveltimes were then used to calculate the velocities for each raypath, assuming straight raypaths, and the velocities were then plotted against elevation (Figure 5.12). Note that the observed velocities from the eastern shotpoints are faster than those from the western shotpoints. This is because the raypaths from the eastern shots are approximately parallel-to-bedding (i.e. travelling at the fast velocity of the strata), whereas the western raypaths are more perpendicular-to-bedding. It can also be seen that

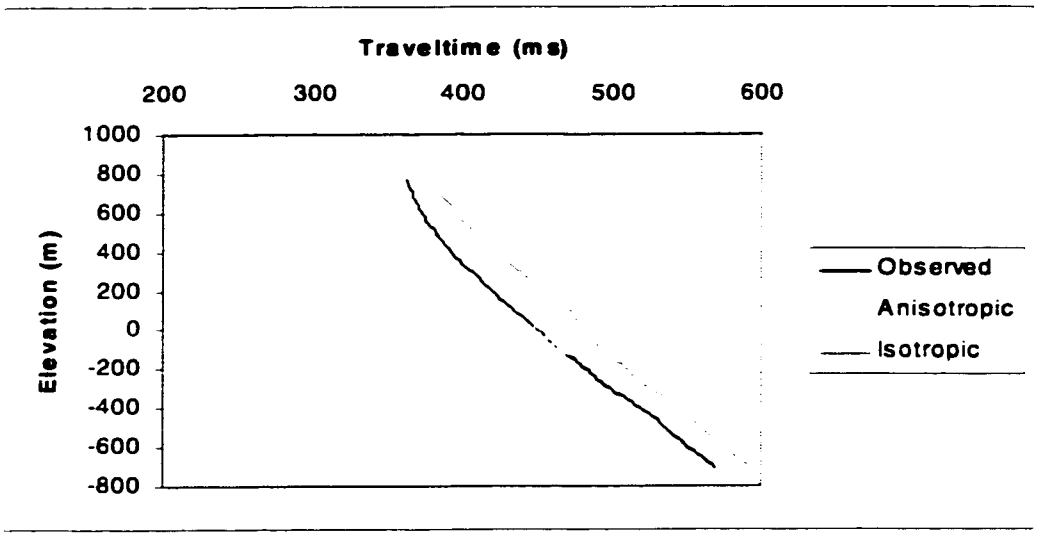

Figure 5.11a. Traveltime vs. Elevation plots for shot E2, comparing the observed data to both the isotropic and anisotropic solutions.

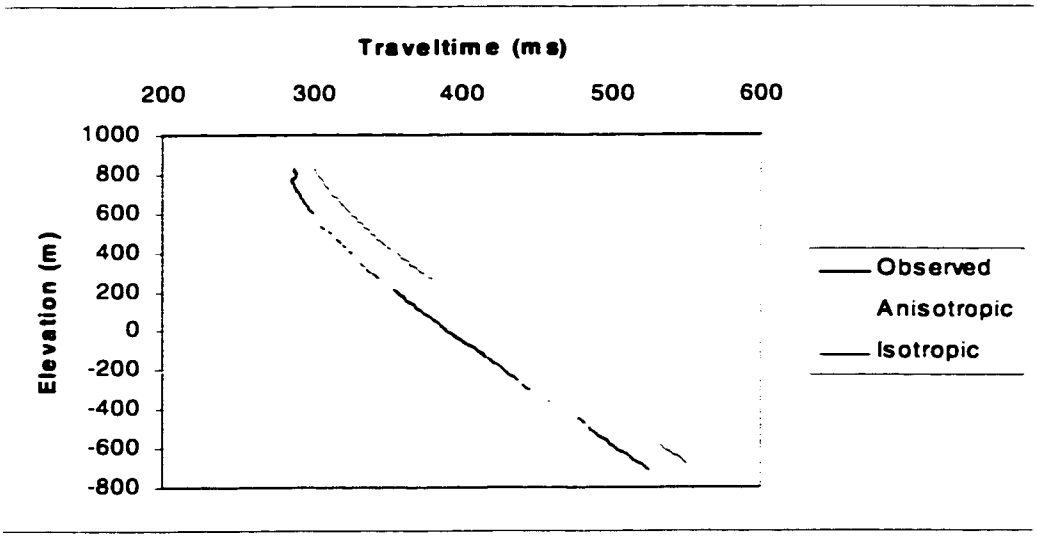

Figure 5.11b. Traveltime vs. Elevation plots for shot E1, comparing the observed data to both the isotropic and anisotropic solutions. Note the lack of data in the isotropic solution, due to the shadow zones present in the raytracing model.

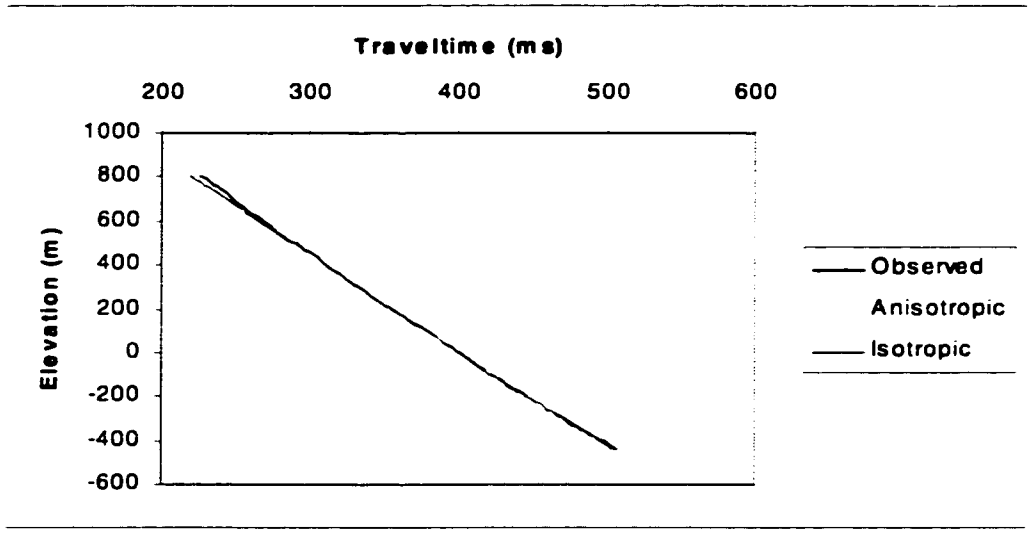

Figure 5.11c. Traveltime vs. Elevation plots for shot W0, comparing the observed data to both the isotropic and anisotropic solutions.

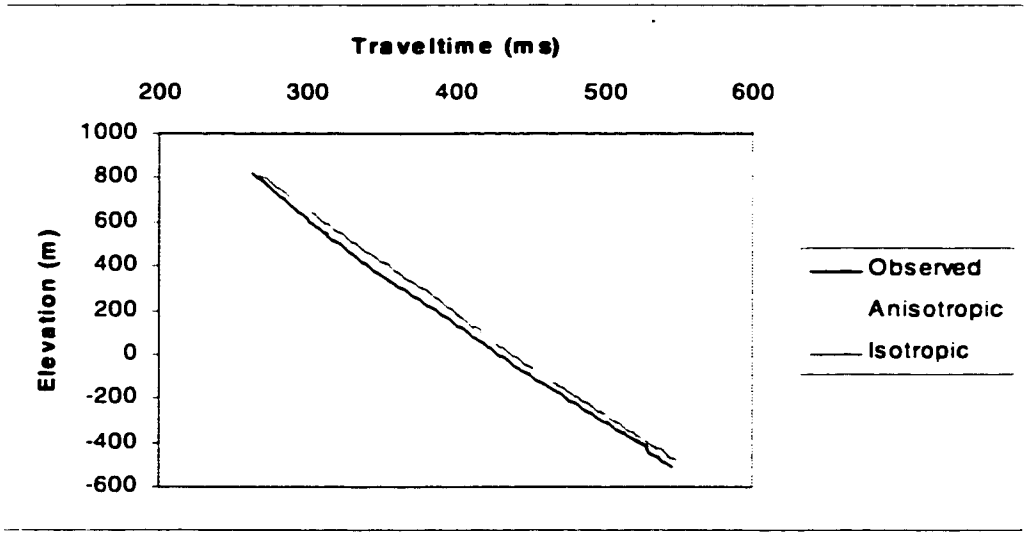

Figure 5.11d. Traveltime vs. Elevation plots for shot W1, comparing the observed data to both the isotropic and anisotropic solutions.

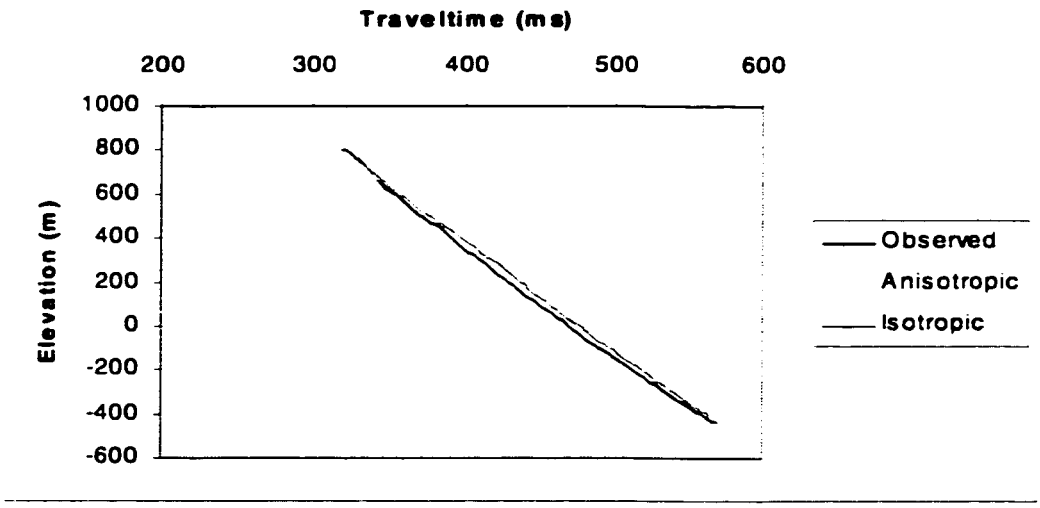

Figure 5.11e. Traveltime vs. Elevation plots for shot W2, comparing the observed data to both the isotropic and anisotropic solutions.

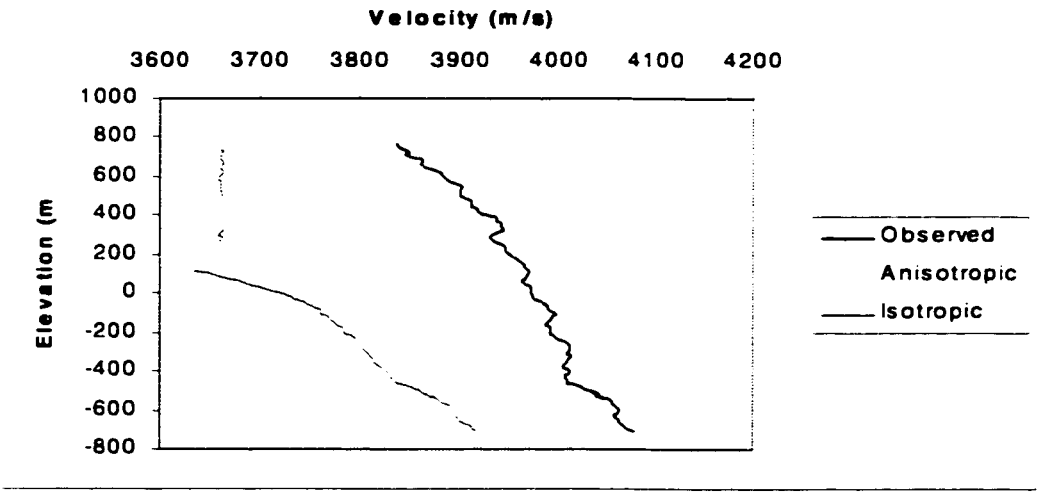

Figure 5.12a. Velocity vs. Elevation plots for shot E2, comparing the observed data to both the isotropic and anisotropic solutions.

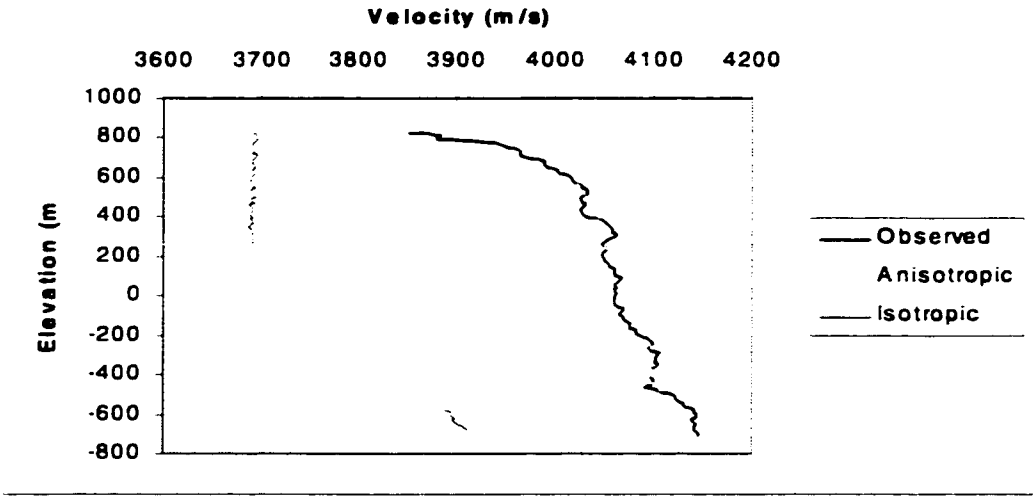

Figure 5.12b. Velocity vs. Elevation plots for shot E1, comparing the observed data to both the isotropic and anisotropic solutions.

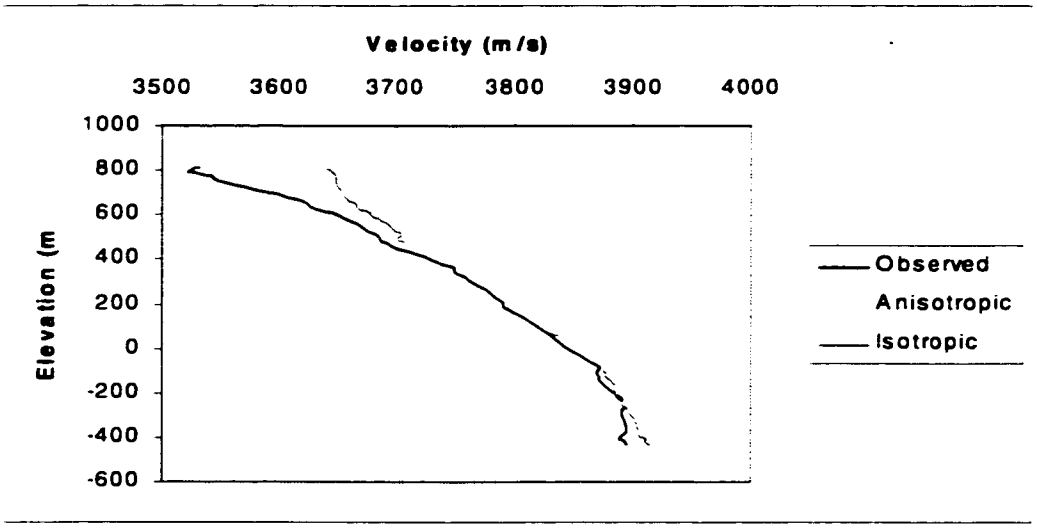

Figure 5.12c. Velocity vs. Elevation plots for shot W0, comparing the observed data to both the isotropic and anisotropic solutions.

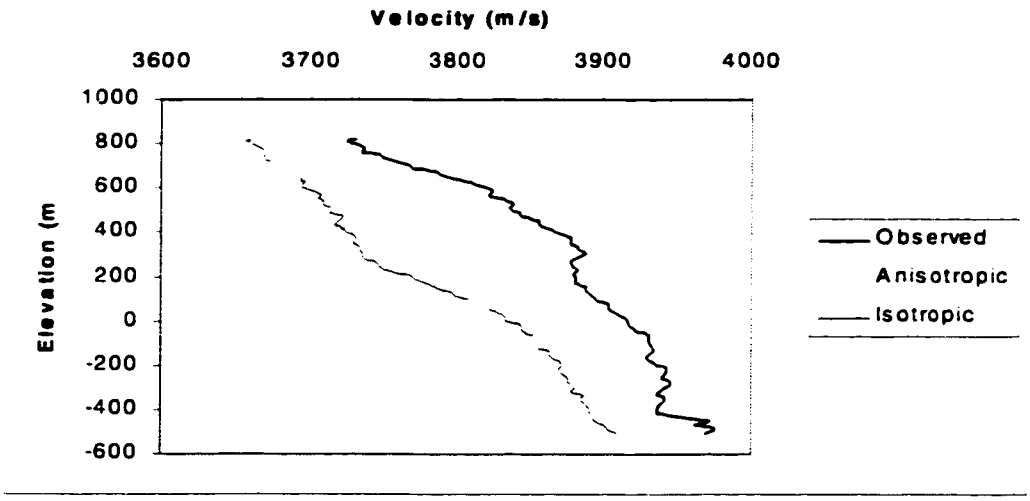

Figure 5.12d. Velocity vs. Elevation plots for shot W1, comparing the observed data to both the isotropic and anisotropic solutions.

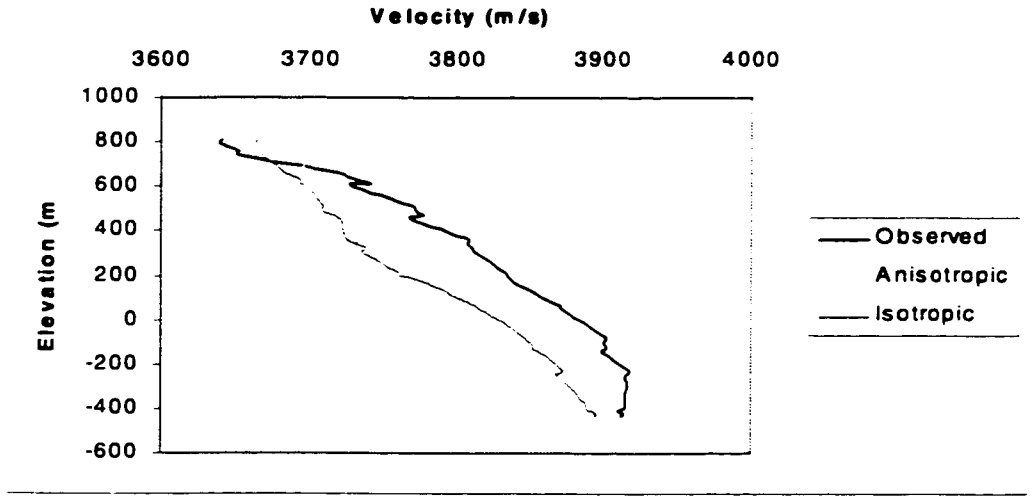

Figure 5.12e. Velocity vs. Elevation plots for shot W2, comparing the observed data to both the isotropic and anisotropic solutions.

the velocities have a larger error associated with them, in general. This is due to the propagation of the error in the traveltimes. It was determined in the refraction surveys that a 10 ms error in the first break picks resulted in approximately ±100 m/s error in the velocity, for typical ray lengths used in these experiments. This further propagates into an order of magnitude error in the calculated anisotropic parameters, especially δ. It is the same for these VSP calculations.

5.9 Discussion

The results of this survey indicate that the anisotropy can be forward modelled in this VSP experiment. This is also an indication that the geological interpretation was well constrained by the available geologic and geophysical data. Minor alterations to the geologic interpretation may be valid; however, it is doubtful that the differences in the modelled traveltimes would be significant. The observed traveltimes were modelled to a precision of ±10 ms which is within the realm of accuracy possible for this experiment. The error in the observed traveltimes is associated with the first break picking; whereas the error in the calculated traveltimes is a result of a variation in shot statics and minor variations in the geologic model.

The anisotropic solution gave a more complete representation of the subsurface than the isotropic solution. The isotropic solution was not comparable in the parallel-to-bedding direction. The Blackstone Formation velocity used in these models is higher than predicted from the sonic data. It is expected that this formation is somewhat fractured at the well location but is more uniform away from the well, resulting in the faster modelling velocity.

The anisotropic parameters used in the anisotropic model were consistent with those obtained from the refraction surveys, within the margin of error. These parameters were also constant within each of the anisotropic formations, whether at surface or at depth. This indicates that the anisotropic parameters are not depth dependent and are not

affected by any compaction gradient. Thus, the anisotropic parameters obtained from surface methods are applicable at depth and are valid in the depth migration process.

Due to the complicated structural geology at this location, the anisotropic parameters could not be determined by direct traveltime inversion assuming straight raypaths. However, the anisotropy was modelled successfully using the forward modelling techniques. Nevertheless, it is expected that the anisotropic parameters could be directly determined from the data if the geology were sufficiently simple, such as a 2 km, uniform panel of shales. Hence, this experiment is expected to provide another method to measure velocity anisotropy, *in situ*, where steeply dipping strata outcrop. This, in turn, allows for the accurate determination of the anisotropic parameters for use in depth migration routines.

CHAPTER 6 ANISOTROPIC DEPTH MIGRATION OF A CANADIAN ROCKY MOUNTAIN FOOTHILLS DATASET

6.1 Introduction

The physical modelling showed that dipping anisotropic strata will cause problems for time-to-depth conversion of seismic data when isotropic velocities are assumed during depth migration. Anomalies seen in time data can be removed effectively from the model data using anisotropic depth migration, if the anisotropic parameters are known and the correct geometric velocity model is used. The refraction and VSP surveys, described in Chapters 4 and 5, demonstrate that geologic formations, comprising a significant amount of clastic strata, will be anisotropic. The differences in velocity were measured and the Thomsen (1986) anisotropic parameters calculated for several formations in the Alberta Foothills. This allows for extra information to be included in the time-to-depth conversion of anisotropic data. The final step in this thesis is to evaluate anisotropic depth migration by the processing of a real dataset.

A modern dataset from the Canadian Rocky Mountain Foothills was graciously donated for the purpose of analysis; however, the donor and exact location cannot be published due to the confidential nature of the data. Anisotropy was suspected to be present. A geologic interpretation of the pre-stack time migrated section was necessary to identify the main velocity contrasts and the anisotropic formations, in order to build the velocity model for the anisotropic depth migration. Equipped with a geologically controlled velocity model, and the anisotropic parameters determined from the refraction surveys, the anisotropic depth migration was tested. The Kelman Technologies Inc. Kirchhoff migration algorithm was used, as described in Chapter 3.

The objective of depth migration of the data, including anisotropic effects, was to determine the most coherent and correct depth section result that could be obtained. Kelman Technologies Inc. had provided a pre-stack time migrated section; however, the image contained time structural anomalies, which were interpreted to be caused by

seismic velocity anisotropy in overlying, dipping clastic rocks. Also, there was no depth control for the line. Anisotropic depth migration was used to provide an optimally imaged depth section to compare with isotropic depth migration.

6.2 Interpretation

The stratigraphy of the study area is summarized in Figure 1.3. The main stratigraphic units identified in the seismic data were; Cambrian, Devonian, Mississippian, Kootenay/Fernie, Blairmore, Blackstone, Cardium, Wapiabi, Belly River and Bearpaw/St. Mary River/Willow Creek. The Wapiabi and Blackstone formations are known to consist of marine shales and the Belly River Formation is an interbedded sequence of shales and sandstones. The refraction surveys have shown that these formations are anisotropic and require the assignment of anisotropic parameters in the migration process. As such, particular attention was made to these units in the interpretation. Data from two wells, located off the southwest end of the section, were available and were considered in the interpretation. The surface geology was also used to constrain the location of faults and formation boundaries at the surface, across the section [Stockmal,1996].

A time migrated section of the data is presented in Figure 6.1 and is approximately 20 km in length. The group interval was 20 m, the crooked line CDP spacing is 10 m and the nominal fold is 60. The shot interval was variable but the average shot interval was 100 m. These data were processed using surface consistent deconvolution, refraction statics, residual statics, pre-stack migration velocity analysis, mute, pre-stack time migration and filter (4-8, 40-50 Hz). The data quality is good but there are few reflectors in the upper portion of the section. The Paleozoic section is well defined and there is one major reflector that runs part way across the middle section, from the southwest to the triangle zone, at a time of approximately 1800 ms. There is virtually no coherent reflectivity in the triangle zone. There is evidence of steeply dipping strata in the upper, central portion of the section, immediately west of the triangle zone. The eastward dips of reflectors on the eastern flank of the triangle zone, are also evident. The interpretation of this time section is presented in Figure 6.2. In the interpretation, the section can be broken into

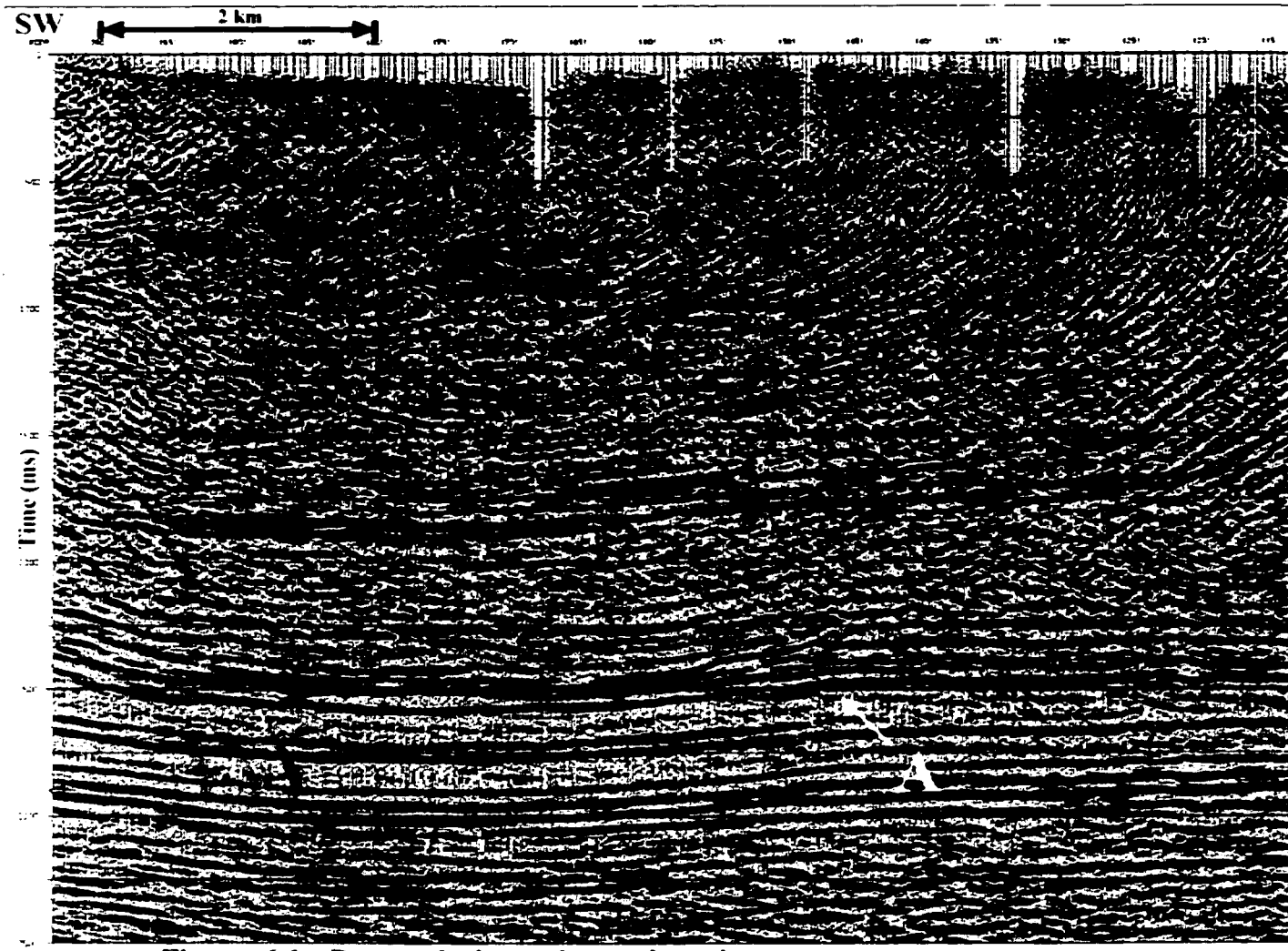

Figure 6.1. Pre-stack time migrated section.

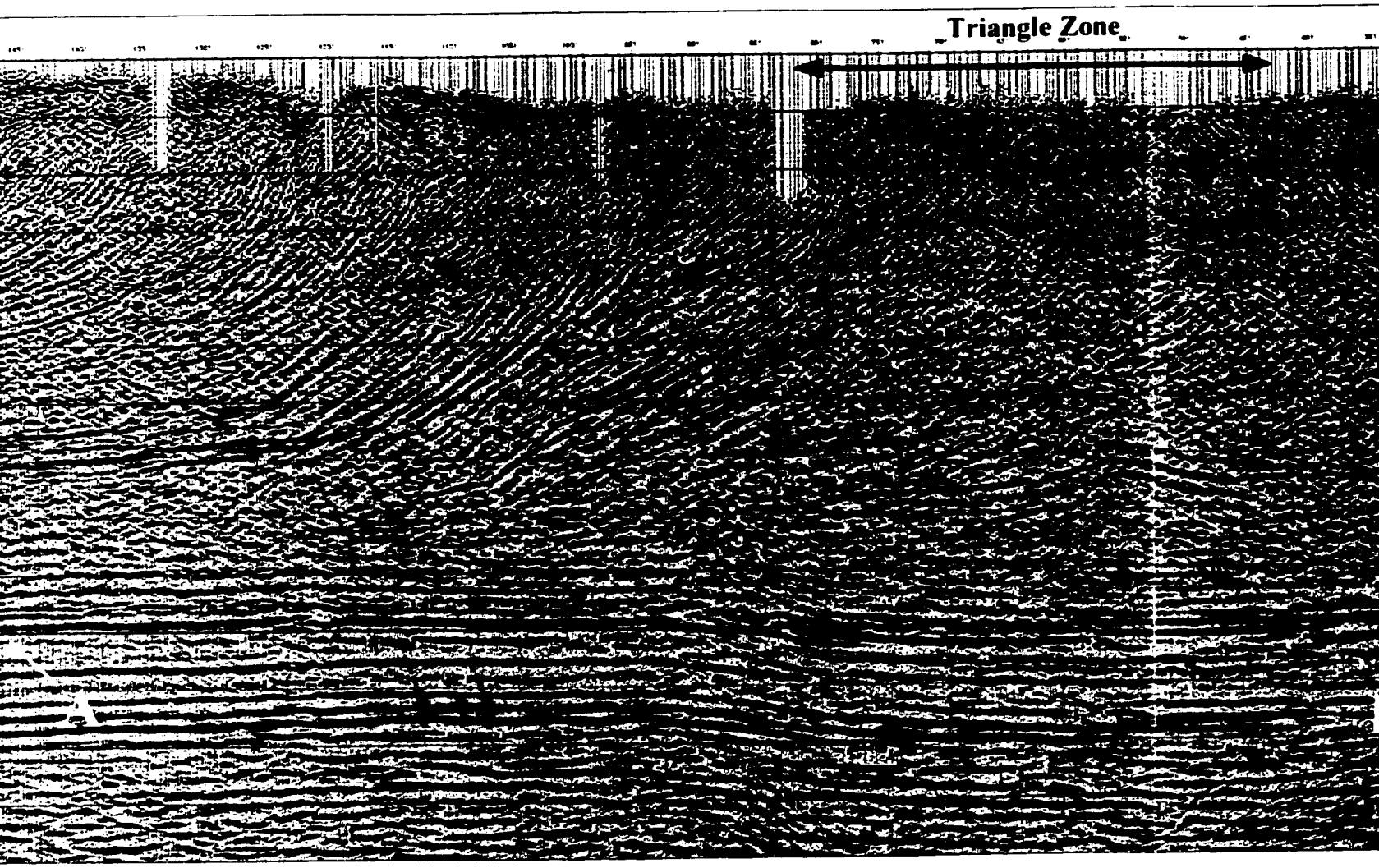
Triangle Zone

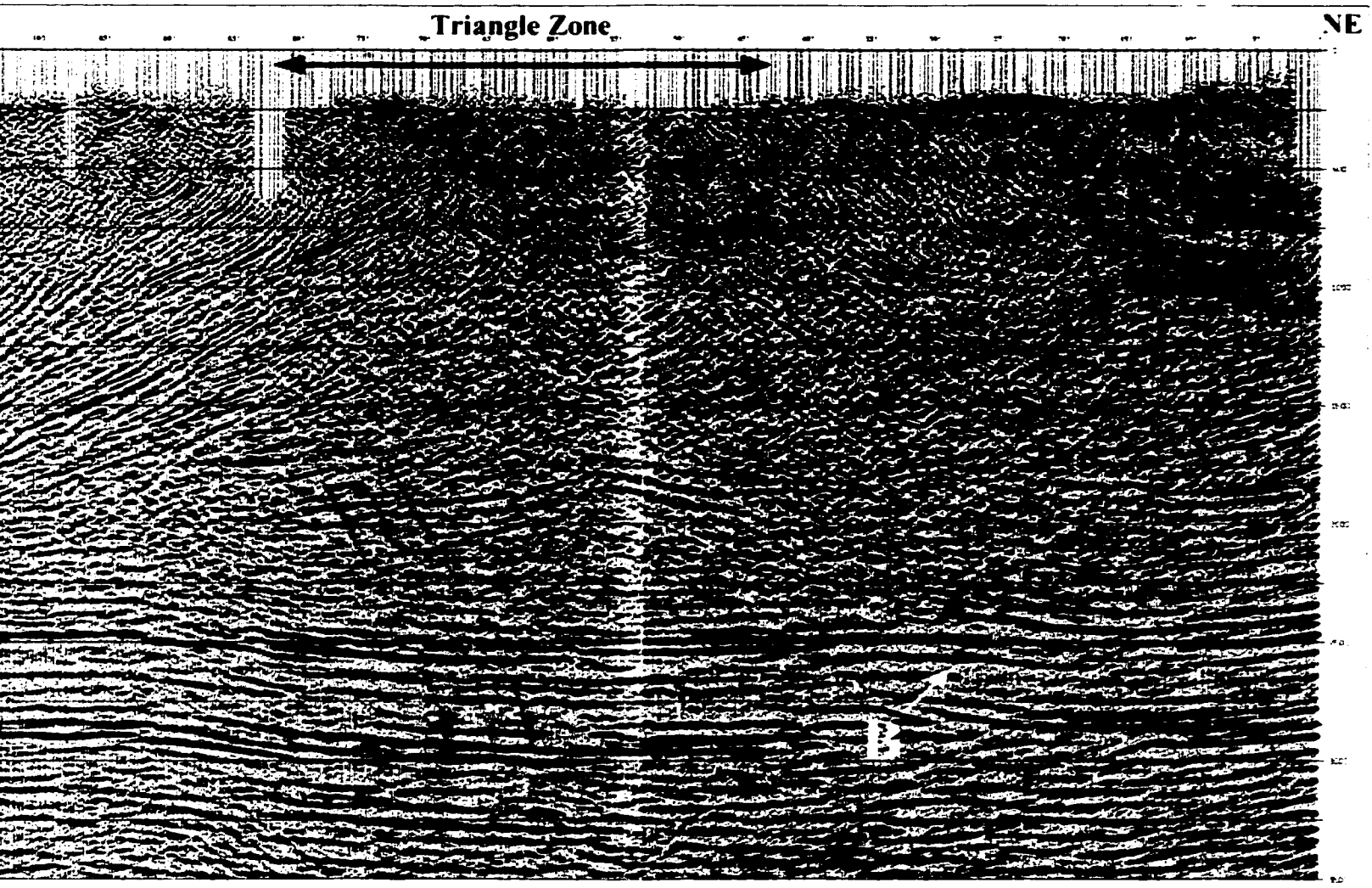
Triangle Zone
NE

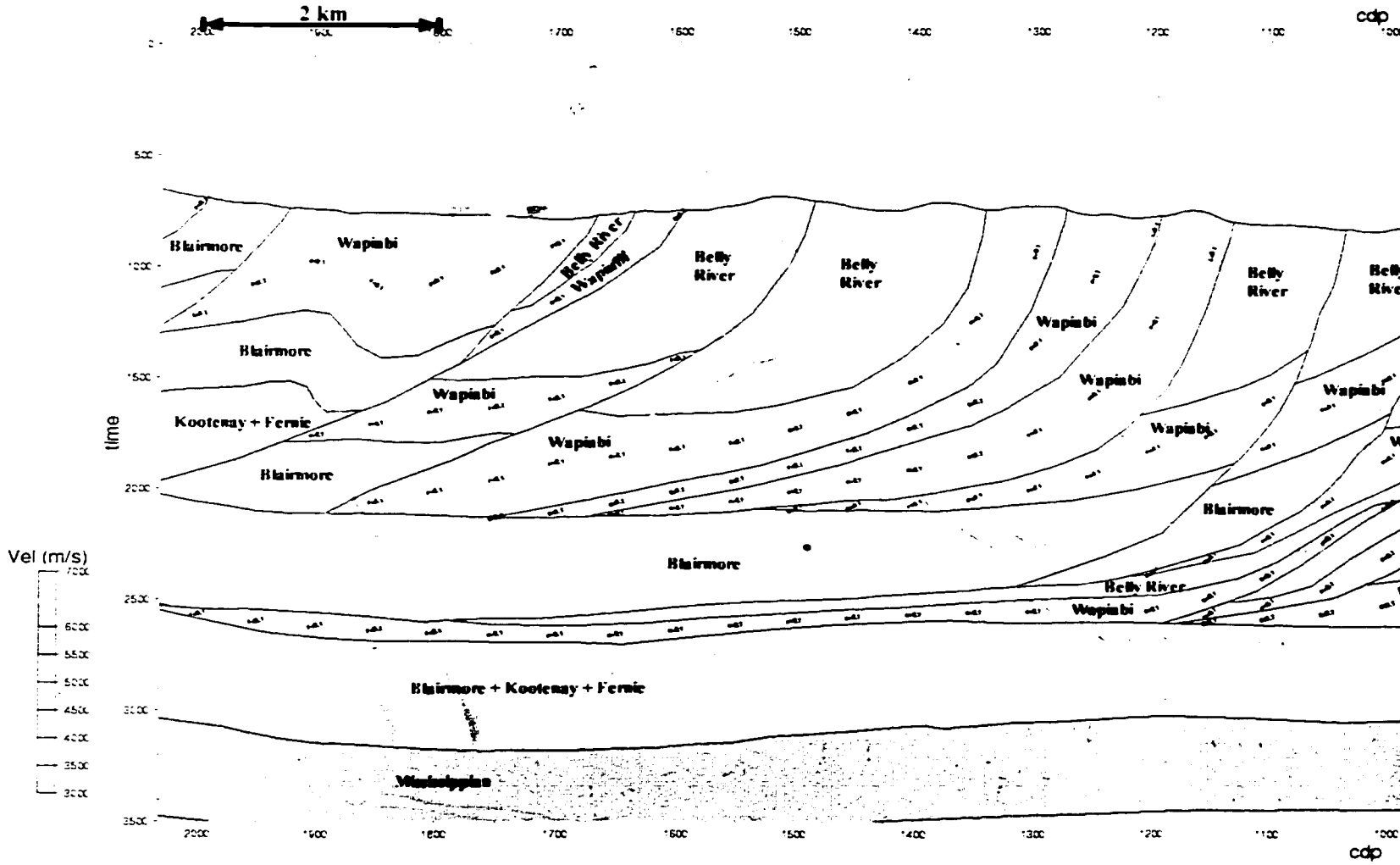

Figure 6.2. Interpretation of time migrated data. Dips of anisotropic strata are indicated by the text within the anisot

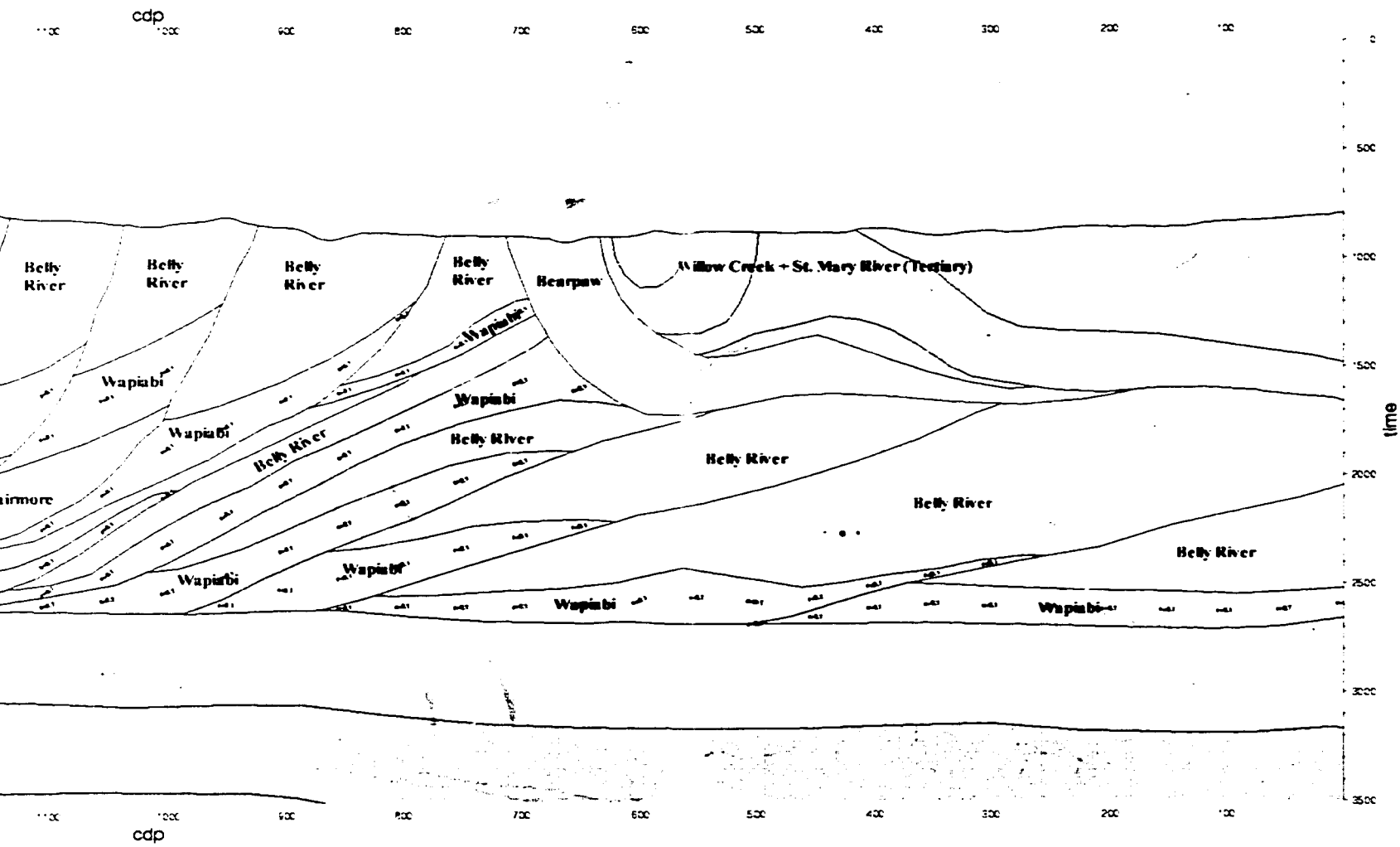

within the anisotropic formations.

three main regions: a region dominated by west-dipping reflectors; a region at the east end of the section incorporating the triangle zone and east-dipping events; and a lower region with essentially flat, coherent events below the overlying dipping sections. The upper west region of the section is dominated by lower to middle Cretaceous sediments, which have been thrusted steeply to the surface. These formations are the west dipping strata that form the western edge of the triangle zone and the hinterland. The upper eastern portion of the data contains the triangle zone structure and the gently dipping foreland structures of the Upper Brazeau and Tertiary strata. These strata dip mainly to the east. While the Mesozoic strata have been substantially folded and faulted, the deeper autochthonous Paleozoic and older basement strata are structurally undeformed. There are two locations in the basement Paleozoic strata, labelled 'A' and 'B', in Figure 6.1, where positive time structures are present. These occur below steeply dipping strata that outcrop at surface west of, and at, the triangle zone, respectively.

The west region extends from the edge of the section in the SW, to the western boundary of the triangle zone. There are two major, lower detachments located in this region. The upper of the two detachments runs through the base of the Blairmore, or top Kootenay strata, and carries all the surficial, middle and lower Cretaceous rock units. These rocks are highly faulted by several, west dipping, steep splays off the main detachment. As a result, the rocks are also steeply dipping to the west, some almost vertically dipping, as confirmed by the surface geology. This shallowest detachment is interpreted to eventually thrust to the surface as a major fault. The deeper detachment runs through the Blairmore unit, above the Paleozoic section. The rocks carried on this second detachment are interpreted to be the rocks which make up the core of the triangle zone. These consist primarily of rocks of the Belly River and Wapiabi formations, with smaller amounts of Blairmore Group strata.

The NE portion of the section contains the core of the triangle zone as well as a major eastward dipping fault, which carries the foreland dipping strata on the east side of the triangle zone. This fault is a major backthrust that brings the Bearpaw, St. Mary River

and Willow Creek formations to surface. A second east-dipping backthrust is also present in this region and converges to the first fault, at depth. In the core of the triangle zone, it has been interpreted that the rocks carried above the deep detachment of the middle region have been rotated to steep angles, which dip to the west, due to the compression of the underlying antiformal stack. Below the Upper Cretaceous/Tertiary strata, riding on the major backthrust in this region, several east-verging horses containing Belly River and Wapiabi strata have also been interpreted. These units have not been rotated to steep dip angles, as is the case in the core of the triangle zone.

6.3 Anisotropic Pre-Stack Depth Migration

Once the interpretation of the time migrated seismic section was completed, the interpretation was digitized into a velocity model builder. All the main horizons and major velocity contrast boundaries were included (Figure 6.2). The velocities assigned to each section, in the first migration model, were based on sonic log information provided by the two wells used in the interpretation of the seismic data. An initial value of ε = 0.10 was assigned to all the Wapiabi shale locations, which was determined from the refraction surveys (Chapter 4). δ, set to 0.025, remained constant throughout the initial depth migrations and was subsequently investigated in the final series of migrations. The dip was assigned based on the reflectors in the data. The depth migration routine used in the processing is the same as that used and described in Chapter 3. The results of this initial migration are shown in Figure 6.3. The image produced was not as coherent as the original time section (Figure 6.1). This is not unexpected since depth migration is more sensitive to migration velocities than is time migration.

Once an initial result was produced, an iterative process was then developed to improve the migrated image (Table 6.1). A velocity analysis tool was first used to refine the velocities, which allows the user to scan through several migrated sections, each with slightly different migration parameters applied. In this case, each section is migrated using a percentage of the current model velocities, typically 90 - 110%, in 2% increments. The velocity panel is then picked according to reflector continuity at the top and bottom

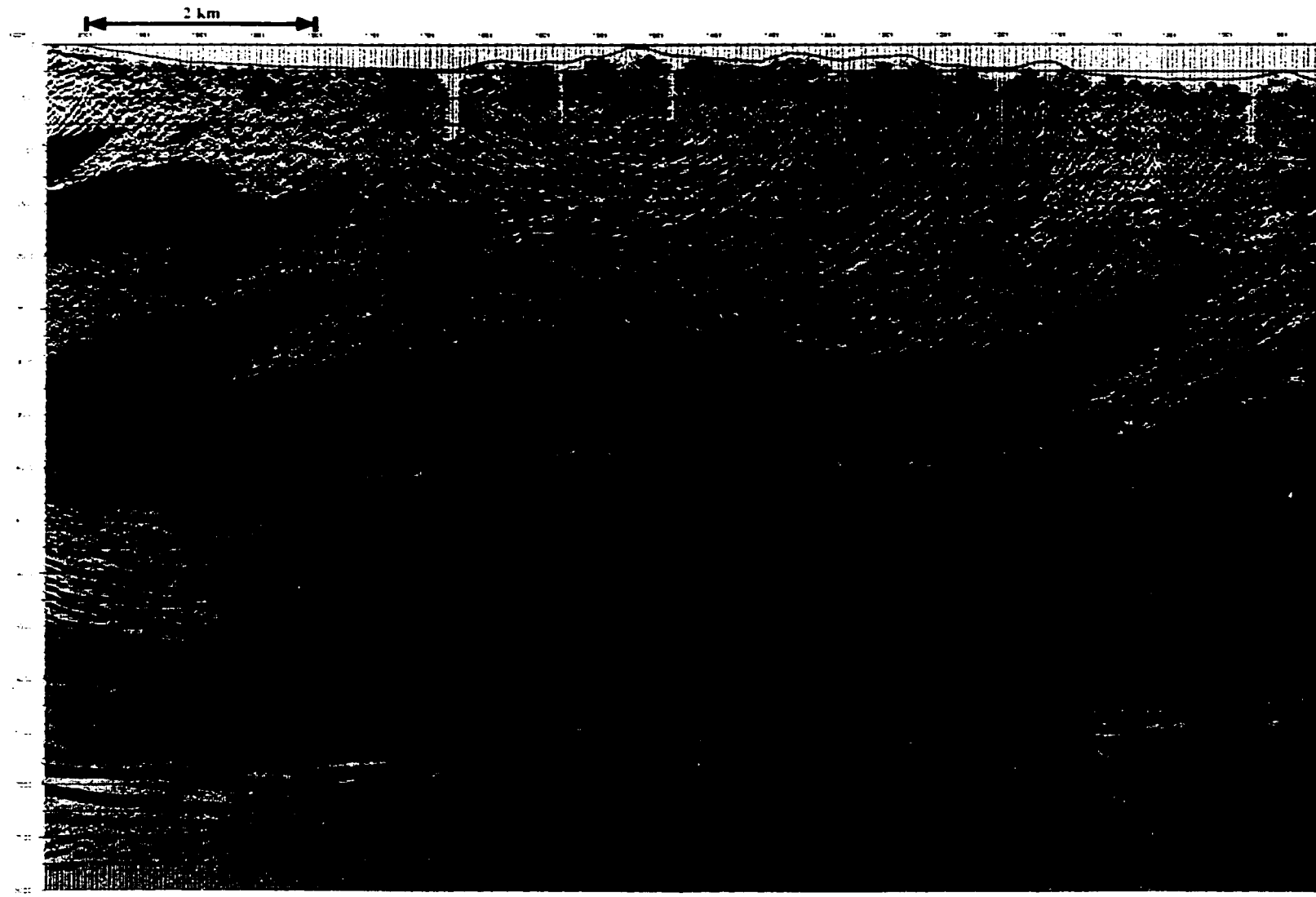

Figure 6.3. Anisotropic depth migrated section, using initial interpretation.

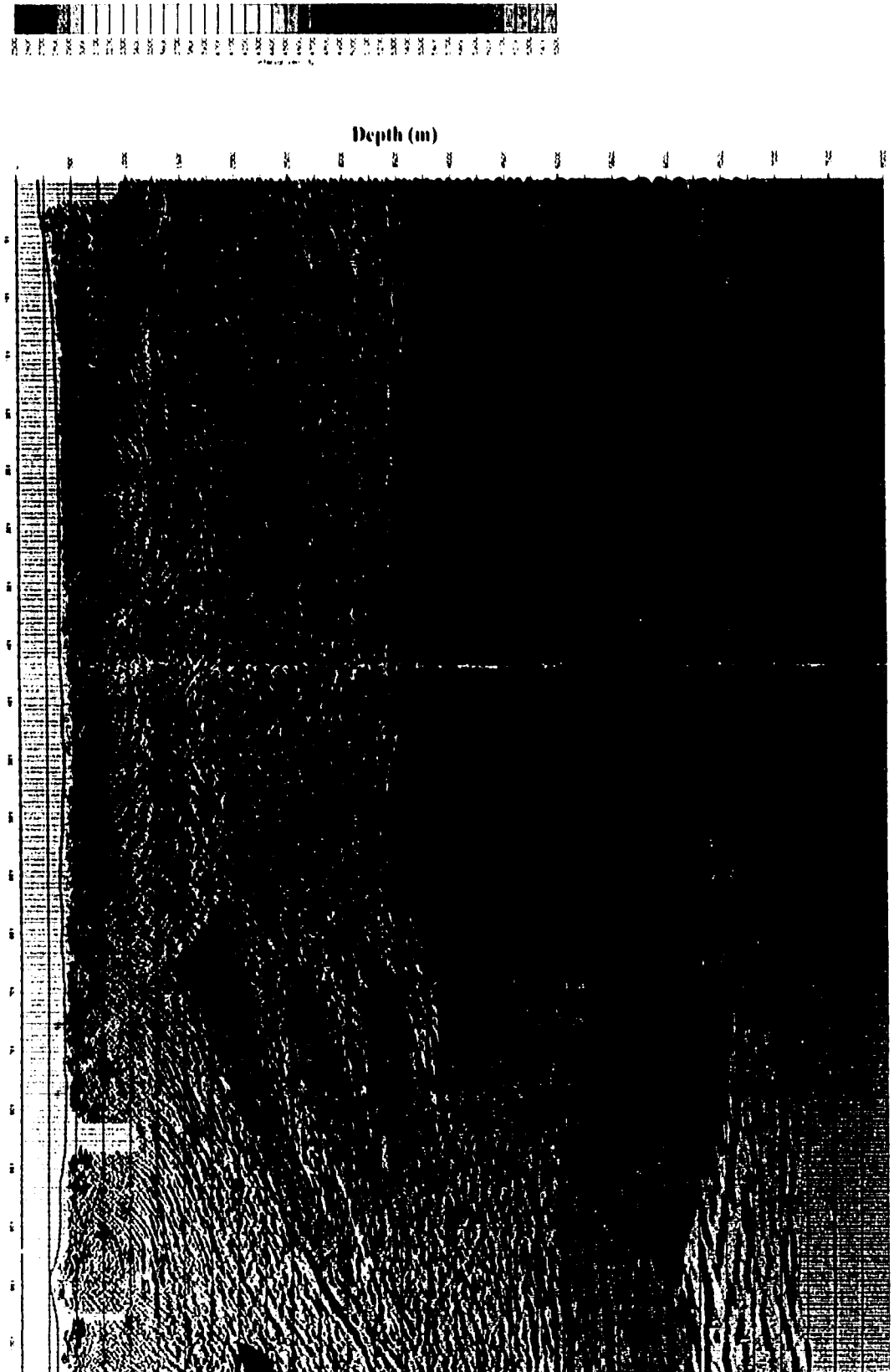
Depth (m)

of each velocity zone. These velocity zones do not change location in time, but they do have different depths after depth migration using each of the interpreted velocity models. The depth changes for each horizon are reflected in changes in the interpreted interval velocity in the model. The interpreted velocities were then assigned in the velocity builder and the migration was rerun. Secondly, the updated migrated section was used to further refine the velocities by evaluating the common image gathers (CIG) [Zhu et al., 1998; Chapter 3]. The velocity model builder allowed for the gathers to be recalculated based on any velocity changes in the model. This meant that the velocities could be modified, according to whether the gather indicated that the velocity was too high or too low [Zhu et al., 1998]. Again the velocity model was updated and the migration rerun. The final result, after changes to the interval velocities and gathers, is shown in Figure 6.4. There is substantial improvement to the section, from the first iteration (Figure 6.3).

Table 6.1. Methodology used to produce final ADM section.

Step	***Procedure***
1	Time migrated section
2	Interpretation
3	Velocity model (time), assigning initial v_o, ε and δ
4	Velocity model (depth)
5	Depth migration
6	Iterate over v_o
7	Check CIG (smiles and frowns) (back to **4**)
8	Check velocity boundaries (back to **4**)
9	Iterate over ε
10	Iterate over δ
11	Final section

It was decided that Figure 6.4 was the best anisotropic depth migrated image that could be obtained using the original geometric interpretation. Since the migrated image had been improved through several iterations, it was evident that some of the original horizon boundaries, from the initial geometric interpretation, had changed. As such, modification of the geologic model was deemed necessary. Using the velocity model builder, it was possible to make the necessary adjustments to the time horizons in order to match the data more correctly. The migration was then updated and the previous steps repeated.

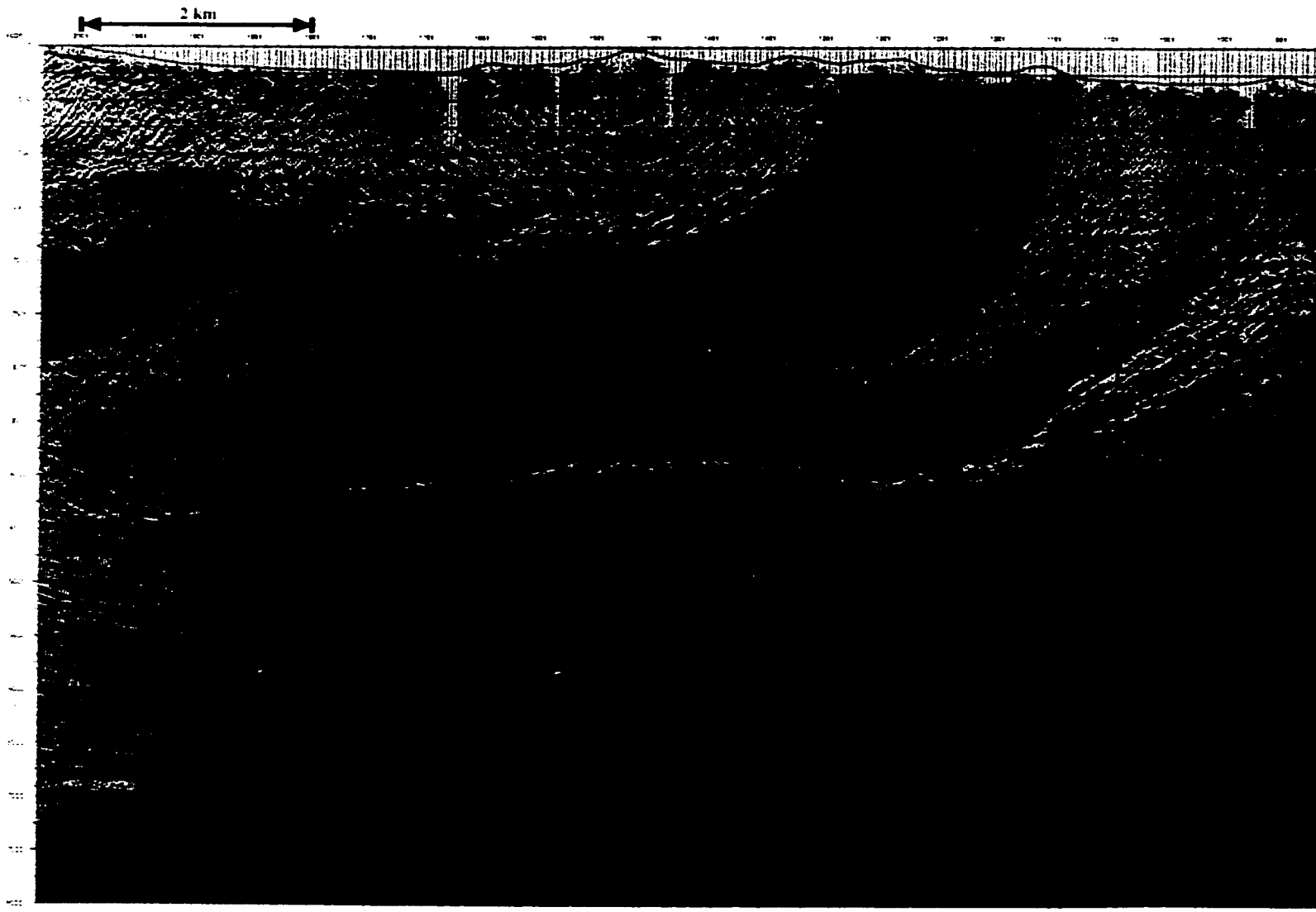

Figure 6.4. Anisotropic depth migrated section, using updated velocity model and original interpretation.

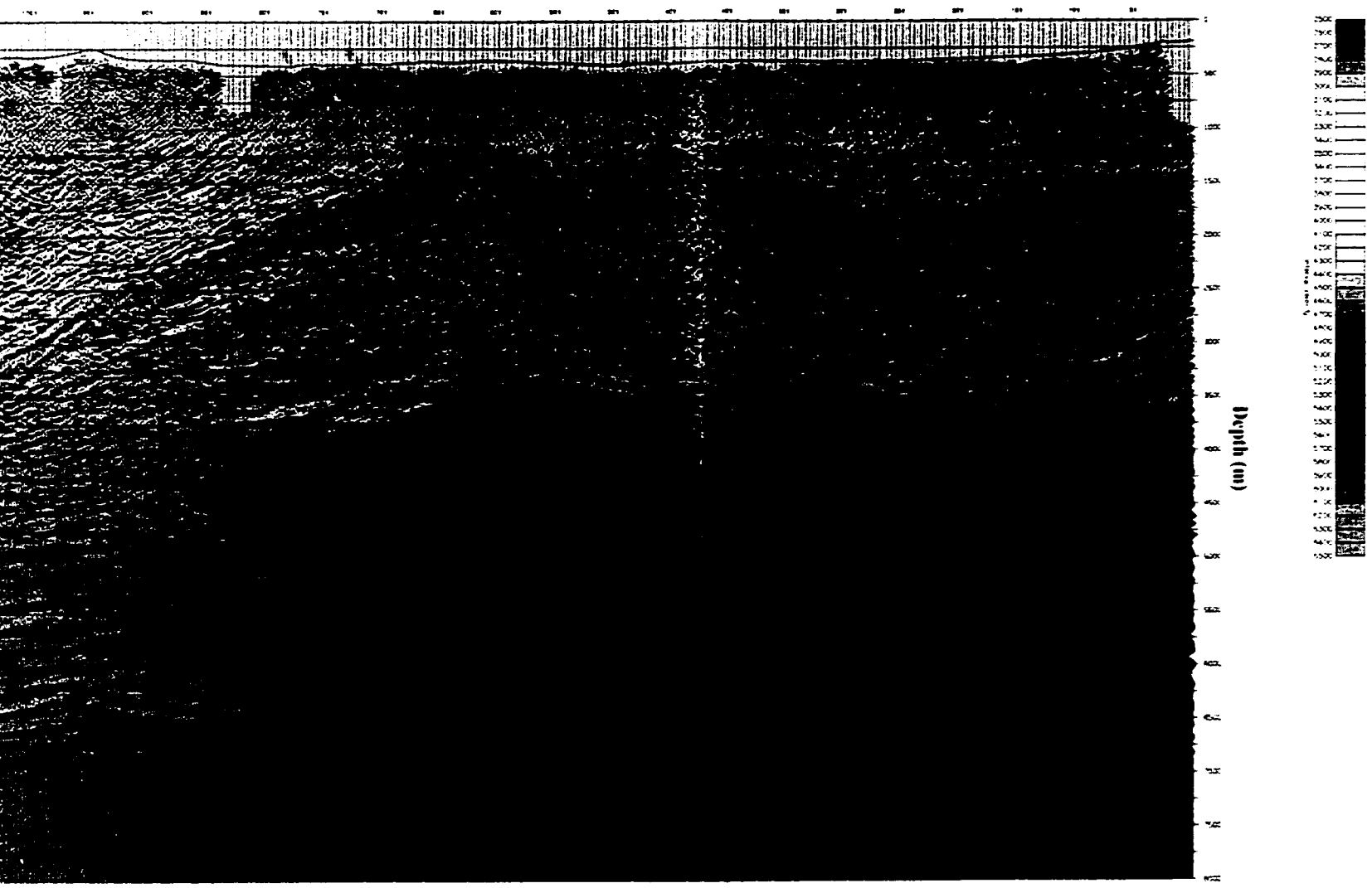

retation.

The velocity analysis tool was again used and the interval velocities were updated. Then the common image gathers were scrutinized [Zhu et al., 1998] and the velocities were updated again. The results of these changes are seen in Figure 6.5 and, once again, improvement to the image was obtained as compared to the section in Figure 6.4.

After the optimal migrated section was obtained, additional iterations were undertaken to examine the effects of the anisotropic parameters in the migration process. The velocity analysis tool was again used to independently increase and decrease the values of ε and δ in the portions of the velocity model interpreted to be Wapiabi shales. Final anisotropic parameters of $\varepsilon = 0.12$ and $\delta = -0.03$ were chosen based on the values that best focussed the migrated image. These parameters were updated in the velocity model builder and the whole section was fine-tuned, again using the velocity analysis tool. The final result is depicted in Figure 6.6. The section has been greatly improved over the previous results (Figures 6.3-6.5) and it is comparable to the original time section (Figure 6.1) in terms of image quality and overall signal-to-noise ratio. In addition, for comparison, the anisotropic parameters were set to zero in the velocity model and the data were migrated using an isotropic velocity model (Figure 6.7).

6.4 Comparison of Migrated Sections

In order to assess the effectiveness of the anisotropic depth migration (ADM), the final anisotropic depth image was compared to both the isotropic depth (IDM) and time migrated sections. In Figure 6.8, CDP's 151-351 were compared. It can be seen that there is a time discontinuity in the Paleozoic portion of the section, at ~2500 ms, which may be interpreted as a normal fault. However this structure is not present in the ADM section. Therefore this interpreted basement fault is probably not a real structure, but rather a manifestation of the steeply dipping strata, constituting part of the triangle zone, in the shallow part of the section.

From CDP's 401-601 (Figure 6.9), it is seen that the depth images, both isotropic and anisotropic, are very similar. Some new reflectors have been imaged in these depth

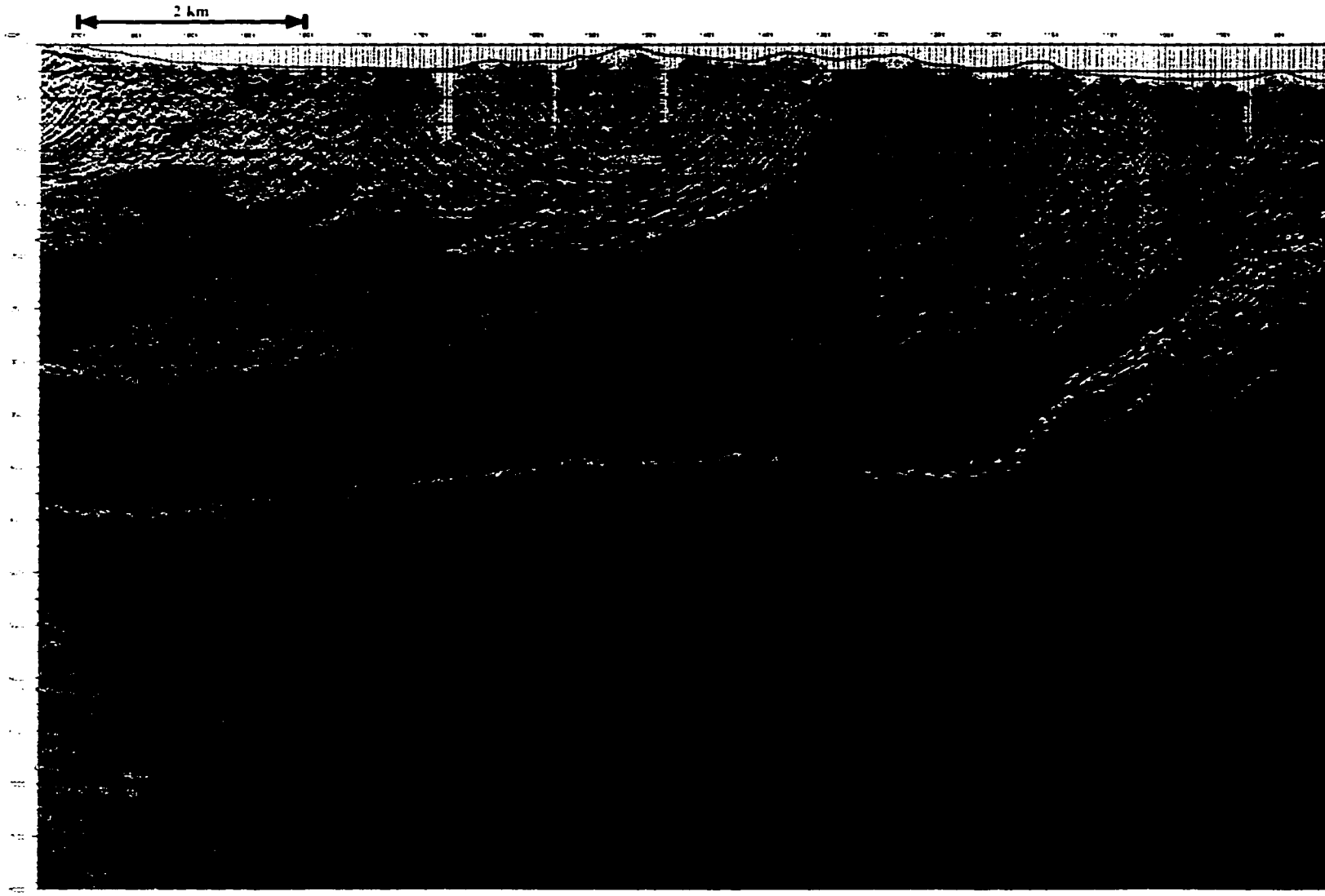

Figure 6.5. Anisotropic depth migrated section, using updated interpretational model.

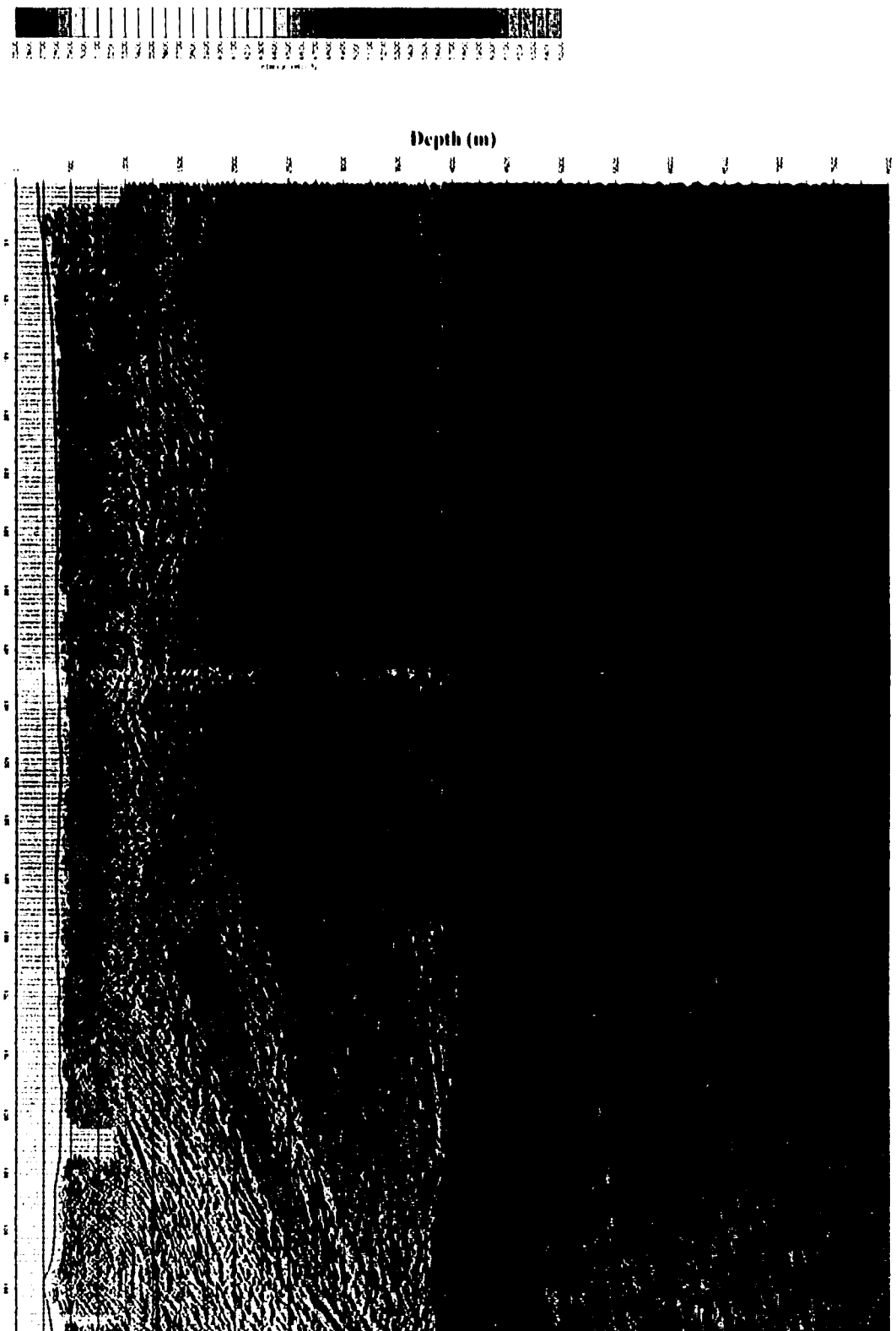
Depth (m)

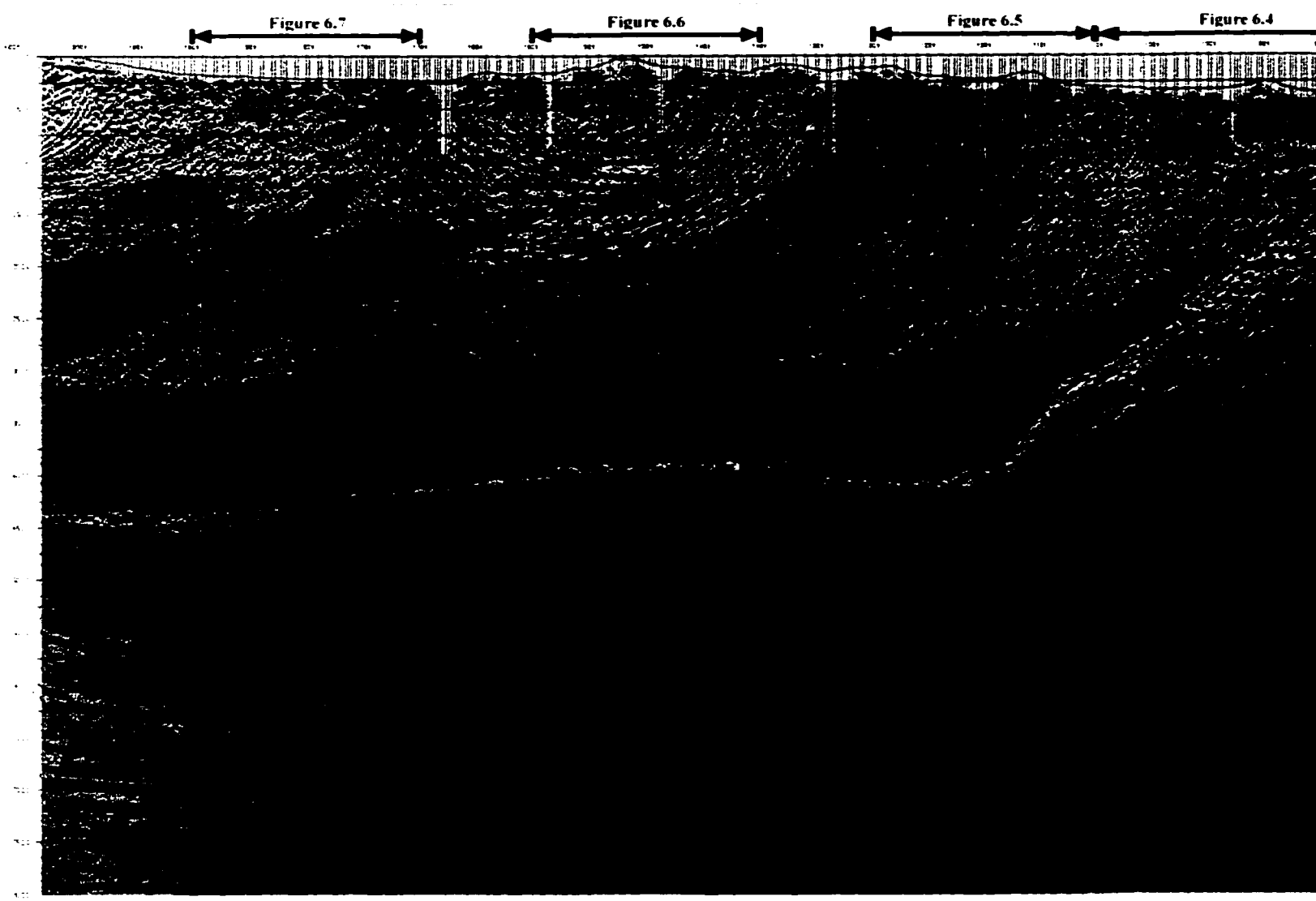

Figure 6.6. Final anisotropic depth migrated section.

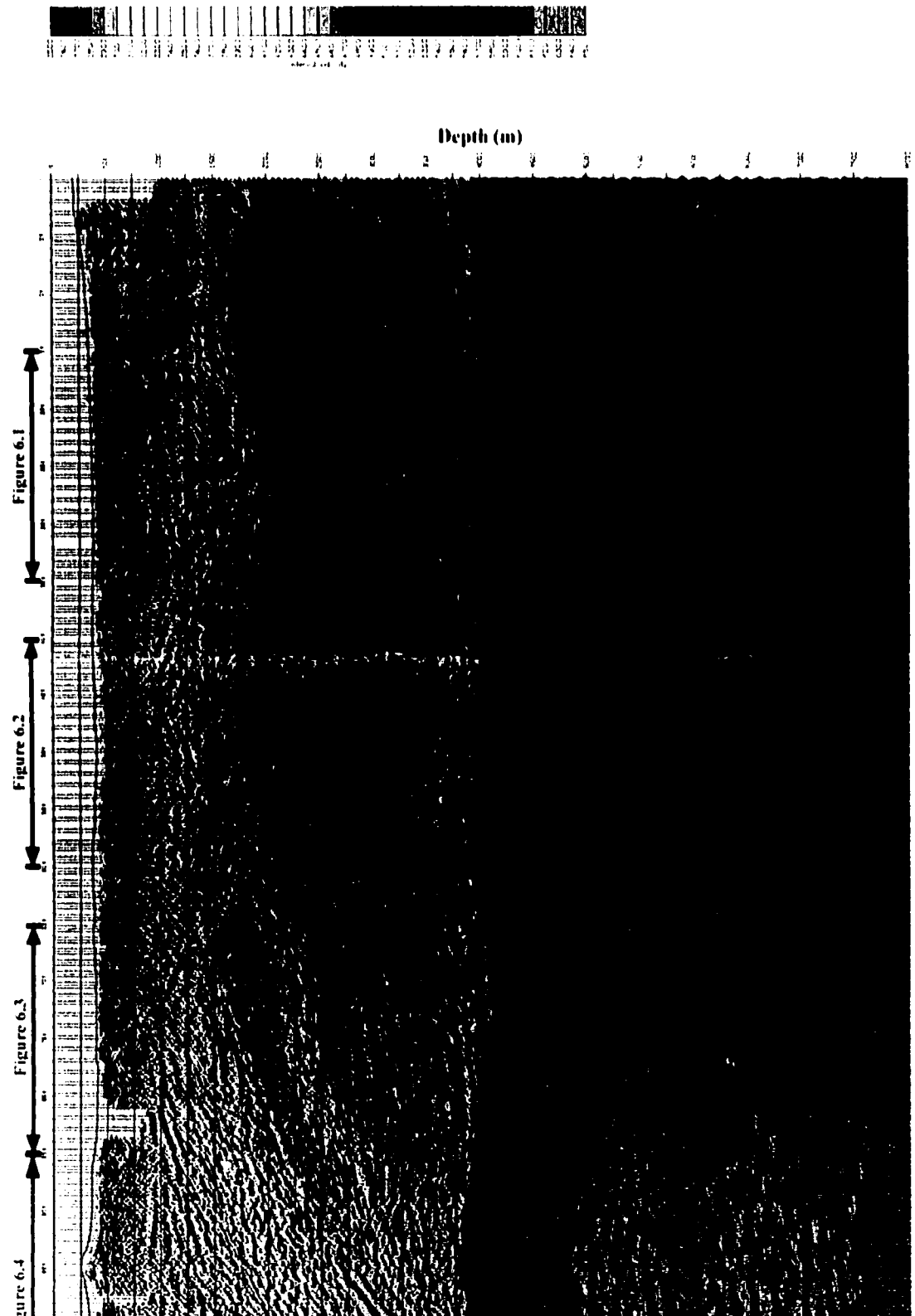
Depth (m)
Figure 6.1
Figure 6.2
Figure 6.3
Figure 6.4

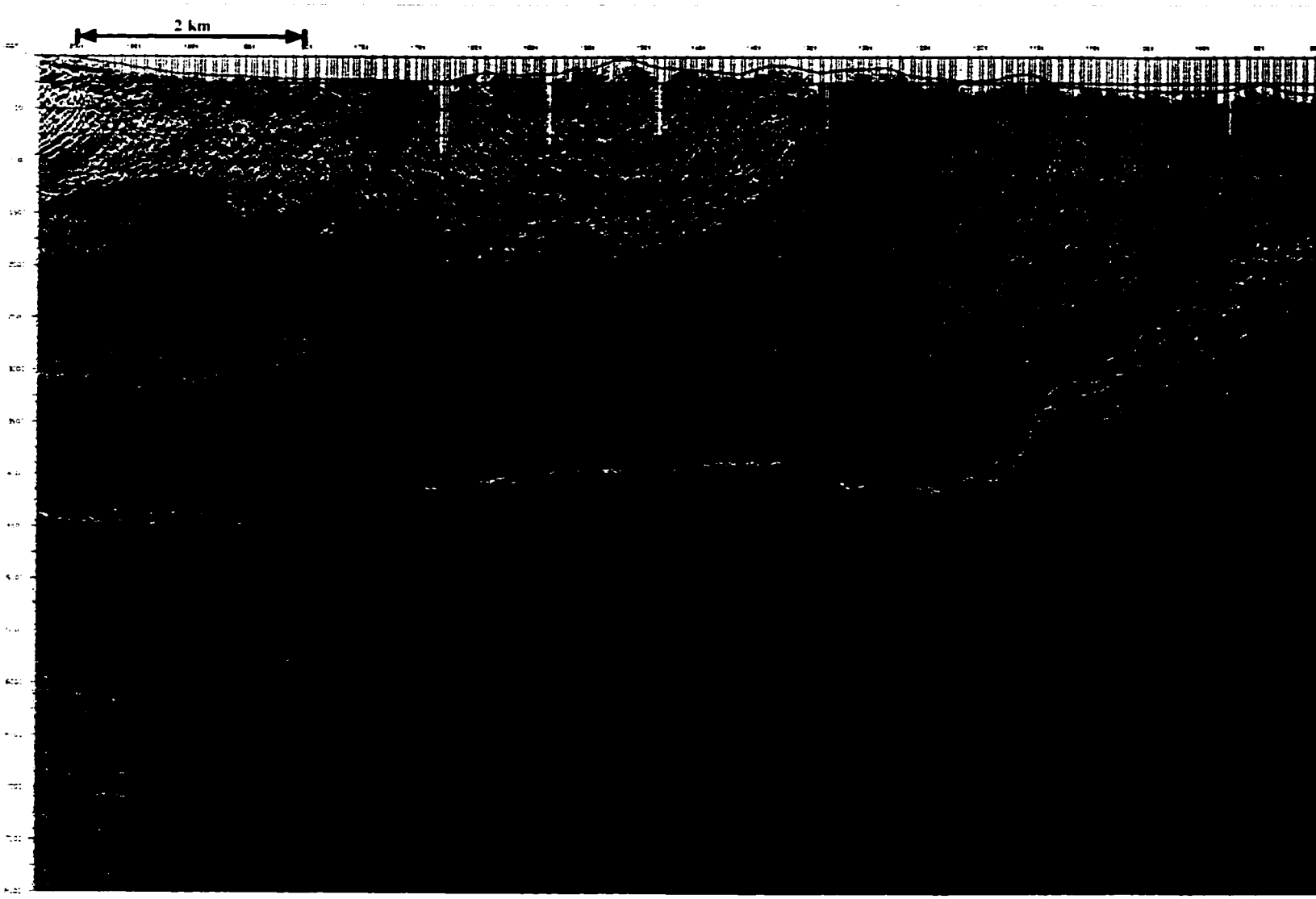

Figure 6.7. Final isotropic depth migrated section.

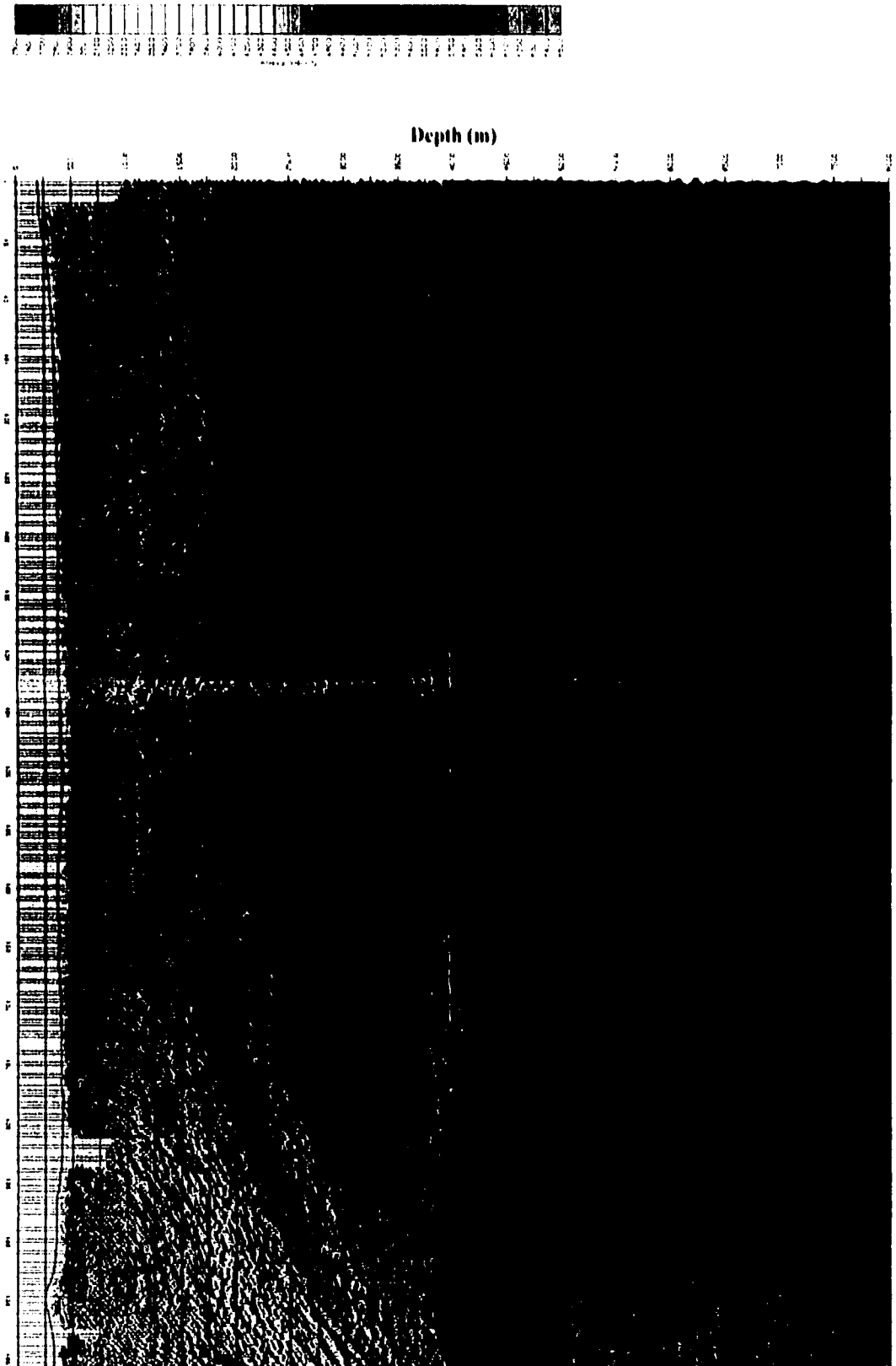
Depth (m)

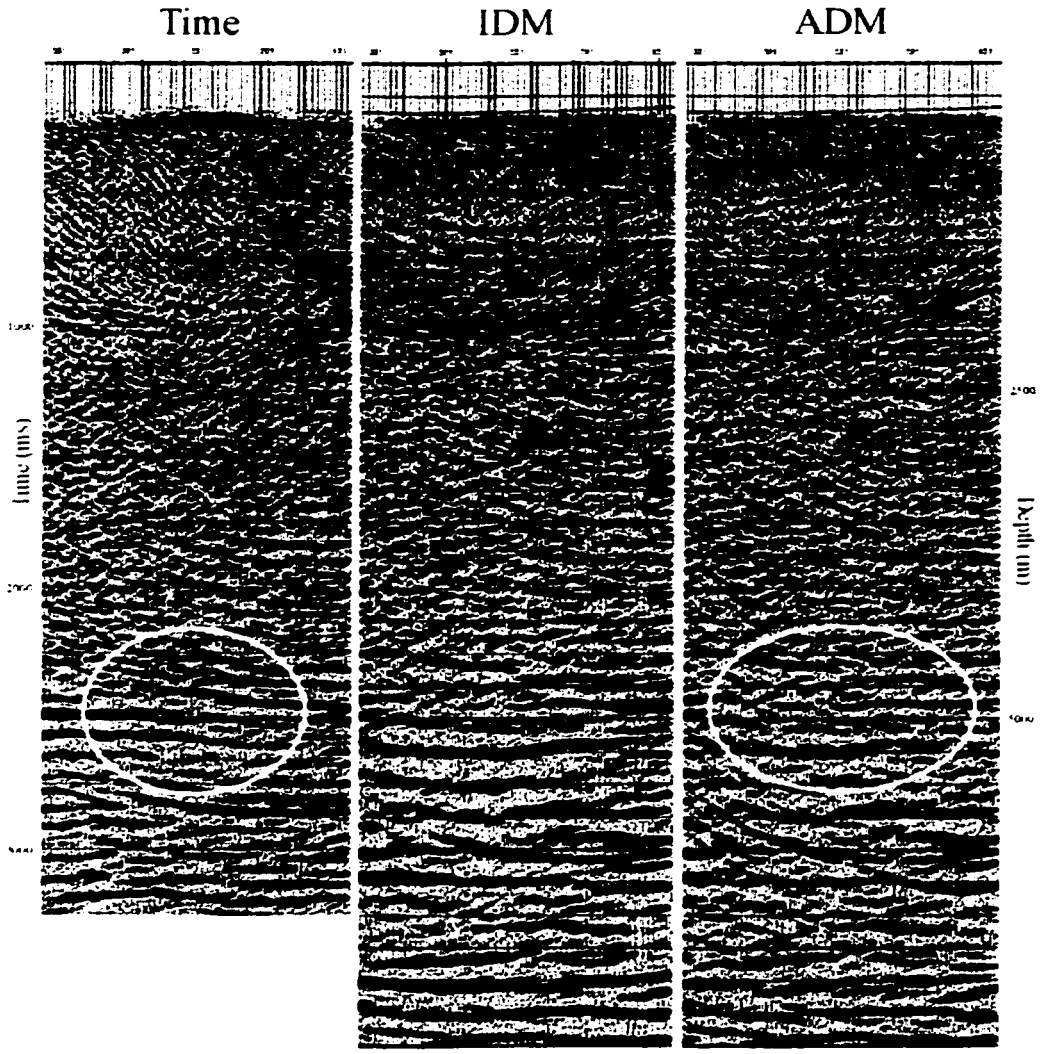

Figure 6.8. Comparison of migrated sections: at left is the pre-stack time migration; in the centre is the isotropic depth migrated section (IDM); and at right is the optimal anisotropic depth migrated section (ADM). The fault interpreted in the time section is not present in the ADM section; hence, it is considered to be a time anomaly. The ADM section also gives a more continuous, hence more interpretable, image of these deeper reflectors than the IDM section.

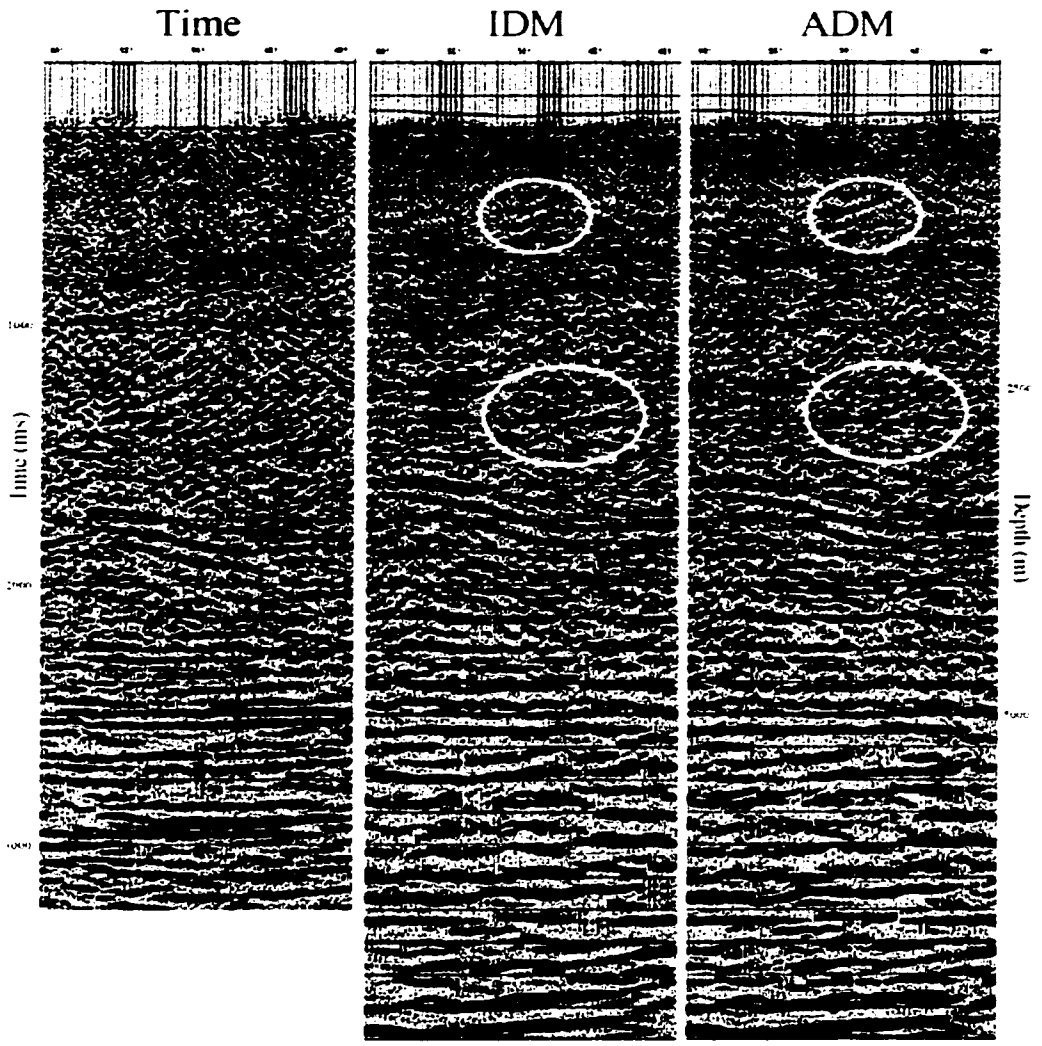

Figure 6.9. Comparison of migrated sections: at left is the pre-stack time migration; in the centre is the isotropic depth migrated section (IDM); and at right is the optimal anisotropic depth migrated section (ADM). The two depth images are very similar in this section of the data. The structures are not complicated in this area and thus the anisotropy does not significantly affect the results.

sections that were not seen in the time section. The similarity between the two depth images results from the relatively unstructured nature and gentle dips of the strata in this area.

In the triangle zone, CDP's 651-851, the ADM section has more reflectors than the time section and better continuity of reflectors than in the IDM section (Figure 6.10). The structural complexity of the triangle zone, in addition to the anisotropy, is best treated by the ADM.

In the presence of steeply dipping reflectors, CDP's 851-1101, the isotropic and anisotropic depth images give better dip images in the shallow part of the section; however, it compromises the basement structures at depth, as a direct consequence (Figure 6.11). Since imaging these dips in the near surface was one focus during the depth migrations, the assignment of short wavelength structure and dips in the shallow portion of the section complicated the migration velocity model in the near surface. The addition of structural complexity in the near surface velocity model thus complicates the imaging of deeper structures, resulting in the near surface, dipping strata being imaged better than the deeper strata, in both migrated sections (IDM and ADM). In addition, the deeper reflectors in the ADM section are imaged slightly better than in the IDM section, since the overmigration of the deeper reflectors in the ADM section is less pronounced.

Figure 6.12, CDP's 1101-1301, indicates that different depth locations of the Paleozoic strata, between the IDM and ADM sections, occur under steeply dipping surface reflectors. The IDM section places the Mississippian reflector shallower in depth than in the ADM section, as expected, since the rotation of the strata is not taken into account in the IDM result. As such, the migration velocities are too low, placing the reflector shallower in depth in the final image. Unfortunately, there were no wells on the line directly to evaluate the tie to the migrated data. Judging from the modelling results in Chapter 3; however, the ADM result is considered to be the more correct image.

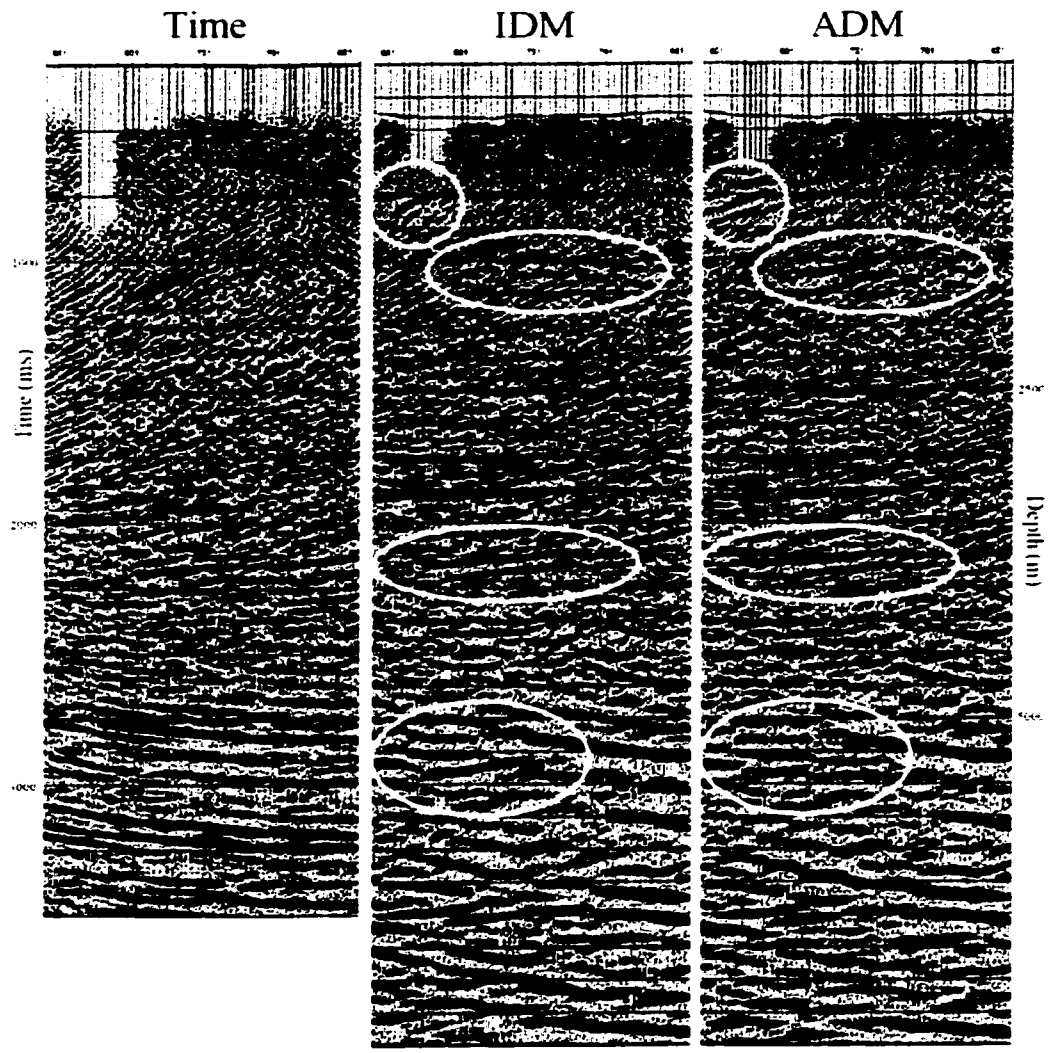

Figure 6.10. Comparison of migrated sections: at left is the pre-stack time migration; in the centre is the isotropic depth migrated section (IDM); and at right is the optimal anisotropic depth migrated section (ADM). In this section, the ADM brings out more reflectors than the time section and better continuity of these reflectors than the isotropic solution.

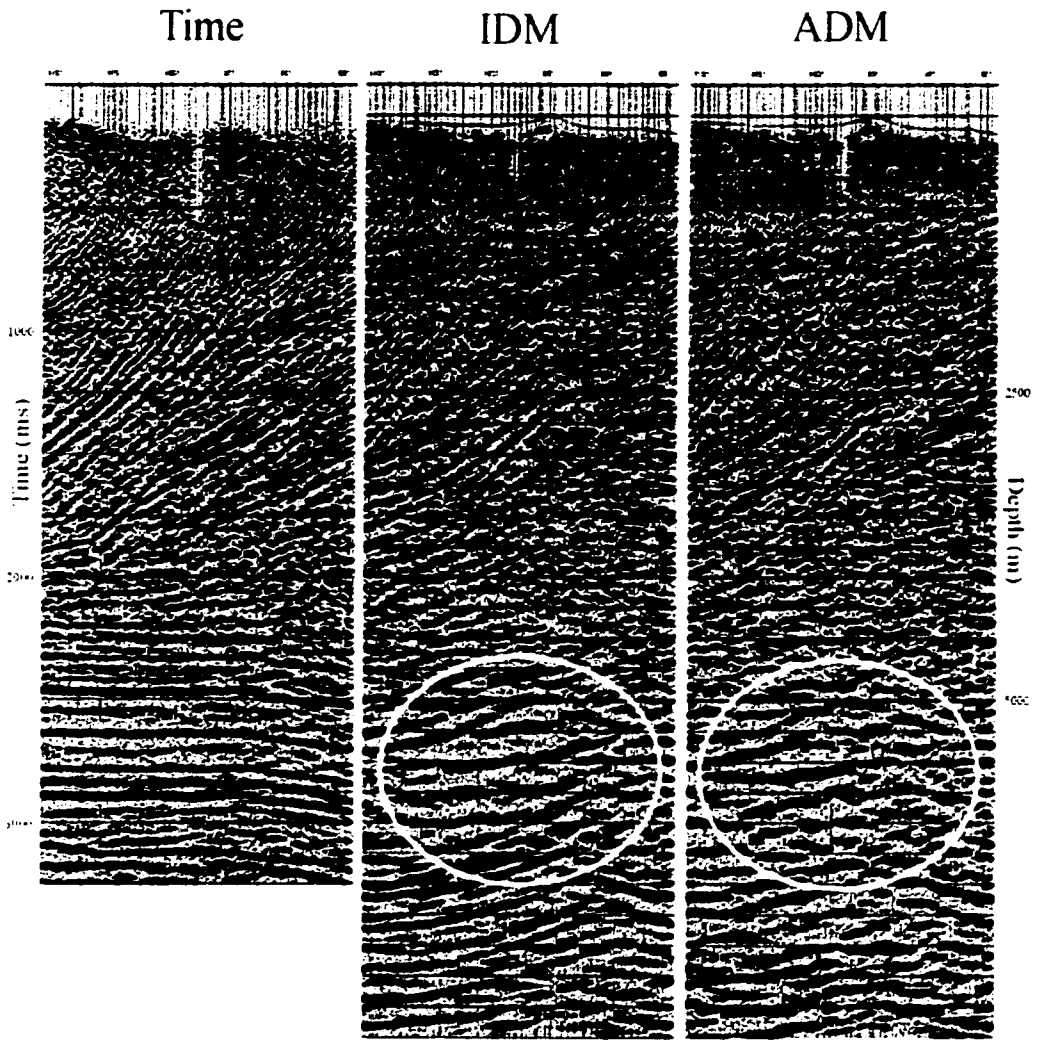

Figure 6.11. Comparison of migrated sections: at left is the pre-stack time migration; in the centre is the isotropic depth migrated section (IDM); and at right is the optimal anisotropic depth migrated section (ADM). The depth migrations give better dip information in the shallow portion of the section, however, they complicate the basement structures, as a direct result. As well, the ADM section is not as overmigrated as the IDM section, in the highlighted area.

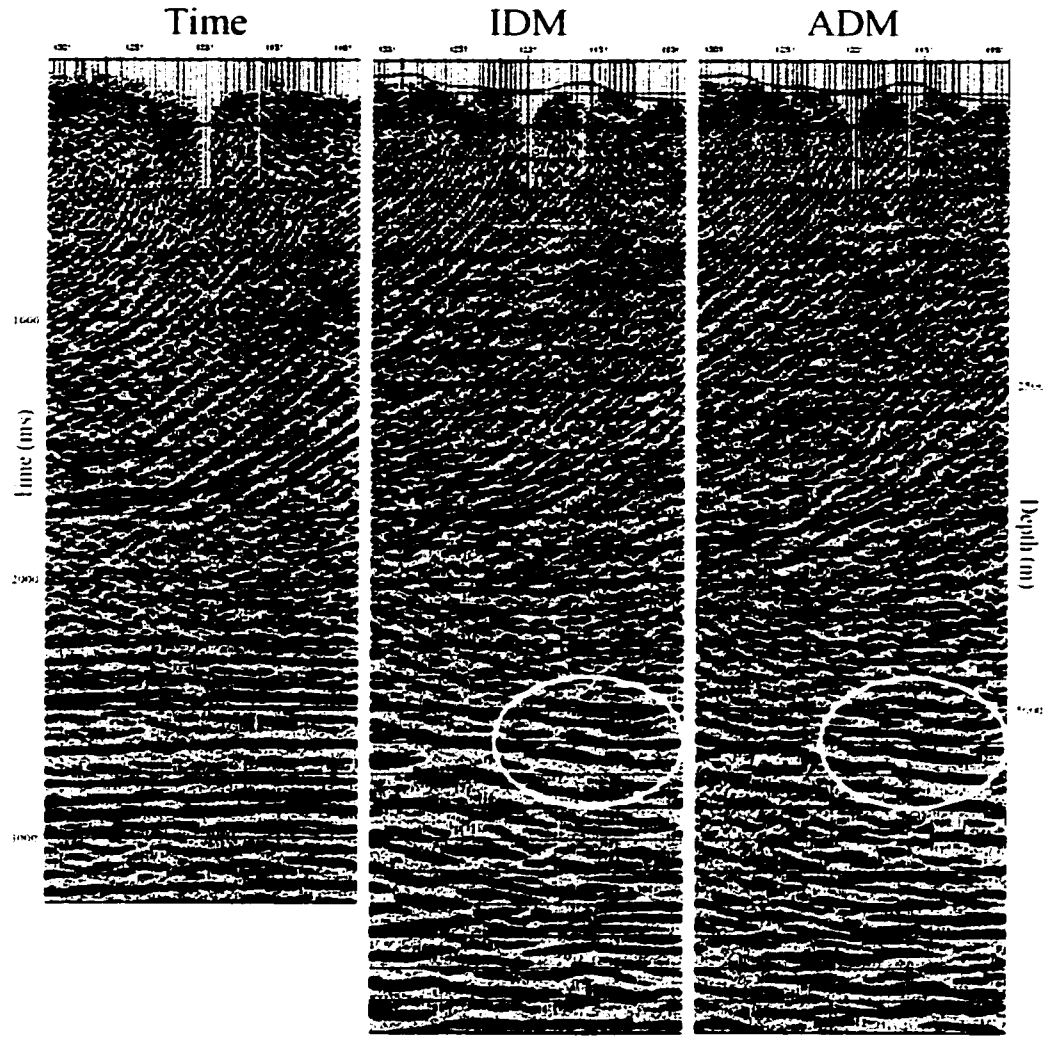

Figure 6.12. Comparison of migrated sections: at left is the pre-stack time migration; in the centre is the isotropic depth migrated section (IDM); and at right is the optimal anisotropic depth migrated section (ADM). Note the different depth location of the Mississippian reflector between the isotropic and ADM solutions. The steeply dipping strata in the near surface seriously affect the isotropic migration.

In the location of CDP's 1401-1601, in Figure 6.13, the time discontinuity of the Mississippian reflector has been enhanced in the ADM section. Since this structure remains in the depth section, it is considered a real structure, such as a duplex involving Fernie strata, and not a manifestation of the processing algorithms. In addition, the ADM section displays better continuity in the shallow reflectors than both the IDM and time sections.

In the relatively flat-lying reflectors found at CDP's 1701-1901, the three sections are comparable (Figure 6.14). Since no anisotropy was considered in this portion of the data and the structures are not complicated, the three migrations are expected to be similar in terms of image quality.

Due to the complexity of the section, it is doubtful whether any further major improvements can be made to the anisotropic depth image, at this time. In the future, with better control of the anisotropic parameters and refined migration processes, it will be possible to improve on this final image.

6.5 Discussion

Anisotropic depth migration is an effective tool in areas of steeply dipping anisotropic strata. Depth migration is preferred to time migration since the ultimate goal must be comparable to a geologic cross-section. Depth migration of this data resulted in better imaging of the dipping reflectors in the shallow portion of the section; however, often at the expense of the quality of the image of the deeper reflectors. If less detail is incorporated in the shallow portions of the velocity model, a better image of the deeper reflectors may be obtained. Hence, the focus of the migration needs to be determined before the data are migrated.

Anisotropic depth migration yields a more complete image than the isotropic image. The incorporation of anisotropy into the migration code adjusts for the lateral and depth mispositioning errors often found if the data were migrated isotropically. This was seen

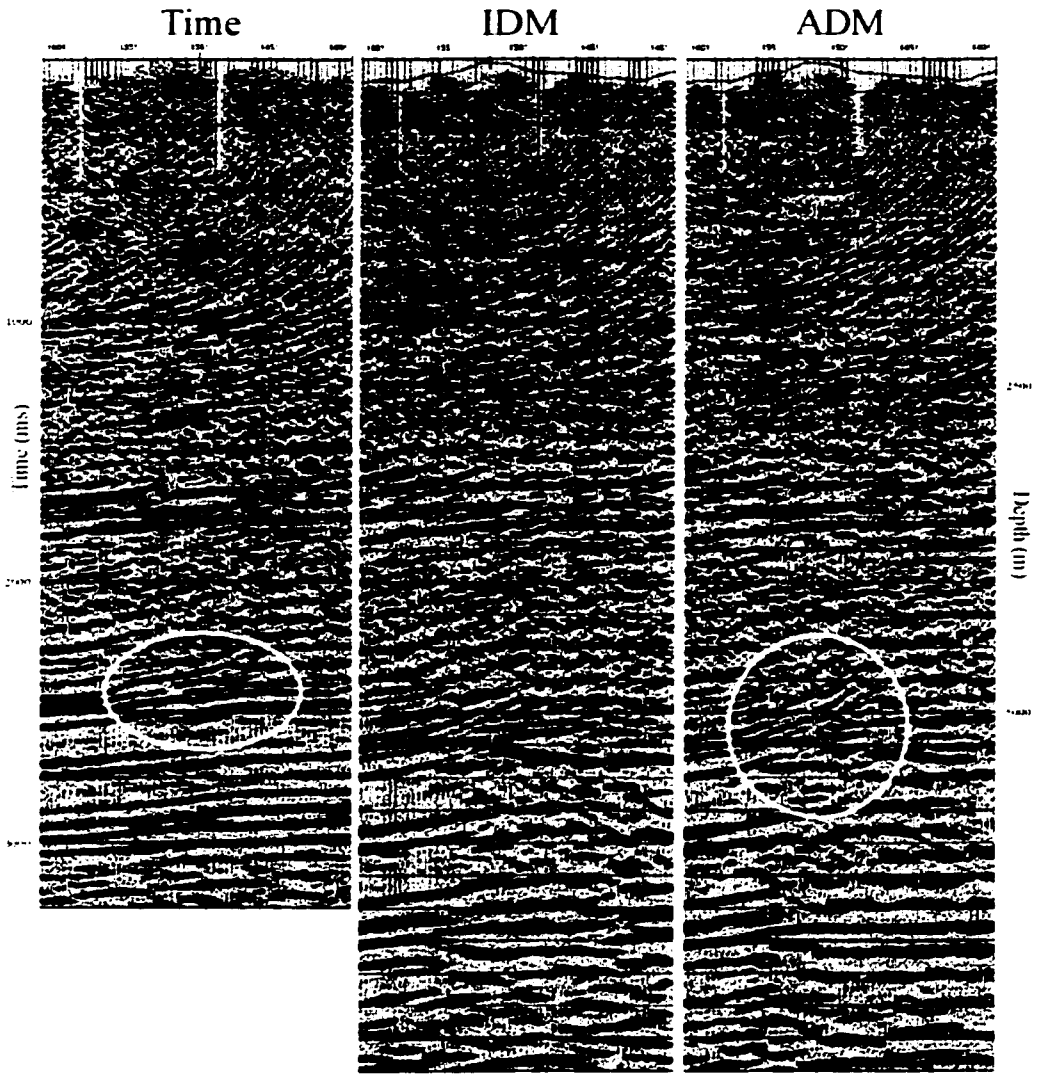

Figure 6.13. Comparison of migrated sections: at left is the pre-stack time migration; in the centre is the isotropic depth migrated section (IDM); and at right is the optimal anisotropic depth migrated section (ADM). The time structure present in the time data is also present in the ADM section. This may be a real subsurface structure, such as a duplex involving Fernie strata. Note also that the ADM image is more continuous than the IDM image. Also, the shallow portion of the section shows better continuity in the ADM section, than in both the IDM and time sections.

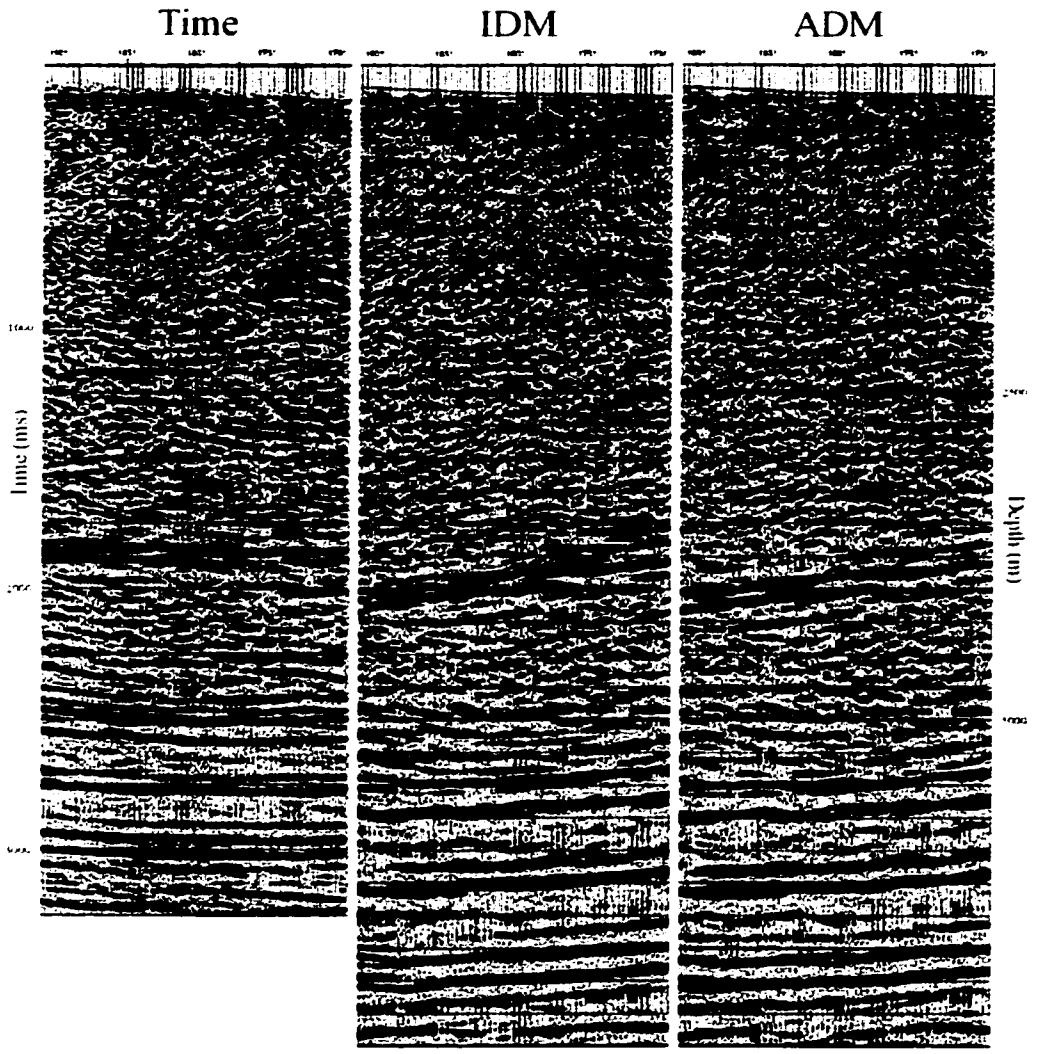

Figure 6.14. Comparison of migrated sections: at left is the pre-stack time migration; in the centre is the isotropic depth migrated section (IDM); and at right is the optimal anisotropic depth migrated section (ADM). In this section of the data, the strata are relatively flat lying and no anisotropy has been assigned to the structures. This results in all three images being similar.

in Figure 6.12 where the depth of the Mississippian reflector was located too shallow in depth in the isotropic image. In Figure 6.13, the apparent time structure was also better imaged with the anisotropic result than with the isotropic result. This reinforces the idea that the structure may be real.

The complexity of the section, at present, seems to hinder the resolution of the overall anisotropic image. With better acquisition and migration routines as well as better knowledge of the anisotropic parameters of rocks in the area, more improvement could be expected.

CHAPTER 7 CONCLUSIONS

7.1 Conclusions

One of the important contributions of this thesis is the demonstrated evidence of traveltime anomalies, in time recorded data, which are due to seismic velocity anisotropy. Traveltime anomalies were identified in the seismic data from two physical models containing dipping anisotropic layers and these anomalies could be successfully predicted using numerical modelling techniques (Chapter 2), a result considered to be significant. The close correlation between the model data and the predicted results indicates that a general anisotropic raytracer has been successfully developed. The depth migration of these model data, discussed in Chapter 3, has demonstrated that isotropic pre-stack depth migration is limited in its ability to correctly migrate data from these anisotropic physical models, as it leads to discrepancies and conflicts between the correct reflector depth and the residual moveout in image gathers. In order to account for these discrepancies correctly, anisotropic depth migration routines need to be used. However, prior knowledge of the anisotropic parameters and geometry of the velocity model is necessary for this process.

Measuring the anisotropic parameters of rocks is not an easy task. In this thesis, two new methods were developed, that allow for the *in situ* measurement of seismic velocities at various angles through bedding, from which the anisotropic parameters can be computed. These methods have not previously been considered by other researchers. By measuring the velocity of rocks *in situ*, a more accurate determination of these parameters is possible, instead of attempting to recreate these conditions in the laboratory, which is difficult. In addition, these methods allow for measurements using true seismic wavelengths, instead of high frequencies (i.e. short wavelengths), which are necessary for laboratory measurements. By using refraction techniques, developed in Chapter 4, the anisotropic parameters of steeply dipping rock formations were determined. In Chapter 5, VSP methods were extended to measure the anisotropic parameters of moderately dipping strata. Both of these methods were successful and can be performed in the Alberta

Foothills, in order to quantify the anisotropy of various anisotropic rock units. This allows for the accurate determination of the anisotropic parameters for use in depth migration routines.

Anisotropic pre-stack depth migration (ADM) methodologies were developed and tested using both synthetic data as well as a real dataset from the Alberta Foothills. The two physical model datasets were migrated using ADM techniques, presented in Chapter 3, which successfully eliminated the traveltime anomalies from the final depth sections. In Chapter 6, it was demonstrated that ADM is an effective tool in the processing of real seismic data, especially in the presence of steeply dipping strata. The depth migrated data offered a more robust section than the time migrated data and thus, yielded a more complete image of the subsurface. Also, the inclusion of anisotropic velocity models in the pre-stack depth migration process does not further complicate the problem, but allows for improved focussing of the final section through an iterative process of varying individual parameters. The key to using ADM successfully is the development of the velocity model. The assignment of the various parameters, such as perpendicular-to-bedding velocity, dip and anisotropic parameters, as well as the geologic boundaries, is very important to the ADM process. Variation of these parameters, within geologic and well log constraints as developed in Chapter 6, allowed for a complete and accurate depth migrated image to be produced.

This thesis has yielded a deeper understanding of the effects of seismic velocity anisotropy on seismic imaging and has developed new methods to predict and compensate for these effects. ADM is necessary for the correct processing of seismic data recorded over anisotropic strata but it requires more input parameters than conventional processing. By incorporating the anisotropic parameters, determined through *in situ* techniques, into processing routines, velocity anomalies and other depth and lateral mispositioning errors due to anisotropy, can be mitigated in the seismic data. Consequently, the correct positioning of exploration targets, both laterally as well as in

depth, can be achieved, particularly in structurally complex areas. As a result, a more accurate depth image of the subsurface exploration target can be obtained.

REFERENCES

Alkhalifah, T. and Tsvankin, I., 1995, Velocity analysis for transversely isotropic media: Geophysics, **60**, p. 1550-1566.

Banik, N.C., 1984, Velocity anisotropy of shales and depth estimation in the North Sea basin: Geophysics, **49**, p.1411-1419.

Backus, G.E., 1962, Long-wave elastic anisotropy produced by horizontal layering: J. Geophys. Res., **67**, No. 11, p.4427-4440.

Berryman, J.G., 1979, Long wavelength anisotropy in TI media: Geophysics, **44**, p.896-917.

Byun, B.S., 1982, Seismic parameters for media with elliptical velocity dependencies: Geophysics, **47**, p.1621-1626.

Cassell, B., 1984, Vertical seismic profiles – an introduction: First Break, November, p.9-19.

Chapman, C.H., and Pratt, R.G., 1992, Traveltime tomography in anisotropic media -I. Theory: Geophys. J. Int., **109**, p.1-19.

Cheadle, S.P., Brown, R.J. and Lawton, D.C., 1991, Orthorhombic anisotropy: a physical seismic modeling study: Geophysics, **56**, p.1603-1613.

Crampin, S., 1977, A review of the effects of anisotropic layering on the propagation of seismic waves: Geophys. J. R. astr. Soc., **49**, p.9-27.

Crampin, S., 1986, Anisotropy and transverse isotropy: Geophys. Prosp., **34**, p.94-99.

Daley, P.F., and Hron, F., 1977, Reflection and transmission coefficients for transversely isotropic media: Bull. Seis. Soc. Am., **67**, No. 3, p.661-675.

Dellinger, J., and Vernik, L., 1994, Do traveltimes in pulse-transmission experiments yield anisotropic group or phase velocities?: Geophysics, **59**, p.1774-1779.

Gaiser, J.E., 1990, Transversely isotropic phase velocity analysis from slowness estimates: J. Geophys. Res., **95**, No. B7, p.11,241-11,254.

Gendzwill, D.J., 1993, Seismic velocity, fracture density and anisotropy of some Manitoba limestones: Canadian Journal of Exploration Geophysics, **29**, p.153-162.

Gilpatrick, R. and Fouquet, D., 1989, A users guide to conventional VSP acquisition: The Leading Edge, March, p.34-39.

Gordy, P.L., Frey, F.R. and Norris, D.K., 1977, Geological guide for the Canadian Society of Petroleum Geologists and the 1977 Waterton-Glacier Park Field Conference: Calgary, Alberta, Canadian Society of Petroleum Geologists.

Hagedoorn, J.G., 1959, The plus-minus method of interpreting seismic refraction sections: Geophys. Prosp., **7**, p.158-182.

Helbig, K.,1994, Foundations of anisotropy for exploration seismics: Pergamon.

Hornby, B.E., Schwartz, L.M., and Hudson, J.A., 1994, Anisotropic effective-medium modelling of the elastic properties of shales: Geophysics, **59**, p.1570-1583.

Johnston, J.E., and Christensen, N.I., 1995, Seismic anisotropy of shales: Journal of Geophysical Research, **100**, p.5991-6003.

Jones, L.E.A., and Wang, H.F., 1981, Ultrasonic velocities in cretaceous shales from the Williston Basin: Geophysics, **46**, p.288-297.

Kebaili, A., and Schmitt, D.R., 1996, Velocity anisotropy observed in wellbore seismic arrivals: combined effects of intrinsic properties and layering:. Geophysics, **61**, p.12-20.

Keith, C.M., and Crampin, S., 1977a, Seismic body waves in anisotropic media: reflection and refraction at a plane interface: Geophys. J. R. astr. Soc., **49**, p.181-208.

Keith, C.M., and Crampin, S., 1977b, Seismic body waves in anisotropic media: propagation through a layer: Geophys. J. R. astr. Soc., **49**, p.209-223.

Lafarge Canada Inc., 1998, personal communication.

Lawton, D.C., 1993, Geophysical study of the Taharoa ironsand deposit, west coast, North Island, New Zealand: New Zealand Journal of Geology and Geophysics, **36**, p. 141-160.

Lawton, D.C., Spratt, D.A. and Hopkins, J.C., 1994, Tectonic wedging beneath the Rocky Mountain foreland basin: Geology, **22**, p.519-522.

Levin, F.K., 1978, The reflection, refraction and diffraction of waves in media with an elliptical velocity dependence: Geophysics, **43**, p.528-537.

Levin, F.K., 1979, Seismic velocities in transversely isotropic media: Geophysics, **44**, p.918-936.

MacBeth, C., 1998, Vertical fracture estimation using walkaway VSP: SEG Expanded Abstracts.

Ollerenshaw, N.C., 1972, Wildcat Hills (west half), Alberta: Geological Survey of Canada, scale 1:50 000.

Postma, G.W., 1955, Wave propagation in a stratified medium: Geophysics, **20**, p.780-806.

Pratt, R.G., and Chapman, C.H., 1992, Traveltime tomography in anisotropic media -II.: Applications, Geophys. J. Int., **109**, p.20-37.

Reynolds, J.M., 1997, An introduction to applied and environmental geophysics: Toronto: John Wiley and Sons.

Sayers, C.M., 1994, The elastic anisotropy of shales: J. Geophys. Res., **99**, No. B1, p.767-774.

Sayers, C.M., 1997, Determination of anisotropic velocity models from walkaway VSP data acquired in the presence of dip: Geophysics, **62**, p.723-729.

Schoenberg, M, 1994, Transversely isotropic media equivalent to this isotropic layers: Geophys. Prosp., **42**, p.885-915.

Slawinski, M.A., 1995, The characteristic biquadratic: An illustration of transmission in anisotropic media: CREWES Research Report, **7**, p.8.1-8.5.

Slawinski, M.A. and Parkin, J.M., 1996, Migration of a multioffset VSP: a case study in NE British Columbia: Can. J. of Exp. Geophys., **32**(2) p.104-112.

Slawinski, M.A., Slawinski, R.A., and Brown, R.J., 1995, Energy partition at the boundary between anisotropic media; Part two: Raytracing in layered, anisotropic media - comparison of traveltimes for synthetic and experimental results: CREWES Research Report, **7**, p.9.1-9.14.

Slotboom, R.T., 1992, Geophysical investigation of the triangle zone structure in the Jumpingpound-Wildcat area, southern Alberta foothills: M.Sc. Thesis, University of Calgary.

Slotboom, R.T., Lawton, D.C., and Spratt, D.A., 1996, Seismic interpretation of the triangle zone at Jumping Pound, Alberta: Bulletin of Canadian Petroleum Geology, **44**, p.233-243.

Stewart, R.R. and Disiena, J.P., 1989, The values of VSP in interpretation: The Leading Edge, December, p.16-25.

Stockmal, G.S., 1996, Maycroft (east half), Alberta (preliminary): Geological Survey of Canada, open file #3275, scale 1:50 000, with 1:25 000 inset.

Thomsen, L., 1986, Weak elastic anisotropy: Geophysics, **51**, p.1954-1966.

Tsvankin, I., 1995, Normal moveout from dipping reflectors in anisotropic media: Geophysics, **60**, p. 268-284.

Tsvankin, I., 1996, P-wave signatures and notation for transversely isotropic media: An overview: Geophysics, **61**, p. 467-483.

Tsvankin, I., 1997, Reflection moveout and parameter estimation for horizontal transverse isotropy: Geophysics, **62**, p.614-629.

Tsvankin, I. and Thomsen, L., 1994, Nonhyperbolic reflection moveout in anisotropic media: Geophysics, **59**, 1290-1304.

Vernik, L. and Liu, X., 1997, Velocity anisotropy in shales: a petrophysical study: Geophysics, **62**, p.521-532.

Vestrum, R.W., 1994, Group- and phase-velocity inversion for the general anisotropic stiffness tensor: M.Sc. thesis, University of Calgary.

Vestrum, R.W., Lawton, D.C., and Schmid, R., 1999, Imaging structures below dipping TI media: Geophysics, **64**, p.1239-1246.

Winterstein, D.F., 1990, Velocity anisotropy terminology for geophysicists: Geophysics, **55**, p.1070-1088.

Zhu, J., Lines, L. and Gray, S., 1998, Smiles and frowns in migration/velocity analysis: Geophysics, **63**, p. 1200-1209.

APPENDIX I ELLIPTICAL RAYTRACING SUBROUTINE

```
implicit real (a-z)
integer med1, med2

pi = 4.0 * atan(1.0)

print *,' Enter incident medium (iso = 1,aniso = 2):    '
read(5,*) med1
print *,' Enter refractive medium (iso = 1,aniso = 2):    '
read(5,*) med2

if (med1 .eq. 1) then
   print *,' The incident medium is isotropic.'
else if (med1 .eq. 2) then
   print *,' The incident medium is anisotropic.'
else if (med1 .ne. 1 .and. med1 .ne. 2) then
   print *,' Please enter incident medium (iso = 1,aniso = 2):'
   read(5,*) med1
end if

 ---------------------------------------------------------------------
if (med2 .eq. 1) then
   print *,' The refractive medium is isotropic.'
else if (med2 .eq. 2) then
   print *,' The refractive medium is anisotropic.'
else if (med2 .ne. 1 .and. med2 .ne. 2) then
   print *,' Please enter refractive medium (iso = 1,aniso = 2):'
   read(5,*) med2
end if
```

```
print *,' Incident ray angle (deg) =      '
read(5,*) alpha1
print *,' Incident gamma (deg) =      '
read(5,*) gamma1
print *,' Refracted gamma (deg) =      '
read(5,*) gamma2

viso = 2740.0
vfast = 3365.0
vslow = 2925.0

 ======================================================================
--- Patch for phi > 90.0 or phi < - 90.0

alphar1 = alpha1 * pi/180
gammar1 = gamma1 * pi/180
gammar2 = gamma2 * pi/180

phir1 = alphar1 - gammar1

if (med1 .eq. 1) then
   phi1 = phir1 * 180.0/pi
   rayvel1 = viso
   rayp = sin(phir1) / rayvel1
else if (med1 .eq. 2) then
   if (phir1 .lt. -pi / 2) then
      gammar1 = gammar1 - pi
      phir1 = alphar1 - gammar1
   elseif (phir1 .gt. pi / 2) then
      gammar1 = gammar1 + pi
```

```
      phir1 = alphar1 - gammar1
   endif
   phi1 = phir1 * 180 / pi
   tanphs = (vslow**2 / vfast**2) * tan(phir1)
   phsr1 = atan(tanphs)
   betar1 = phsr1 + gammar1
   phs1 = phsr1 * 180.0 / pi
   beta1 = betar1 * 180 / pi
   rvel1 = (sin(phir1)**2 / vfast**2) + (cos(phir1)**2 / vslow**2)
   rayvel1 = sqrt(1 / rvel1)
   raypnum = (sin(gammar1) / vslow**2) +
      ((cos(gammar1) * tan(phir1)) / vfast**2)
   raypdenom = sqrt(1 / (vslow**2) + (tan(phir1)**2 / vfast**2))
   rayp = raypnum / raypdenom
else if (med1 .ne. 1 .and. med1 .ne. 2) then
   print *,'Incident medium was not entered.'
end if

if (med2 .eq. 1) then
   rayvel2 = viso
   crit = abs(rayp * rayvel2)
   if (crit .gt. 1) then
      print *,'Incident Angle is past critical'
      print *,'Ray Parameter =',rayp
      print *,'Incident Angle =',alpha1
      print *,'Incident Ray Velocity =',rayvel1
   else
      phir2 = asin(rayp * rayvel2)
      phi2 = phir2 * 180.0 / pi
      print *,'Ray Parameter =',rayp
```

```
      print *,'Incident Angle =',alpha1
      print *,'Incident Ray Velocity =',rayvel1
      print *,'Refracted Angle =',phi2
      print *,'Refracted Ray Velocity =',rayvel2
   endif
else if (med2 .eq. 2) then
   num1 = sin(gammar2) * cos(gammar2)
   num2 = (vslow**2 * cos(gammar2)**2 +
        vfast**2 * sin(gammar2)**2 - (rayp * vslow * vfast)**2)
   if (num2 .lt. 0) then
      print *,'Incident Angle is past critical'
      print *,'Ray Parameter =',rayp
      print *,'Incident Angle =',alpha1
      print *,'Incident Ray Velocity =',rayvel1
   else
      num2 = sqrt(num2)
      phsdenom = (rayp**2 * vfast**2) - cos(gammar2)**2
      tanphs2a = (num1 + rayp * num2) / phsdenom
      tanphs2b = (num1 - rayp * num2) / phsdenom
      phaser2a = atan(tanphs2a)
      phaser2b = atan(tanphs2b)
      betar2 = phaser2b + gammar2
      if(betar2.gt.pi/2) then
         betar2 = betar2 - pi
      elseif(betar2.lt.-pi/2) then
         betar2 = betar2 + pi
      endif
      if (betar1 .gt. 0 .and. betar2 .lt. 0) then
         gammar2 = gammar2 + pi
         betar2 = phaser2b + gammar2
```

```
            num1 = sin(gammar2) * cos(gammar2)
            num2 = (vslow**2 * cos(gammar2)**2 +
            vfast**2 * sin(gammar2)**2 - (rayp * vslow * vfast)**2)
            num2 = sqrt(num2)
         elseif (betar1 .lt. 0 .and. betar2 .gt. 0) then
            gammar2 = gammar2 - pi
            betar2 = phaser2b + gammar2
            num1 = sin(gammar2) * cos(gammar2)
            num2 = (vslow**2 * cos(gammar2)**2 +
     .....       vfast**2 * sin(gammar2)**2 - (rayp * vslow * vfast)**2)
            num2 = sqrt(num2)
         endif

         phase2a = phaser2a * 180 / pi
         phase2b = phaser2b * 180 / pi
         beta2 = betar2 * 180 / pi

         denom = (vslow**2 / vfast**2) *
              ((rayp**2 * vfast**2) - cos(gammar2)**2)
         tanphi2a = (num1 + rayp * num2) / denom
         tanphi2b = (num1 - rayp * num2) / denom

         phir2a = atan(tanphi2a)
         phir2b = atan(tanphi2b)
         alphar2a = phir2a + gammar2
         alphar2b = phir2b + gammar2
         if (alphar2b .gt. pi / 2) then
            alphar2b = alphar2b - pi
            print *,'Refracted alpha out of range (>+90)'
         elseif (alphar2b .lt. -pi / 2) then
```

```
      alphar2b = alphar2b + pi
      print *,'Refracted alpha out of range (>-90)'
   endif
   alpha2a = alphar2a * 180.0 / pi
   alpha2b = alphar2b * 180.0 / pi
   phi2a = phir2a * 180.0 / pi
   phi2b = phir2b * 180.0 / pi
   gamma2 = gammar2 * 180 /pi

   rvel2 = (sin(phir2b)**2 / vfast**2) +
        (cos(phir2b)**2 / vslow**2)
   rayvel2 = sqrt(1 / rvel2)

   print *,'Ray Parameter =',rayp
   print *,'Incident Gamma =',gamma1
   print *,'Incident Angle =',alpha1
   print *,'Incident Phi =',phi1
   print *,'Incident Phase =',phs1
   print *,'Incident Beta =',beta1
   print *,'Incident Ray Velocity =',rayvel1
   print *,'Refracted Gamma =',gamma2
   print *,'Refracted Angle (a) =',alpha2a
   print *,'Refracted Phase (a) =',phase2a
   print *,'Refracted Phi (a) =',phi2a
   print *,'Refracted Angle (b) =',alpha2b
   print *,'Refracted Phi (b) =',phi2b
   print *,'Refracted Phase (b) =',phase2b
   print *,'Refracted Beta (b) =',beta2
   print *,'Refracted Ray Velocity =',rayvel2
endif
```

```
else if (med2 .ne. 1 .and. med2 .ne. 2) then
   print *,'Refractive medium was not entered.'
end if

end
```

APPENDIX II VSP DATA

The following table contains all the data acquired from the VSP experiment. This includes the transformation of the well into the plane of the shots for the 2D analysis of the data. Note that the transformation was not performed on the data from the two zero-offset shot locations (E0 and Zero). The headings for the accompanying table are as follows:

Column A - Source location.

Column B - Source elevation (m).

Column C - Source northing direction (m).

Column D - Source easting direction (m).

Column E - Field file identification number (FFID).

Column F - Measured depth of receiver in well (m).

Column G - Total vertical depth of receiver in well (m).

Column H - Total vertical depth to receiver with respect to kellybushing (m). Factor **z** from Figure 5.8.

Column I - Receiver northing direction (m).

Column J - Receiver easting direction (m).

Column K - First arrival times (ms) from experiment.

Column L - Horizontal distance from shotpoint to well (m). Factor **h** from Figure 5.8.

Column M - Total distance between shotpoint and receiver location in well (m). Factor **d** from Figure 5.8.

Column N - Calculated velocity from shotpoint to receiver in well, assuming straight raypaths (m/s).

Column O - Bearing direction between source location and well (°).

Column P - Transformation angle between h and h' planes (°). Factor θ from Figure 5.8.

Column Q - Transformed horizontal distance from shotpoint to well (m). Factor **h'** from Figure 5.8.

Column R - Transformed total distance between shotpoint and receiver in well (m). Factor **d'** from Figure 5.8.

Column S - Inclination angle (°). Factor **I** from Figure 5.8.

Column T - Transformed inclination angle (radians). Factor **I'** from Figure 5.8.

Column U - Transformed first arrival times (ms). Factor **t'** from Figure 5.8.

A	B	C	D	E	F	G	H	I	J	K	L	M	N	O	P	Q	R	S	T	U
E2	1397 9	302 58	1272 86	512	629 63	627 369	766 401	16 1451	36 13025	369 48	1269 467	1417 863	3837 456	256 9598	11 95983	1241 91	1393 245	26 44815	0 470416	363 0648
E2	1397 9	302 58	1272 86	512	644 74	642 1718	751 5982	17 68092	38 73029	370 44	1266 587	1421 953	3838 551	257 001	12 00098	1238 905	1397 352	27 03387	0 480834	364 031
E2	1397 9	302 58	1272 86	512	659 86	656 947	736 823	19 31367	41 48355	371 02	1263 538	1426 026	3843 529	257 045	12 04504	1235 72	1401 437	27 61835	0 491233	364 6225
E2	1397 9	302 58	1272 86	512	674 98	671 6855	722 0845	21 04372	44 38518	371 54	1260 323	1430 084	3849 071	257 0921	12 09211	1232 359	1405 502	28 20129	0 501608	365 1534
E2	1397 9	302 58	1272 86	512	690 1	686 4798	707 2902	22 65446	47 07522	373 07	1257 341	1434 52	3845 177	257 1363	12 13627	1229 24	1409 955	28 77832	0 511872	366 6814
E2	1397 9	302 58	1272 86	507	704 48	700 5967	693 1733	24 03785	49 42652	373 14	1254 741	1439 102	3856 735	257 174	12 17396	1226 524	1414 568	29 32079	0 521513	366 7785
E2	1397 9	302 58	1272 86	507	719 6	715 4895	678 2805	25 38032	51 68245	373 8	1252 244	1444 268	3863 798	257 2109	12 21093	1223 912	1419 794	29 88444	0 531524	367 4606
E2	1397 9	302 58	1272 86	507	734 72	730 3822	663 3878	26 73929	53 87792	375 49	1249 602	1449 66	3860 715	257 2494	12 24941	1221 348	1425 202	30 44287	0 541444	369 1549
E2	1397 9	302 58	1272 86	507	749 84	745 2817	648 4883	28 07975	56 08292	376 42	1247 356	1455 168	3865 81	257 2871	12 28711	1218 783	1430 752	30 99746	0 551293	370 104
E2	1397 9	302 58	1272 86	507	764 96	760 18	633 59	29 38133	58 352	377 26	1244 856	1460 766	3872 04	257 3226	12 32256	1216 177	1436 404	31 54886	0 561079	370 9682
E2	1397 9	302 58	1272 86	502	779 5	774 485	619 285	30 65406	60 58625	377 92	1242 397	1466 217	3879 702	257 3572	12 35721	1213 614	1441 909	32 07552	0 570424	371 6544
E2	1397 9	302 58	1272 86	502	794 61	789 3708	604 3992	31 89014	62 8938	379 43	1239 875	1472 051	3879 638	257 3896	12 38961	1211	1447 814	32 6186	0 580053	373 1827
E2	1397 9	302 58	1272 86	502	809 73	804 2544	589 5156	33 06184	65 25277	380 56	1237 318	1477 985	3883 712	257 4187	12 41871	1208 367	1453 835	33 15803	0 589609	374 3417
E2	1397 9	302 58	1272 86	502	824 88	819 1669	574 6031	34 25306	67 65844	381 59	1234 711	1484 024	3889 054	257 4483	12 44834	1205 683	1459 962	33 6951	0 599121	375 4029
E2	1397 9	302 58	1272 86	502	840	834 056	559 714	35 3601	70 03608	382 52	1232 149	1490 217	3895 789	257 4746	12 47457	1203 061	1466 257	34 22602	0 608515	376 3698
E2	1397 9	302 58	1272 86	497	854 57	848 4218	545 3482	36 34469	72 27353	383 47	1229 752	1496 374	3902 192	257 4967	12 49674	1200 617	1472 523	34 73247	0 617469	377 358
E2	1397 9	302 58	1272 86	497	869 69	863 3245	530 4455	37 38883	74 61318	385 36	1227 242	1502 864	3899 895	257 5207	12 52068	1198 055	1479 126	35 25392	0 626687	379 2732
E2	1397 9	302 58	1272 86	497	884 8	878 2063	515 5638	38 45125	76 96625	386 95	1224 715	1509 451	3900 895	257 5454	12 54542	1195 473	1485 824	35 77058	0 635818	380 8932
E2	1397 9	302 58	1272 86	497	899 92	893 1055	500 6645	39 58224	79 30402	388 71	1222 188	1516 171	3900 52	257 5736	12 57356	1192 877	1492 644	36 28322	0 644883	382 6782
E2	1397 9	302 58	1272 86	497	915 04	907 9966	485 7734	40 74274	81 65438	389 98	1219 643	1522 992	3905 308	257 603	12 60304	1190 256	1499 561	36 79147	0 653869	383 9803
E2	1397 9	302 58	1272 86	492	929 49	922 2215	471 5485	41 8482	83 92076	391 07	1217 193	1529 603	3911 327	257 631	12 63096	1187 735	1506 267	37 27316	0 662384	385 1039
E2	1397 9	302 58	1272 86	492	944 61	937 1085	456 6615	42 95722	86 31667	392 99	1214 615	1536 626	3910 089	257 6579	12 65785	1185 095	1513 4	37 77309	0 671213	387 05
E2	1397 9	302 58	1272 86	492	959 72	952 0139	441 7561	43 94881	88 60678	394 77	1212 166	1543 877	3910 827	257 6805	12 6805	1182 0	1520 774	38 26601	0 679906	388 8626
E2	1397 9	302 58	1272 86	492	974 84	966 9461	426 8239	44 89788	90 79882	396	1209 822	1551 341	3917 527	257 7023	12 70226	1180 212	1528 362	38 75263	0 688488	390 1344
E2	1397 9	302 58	1272 86	492	989 96	981 8901	411 8799	45 84927	92 88561	397 67	1207 58	1559 002	3920 34	257 7253	12 72528	1177 919	1536 141	39 23251	0 696949	391 6387
E2	1397 9	302 58	1272 86	487	1004 47	996 2397	397 5303	46 78195	94 81391	398 41	1205 498	1566 514	3931 913	257 7491	12 74911	1175 777	1543 759	39 68722	0 704967	392 6228
E2	1397 9	302 58	1272 86	487	1019 59	1011 202	382 5678	47 76633	96 78266	399 88	1203 365	1574 48	3937 381	257 775	12 77502	1173 577	1551 832	40 1558	0 71323	394 1279
E2	1397 9	302 58	1272 86	487	1034 7	1026 155	367 6152	48 72677	98 69578	401 89	1201 292	1582 59	3937 868	257 8005	12 80047	1171 437	1560 049	40 61794	0 721376	396 1659
E2	1397 9	302 58	1272 86	487	1049 82	1041 126	352 6441	49 7059	100 5592	403 74	1199 264	1590 847	3940 276	257 8274	12 82738	1169 335	1568 408	41 07479	0 729429	398 0452
E2	1397 9	302 58	1272 86	487	1064 94	1056 098	337 672	50 68624	102 4335	405 86	1197 225	1599 197	3940 268	257 8543	12 85433	1167 222	1576 861	41 52717	0 737401	400 1912
E2	1397 9	302 58	1272 86	482	1079 66	1070 669	323 1013	51 63213	104 3085	407 65	1195 193	1607 383	3943 046	257 8797	12 87974	1165 122	1585 151	41 96402	0 745095	402 0117
E2	1397 9	302 58	1272 86	482	1094 78	1085 623	308 1468	52 595	106 3094	410 34	1193 035	1615 826	3937 774	257 9048	12 90478	1162 902	1593 707	42 40949	0 752937	404 7229
E2	1397 9	302 58	1272 86	482	1109 9	1100 577	293 1929	53 62162	108 3188	413 23	1190 855	1624 35	3930 863	257 9328	12 93282	1160 647	1602 336	42 8508	0 760709	407 6295
E2	1397 9	302 58	1272 86	482	1125 02	1115 518	278 2522	54 70365	110 3685	415 55	1188 625	1632 924	3929 549	257 9632	12 96317	1158 332	1611 007	43 28837	0 768418	409 9726
E2	1397 9	302 58	1272 86	482	1140 13	1130 437	263 3332	55 79127	112 4881	417 26	1186 325	1641 527	3934 062	257 9932	12 99319	1155 952	1619 712	43 72245	0 776062	411 7149
E2	1397 9	302 58	1272 86	476	1154 52	1144 638	249 1316	56 77694	114 5985	418 36	1184 056	1649 745	3943 362	258 0186	13 0186	1153 622	1628 04	44 13337	0 78329	412 6558
E2	1397 9	302 58	1272 86	476	1169 64	1159 555	234 2155	57 65187	116 9259	420 32	1181 598	1658 413	3945 597	258 0367	13 03667	1151 143	1636 854	44 56238	0 790816	414 8559
E2	1397 9	302 58	1272 86	476	1184 76	1174 47	219 3001	58 48688	119 2629	422 65	1179 139	1667 173	3944 571	258 0528	13 05283	1148 672	1645 766	44 98691	0 798257	417 2231
E2	1397 9	302 58	1272 86	476	1199 88	1189 388	204 3816	59 34541	121 5754	424 48	1176 698	1676 039	3948 451	258 0704	13 07042	1146 214	1654 778	45 40659	0 805613	419 0956
E2	1397 9	302 58	1272 86	476	1214 99	1204 302	189 468	60 20641	123 8392	426 46	1174 306	1685 023	3951 186	258 0887	13 08869	1143 798	1663 906	45 82055	0 812869	421 1155
E2	1397 9	302 58	1272 86	470	1229 5	1218 629	175 1412	60 98476	125 9545	428 07	1172 075	1693 783	3956 789	258 1046	13 10458	1141 552	1672 806	46 21241	0 819732	422 7686
E2	1397 9	302 58	1272 86	470	1244 62	1233 575	160 1953	61 70514	128 1393	429 97	1169 789	1703 032	3960 817	258 117	13 11704	1139 267	1682 214	46 61589	0 826787	424 7139
E2	1397 9	302 58	1272 86	470	1259 74	1248 505	145 2647	62 54103	130 3749	431 93	1167 429	1712 304	3964 31	258 1346	13 1346	1136 888	1691 629	47 01645	0 8338	426 7147
E2	1397 9	302 58	1272 86	470	1274 86	1263 42	130 3498	63 49313	132 6757	434 18	1164 982	1721 588	3965 149	258 1572	13 15715	1134 4	1701 043	47 41446	0 840776	428 9986
E2	1397 9	302 58	1272 86	470	1289 97	1278 308	115 4622	64 54728	135 0557	436 09	1162 436	1730 868	3969 062	258 1839	13 18393	1131 798	1710 442	47 80999	0 847714	430 9437
E2	1397 9	302 58	1272 86	463	1304 48	1292 592	101 1777	65 50961	137 4089	438 28	1159 936	1739 81	3969 632	258 2067	13 20666	1129 258	1719 51	48 18693	0 854318	433 166
E2	1397 9	302 58	1272 86	463	1319 6	1307 482	86 28827	66 49503	139 8366	440 96	1157 358	1749 229	3966 866	258 2298	13 22985	1126 642	1729 06	48 57501	0 861115	435 8754
E2	1397 9	302 58	1272 86	463	1334 72	1322 377	71 39279	67 55711	142 2125	443 66	1154 816	1758 756	3964 197	258 2574	13 25739	1124 04	1738 703	48 95819	0 867832	438 6015
E2	1397 9	302 58	1272 86	463	1349 84	1337 27	56 49954	68 69329	144 5658	446 23	1152 281	1768 363	3962 895	258 2889	13 28889	1121 427	1748 414	49 33699	0 874479	441 1963
E2	1397 9	302 58	1272 86	463	1364 96	1352 148	41 62196	69 84846	146 966	448 24	1149 696	1778 002	3966 63	258 321	13 32098	1118 763	1758 158	49 71256	0 881069	443 2373
E2	1397 9	302 58	1272 86	456	1379 49	1366 443	27 32656	70 90037	149 3601	450 01	1147 119	1787 276	3971 635	258 348	13 34802	1116 131	1767 546	50 07191	0 887365	445 0424
E2	1397 9	302 58	1272 86	456	1394 61	1381 3	12 47023	72 01184	151 9396	452 39	1144 388	1796 953	3972 132	258 3766	13 37664	1113 341	1777 342	50 44272	0 89386	447 4528
E2	1397 9	302 58	1272 86	456	1409 73	1396 15	-2 38046	73 15857	154 5212	454 86	1141 629	1806 682	3971 953	258 4069	13 40691	1110 517	1787 186	50 81013	0 900297	449 9514
E2	1397 9	302 58	1272 86	456	1424 85	1411 005	-17 2347	74 31794	157 1009	457 03	1138 869	1816 488	3974 548	258 438	13 43797	1107 689	1797 103	51 17367	0 906666	452 1529
E2	1397 9	302 58	1272 86	456	1440	1425 905	-32 1349	75 40841	159 6397	459 33	1136 183	1826 435	3976 303	258 4662	13 46618	1104 927	1807 17	51 53285	0 912951	454 485

E2	1397 9	302 58	1272 86	449	1439 6	1425 512	-31 7415	75 37962	159 5727	458 92	1136 234	1826 172	3979 281	258 4654	13 46543	1105	1806 903	51 52342	0 912786	454 0778
E2	1397 9	302 58	1272 86	449	1454 72	1440 396	-46 6259	76 32658	162 051	461 01	1133 617	1836 23	3983 06	258 4873	13 48728	1102 354	1817 096	51 87633	0 918948	456 2061
E2	1397 9	302 58	1272 86	449	1469 84	1455 284	-61 5137	77 22823	164 5261	463 2	1131 012	1846 368	3986 115	258 507	13 50701	1099 729	1827 373	52 22515	0 925032	458 4347
E2	1397 9	302 58	1272 86	449	1484 96	1470 174	-76 4036	78 12545	166 9879	465 44	1128 421	1856 584	3988 879	258 5268	13 52675	1097 119	1837 727	52 56984	0 931043	460 7127
E2	1397 9	302 58	1272 86	449	1500 07	1485 054	-91 2844	79 05503	169 4301	467 77	1125 842	1866 867	3990 993	258 5484	13 54839	1094 513	1848 142	52 91026	0 936981	463 0782
E2	1397 9	302 58	1272 86	444	1514 55	1499 313	-105 543	80 05237	171 772	469 56	1123 349	1876 767	3996 863	258 5745	13 57453	1091 969	1858 154	53 23348	0 942629	464 9031
E2	1397 9	302 58	1272 86	444	1529 67	1514 186	-120 416	81 14702	174 2507	472 45	1120 703	1887 129	3994 347	258 6043	13 60429	1089 26	1868 628	53 56813	0 948479	467 818
E2	1397 9	302 58	1272 86	444	1544 79	1529 05	-135 28	82 26237	176 7878	475 3	1117 996	1897 513	3992 243	258 6346	13 63463	1086 489	1879 122	53 90045	0 954288	470 6933
E2	1397 9	302 58	1272 86	444	1559 91	1543 906	-150 136	83 37919	179 3877	478 23	1115 227	1907 917	3989 538	258 6646	13 66456	1083 661	1889 639	54 2305	0 960055	473 6486
E2	1397 9	302 58	1272 86	444	1575 02	1558 734	-104 964	84 48446	182 0356	481 21	1112 413	1918 335	3986 482	258 6936	13 69357	1080 794	1900 174	54 55755	0 965766	476 6543
E2	1397 9	302 58	1272 86	438	1589 5	1572 957	-179 187	85 59131	184 5526	483 19	1109 728	1928 393	3990 962	258 7241	13 72413	1078 045	1910 336	54 86759	0 971184	478 6655
E2	1397 9	302 58	1272 86	438	1604 62	1587 815	-194 045	86 68805	187 1276	485 73	1106 989	1938 998	3991 925	258 7537	13 75374	1075 248	1921 053	55 18646	0 976751	481 2348
E2	1397 9	302 58	1272 86	438	1619 74	1602 676	-208 906	87 70154	189 7082	488 39	1104 26	1949 671	3992 036	258 7792	13 7792	1072 481	1931 849	55 50162	0 982244	483 9256
E2	1397 9	302 58	1272 86	438	1634 89	1617 563	-223 793	88 6495	192 3424	490 52	1101 492	1960 401	3996 577	258 8009	13 80091	1069 692	1942 712	55 81472	0 987692	486 0939
E2	1397 9	302 58	1272 86	438	1650	1632 396	-238 626	89 63838	195 0401	492 73	1098 654	1971 105	4000 376	258 8242	13 82417	1066 83	1953 546	56 12523	0 993096	488 3406
E2	1397 9	302 58	1272 86	431	1664 54	1646 684	-252 914	90 75656	197 5005	494 68	1096 023	1981 528	4005 677	258 8566	13 85659	1064 127	1964 066	56 41866	0 998221	490 3205
E2	1397 9	302 58	1272 86	431	1679 66	1661 559	-267 789	91 99517	199 9283	496 85	1093 402	1992 498	4010 261	258 8957	13 89568	1061 403	1975 12	56 71605	1 003461	492 5165
E2	1397 9	302 58	1272 86	431	1694 78	1676 447	-282 677	93 23781	202 273	499 43	1090 862	2003 576	4011 726	258 936	13 93601	1058 753	1986 277	57 01239	1 008614	495 1178
E2	1397 9	302 58	1272 86	431	1709 9	1691 34	-297 57	94 40074	204 6033	502 22	1088 352	2014 728	4011 645	258 9725	13 97255	1056 15	1997 516	57 30287	1 013691	497 9295
E2	1397 9	302 58	1272 86	431	1725 02	1706 244	-312 474	95 48874	206 9073	505 33	1085 883	2025 962	4009 186	259 0056	14 00564	1053 602	2008 844	57 58933	1 01869	501 0605
E2	1397 9	302 58	1272 86	426	1739 52	1720 546	-326 778	96 62338	208 9792	507 6	1083 633	2036 854	4012 716	259 0436	14 04364	1051 244	2019 81	57 85844	1 023398	503 3523
E2	1397 9	302 58	1272 86	426	1754 64	1735 468	-341 698	97 89031	211 0629	510 9	1081 347	2048 295	4009 19	259 0886	14 08856	1048 821	2031 312	58 13462	1 02824	506 6638
E2	1397 9	302 58	1272 86	426	1769 76	1750 391	-356 621	99 19527	213 1034	513 78	1079 097	2059 805	4009 118	259 1361	14 13609	1046 42	2042 875	58 40692	1 033018	509 5573
E2	1397 9	302 58	1272 86	426	1784 88	1765 322	-371 552	100 4302	215 1537	517 15	1076 851	2071 368	4005 353	259 1801	14 18006	1044 04	2054 502	58 6762	1 037736	512 939
E2	1397 9	302 58	1272 86	426	1800	1780 262	-386 492	101 5689	217 1803	519 97	1074 646	2083 008	4006 015	259 2194	14 21941	1041 722	2066 214	58 94163	1 042376	515 7779
E2	1397 9	302 58	1272 86	421	1814 5	1794 579	-400 809	102 596	219 2196	522 2	1072 451	2094 16	4010 264	259 2529	14 25293	1039 439	2077 448	59 19517	1 0468	518 0326
E2	1397 9	302 58	1272 86	421	1829 62	1809 485	-415 715	103 6289	221 5277	525 31	1069 991	2105 726	4008 539	259 2842	14 28422	1036 911	2089 111	59 46037	1 051418	521 1651
E2	1397 9	302 58	1272 86	421	1844 74	1824 362	-430 592	104 6472	224 0488	528 31	1067 325	2117 207	4007 509	259 3128	14 31277	1034 198	2100 701	59 7271	1 056055	524 1912
E2	1397 9	302 58	1272 86	421	1859 86	1839 238	-445 468	105 6631	226 5609	531 09	1064 668	2128 738	4008 243	259 3414	14 34142	1031 49	2112 339	59 9907	1 060637	526 9988
E2	1397 9	302 58	1272 86	421	1874 98	1854 141	-460 371	106 6486	228 8885	533 93	1062 198	2140 429	4008 819	259 3704	14 37045	1028 964	2124 132	60 24746	1 065101	529 8647
E2	1397 9	302 58	1272 86	416	1889 61	1868 57	-474 8	107 5992	231 1143	535 45	1059 836	2151 803	4018 681	259 3988	14 39875	1026 545	2135 603	60 49274	1 069365	531 4187
E2	1397 9	302 58	1272 86	416	1904 73	1883 483	-489 713	108 571	233 4188	537 46	1057 392	2163 599	4025 599	259 4275	14 42755	1024 045	2147 499	60 74358	1 073723	533 4606
E2	1397 9	302 58	1272 86	416	1919 84	1898 377	-504 607	109 512	235 7469	539 31	1054 931	2175 411	4033 693	259 4546	14 45458	1021 538	2159 415	60 99185	1 078033	535 3444
E2	1397 9	302 58	1272 86	416	1934 96	1913 265	-519 495	110 448	238 2109	541 52	1052 337	2187 194	4038 99	259 4801	14 48013	1018 909	2171 308	61 2404	1 082343	537 5869
E2	1397 9	302 58	1272 86	416	1950 08	1928 103	-534 333	111 4762	240 9465	543 88	1049 46	2198 838	4042 874	259 5081	14 50805	1015 995	2183 064	61 49214	1 086711	539 9783
E2	1397 9	302 58	1272 86	411	1919 6	1898 141	-504 371	109 4971	235 7078	539	1054 972	2175 224	4035 666	259 4542	14 45418	1021 579	2159 226	60 98788	1 077964	535 0359
E2	1397 9	302 58	1272 86	411	1934 72	1913 029	-519 259	110 4331	238 1718	541 28	1052 378	2187 007	4040 435	259 4797	14 47973	1018 951	2171 119	61 23647	1 082275	537 3479
E2	1397 9	302 58	1272 86	411	1949 84	1927 867	-534 097	111 4595	240 902	544 34	1049 507	2198 654	4039 119	259 5076	14 5076	1016 043	2182 878	61 48815	1 086642	540 4343
E2	1397 9	302 58	1272 86	411	1964 95	1942 633	-548 863	112 6033	243 8916	545 52	1046 359	2210 148	4051 452	259 5394	14 53937	1012 85	2194 482	61 74257	1 091062	541 6533
E2	1397 9	302 58	1272 86	411	1980 07	1957 338	-563 568	113 9027	247 144	547 8	1042 925	2221 497	4055 307	259 5771	14 57714	1009 353	2205 935	62 00014	1 095545	543 9626
E2	1397 9	302 58	1272 86	405	1994 52	1971 319	-577 549	115 3326	250 4955	550 27	1039 37	2232 194	4056 543	259 6212	14 62123	1005 711	2216 721	62 24917	1 099891	546 4558
E2	1397 9	302 58	1272 86	405	2009 64	1985 86	-592 09	117 0409	254 2801	552 33	1035 34	2243 209	4061 357	259 6765	14 67649	1001 559	2227 819	62 5132	1 104513	548 5406
E2	1397 9	302 58	1272 86	405	2024 76	2000 409	-606 639	118 7591	258 0265	555 13	'031 347	2254 297	4060 845	259 7331	14 7331	997 4376	2238 986	62 77391	1 109079	551 3597
E2	1397 9	302 58	1272 86	405	2039 87	2014 978	-621 208	120 4657	261 6562	558 29	1027 472	2265 501	4057 928	259 7907	14 79067	993 4267	2250 265	63 02962	1 113559	554 5354
E2	1397 9	302 58	1272 86	405	2054 99	2029 591	-635 821	122 1618	265 1417	561 31	1023 742	2276 855	4056 324	259 8495	14 84951	989 551	2261 688	63 28007	1 117949	557 5709
E2	1397 9	302 58	1272 86	398	2069 53	2043 672	-649 902	123 8071	268 3635	563 42	1020 281	2287 896	4060 729	259 9086	14 90858	985 9357	2272 788	63 51604	1 12209	559 6994
E2	1397 9	302 58	1272 86	398	2084 65	2058 312	-664 542	125 5368	271 7177	566 22	1016 676	2299 413	4060 988	259 9714	14 97143	982 1648	2284 363	63 75911	1 126358	562 5142
E2	1397 9	302 58	1272 86	398	2099 77	2072 922	-679 152	127 308	275 1779	568 5	1012 961	2310 895	4064 898	260 036	15 036	978 2802	2295 904	64 00189	1 130621	564 8122
E2	1397 9	302 58	1272 86	398	2114 89	2087 496	-693 726	129 1389	278 7527	570 66	1009 124	2322 333	4069 557	260 1033	15 10327	974 2665	2307 4	64 2446	1 134886	566 9906
E2	1397 9	302 58	1272 86	398	2130	2102 031	-708 261	131 0407	282 416	572 51	1005 189	2333 735	4076 321	260 1742	15 17417	970 1428	2318 855	64 48666	1 139145	568 8598

A	B	C	D	E	F	G	H	I	J	K	L	M	N	O	P	Q	R	S	T	U
E1	1355 6	199 38	1013 12	392	569 49	568 2013	825 5687	10 69293	26 9616	294 65	1004 047	1135 361	3853 253	259 1682	14 1682	973 5056	1108 443	27 82933	0 498577	287 6643
E1	1355 6	199 38	1013 12	392	584 61	583 1236	810 6464	11 94033	29 04642	293 62	1001 766	1140 399	3883 927	259 2159	14 21587	971 089	1113 548	28 54588	0 511384	286 7066
E1	1355 6	199 38	1013 12	392	599 72	598 036	795 734	13 1869	31 12985	295 22	999 4861	1145 61	3880 53	259 2637	14 26372	968 6739	1118 829	29 25554	0 524065	288 3187
E1	1355 6	199 38	1013 12	392	614 84	612 8796	780 8904	14 64181	33 56528	293 93	996 8031	1150 612	3914 578	259 3196	14 31959	965 8337	1123 689	29 96572	0 536764	287 1034
E1	1355 6	199 38	1013 12	392	629 96	627 6923	766 0777	16 17864	36 18704	292 82	993 9621	1155 637	3946 579	259 3788	14 37885	962 8262	1128 969	30 67232	0 549402	286 0627
E1	1355 6	199 38	1013 12	387	644 56	641 9955	751 7745	17 66263	38 69932	293 58	991 2199	1160 656	3953 457	259 4364	14 43639	959 9221	1134 044	31 34869	0 561496	286 8487
E1	1355 6	199 38	1013 12	387	659 68	656 7716	736 9984	19 29296	41 44877	294 17	988 2188	1165 866	3963 24	259 5001	14 50009	956 7413	1139 308	32 04559	0 573961	287 4687
E1	1355 6	199 38	1013 12	387	674 8	671 51	722 26	21 0232	44 3508	295 29	985 0507	1171 087	3965 887	259 5683	14 56828	953 3799	1144 575	32 73906	0 586369	288 6051
E1	1355 6	199 38	1013 12	387	689 95	686 3327	707 4373	22 63929	47 04978	296 71	982 1043	1176 709	3965 855	259 6325	14 6325	950 2508	1150 257	33 42375	0 598609	290 0401
E1	1355 6	199 38	1013 12	387	705 06	701 1665	692 6035	24 09209	49 51943	297 46	979 4141	1182 716	3976 049	259 6901	14 6901	947 3986	1156 343	34 09532	0 610597	290 827
E1	1355 6	199 38	1013 12	381	719 57	715 4599	678 3101	25 37767	51 67814	298 09	977 0605	1188 852	3988 231	259 7416	14 74161	944 8988	1162 564	34 72936	0 621903	291 4987
E1	1355 6	199 38	1013 12	381	734 69	730 3526	663 4174	26 7366	53 87354	299 62	974 6587	1195 44	3989 853	259 7972	14 79724	942 3348	1169 236	35 38159	0 633533	293 0523
E1	1355 6	199 38	1013 12	381	749 81	745 2521	648 5179	28 07713	56 07854	300 99	972 2515	1202 181	3994 068	259 852	14 85197	939 7698	1176 067	36 02699	0 645035	294 4518
E1	1355 6	199 38	1013 12	381	764 93	760 1505	633 6195	29 37874	58 34741	302 13	969 7892	1209 027	4001 679	259 9041	14 90405	937 1635	1183 018	36 66663	0 656423	295 6304
E1	1355 6	199 38	1013 12	381	780 07	775 0455	618 7245	30 70453	60 67413	303 59	967 2665	1215 973	4005 313	259 9572	14 95721	934 4944	1190 069	37 30059	0 667707	297 1227
E1	1355 6	199 38	1013 12	376	794 55	789 3116	604 4584	31 68557	62 68459	304 72	964 8843	1222 79	4012 832	260 0034	15 00337	931 992	1197 006	37 89999	0 67836	298 2945
E1	1355 6	199 38	1013 12	376	809 67	804 1953	589 5747	33 05713	65 24331	306 15	962 3583	1230 012	4017 676	260 0477	15 04769	929 3591	1204 368	38 51936	0 689354	299 7674
E1	1355 6	199 38	1013 12	376	824 79	819 0783	574 6917	34 24598	67 64414	307 76	959 7884	1237 341	4020 472	260 0928	15 09282	926 6808	1211 84	39 13268	0 700237	301 4172
E1	1355 6	199 38	1013 12	376	839 91	833 9672	559 8028	35 35407	70 02226	309 21	957 2554	1244 842	4025 878	260 1337	15 13367	924 0572	1219 498	39 73784	0 71096	302 9147
E1	1355 6	199 38	1013 12	376	855 03	848 8749	544 8951	36 37624	72 34414	311 02	954 7929	1252 548	4027 221	260 1702	15 17022	921 5209	1227 372	40 33425	0 721512	304 7691
E1	1355 6	199 38	1013 12	370	869 56	863 1964	530 5736	37 37969	74 59294	312 45	952 406	1260 058	4032 83	260 2066	15 20661	919 0587	1235 046	40 90091	0 731535	306 2478
E1	1355 6	199 38	1013 12	370	884 68	878 0881	515 6819	38 44281	76 84756	314 45	949 9051	1267 983	4032 385	260 2456	15 24564	916 4754	1243 137	41 48352	0 741838	308 2883
E1	1355 6	199 38	1013 12	370	899 83	893 0168	500 7532	39 57543	79 29012	316 95	947 4047	1276 064	4026 073	260 2891	15 28914	913 8736	1251 37	42 06005	0 752038	310 8166
E1	1355 6	199 38	1013 12	370	914 95	907 908	485 862	40 73576	81 64031	319 02	944 8928	1284 238	4025 571	260 3345	15 33446	911 2532	1259 693	42 62839	0 762092	312 9228
E1	1355 6	199 38	1013 12	370	930 07	922 7926	470 9774	41 89078	84 01269	320 85	942 3605	1292 517	4028 415	260 3795	15 37947	908 615	1268 124	43 18989	0 77202	314 7947
E1	1355 6	199 38	1013 12	365	944 54	937 0395	456 7305	42 95263	86 30606	322 74	939 9221	1300 546	4029 702	260 4199	15 41992	906 0878	1276 308	43 72103	0 781399	316 7251
E1	1355 6	199 38	1013 12	365	959 66	951 9547	441 8153	43 94488	88 59769	325 19	937 4975	1309 162	4025 836	260 4564	15 45641	903 5915	1285 099	44 26615	0 791007	319 213
E1	1355 6	199 38	1013 12	365	974 78	966 8868	426 6832	44 89417	90 79026	327 36	935 1781	1317 981	4026 089	260 4915	15 49149	901 2032	1294 095	44 80138	0 800432	321 4273
E1	1355 6	199 38	1013 12	365	989 9	981 8308	411 9392	45 84543	92 87758	329 39	932 9625	1326 995	4028 643	260 5279	15 52793	898 9094	1303 278	45 32663	0 809681	323 503
E1	1355 6	199 38	1013 12	365	1005 05	996 8136	396 9564	46 81971	94 88943	331 19	930 8179	1336 196	4034 53	260 5667	15 56671	896 6743	1312 639	45 84372	0 818787	325 3513
E1	1355 6	199 38	1013 12	359	1019 56	1011 173	382 5975	47 76438	96 77875	332 36	928 7995	1345 14	4047 239	260 6051	15 60509	894 5627	1321 732	46 33147	0 827375	326 5763
E1	1355 6	199 38	1013 12	359	1034 67	1026 125	367 6449	48 72486	98 69198	334 37	926 7554	1354 596	4051 189	260 6444	15 64437	892 4228	1331 343	46 83072	0 836159	328 6301
E1	1355 6	199 38	1013 12	359	1049 79	1041 096	352 6739	49 70395	100 5556	336 5	924 7577	1364 199	4054 082	260 6855	15 68545	890 3201	1341 093	47 3221	0 844806	330 8007
E1	1355 6	199 38	1013 12	359	1064 91	1056 068	337 7017	50 68431	102 4297	338 46	922 7498	1373 894	4059 25	260 7267	15 72669	888 2072	1350 936	47 80692	0 853333	332 8044
E1	1355 6	199 38	1013 12	359	1080 03	1071 035	322 7354	51 65569	104 3575	340 95	920 691	1383 648	4058 213	260 767	15 76702	886 0496	1360 843	48 28633	0 861759	335 3305
E1	1355 6	199 38	1013 12	354	1094 63	1085 475	308 2952	52 58544	106 2896	342 9	918 6349	1393 104	4062 711	260 8049	15 80492	883 9055	1370 451	48 74465	0 869807	337 3243
E1	1355 6	199 38	1013 12	354	1109 75	1100 429	293 3413	53 61134	108 2988	345 78	916 4878	1402 977	4057 426	260 8482	15 84816	881 651	1380 472	49 21327	0 878042	340 2334
E1	1355 6	199 38	1013 12	354	1124 89	1115 389	278 3805	54 69408	110 3506	348 72	914 2902	1412 915	4051 717	260 8947	15 8947	879 3338	1390 55	49 67706	0 886195	343 2002
E1	1355 6	199 38	1013 12	354	1140 01	1130 318	263 4516	55 78304	112 4705	351 57	912 025	1422 877	4047 207	260 9412	15 94117	876 9524	1400 655	50 13561	0 894253	346 0793
E1	1355 6	199 38	1013 12	354	1155 13	1145 24	248 5298	56 81224	114 6924	353 84	909 669	1432 865	4049 472	260 9832	15 98315	874 5037	1410 802	50 59038	0 902228	348 3915
E1	1355 6	199 38	1013 12	348	1169 55	1159 466	234 3043	57 64666	116 9121	355 88	907 3461	1442 422	4053 113	261 0132	16 01323	872 1393	1420 539	51 02041	0 909742	350 481
E1	1355 6	199 38	1013 12	348	1184 67	1174 381	219 3889	58 48195	119 249	358 75	904 9076	1452 527	4048 855	261 0424	16 04235	869 6684	1430 839	51 46529	0 917505	353 3934
E1	1355 6	199 38	1013 12	348	1199 78	1189 29	204 4803	59 33957	121 5602	361 36	902 4911	1462 726	4047 835	261 0733	16 07329	867 2112	1441 226	51 90315	0 925146	356 0485
E1	1355 6	199 38	1013 12	348	1214 9	1204 213	189 5568	60 20158	123 8261	363 64	900 1191	1473 048	4050 842	261 1051	16 10511	864 7934	1451 731	52 3339	0 932662	358 3777
E1	1355 6	199 38	1013 12	348	1230 02	1219 143	174 6271	61 00954	126 0296	366 3	897 8172	1483 5	4049 959	261 1343	16 13431	862 4548	1462 37	52 75662	0 940028	361 0826
E1	1355 6	199 38	1013 12	343	1244 5	1233 456	160 3139	61 69942	128 122	368 33	895 6436	1493 615	4055 1	261 1573	16 15729	860 2669	1472 674	53 1553	0 94696	363 1658
E1	1355 6	199 38	1013 12	343	1259 62	1248 387	145 3831	62 53408	130 857	370 76	893 307	1504 202	4057 076	261 1881	16 18815	857 8886	1483 441	53 56756	0 954141	365 6429
E1	1355 6	199 38	1013 12	343	1274 73	1263 292	130 4779	63 48398	132 6553	373 1	890 8904	1514 797	4060 029	261 2259	16 22587	855 4041	1494 202	53 97591	0 961266	368 0274
E1	1355 6	199 38	1013 12	343	1289 85	1278 19	115 5803	64 53933	135 0362	375 67	888 3767	1525 405	4060 493	261 2697	16 26972	852 8003	1504 964	54 38138	0 968352	370 6358
E1	1355 6	199 38	1013 12	343	1304 97	1293 075	100 6953	65 5421	137 4883	378 3	885 801	1536 043	4060 384	261 3098	16 30976	850 1541	1515 766	54 78264	0 975355	373 3062
E1	1355 6	199 38	1013 12	337	1319 6	1307 482	86 28827	66 49503	139 8366	380 3	883 3359	1546 426	4066 333	261 3478	16 34784	847 6232	1526 308	55 16528	0 982022	375 3525
E1	1355 6	199 38	1013 12	337	1334 72	1322 377	71 39279	67 55711	142 2125	383 21	880 8276	1557 256	4063 714	261 3929	16 39289	845 021	1537 286	55 55408	0 988811	378 2959
E1	1355 6	199 38	1013 12	337	1349 84	1337 27	56 49954	68 69329	144 5658	386 1	878 3311	1568 161	4061 54	261 4432	16 4432	842 4081	1548 326	55 93709	0 995508	381 2165
E1	1355 6	199 38	1013 12	337	1364 96	1352 148	41 62196	69 84846	146 966	388 69	875 7861	1579 095	4062 607	261 4946	16 49457	839 7445	1559 394	56 31595	1 002132	383 8407
E1	1355 6	199 38	1013 12	337	1380 07	1367 014	26 75592	70 94236	149 4764	391 49	873 1417	1590 032	4061 489	261 5412	16 5412	837 007	1570 48	56 69234	1 008698	386 6759

E1	1355 6	199 38	1013 12	332	1394 61	1381 3	12 47023	72 01184	151 9396	393 9	870 5483	1600 579	4063 414	261 587	16 56697	834 3227	1581 168	57 05075	1 01495	389 123
E1	1355 6	199 38	1013 12	332	1409 73	1396 15	2 38046	73 15857	154 5212	396 85	867 827	1611 594	4060 965	261 6369	16 63693	831 4983	1592 325	57 4191	1 021378	392 1052
E1	1355 6	199 38	1013 12	332	1424 85	1411 005	-17 2347	74 31794	157 1009	399 64	865 1065	1622 678	4060 35	261 688	16 68805	828 6703	1603 549	57 78248	1 027719	394 9288
E1	1355 6	199 38	1013 12	332	1439 97	1425 875	32 1054	75 40625	159 6347	402 29	862 4423	1633 871	4061 425	261 7353	16 73525	825 9139	1614 887	58 13955	1 033939	397 6159
E1	1355 6	199 38	1013 12	332	1455 08	1440 75	-46 9803	76 34896	162 1099	405 03	859 8574	1645 171	4061 849	261 7737	16 77371	823 2722	1626 348	58 48945	1 040013	400 3961
E1	1355 6	199 38	1013 12	326	1469 56	1455 008	-61 238	77 21187	164 4803	407 08	857 3881	1656 063	4068 151	261 8081	16 80812	820 7593	1637 399	58 82011	1 045744	402 4922
E1	1355 6	199 38	1013 12	326	1484 68	1469 898	-76 1279	78 10848	166 9426	409 84	854 8233	1667 503	4068 669	261 8441	16 84408	818 1487	1649 003	59 16039	1 05164	405 293
E1	1355 6	199 38	1013 12	326	1499 83	1484 818	-91 0481	79 03849	169 3913	413 02	852 2677	1679 033	4065 258	261 8826	16 88262	815 5364	1660 69	59 49627	1 057464	408 5079
E1	1355 6	199 38	1013 12	326	1514 95	1499 707	-105 937	80 07992	171 8367	415 52	849 7	1690 586	4068 602	261 9289	16 92886	812 88	1672 383	59 82738	1 063219	411 046
E1	1355 6	199 38	1013 12	326	1530 07	1514 579	-120 809	81 17639	174 3165	418 29	847 0911	1702 159	4069 328	261 9787	16 97874	810 1691	1684 089	60 15491	1 068919	413 8495
E1	1355 6	199 38	1013 12	321	1544 6	1528 863	-135 093	82 24829	176 7553	420 28	844 527	1713 299	4070 565	262 0277	17 02766	807 5059	1695 356	60 46702	1 074349	415 8786
E1	1355 6	199 38	1013 12	321	1559 72	1543 72	-149 95	83 36531	179 3544	423 2	841 7984	1724 907	4075 868	262 0784	17 07842	804 6782	1707 099	60 78913	1 079951	418 8308
E1	1355 6	199 38	1013 12	321	1574 84	1558 558	-164 788	84 4707	182 0043	425 93	839 0217	1736 53	4077 031	262 1282	17 12824	801 8094	1718 859	61 10801	1 085492	421 5958
E1	1355 6	199 38	1013 12	321	1589 96	1573 408	-179 638	85 62647	184 6325	428 22	836 2603	1748 224	4082 538	262 182	17 18202	798 939	1730 682	61 42241	1 090962	423 9231
E1	1355 6	199 38	1013 12	321	1605 08	1588 267	-194 497	86 7207	187 2053	431 04	833 5629	1760 008	4083 166	262 2325	17 23248	796 1448	1742 598	61 73091	1 09632	426 7761
E1	1355 6	199 38	1013 12	314	1619 59	1602 528	-208 758	87 69224	189 6822	432 96	830 9777	1771 367	4091 295	262 2758	17 27577	793 4893	1754 093	62 02303	1 101382	428 7379
E1	1355 6	199 38	1013 12	314	1634 7	1617 376	-223 606	88 63707	192 3085	435 41	828 2485	1783 224	4095 505	262 3161	17 31612	790 7099	1766 101	62 32427	1 106588	431 2292
E1	1355 6	199 38	1013 12	314	1649 82	1632 219	-238 449	89 6266	195 0079	437 93	825 4412	1795 089	4099 032	262 3591	17 35914	787 8451	1778 115	62 62367	1 111766	433 7889
E1	1355 6	199 38	1013 12	314	1664 94	1647 077	-253 307	90 78781	197 5678	440 88	822 75	1807 07	4098 779	262 4156	17 41558	785 0343	1790 213	62 91607	1 116851	436 7674
E1	1355 6	199 38	1013 12	314	1680 06	1661 953	-268 183	92 02895	199 9905	444 1	820 1853	1819 169	4096 304	262 4792	17 47919	782 3141	1802 411	63 20131	1 121827	440 0091
E1	1355 6	199 38	1013 12	309	1694 6	1676 269	-282 499	93 22387	202 2452	445 81	817 794	1830 889	4106 883	262 5415	17 54151	779 7657	1814 223	63 47009	1 126517	441 7517
E1	1355 6	199 38	1013 12	309	1709 71	1691 153	-297 383	94 38707	204 5744	449 09	815 334	1843 128	4104 14	262 6013	17 60131	777 1631	1826 564	63 74517	1 131306	445 0539
E1	1355 6	199 38	1013 12	309	1724 83	1706 057	-312 287	95 47507	206 8784	452 23	812 9095	1855 443	4102 874	262 6564	17 65645	774 6152	1838 987	64 01591	1 136008	448 2193
E1	1355 6	199 38	1013 12	309	1739 95	1720 973	-327 203	96 65756	209 0399	455 3	810 615	1867 666	4102 494	262 7198	17 71981	772 1565	1851 5	64 27963	1 140606	451 3107
E1	1355 6	199 38	1013 12	309	1755 07	1735 893	-342 123	97 9281	211 1208	458 44	808 3905	1880 361	4101 651	262 7904	17 79045	769 7335	1864 069	64 538	1 145125	454 4679
E1	1355 6	199 38	1013 12	302	1769 55	1750 184	-356 414	99 17812	213 0749	461 07	806 2955	1892 381	4104 324	262 8611	17 86115	767 4342	1876 152	64 78129	1 149387	457 116
E1	1355 6	199 38	1013 12	302	1784 67	1765 114	-371 344	100 413	215 1253	464 84	804 1082	1904 974	4098 129	262 9303	17 9303	765 0541	1888 821	65 03214	1 15377	460 8984
E1	1355 6	199 38	1013 12	302	1799 81	1780 074	-386 304	101 5546	217 1548	468 07	801 9541	1917 645	4096 919	262 9934	17 99339	762 7322	1901 576	65 27916	1 158073	464 1479
E1	1355 6	199 38	1013 12	302	1814 93	1795 004	-401 234	102 6256	219 2813	471 08	799 7133	1930 286	4097 577	263 051	18 05097	760 3524	1914 314	65 5249	1 16234	467 1821
E1	1355 6	199 38	1013 12	302	1830 05	1809 908	-416 138	103 6579	221 5995	474 24	797 2876	1942 865	4096 796	263 1044	18 10445	757 8151	1927 003	65 77211	1 166621	470 3682
E1	1355 6	199 38	1013 12	295	1844 56	1824 185	-430 415	104 6351	224 0189	476 81	794 7686	1954 868	4099 888	263 1535	18 15345	755 2094	1939 121	66 01115	1 170752	472 9693
E1	1355 6	199 38	1013 12	295	1859 68	1839 061	-445 291	105 651	226 531	479 94	792 1536	1967 413	4099 29	263 2047	18 20474	752 5033	1951 786	66 25686	1 174997	476 1278
E1	1355 6	199 38	1013 12	295	1874 79	1853 954	-460 184	106 6363	228 8596	483 85	789 7251	1980 085	4092 353	263 2557	18 25574	749 9765	1964 57	66 49469	1 179106	480 0588
E1	1355 6	199 38	1013 12	295	1889 91	1868 866	-475 096	107 6187	231 1599	485 71	787 3257	1992 819	4102 899	263 3071	18 30707	747 4765	1977 414	66 72895	1 183154	481 9554
E1	1355 6	199 38	1013 12	295	1905 03	1883 778	-490 008	108 5897	233 4649	488 14	784 9235	2005 586	4108 629	263 3579	18 35786	744 9771	1990 [illegible]	66 96031	1 187149	484 4175
E1	1355 6	199 38	1013 12	288	1919 57	1898 111	-504 341	109 4953	235 7029	489 83	782 5961	2017 88	4119 551	263 4048	18 40476	742 5661	2002 695	67 1604	1 190944	486 1439
E1	1355 6	199 38	1013 12	288	1934 69	1912 999	-519 229	110 4313	238 1669	492 62	780 0412	2030 628	4122 098	263 4523	18 45227	739 9374	2015 562	67 40977	1 194894	488 9652
E1	1355 6	199 38	1013 12	288	1949 81	1927 838	-534 068	111 4574	240 8965	495 38	777 2127	2043 258	4124 628	263 5045	18 50448	737 0299	2028 314	67 64284	1 198913	491 7568
E1	1355 6	199 38	1013 12	288	1964 92	1942 604	-548 834	112 6008	243 8654	497 74	774 114	2055 753	4130 175	263 5635	18 56354	733 6378	2040 928	67 87925	1 202999	494 1505
E1	1355 6	199 38	1013 12	288	1980 04	1957 309	-563 539	113 8998	247 137	500 32	770 7378	2068 123	4133 6	263 6324	18 6324	730 3418	2053 41	68 11931	1 207163	496 7608
E1	1355 6	199 38	1013 12	282	1994 61	1971 406	-577 636	115 3415	250 5164	502 26	767 2202	2079 911	4141 103	263 7114	18 71141	726 6698	2065 297	68 35395	1 211252	498 731
E1	1355 6	199 38	1013 12	282	2009 73	1985 946	-592 176	117 0511	254 3027	505 15	763 2704	2091 988	4141 32	263 8078	18 80784	722 5157	2077 465	68 6014	1 215586	501 6432
E1	1355 6	199 38	1013 12	282	2024 85	2000 496	-606 726	118 7694	258 0486	507 81	759 3621	2104 128	4143 533	263 9062	18 90624	718 3946	2089 692	68 84503	1 219857	504 3261
E1	1355 6	199 38	1013 12	282	2039 97	2015 074	-621 304	120 4769	261 6794	511 09	755 5718	2116 374	4140 903	264 0058	19 00577	714 3824	2102 021	69 08317	1 224034	507 6239
E1	1355 6	199 38	1013 12	282	2055 08	2029 679	-635 909	122 1719	265 1617	514 17	751 9327	2128 734	4140 137	264 1065	19 10651	710 51	2114 458	69 315	1 228103	510 7217
E1	1355 6	199 38	1013 12	277	2069 62	2043 759	-649 989	123 8173	268 3834	516 65	748 5601	2140 731	4143 485	264 2065	19 20646	706 6947	2126 52	69 53257	1 23193	513 2203
E1	1355 6	199 38	1013 12	277	2084 74	2058 399	-664 629	125 5471	271 7376	519 9	745 0497	2153 236	4141 635	264 3128	19 31277	703 1238	2139 091	69 7563	1 235867	516 4846
E1	1355 6	199 38	1013 12	277	2099 86	2073 009	-679 239	127 3186	275 1989	523 03	741 4313	2165 707	4140 695	264 4225	19 42249	699 2381	2151 628	69 97985	1 239805	519 6297
E1	1355 6	199 38	1013 12	277	2114 98	2087 583	-693 813	129 1502	278 7745	525 42	737 6961	2178 139	4145 52	264 5371	19 53708	695 2234	2164 123	70 20342	1 243748	522 0391
E1	1355 6	199 38	1013 12	277	2130 09	2102 117	-708 347	131 0524	282 4381	528 26	733 8696	2190 535	4146 698	264 6577	19 65769	691 0991	2176 579	70 42634	1 247687	524 8945

A	B	C	D	E	F	G	H	I	J	K	L	M	N	O	P	Q	R	S	T	U
E0	1367 8	-196 34	21 48	270	614 51	612 5563	781 2137	14 60826	33 5285	153 79	211 2921	623 4805	4054 103	3 268948				70 19066		
E0	1367 8	-196 34	21 48	270	629 63	627 369	766 401	16 1451	36 13025	157 39	212 9896	638 001	4053 631	3 944142				70 49805		
E0	1367 8	-196 34	21 48	270	644 77	642 2012	751 5688	17 68397	38 73545	160 88	214 7184	652 5679	4056 24	4 609441				70 78972		
E0	1367 8	-196 34	21 48	270	659 89	656 9762	736 7938	19 31712	41 48935	164 34	216 5834	667 1411	4059 517	5 300906				71 05599		
E0	1367 8	-196 34	21 48	270	675 01	671 7148	722 0553	21 04714	44 39091	167 7	218 5911	681 7392	4065 231	6 016319				71 29852		
E0	1367 8	-196 34	21 48	265	689 61	685 9994	707 7706	22 60492	46 99213	171 03	220 4263	695 8639	4068 666	6 646307				71 53252		
E0	1367 8	-196 34	21 48	265	704 73	700 8423	692 9277	24 06123	49 46656	174 48	222 171	710 5017	4072 11	7 236694				71 77822		
E0	1367 8	-196 34	21 48	265	719 88	715 7656	678 0044	25 40504	51 72266	178 2	223 7979	725 192	4069 54	7 766358				72 02482		
E0	1367 8	-196 34	21 48	265	734 99	730 6483	663 1217	26 76348	53 91729	181 78	225 4492	739 864	4070 107	8 272341				72 25886		
E0	1367 8	-196 34	21 48	265	750 11	745 5478	648 2222	28 10338	56 12229	185 45	227 1011	754 5642	4068 828	8 774225				72 48413		
E0	1367 8	-196 34	21 48	259	764 5	759 7272	634 0428	29 34156	58 28156	188 46	228 6625	768 5611	4078 112	9 26162				72 69128		
E0	1367 8	-196 34	21 48	259	779 62	774 603	619 167	30 66469	60 60475	192 21	230 3516	783 2709	4075 079	9 778978				72 89706		
E0	1367 8	-196 34	21 48	259	794 74	789 4989	604 2711	31 90006	62 91377	195 96	231 9704	797 9891	4072 204	10 28919				73 10051		
E0	1367 8	-196 34	21 48	259	809 85	804 3724	589 3976	33 07124	65 2717	199 56	233 5535	812 6854	4072 386	10 80703				73 29854		
E0	1367 8	-196 34	21 48	259	824 97	819 2555	574 5145	34 26014	67 67273	203 39	235 1812	827 4129	4068 11	11 3273				73 48677		
E0	1367 8	-196 34	21 48	254	839 78	833 8389	559 9311	35 34536	70 00229	206 67	236 7119	841 8341	4073 325	11 8286				73 669		
E0	1367 8	-196 34	21 48	254	854 9	848 7469	545 0231	36 36733	72 32419	210 43	238 197	856 5627	4070 535	12 32486				73 85407		
E0	1367 8	-196 34	21 48	254	870 02	863 6495	530 1205	37 41203	74 66457	214 28	239 7261	871 3068	4066 207	12 81804				74 03		
E0	1367 8	-196 34	21 48	254	885 14	878 5411	515 2289	38 47516	77 0192	218 06	241 2939	886 0588	4063 372	13 30722				74 19747		
E0	1367 8	-196 34	21 48	254	900 26	893 4405	500 3295	39 60796	79 35652	222 02	242 9426	900 8475	4057 506	13 78217				74 35464		
E0	1367 8	-196 34	21 48	247	914 52	907 4847	486 2853	40 70239	81 57313	225 47	244 5409	914 8051	4057 325	14 22548				74 49546		
E0	1367 8	-196 34	21 48	247	929 64	922 3692	471 4008	41 85921	83 94453	229 51	246 2533	929 6087	4050 406	14 69418				74 63899		
E0	1367 8	-196 34	21 48	247	944 76	937 2565	456 5135	42 96706	86 33941	233 61	247 9407	944 4139	4042 695	15 16457				74 77953		
E0	1367 8	-196 34	21 48	247	959 91	952 2013	441 5687	43 96128	88 63558	237 23	249 5087	959 2492	4043 541	15 61377				74 92351		
E0	1367 8	-196 34	21 48	247	975 02	967 1239	426 6461	44 90899	90 82449	241 02	251 0174	974 0536	4041 381	16 03674				75 06614		
E0	1367 8	-196 34	21 48	242	989 62	981 554	412 216	45 82752	92 8401	244 18	252 4626	988 3714	4047 717	16 41879				75 20076		
E0	1367 8	-196 34	21 48	242	1004 74	996 5069	397 2631	46 79953	94 84906	247 83	253 9682	1003 216	4047 999	16 79156				75 33576		
E0	1367 8	-196 34	21 48	242	1019 86	1011 469	382 3006	47 78381	96 81759	251 7	255 4842	1018 077	4044 804	17 15044				75 4664		
E0	1367 8	-196 34	21 48	242	1034 98	1026 432	367 3381	48 74456	98 73122	255 46	256 9712	1032 937	4043 438	17 49497				75 59483		
E0	1367 8	-196 34	21 48	242	1050 1	1041 403	352 3668	49 72417	100 5934	259 25	258 4695	1047 812	4041 707	17 82339				75 71914		
E0	1367 8	-196 34	21 48	236	1064 57	1055 732	338 0383	50 66241	102 3868	262 1	259 9156	1062 057	4052 106	18 13646				75 83421		
E0	1367 8	-196 34	21 48	236	1079 69	1070 698	323 0716	51 63404	104 3125	266 07	261 4428	1076 945	4047 599	18 47122				75 9503		
E0	1367 8	-196 34	21 48	236	1094 81	1085 653	308 1171	52 59691	106 3134	269 96	262 9948	1091 831	4044 117	18 81823				76 0618		
E0	1367 8	-196 34	21 48	236	1109 93	1100 607	293 1633	53 62368	108 3228	273 8	264 6196	1106 737	4042 138	19 15833				76 16664		
E0	1367 8	-196 34	21 48	236	1125 05	1115 547	278 2225	54 70585	110 3726	277 77	266 3192	1121 653	4038 063	19 4985				76 26462		
E0	1367 8	-196 34	21 48	231	1139 56	1129 874	263 8958	55 75218	112 4045	281 07	267 9883	1135 968	4041 582	19 83334				76 35462		
E0	1367 8	-196 34	21 48	231	1154 67	1144 786	248 9836	56 78562	114 0216	284 65	269 7182	1150 868	4043 1	20 20189				76 44606		
E0	1367 8	-196 34	21 48	231	1169 79	1159 702	234 0675	57 66054	116 949	288 4	271 3496	1165 753	4042 139	20 59931				76 53993		
E0	1367 8	-196 34	21 48	231	1184 91	1174 618	219 1521	58 49508	119 2861	292 07	272 9596	1180 635	4042 301	20 99688				76 63243		
E0	1367 8	-196 34	21 48	231	1200 03	1189 536	204 2336	59 35417	121 5981	295 77	274 5963	1195 529	4042 091	21 38304				76 72141		
E0	1367 8	-196 34	21 48	225	1214 57	1203 887	189 8827	60 18386	123 7779	298 98	276 1691	1209 859	4046 622	21 74139				76 80502		
E0	1367 8	-196 34	21 48	225	1229 69	1218 817	174 9533	60 99382	125 9819	302 84	277 7433	1224 755	4044 231	22 10181				76 89275		
E0	1367 8	-196 34	21 48	225	1244 8	1233 753	160 0174	61 71372	128 1653	306 62	279 2373	1239 642	4042 926	22 46133				76 98204		
E0	1367 8	-196 34	21 48	225	1259 92	1248 683	145 087	62 55146	130 4017	310 01	280 8714	1254 558	4046 831	22 81763				77 06293		
E0	1367 8	-196 34	21 48	225	1275 04	1263 598	130 1725	63 50578	132 7039	313 77	282 6492	1269 493	4045 935	23 17278				77 13543		
E0	1367 8	-196 34	21 48	220	1289 58	1277 924	115 8461	64 52142	134 9925	316 93	284 4886	1283 87	4050 958	23 51601				77 19775		
E0	1367 8	-196 34	21 48	220	1304 7	1292 809	100 9611	65 5242	137 4446	320 88	286 3925	1298 808	4047 643	23 88579				77 26136		
E0	1367 8	-196 34	21 48	220	1319 81	1307 689	86 08146	66 50866	139 8702	324 23	288 2805	1313 738	4051 871	24 24738				77 32413		
E0	1367 8	-196 34	21 48	220	1334 93	1322 584	71 18585	67 57276	142 245	327 97	290 2311	1328 699	4051 284	24 58856				77 38302		
E0	1367 8	-196 34	21 48	220	1350 05	1337 477	56 2929	68 70942	144 599	331 54	292 249	1343 674	4052 827	24 91549				77 43777		
E0	1367 8	-196 34	21 48	214	1364 65	1351 843	41 92695	69 82602	146 9145	334 33	294 2417	1358 13	4062 244	25 23281				77 48753		
E0	1367 8	-196 34	21 48	214	1379 77	1366 719	27 05108	70 92064	149 4266	338 02	296 3082	1373 101	4062 189	25 58199				77 53783		
E0	1367 8	-196 34	21 48	214	1394 89	1381 575	12 1951	72 03251	151 9872	341 72	298 4224	1388 063	4061 991	25 93325				77 58495		
E0	1367 8	-196 34	21 48	214	1410	1396 416	-2 64564	73 17955	154 5674	345 23	300 5878	1403 023	4064 025	26 27993				77 62888		
E0	1367 8	-196 34	21 48	214	1425 12	1411 27	-17 5002	74 33737	157 1461	348 75	302 7731	1418 001	4065 954	26 62047				77 67123		

E0	1367 8	-196 34	21 48	209	1439 54	1425 453	-31 6825	75 3753	159 5626	351 84	304 7885	1432 287	4070 849	26 93916	77 7136
E0	1367 8	-196 34	21 48	209	1454 66	1440 337	-46 5668	76 32285	162 0412	355 48	306 7613	1447 251	4071 259	27 27168	77 76268
E0	1367 8	-196 34	21 48	209	1469 78	1455 225	-61 4546	77 22473	164 5163	359 24	308 7022	1462 213	4070 295	27 60331	77 81201
E0	1367 8	-196 34	21 48	209	1484 89	1470 105	-76 3347	78 12121	166 9766	362 63	310 6416	1477 167	4073 483	27 92882	77 86033
E0	1367 8	-196 34	21 48	209	1500 01	1484 995	-91 2254	79 05089	169 4204	366 22	312 6124	1492 14	4074 436	28 24476	77 90659
E0	1367 8	-196 34	21 48	203	1514 55	1499 313	-105 543	80 05237	171 772	369 45	314 6116	1506 559	4077 842	28 53572	77 94633
E0	1367 8	-196 34	21 48	203	1529 67	1514 186	-120 416	81 14702	174 2507	373 39	316 7616	1521 553	4074 97	28 83502	77 9841
E0	1367 8	-196 34	21 48	203	1544 79	1529 05	-135 28	82 26237	176 7878	377 45	318 9667	1536 551	4070 874	29 13762	78 01907
E0	1367 8	-196 34	21 48	203	1559 91	1543 906	-150 136	83 37919	179 3877	381 21	321 2128	1551 55	4070 067	29 44569	78 05182
E0	1367 8	-196 34	21 48	203	1575 02	1558 734	-164 964	84 48446	182 0356	384 84	323 4818	1566 527	4070 593	29 75788	78 0829
E0	1367 8	-196 34	21 48	198	1589 47	1572 927	-179 157	85 58902	184 5474	387 91	325 6915	1580 87	4075 353	30 04503	78 11076
E0	1367 8	-196 34	21 48	198	1604 59	1587 786	-194 016	86 68592	187 1226	391 7	327 9346	1595 872	4074 221	30 33855	78 14186
E0	1367 8	-196 34	21 48	198	1619 71	1602 646	-208 876	87 69968	189 703	395 38	330 1174	1610 865	4074 22	30 63621	78 17449
E0	1367 8	-196 34	21 48	198	1634 83	1617 504	-223 734	88 64558	192 3317	398 65	332 2756	1625 849	4078 388	30 94311	78 20735
E0	1367 8	-196 34	21 48	198	1649 94	1632 337	-238 567	89 63445	195 0293	402	334 5157	1640 828	4081 66	31 25231	78 23663
E0	1367 8	-196 34	21 48	192	1664 57	1646 714	-252 944	90 75891	197 5056	405 36	336 7652	1655 361	4083 682	31 51322	78 26186
E0	1367 8	-196 34	21 48	192	1679 69	1661 589	-267 819	91 9977	199 933	409 18	339 093	1670 399	4082 308	31 75347	78 28748
E0	1367 8	-196 34	21 48	192	1694 81	1676 476	-282 706	93 24013	202 2776	413 34	341 386	1685 442	4077 617	31 97835	78 31389
E0	1367 8	-196 34	21 48	192	1709 93	1691 37	-297 6	94 4029	204 6079	417 15	343 6092	1700 477	4076 417	32 20527	78 34218
E0	1367 8	-196 34	21 48	192	1725 05	1706 274	-312 504	95 4909	206 9119	421 51	345 7604	1715 509	4069 912	32 43223	78 3724
E0	1367 8	-196 34	21 48	187	1739 52	1720 548	-326 778	96 62338	208 9792	424 04	347 8268	1729 907	4079 585	32 61961	78 40065
E0	1367 8	-196 34	21 48	187	1754 64	1735 468	-341 698	97 69031	211 0629	428 08	350 0188	1744 963	4076 255	32 7951	78 42865
E0	1367 8	-196 34	21 48	187	1769 76	1750 391	-356 621	99 19527	213 1034	432 01	352 2224	1760 026	4074 039	32 95915	78 45582
E0	1367 8	-196 34	21 48	187	1784 88	1765 322	-371 552	100 4302	215 1537	435 7	354 3756	1775 085	4074 098	33 12867	78 48417
E0	1367 8	-196 34	21 48	187	1800	1780 262	-386 492	101 5689	217 1803	439 52	356 4384	1790 137	4072 936	33 30145	78 51494
E0	1367 8	-196 34	21 48	181	1814 57	1794 648	-400 878	102 6008	219 2296	442 54	358 4279	1804 631	4077 894	33 48467	78 54399
E0	1367 8	-196 34	21 48	181	1829 68	1809 544	-415 774	103 6329	221 5377	446 55	360 5646	1819 655	4074 918	33 70009	78 5712
E0	1367 8	-196 34	21 48	181	1844 8	1824 421	-430 651	104 6513	224 0588	450 48	362 8138	1834 683	4072 729	33 94208	78 59441
E0	1367 8	-196 34	21 48	181	1859 92	1839 297	-445 527	105 6671	226 5709	454 07	365 0624	1849 71	4073 622	34 18015	78 61726
E0	1367 8	-196 34	21 48	181	1875 04	1854 2	-460 43	106 6525	228 8977	457 57	367 1874	1864 739	4075 309	34 39412	78 64363
E0	1367 8	-196 34	21 48	176	1844 44	1824 067	-430 297	104 6271	223 9989	450	362 7604	1834 325	4076 278	33 93637	78 59386
E0	1367 8	-196 34	21 48	176	1859 55	1838 933	-445 163	105 6423	226 5094	453 87	365 0073	1849 342	4074 607	34 17435	78 61671
E0	1367 8	-196 34	21 48	176	1874 67	1853 835	-460 065	106 6285	228 8413	457 93	367 1357	1864 371	4071 302	34 38898	78 64298
E0	1367 8	-196 34	21 48	176	1889 79	1868 747	-474 977	107 6109	231 1417	460 85	369 2481	1879 407	4078 133	34 59745	78 66936
E0	1367 8	-196 34	21 48	176	1904 91	1883 66	-489 89	108 5823	233 4465	464 37	371 3588	1894 445	4079 602	34 80506	78 69538
E0	1367 8	-196 34	21 48	169	1919 57	1898 111	-504 341	109 4953	235 7029	467 14	373 3988	1909 015	4086 602	35 00939	78 72036
E0	1367 8	-196 34	21 48	169	1934 69	1912 999	-519 229	110 4313	238 1669	470 57	375 582	1924 043	4088 75	35 23535	78 74333
E0	1367 8	-196 34	21 48	169	1949 81	1927 838	-534 068	111 4574	240 8965	473 85	377 9985	1939 068	4092 156	35 48355	78 75889
E0	1367 8	-196 34	21 48	169	1964 92	1942 604	-548 834	112 6008	243 8854	477 21	380 6686	1954 072	4094 783	35 74998	78 7665
E0	1367 8	-196 34	21 48	169	1980 07	1957 338	-563 568	113 9027	247 144	479 86	383 6337	1969 1	4103 49	36 03135	78 76539
E0	1367 8	-196 34	21 48	163	1994 55	1971 348	-577 578	115 3356	250 5024	483 08	386 7725	1983 454	4105 849	36 30883	78 75531
E0	1367 8	-196 34	21 48	163	2009 67	1985 888	-592 118	117 0443	254 2877	486 33	390 3961	1998 422	4109 189	36 60801	78 7347
E0	1367 8	-196 34	21 48	163	2024 79	2000 438	-606 668	118 7625	258 0339	490 19	394 0144	2013 398	4107 383	36 8963	78 7146
E0	1367 8	-196 34	21 48	163	2039 9	2015 007	-621 237	120 4691	261 6631	493 71	397 5625	2028 379	4108 443	37 16693	78 69685
E0	1367 8	-196 34	21 48	163	2055 02	2029 62	-635 85	122 1652	265 1484	497 26	401 0235	2043 388	4109 295	37 41734	78 682
E0	1367 8	-196 34	21 48	158	2069 56	2043 701	-649 931	123 8105	268 3701	500 29	404 2908	2057 836	4113 287	37 6383	78 66974
E0	1367 8	-196 34	21 48	158	2084 68	2058 341	-664 571	125 5402	271 7243	503 92	407 712	2072 863	4113 477	37 86312	78 65652
E0	1367 8	-196 34	21 48	158	2099 8	2072 951	-679 181	127 3115	275 1849	507 63	411 2378	2087 881	4112 998	38 09229	78 64051
E0	1367 8	-196 34	21 48	158	2114 92	2087 525	-693 755	129 1427	278 76	510 58	414 8879	2102 889	4118 628	38 32485	78 62122
E0	1367 8	-196 34	21 48	158	2130 03	2102 059	-708 289	131 0446	282 4234	513 96	418 6551	2117 881	4120 712	38 55676	78 59868

A	B	C	D	E	F	G	H	I	J	K	L	M	N	O	P	Q	R	S	T	U
Zero	1388 1	10 32	37 46	49	589 64	588 0878	805 6822	12 3553	29 73998	143 27	7 983809	582 4725	4065 558	284 7693				89 21464		
Zero	1388 1	10 32	37 46	49	604 75	602 9948	790 7752	13 61623	31 84906	147 44	6 507522	597 3602	4051 548	300 4327				89 37582		
Zero	1388 1	10 32	37 46	49	619 87	617 8074	775 9626	15 15307	34 45081	150 91	5 693309	612 1639	4056 483	328 0926				89 46712		
Zero	1388 1	10 32	37 46	49	634 99	632 62	761 15	16 68991	37 05257	154 94	6 382924	626 9825	4046 615	356 3403				89 4167		
Zero	1388 1	10 32	37 46	49	650 11	647 4327	746 3373	18 22675	39 65433	158 2	8 20559	641 8151	4056 986	15 51073				89 26745		
Zero	1388 1	10 32	37 46	46	739 63	735 2206	658 5494	27 17915	54 59396	179 11	24 03754	729 9465	4075 409	45 46319				88 11288		
Zero	1388 1	10 32	37 46	46	754 75	750 1204	643 6496	28 50541	56 60856	182 5	26 55326	744 9238	4081 774	48 77498				87 95722		
Zero	1388 1	10 32	37 46	46	769 86	765 0034	628 7666	29 80498	59 10231	186 53	29 12137	759 8917	4073 831	48 0027				87 80371		
Zero	1388 1	10 32	37 46	46	784 98	779 8807	613 8893	31 11815	61 42404	190 07	31 73071	774 8607	4076 712	49 04562				87 65307		
Zero	1388 1	10 32	37 46	46	800 1	794 7815	598 9885	32 30897	63 73711	194 26	34 2637	789 8551	4065 969	50 07705				87 51374		
Zero	1388 1	10 32	37 46	43	889 53	882 8662	510 9038	38 79626	77 69976	216 16	49 29641	878 5803	4064 491	54 7143				86 78349		
Zero	1388 1	10 32	37 46	43	904 65	897 7668	496 0032	39 94005	80 03435	220 24	51 86447	893 6032	4057 407	55 17269				86 6727		
Zero	1388 1	10 32	37 46	43	919 76	912 6428	481 1272	41 10903	82 39188	224 16	54 46869	908 6069	4053 386	55 57957				86 5632		
Zero	1388 1	10 32	37 46	43	934 88	927 5284	466 2416	42 24385	84 77513	228 04	57 07761	923 6237	4050 271	55 99218				86 45701		
Zero	1388 1	10 32	37 46	43	950	942 4255	451 3445	43 31094	87 13359	231 94	59 6311	938 6516	4046 959	56 4097				86 35763		
Zero	1388 1	10 32	37 46	40	1039 52	1030 925	362 845	49 03393	99 3034	253 33	72 96146	1027 648	4057 347	57 95346				85 92945		
Zero	1388 1	10 32	37 46	40	1054 64	1045 899	347 8705	50 02036	101 1469	257 59	75 04759	1042 933	4048 811	58 06192				85 87353		
Zero	1388 1	10 32	37 46	40	1069 76	1060 87	332 9	50 99664	103 0417	261 09	77 1722	1058 018	4052 312	58 191				85 81711		
Zero	1388 1	10 32	37 46	40	1084 87	1075 822	317 9483	51 96391	104 998	265 37	79 34477	1073 089	4043 747	58 34202				85 75965		
Zero	1388 1	10 32	37 46	40	1099 99	1090 776	302 994	52 94193	107 0009	268 97	81 56328	1088 167	4045 682	58 49569				85 70138		
Zero	1388 1	10 32	37 46	37	1189 57	1179 215	214 5552	58 74992	120 0069	290 53	95 70502	1177 441	4052 734	59 60004				85 33773		
Zero	1388 1	10 32	37 46	37	1204 69	1194 135	199 6349	59 62642	122 3045	294 54	98 13108	1192 51	4048 719	59 83747				85 27982		
Zero	1388 1	10 32	37 46	37	1219 81	1209 061	184 7089	60 46517	124 5419	297 86	100 4878	1207 579	4054 185	60 06497				85 22666		
Zero	1388 1	10 32	37 46	37	1234 93	1223 996	169 7737	61 24347	126 7391	301 8	102 7811	1222 654	4051 206	60 30021				85 1778		
Zero	1388 1	10 32	37 46	37	1250 05	1238 94	154 83	61 97978	128 931	298 53	105 0508	1237 736	4146 103	60 54367				85 13126		
Zero	1388 1	10 32	37 46	34	1339 57	1327 156	66 61352	67 91834	142 9627	326 75	120 2015	1326 942	4061 031	61 36803				84 80272		
Zero	1388 1	10 32	37 46	34	1354 68	1342 033	51 73708	69 06498	145 3305	330 35	122 8293	1341 996	4062 346	61 42783				84 74852		
Zero	1388 1	10 32	37 46	34	1369 8	1356 91	36 8601	70 19885	147 7701	333 92	125 5141	1357 057	4064 018	61 50588				84 69313		
Zero	1388 1	10 32	37 46	34	1384 92	1371 782	21 98774	71 2965	150 2907	337 31	128 2533	1372 119	4067 829	61 61212				84 63668		
Zero	1388 1	10 32	37 46	34	1400 07	1386 663	7 107424	72 41491	152 8686	341 29	131 0531	1387 197	4064 57	61 7178				84 57899		
Zero	1388 1	10 32	37 46	31	1489 56	1474 704	-80 9339	78 40424	167 7313	361 7	146 9901	1476 369	4081 751	62 40689				84 28606		
Zero	1388 1	10 32	37 46	31	1504 68	1489 594	-95 8239	79 37255	170 1757	365 4	149 6052	1491 446	4081 681	62 51184				84 24305		
Zero	1388 1	10 32	37 46	31	1519 79	1504 47	-110 7	80 42145	172 6246	369 51	152 2619	1506 514	4077 06	62 58705				84 19927		
Zero	1388 1	10 32	37 46	31	1534 91	1519 338	-125 568	81 53183	175 1131	373 07	154 9823	1521 582	4078 542	62 6462				84 15394		
Zero	1388 1	10 32	37 46	31	1550 03	1534 201	-140 431	82 65062	177 6837	377 22	157 7796	1536 652	4073 624	62 71428				84 10663		
Zero	1388 1	10 32	37 46	28	1639 64	1622 225	-228 455	88 96037	193 1904	398 18	174 46	1625 942	4083 435	63 20725				83 84043		
Zero	1388 1	10 32	37 46	28	1654 76	1637 072	-243 302	89 9925	195 8553	401 89	177 3042	1641 009	4083 229	63 29769				83 79732		
Zero	1388 1	10 32	37 46	28	1669 88	1651 932	-258 162	91 17375	198 3989	405 59	180 1073	1656 085	4083 151	63 3256				83 75646		
Zero	1388 1	10 32	37 46	28	1685	1666 816	-273 046	92 44617	200 7583	409 61	182 7869	1671 173	4079 911	63 30122				83 72063		
Zero	1388 1	10 32	37 46	28	1700 11	1681 696	-287 926	93 65045	203 0954	411 94	185 4159	1686 251	4093 439	63 29323				83 68714		
Zero	1388 1	10 32	37 46	25	1789 6	1769 985	-376 215	100 7862	215 7865	435 65	199 9612	1775 611	4075 774	63 10102				83 53389		
Zero	1388 1	10 32	37 46	25	1804 72	1784 926	-391 156	101 9221	217 8159	439 24	202 2849	1790 718	4076 855	63 07417				83 51385		
Zero	1388 1	10 32	37 46	25	1819 84	1799 85	-406 08	102 964	219 988	443 2	204 6916	1805 819	4074 5	63 0892				83 49147		
Zero	1388 1	10 32	37 46	25	1834 96	1814 739	-420 969	103 9887	222 4187	447 09	207 3247	1820 911	4072 806	63 14096				83 46226		
Zero	1388 1	10 32	37 46	25	1850 07	1829 606	-435 836	105 0053	224 9343	450 88	210 0284	1835 989	4072 012	63 2036				83 43125		

A	B	C	D	E	F	G	H	I	J	K	L	M	N	O	P	Q	R	S	T	U
W0	1372	-417 34	-389 16	146	589 67	588 1174	805 6526	12 35778	29 74411	233 72	600 1007	825 1486	3530 501	44 27127	20 72873	561 2542	797 3429	43 34251	0 789915	225 8441
W0	1372	-417 34	-389 16	146	604 78	603 0241	790 7459	13 61928	31 85422	237 67	602 4773	837 159	3522 359	44 33122	20 66878	563 6997	809 6998	43 97285	0 800729	229 8743
W0	1372	-417 34	-389 16	146	619 9	617 8368	775 9332	15 15612	34 45598	239 94	605 3952	849 5875	3540 833	44 40571	20 59429	566 7072	822 4674	44 55515	0 810642	232 2608
W0	1372	-417 34	-389 16	146	635 02	632 6494	761 1206	16 69296	37 05773	243 32	608 3142	862 102	3543 079	44 47949	20 52051	569 7147	835 3134	45 12055	0 820252	235 7592
W0	1372	-417 34	-389 16	146	650 14	647 462	746 308	18 22979	39 65949	246 12	611 2342	874 6987	3553 952	44 55257	20 44743	572 7222	848 2342	45 66967	0 829569	238 6735
W0	1372	-417 34	-389 16	138	739 51	735 1024	658 6676	27 1684	54 57646	262 64	628 0842	950 4382	3618 787	44 95021	20 04979	590 0192	925 7244	48 63631	0 87973	255 8107
W0	1372	-417 34	-389 16	138	754 62	749 9923	643 7777	28 49429	56 78899	265 7	630 586	963 2998	3625 517	45 00737	19 99263	592 5848	938 8634	49 10989	0 887732	258 9599
W0	1372	-417 34	-389 16	138	769 77	764 9148	628 8552	29 7972	59 08853	268 91	633 1338	976 28	3630 508	45 07111	19 92889	595 2195	952 1294	49 57015	0 895478	262 2579
W0	1372	-417 34	-389 16	138	784 89	779 792	613 978	31 11074	61 41035	271 65	635 7057	989 3023	3641 827	45 13509	19 86491	597 8789	965 4308	50 01554	0 902962	265 0952
W0	1372	-417 34	-389 16	138	800 01	794 6928	599 0772	32 3021	63 72329	274 66	638 1659	1002 343	3649 395	45 20576	19 79424	600 4786	978 7667	50 45424	0 910304	268 1997
W0	1372	-417 34	-389 16	131	889 56	882 8958	510 8742	38 79853	77 70439	293 41	652 7057	1080 538	3682 69	45 66578	19 33422	615 8953	1058 709	52 83904	0 949928	287 4825
W0	1372	-417 34	-389 16	131	904 68	897 7964	495 9736	39 94232	80 03898	296 72	655 1754	1093 927	3686 733	45 73691	19 26309	618 4946	1072 361	53 20738	0 95604	290 8702
W0	1372	-417 34	-389 16	131	919 79	912 6723	481 0977	41 11136	82 39656	300 24	657 6802	1107 362	3688 256	45 80733	19 19267	621 1253	1086 05	53 56459	0 961961	294 4616
W0	1372	-417 34	-389 16	131	934 91	927 5579	466 2121	42 24605	84 77988	303 39	660 1805	1120 843	3694 398	45 88091	19 11909	623 7649	1099 788	53 91369	0 967733	297 6908
W0	1372	-417 34	-389 16	131	950 03	942 4551	451 3149	43 31291	87 13814	306 61	662 6168	1134 338	3699 611	45 95664	19 04336	626 353	1113 544	54 25745	0 973406	300 9894
W0	1372	-417 34	-389 16	122	1039 52	1030 925	362 845	49 03393	99 3034	323 84	675 3526	1214 288	3749 654	46 32526	18 67474	639 7963	1194 878	56 20854	1 005757	318 6635
W0	1372	-417 34	-389 16	122	1054 64	1045 899	347 8705	50 02036	101 1469	327 48	677 3674	1227 871	3749 454	46 37259	18 62741	641 884	1208 659	56 51903	1 010932	322 356
W0	1372	-417 34	-389 16	122	1069 76	1060 87	332 9	50 99664	103 0417	330 86	679 4128	1241 503	3752 353	46 42325	18 57675	644 0139	1222 49	56 82144	1 015959	325 793
W0	1372	-417 34	-389 16	122	1084 87	1075 822	317 9483	51 96391	104 998	333 83	681 4971	1255 175	3759 921	46 47771	18 52229	646 1956	1236 363	57 11531	1 02083	328 8268
W0	1372	-417 34	-389 16	122	1099 99	1090 776	302 994	52 94193	107 0009	337 29	683 6233	1268 903	3762 053	46 53388	18 46612	648 4242	1250 291	57 40132	1 025562	332 3428
W0	1372	-417 34	-389 16	115	1189 51	1179 156	214 6144	58 74664	119 9976	356 49	697 0653	1351 089	3789 977	46 92249	18 07751	662 6564	1333 662	58 94046	1 050808	351 8919
W0	1372	-417 34	-389 16	115	1204 63	1194 076	199 6941	59 62291	122 2954	360 08	699 3427	1365 057	3790 983	46 99862	18 00138	665 1092	1347 84	59 18168	1 054729	355 5382
W0	1372	-417 34	-389 16	115	1219 75	1209 002	184 7681	60 46195	124 5331	363 72	701 5521	1379 02	3791 432	47 07315	17 92685	667 4919	1362 008	59 42056	1 058615	359 2331
W0	1372	-417 34	-389 16	115	1234 87	1223 937	169 833	61 24061	126 7304	366 92	703 6919	1392 978	3796 408	47 14857	17 85143	669 8124	1376 174	59 6573	1 062464	362 4936
W0	1372	-417 34	-389 16	115	1249 98	1238 871	154 899	61 97572	128 9205	369 93	705 7981	1406 942	3803 265	47 22574	17 77426	672 108	1390 347	59 89051	1 06625	365 5666
W0	1372	-417 34	-389 16	106	1339 57	1327 156	66 61352	67 91834	142 9627	389 26	720 1599	1490 86	3829 986	47 63739	17 36261	687 346	1475 289	61 11521	1 086138	385 1945
W0	1372	-417 34	-389 16	106	1354 68	1342 033	51 73708	69 06498	145 3305	392 87	722 6825	1505 113	3831 07	47 69672	17 30328	689 9766	1489 685	61 30469	1 089228	388 8431
W0	1372	-417 34	-389 16	106	1369 8	1356 91	36 8601	70 19885	147 7701	396 25	725 2504	1519 403	3834 456	47 76018	17 23982	692 6668	1504 123	61 48911	1 092224	392 265
W0	1372	-417 34	-389 16	106	1384 92	1371 782	21 98774	71 2965	150 2907	399 5	727 8549	1533 723	3839 106	47 8296	17 1704	695 4151	1518 596	61 66881	1 095128	395 5599
W0	1372	-417 34	-389 16	106	1400 04	1386 633	7 13689	72 41269	152 8635	402 91	730 5116	1548 063	3842 205	47 90018	17 09982	698 2186	1533 089	61 84311	1 097938	399 0127
W0	1372	-417 34	-389 16	99	1489 56	1474 704	-80 9339	78 40424	167 7313	421 96	745 5805	1633 067	3870 193	48 32455	16 67545	714 2255	1618 992	62 83514	1 113912	418 3233
W0	1372	-417 34	-389 16	99	1504 68	1489 594	-95 8239	79 37255	170 1757	425 64	748 0507	1647 449	3870 521	48 39364	16 60636	716 8501	1633 518	62 99513	1 116491	422 0409
W0	1372	-417 34	-389 16	99	1519 79	1504 47	-110 7	80 42145	172 6246	429 48	750 5787	1661 857	3869 463	48 4579	16 5421	719 5128	1648 059	63 15036	1 119	425 9142
W0	1372	-417 34	-389 16	99	1534 91	1519 338	-125 568	81 53183	175 1131	433 04	753 1781	1676 302	3871 009	48 52022	16 47978	722 2375	1662 63	63 30062	1 12143	429 5081
W0	1372	-417 34	-389 16	99	1550 06	1534 23	-140 46	82 65284	177 6889	436 78	755 8508	1690 812	3871 084	48 58588	16 41412	725 0456	1677 268	63 44644	1 123779	433 2811
W0	1372	-417 34	-389 16	92	1638 48	1621 087	-227 317	88 88445	192 9833	456 36	771 4623	1775 66	3890 919	48 99019	16 00981	741 5407	1762 866	64 24874	1 13664	453 0719
W0	1372	-417 34	-389 16	92	1653 6	1635 932	-242 162	89 90188	195 6601	460 01	774 1504	1790 203	3891 662	49 06337	15 93663	744 3967	1777 539	64 37767	1 138696	456 7558
W0	1372	-417 34	-389 16	92	1668 75	1650 822	-257 052	91 08547	198 2088	463 9	776 6517	1804 801	3890 497	49 12059	15 87941	747 2068	1792 241	64 50476	1 140751	460 6715
W0	1372	-417 34	-389 16	92	1683 87	1665 704	-271 934	92 35073	200 5827	467 33	779 4749	1819 368	3893 112	49 16447	15 83553	749 893	1806 892	64 63193	1 142833	464 1253
W0	1372	-417 34	-389 16	92	1698 99	1680 593	-286 823	93 56374	202 9226	471 24	782 0386	1833 924	3891 699	49 20933	15 79067	752 5263	1821 535	64 75885	1 144911	468 0565
W0	1372	-417 34	-389 16	83	1789 54	1769 926	-376 156	100 7617	215 7785	493 32	796 4927	1921 055	3894 135	49 42039	15 57961	767 2281	1909 107	65 5051	1 157229	490 2519
W0	1372	-417 34	-389 16	83	1804 66	1784 867	-391 097	101 9179	217 8073	497 31	798 7729	1935 6	3892 14	49 45315	15 54685	769 5471	1923 724	65 62704	1 159247	494 2566
W0	1372	-417 34	-389 16	83	1819 78	1799 791	-406 021	102 9599	219 9774	501 32	801 0994	1950 159	3890 047	49 49742	15 50258	771 9542	1938 368	65 74573	1 161189	498 2891
W0	1372	-417 34	-389 16	83	1834 9	1814 68	-420 91	103 9847	222 4087	504 71	803 6141	1964 77	3892 87	49 55445	15 44555	774 5908	1953 079	65 85723	1 162986	501 7067
W0	1372	-417 34	-389 16	83	1850 01	1829 547	-435 777	105 0013	224 9244	508 24	806 1886	1979 393	3894 604	49 61545	15 38455	777 3004	1967 804	65 96524	1 164719	505 2643

A	B	C	D	E	F	G	H	I	J	K	L	M	N	O	P	Q	R	S	T	U
W1	1399 3	-511 08	-600 9	109	573 48	572 1391	821 6309	11 0221	27 51176	268 22	817 0018	1000 597	3730 507	50 27925	14 72075	790 1844	978 8222	35 26259	0 631266	262 3832
W1	1399 3	-511 08	-600 9	109	588 6	587 0614	806 7086	12 2695	29 59658	271 46	819 4026	1011 23	3725 151	50 30532	14 69468	792 601	989 6368	35 87443	0 641998	265 6635
W1	1399 3	-511 08	-600 9	109	603 72	601 9837	791 7863	13 5169	31 68139	273 86	821 8036	1021 976	3731 744	50 33124	14 66876	795 0177	1000 563	36 47346	0 652496	268 122
W1	1399 3	-511 08	-600 9	109	618 84	616 7983	776 9717	15 04838	34 27358	276 57	824 7767	1033 223	3735 845	50 36429	14 63571	798 0142	1011 988	37 03607	0 662331	270 8859
W1	1399 3	-511 08	-600 9	109	633 95	631 6012	762 1688	16 5842	36 87361	279 71	827 7588	1044 567	3734 485	50 39723	14 60277	801 0197	1023 508	37 5857	0 67193	274 0708
W1	1399 3	-511 08	-600 9	106	648 49	645 8456	747 9244	18 06208	39 37557	281 78	830 6288	1055 573	3746 089	50 4287	14 5713	803 9118	1034 681	38 10339	0 680964	276 2029
W1	1399 3	-511 08	-600 9	106	663 61	660 6011	733 1689	19 74506	42 20817	284 68	833 8845	1067 283	3749 064	50 46355	14 53645	807 1903	1046 56	38 61887	0 689947	279 1522
W1	1399 3	-511 08	-600 9	106	678 73	675 3499	718 4201	21 45484	45 0714	287 15	837 1812	1079 106	3757 987	50 49804	14 50196	810 5079	1058 546	39 12148	0 698698	281 6791
W1	1399 3	-511 08	-600 9	106	693 85	690 1564	703 6136	23 03353	47 71109	289 62	840 2224	1090 85	3766 486	50 52948	14 47052	813 5674	1070 454	39 62404	0 707451	284 2049
W1	1399 3	-511 08	-600 9	106	708 96	705 0047	688 7653	24 44118	50 11574	292 45	842 9736	1102 481	3769 81	50 55952	14 44048	816 3417	1082 254	40 12723	0 716212	287 0845
W1	1399 3	-511 08	600 9	103	723 41	719 2468	674 5232	25 71673	52 22963	294 26	845 4165	1113 567	3784 295	50 58376	14 41624	818 7966	1093 494	40 60653	0 724563	288 9558
W1	1399 3	-511 08	-600 9	103	738 53	734 1366	659 6334	27 0806	54 43354	297 05	847 9852	1125 249	3788 08	50 60712	14 39288	821 3704	1105 331	41 09701	0 733106	291 7918
W1	1399 3	-511 08	-600 9	103	753 65	749 0363	644 7337	28 41129	56 64299	299 47	850 5373	1137 007	3796 729	50 63231	14 36769	823 9352	1117 246	41 57829	0 74148	294 2655
W1	1399 3	-511 08	-600 9	103	768 77	763 9305	629 8395	29 71074	58 93541	301 71	853 1339	1148 872	3807 868	50 66249	14 33751	826 562	1129 28	42 04801	0 749636	296 565
W1	1399 3	-511 08	-600 9	103	783 92	778 8362	614 9338	31 03092	61 26283	304 5	855 7709	1160 851	3812 317	50 69291	14 30709	829 2293	1141 425	42 50715	0 757602	299 4046
W1	1399 3	-511 08	-600 9	100	798 52	793 2244	600 5456	32 18843	63 49441	306 85	858 231	1172 42	3820 825	50 72749	14 27251	831 741	1153 17	42 94428	0 76517	301 8118
W1	1399 3	-511 08	-600 9	100	813 63	808 0927	585 6773	33 3683	65 87133	309 71	860 8182	1184 479	3824 477	50 76684	14 23316	834 3938	1165 416	43 3855	0 772795	304 7257
W1	1399 3	-511 08	-600 9	100	828 78	823 0059	570 7641	34 55978	68 27797	313 1	863 4361	1196 659	3821 972	50 80661	14 19339	837 0785	1177 783	43 81833	0 780269	308 181
W1	1399 3	-511 08	-600 9	100	843 9	837 9037	555 8663	35 62144	70 63515	315 67	865 9341	1208 81	3829 348	50 85072	14 14928	839 6636	1190 132	44 24586	0 787638	310 7925
W1	1399 3	-511 08	-600 9	100	859 02	852 8057	540 9643	36 65038	72 9581	318 47	868 3855	1220 997	3833 946	50 89484	14 10516	842 2037	1202 517	44 66653	0 794884	313 6499
W1	1399 3	-511 08	-600 9	97	873 5	867 0769	526 6931	37 65672	75 20651	321 1	870 7652	1232 751	3839 15	50 93677	14 06323	844 6668	1214 457	45 06053	0 801667	316 3348
W1	1399 3	-511 08	-600 9	97	888 61	881 9595	511 8105	38 72666	77 55771	324 55	873 2653	1245 082	3836 334	50 97948	14 02052	847 2498	1226 976	45 46285	0 80859	319 8303
W1	1399 3	-511 08	-600 9	97	903 73	896 8602	496 9098	39 87046	79 8923	327 59	875 7994	1257 51	3838 672	51 0175	13 9825	849 8491	1239 577	45 85673	0 815374	322 9182
W1	1399 3	-511 08	-600 9	97	918 85	911 747	482 023	41 03841	82 24969	330 44	878 3668	1270 01	3843 391	51 05502	13 94498	852 4792	1252 245	46 24136	0 821996	325 8178
W1	1399 3	-511 08	-600 9	97	933 97	926 6324	467 1376	42 17705	84 63088	333 63	880 9347	1282 565	3844 273	51 09477	13 90523	855 1185	1264 972	46 61842	0 828478	329 0536
W1	1399 3	-511 08	-600 9	94	948 51	940 9557	452 8143	43 21316	86 90777	335 76	883 3575	1294 664	3855 922	51 13522	13 86478	857 6199	1277 242	46 97588	0 834616	331 2417
W1	1399 3	-511 08	-600 9	94	963 63	955 8709	437 6991	44 20541	89 19939	338 96	885 7647	1307 238	3856 614	51 17826	13 82174	860 1162	1289 997	47 34479	0 840946	334 4895
W1	1399 3	-511 08	-600 9	94	978 74	970 7992	422 9708	45 1387	91 35505	341 78	888 0294	1319 778	3861 485	51 21854	13 78146	862 4643	1302 714	47 71162	0 847243	337 3608
W1	1399 3	-511 08	-600 9	94	993 86	985 7461	408 0239	46 09878	93 40771	344 75	890 2311	1332 344	3864 666	51 25312	13 74688	864 7304	1315 442	48 07408	0 853475	340 3765
W1	1399 3	-511 08	-600 9	94	1008 98	1000 703	393 0673	47 07557	95 40115	347 58	892 3973	1344 945	3869 455	51 28431	13 71569	866 9499	1328 197	48 43115	0 859618	343 2516
W1	1399 3	-511 08	-600 9	91	1023 49	1015 062	378 7084	48 01447	97 27702	349 91	894 4483	1357 072	3878 346	51 31254	13 68746	869 0468	1340 466	48 76862	0 865425	345 6283
W1	1399 3	-511 08	-600 9	91	1038 6	1030 014	363 7558	48 97458	99 18938	353 24	896 5413	1369 722	3877 596	51 34104	13 65896	871 1857	1353 261	49 11503	0 871385	348 995
W1	1399 3	-511 08	-600 9	91	1053 75	1045 018	348 752	49 9623	101 0384	356 42	898 6022	1382 439	3878 679	51 36551	13 63449	873 279	1366 114	49 45747	0 877283	352 2111
W1	1399 3	-511 08	-600 9	91	1068 87	1059 989	333 7811	50 93932	102 9294	359 36	900 6895	1395 196	3882 447	51 39206	13 60794	875 4057	1379 009	49 79196	0 883037	355 1907
W1	1399 3	-511 08	-600 9	91	1083 99	1074 951	318 8187	51 90787	104 8815	362 57	902 8194	1408 021	3883 446	51 42133	13 57867	877 5842	1391 975	50 11883	0 888651	358 4381
W1	1399 3	-511 08	-600 9	88	1098 5	1089 302	304 4676	52 83974	106 8028	365 29	904 9026	1420 39	3888 389	51 45107	13 54893	879 7193	1404 48	50 42553	0 893913	361 1984
W1	1399 3	-511 08	-600 9	88	1113 62	1104 256	289 5138	53 87676	108 8135	369 15	907 1215	1433 351	3882 841	51 47898	13 52102	881 9799	1417 573	50 73798	0 899277	365 0866
W1	1399 3	-511 08	-600 9	88	1128 73	1119 182	274 5883	54 97661	110 8779	372 97	909 4217	1446 383	3878 015	51 50577	13 49423	884 3157	1430 731	51 04162	0 90449	368 9338
W1	1399 3	-511 08	-600 9	88	1143 85	1134 108	259 6619	56 04641	113 0334	376 36	911 7748	1459 489	3877 907	51 53747	13 46253	886 7214	1443 97	51 33822	0 909569	372 3581
W1	1399 3	-511 08	-600 9	88	1158 97	1149 028	244 7416	57 03444	115 2835	379 61	914 1514	1472 643	3879 358	51 5767	13 4233	889 1782	1457 272	51 62867	0 914526	375 6478
W1	1399 3	-511 08	-600 9	85	1173 51	1163 372	230 3977	57 87164	117 5226	382 53	916 4262	1485 318	3882 88	51 62269	13 37731	891 5614	1470 107	51 90335	0 919195	378 6125
W1	1399 3	-511 08	-600 9	85	1188 63	1178 288	215 4825	58 69852	119 8615	386 19	918 7735	1498 522	3880 272	51 67282	13 32718	894 0306	1483 481	52 18458	0 923969	382 3136
W1	1399 3	-511 08	-600 9	85	1203 75	1193 208	200 5625	59 5715	122 162	389 57	921 1109	1511 765	3880 599	51 71896	13 28104	896 4845	1496 882	52 46103	0 928668	385 7348
W1	1399 3	-511 08	-600 9	85	1218 86	1208 123	185 6469	60 41417	124 4034	392 93	923 4016	1525	3881 098	51 76408	13 23592	898 872	1510 273	52 7345	0 933317	389 1355
W1	1399 3	-511 08	-600 9	85	1233 98	1223 057	170 7128	61 19821	126 6018	396 37	925 614	1538 242	3880 823	51 81018	13 18982	901 1958	1523 673	53 00574	0 937925	392 616
W1	1399 3	-511 08	-600 9	82	1248 49	1237 4	156 3699	61 88952	128 6986	398 83	927 6897	1550 962	3888 78	51 85669	13 14331	903 3682	1536 55	53 26333	0 942295	395 1239
W1	1399 3	-511 08	-600 9	82	1263 61	1252 326	141 4445	62 76518	130 9515	402 3	930 0027	1564 323	3888 448	51 89999	13 10001	905 8002	1550 056	53 52242	0 946698	398 6311
W1	1399 3	-511 08	-600 9	82	1278 73	1267 234	126 5363	63 76523	133 2824	405 58	932 4542	1577 783	3890 189	51 94	13 06	908 3353	1563 65	53 77269	0 950954	401 947
W1	1399 3	-511 08	-600 9	82	1293 84	1282 118	111 6523	64 80395	135 6833	408 76	934 9852	1591 299	3892 992	51 98059	13 01941	910 9503	1577 297	54 01589	0 955086	405 1833
W1	1399 3	-511 08	-600 9	82	1308 96	1297 003	96 76672	65 80426	138 132	411 95	937 5306	1604 854	3895 75	52 0246	12 9754	913 5923	1590 988	54 25461	0 959134	408 3908
W1	1399 3	-511 08	-600 9	79	1323 5	1311 323	82 44749	66 74822	140 4614	414 46	939 948	1617 901	3903 635	52 06661	12 93339	916 1024	1604 165	54 48137	0 962978	410 9412
W1	1399 3	-511 08	-600 9	79	1338 62	1326 22	67 54967	67 84758	142 8158	417 88	942 4809	1631 511	3904 258	52 10189	12 89811	918 7007	1617 891	54 71292	0 966919	414 3913
W1	1399 3	-511 08	-600 9	79	1353 74	1341 108	52 66202	68 9928	145 182	421 37	945 0518	1645 162	3904 316	52 13522	12 86478	921 3293	1631 65	54 93936	0 970774	417 9093
W1	1399 3	-511 08	-600 9	79	1368 86	1355 985	37 78493	70 1308	147 6139	424 38	947 6704	1658 856	3908 892	52 17115	12 82885	924 0143	1645 456	55 1605	0 974532	420 952
W1	1399 3	-511 08	-600 9	79	1383 97	1370 849	22 92083	71 22637	150 1291	427 47	950 3291	1672 586	3912 757	52 21198	12 78802	926 7568	1659 306	55 37663	0 978195	424 076

W1	1399 3	-511 08	-600 9	76	1398 48	1385 101	8 66912	72 29753	152 5981	430 34	952 9389	1685 806	3917 382	52 25204	12 74796	929 4472	1672 641	55 57891	0 98162	426 9791
W1	1399 3	-511 08	-600 9	76	1413 6	1399 951	-6 18149	73 45936	155 1841	433 8	955 6931	1699 626	3917 994	52 29188	12 70812	932 2819	1686 573	55 78525	0 985115	430 4685
W1	1399 3	-511 08	-600 9	76	1428 72	1414 811	-21 0409	74 59649	157 7494	437 31	958 4184	1713 457	3918 174	52 3319	12 6681	935 0874	1700 517	55 98929	0 988571	434 0074
W1	1399 3	-511 08	-600 9	76	1443 84	1429 685	-35 915	75 6501	160 2696	440 39	961 0574	1727 273	3922 145	52 37399	12 62601	937 8168	1714 451	56 1927	0 992012	437 1208
W1	1399 3	-511 08	-600 9	76	1458 95	1444 56	-50 7901	76 58959	162 7436	443 65	963 5907	1741 054	3924 386	52 41956	12 58044	940 456	1728 357	56 3958	0 995441	440 4147
W1	1399 3	-511 08	-600 9	70	1473 49	1458 878	-65 108	77 44147	165 1236	446 14	965 9967	1754 32	3932 22	52 46561	12 53439	942 973	1741 749	56 58916	0 998702	442 9429
W1	1399 3	-511 08	-600 9	70	1488 61	1473 768	-79 9983	78 34667	167 5778	449 76	968 4947	1768 136	3931 288	52 5116	12 4884	945 5799	1755 689	56 78728	1 002045	446 5939
W1	1399 3	-511 08	-600 9	70	1503 73	1488 658	-94 8884	79 30712	170 022	453 29	971 0189	1781 987	3931 229	52 5544	12 4456	948 201	1769 657	56 98162	1 005329	450 1535
W1	1399 3	-511 08	-600 9	70	1518 85	1503 546	-109 776	80 35242	172 4699	456 61	973 5981	1795 885	3933 083	52 59315	12 40685	950 8613	1783 661	57 17144	1 008542	453 502
W1	1399 3	-511 08	-600 9	70	1534	1518 443	-124 673	81 465	174 9633	459 97	976 2548	1809 853	3934 72	52 63018	12 36982	953 5913	1797 729	57 35644	1 011674	456 8888
W1	1399 3	-511 08	-600 9	67	1548 54	1532 736	-138 966	82 54022	177 429	463 31	978 8672	1823 306	3935 39	52 66776	12 33224	956 2803	1811 28	57 52959	1 014602	460 2542
W1	1399 3	-511 08	-600 9	67	1563 65	1547 576	-153 806	83 6525	180 0432	467 26	981 6206	1837 313	3932 1	52 70867	12 29133	959 1197	1825 39	57 7056	1 017573	464 2279
W1	1399 3	-511 08	-600 9	67	1578 77	1562 418	-168 648	84 77111	182 6875	470 97	984 4023	1851 353	3930 936	52 75012	12 24988	961 989	1839 533	57 87822	1 020485	467 9632
W1	1399 3	-511 08	-600 9	67	1593 89	1577 268	-183 498	85 92639	185 3152	474 07	987 1935	1865 423	3934 91	52 78906	12 21094	964 8588	1853 7	58 04816	1 023355	471 0908
W1	1399 3	-511 08	-600 9	67	1609 01	1592 13	-198 36	86 99967	187 8692	477 3	989 8768	1879 461	3937 693	52 82899	12 17101	967 627	1867 638	58 21851	1 026231	474 3483
W1	1399 3	-511 08	-600 9	64	1623 52	1608 391	-212 621	87 93582	190 3618	479 96	992 4289	1892 935	3943 944	52 87287	12 12713	970 2817	1881 419	58 38019	1 028951	477 0399
W1	1399 3	-511 08	-600 9	64	1638 64	1621 244	-227 474	88 89492	193 0119	483 64	995 1211	1907 003	3943 021	52 92094	12 07906	973 0889	1895 599	58 54527	1 031723	480 7479
W1	1399 3	-511 08	-600 9	64	1653 78	1636 109	-242 339	89 91594	195 6904	487 4	997 8739	1921 128	3941 583	52 96689	12 03311	975 9479	1909 831	58 70658	1 034434	484 5339
W1	1399 3	-511 08	-600 9	64	1668 9	1650 969	-257 199	91 09719	198 234	491 05	1000 616	1935 258	3941 06	53 00062	11 99938	978 7525	1924 044	58 86573	1 037128	488 2047
W1	1399 3	-511 08	-600 9	64	1684 02	1665 851	-272 081	92 3634	200 606	494 15	1003 273	1949 377	3944 91	53 02439	11 97561	981 4373	1938 23	59 02506	1 039841	491 3242
W1	1399 3	-511 08	-600 9	61	1698 56	1680 17	-286 4	93 53045	202 8562	497 49	1005 772	1962 947	3945 702	53 04838	11 95162	983 97	1951 866	59 17759	1 042436	494 6816
W1	1399 3	-511 08	-600 9	61	1713 68	1695 066	-301 296	94 67274	205 1793	501 62	1008 316	1977 05	3941 33	53 07586	11 92414	986 5581	1966 043	59 3355	1 045119	498 8272
W1	1399 3	-511 08	-600 9	61	1728 8	1709 971	-316 201	95 77128	207 4674	505 54	1010 805	1991 148	3938 656	53 104	11 896	989 0981	1980 216	59 49263	1 047788	502 7644
W1	1399 3	-511 08	-600 9	61	1743 91	1724 88	-331 11	96 97233	209 5983	509 17	1013 23	2005 232	3938 236	53 12202	11 87798	991 535	1994 357	59 64918	1 050462	506 4087
W1	1399 3	-511 08	-600 9	61	1759 03	1739 8	-346 03	98 27616	211 6544	512 33	1015 657	2019 341	3941 485	53 13279	11 86721	993 9494	2008 51	59 80366	1 053112	509 5821
W1	1399 3	-511 08	-600 9	57	1773 54	1754 124	-360 354	99 504	213 616	515 64	1017 963	2032 887	3942 455	53 14375	11 85625	996 2461	2022 1	59 95054	1 055631	512 9038
W1	1399 3	-511 08	-600 9	57	1788 66	1769 057	-375 287	100 7154	215 6605	519 68	1020 326	2047 003	3938 969	53 15818	11 84182	998 6111	2036 267	60 10259	1 058233	516 9542
W1	1399 3	-511 08	-600 9	57	1803 81	1784 027	-390 257	101 8556	217 6909	523 48	1022 634	2061 139	3937 379	53 17527	11 82473	1000 933	2050 459	60 25438	1 060827	520 7674
W1	1399 3	-511 08	-600 9	57	1818 92	1798 942	-405 172	102 9006	219 854	527 06	1024 992	2075 266	3937 437	53 20098	11 79902	1003 335	2064 655	60 40217	1 063338	524 3652
W1	1399 3	-511 08	-600 9	57	1834 04	1813 834	-420 064	103 9267	222 2652	530 73	1027 538	2089 478	3936 989	53 2357	11 7643	1005 954	2078 949	60 54317	1 065718	528 0555
W1	1399 3	-511 08	-600 9	25	1863 52	1842 843	-449 073	105 9046	227 1425	533 17	1032 63	2117 264	3971 086	53 30975	11 69025	1011 21	2106 9	60 80923	1 070197	530 5602
W1	1399 3	-511 08	-600 9	25	1878 63	1857 739	-463 969	106 8856	229 4446	537 84	1035 062	2131 461	3963 002	53 34235	11 65765	1013 711	2121 175	60 94745	1 072533	535 2445
W1	1399 3	-511 08	-600 9	25	1893 75	1872 654	-478 884	107 8683	231 7436	540 1	1037 493	2145 686	3972 756	53 37462	11 62538	1016 21	2135 476	61 0841	1 074843	537 5301
W1	1399 3	-511 08	-600 9	25	1908 87	1887 564	-493 794	108 829	234 0545	543 27	1039 921	2159 917	3975 771	53 40809	11 59191	1018 711	2149 785	61 21897	1 07712	540 7216
W1	1399 3	-511 08	-600 9	25	1923 99	1902 463	-508 693	109 7689	236 4232	547 78	1042 384	2174 167	3969 052	53 44422	11 55578	1021 255	2164 116	61 35114	1 079348	545 2477

A	B	C	D	E	F	G	H	I	J	K	L	M	N	O	P	Q	R	S	T	U
W2	1431 6	-591 08	-774 7	80	589 54	587 9891	805 7809	12 34705	29 72619	325 28	1005 597	1184 43	3641 264	53 12521	11 87479	984 077	1166 215	31 89548	0 566431	320 2775
W2	1431 6	-591 08	-774 7	80	604 66	602 9066	790 8634	13 60708	31 83357	328 2	1008 039	1194 44	3639 365	53 13979	11 86021	986 5195	1176 335	32 44113	0 576018	323 2253
W2	1431 6	-591 08	-774 7	80	619 78	617 7192	776 0508	15 14392	34 43533	330 56	1011 043	1204 97	3645 238	53 15855	11 84145	989 5269	1186 974	32 95894	0 585104	325 6233
W2	1431 6	-591 08	-774 7	80	634 9	632 5318	761 2382	16 68076	37 03708	332 88	1014 046	1215 597	3651 756	53 1772	11 8228	992 5344	1197 71	33 46774	0 594027	327 9819
W2	1431 6	-591 08	-774 7	80	650 02	647 3445	746 4255	18 2176	39 63884	335 96	1017 05	1226 318	3650 19	53 19575	11 80425	995 5419	1208 54	33 96767	0 602792	331 0895
W2	1431 6	-591 08	-774 7	77	739 44	735 0334	658 7366	27 16213	54 56625	347 19	1034 363	1291 21	3719 03	53 2944	11 7056	1012 851	1274 043	36 76665	0 651806	342 5739
W2	1431 6	-591 08	-774 7	77	754 56	749 9332	643 8368	28 48915	56 77996	349 68	1036 93	1302 227	3724 054	53 30872	11 69128	1015 418	1285 163	37 22418	0 659811	345 0979
W2	1431 6	-591 08	-774 7	77	769 68	764 8263	628 9438	29 78942	59 07475	351 9	1039 548	1313 361	3732 199	53 32683	11 67317	1018 047	1296 409	37 67248	0 667844	347 3581
W2	1431 6	-591 08	-774 7	77	784 8	779 7033	614 0667	31 10333	61 39667	354 12	1042 195	1324 587	3740 503	53 34513	11 65487	1020 707	1307 747	38 11186	0 675319	349 6181
W2	1431 6	-591 08	-774 7	77	799 92	794 6041	599 1659	32 29524	63 70946	358 37	1044 762	1335 842	3727 55	53 36841	11 63159	1023 307	1319 13	38 54676	0 682903	353 8866
W2	1431 6	-591 08	-774 7	74	889 5	882 8366	510 9334	38 79399	77 69513	372 41	1059 867	1403 904	3769 78	53 5376	11 4624	1038 729	1388 014	40 97961	0 725217	368 1951
W2	1431 6	-591 08	-774 7	74	904 62	897 7373	496 0327	39 93778	80 02972	375 39	1062 425	1415 639	3771 114	53 56281	11 43719	1041 328	1399 875	41 36703	0 731951	371 2099
W2	1431 6	-591 08	-774 7	74	919 73	912 6133	481 1567	41 1067	82 38719	378 27	1065 016	1427 446	3773 616	53 58755	11 41245	1043 958	1411 804	41 74642	0 738544	374 1251
W2	1431 6	-591 08	-774 7	74	934 85	927 4989	466 2711	42 24165	84 77037	381 1	1067 607	1439 321	3776 755	53 61445	11 38555	1046 598	1423 807	42 11983	0 745026	376 9923
W2	1431 6	-591 08	-774 7	74	949 97	942 3959	451 3741	43 30897	87 12905	385 18	1070 14	1451 221	3787 643	53 64336	11 35664	1049 187	1435 84	42 48905	0 751431	381 0976
W2	1431 6	-591 08	-774 7	71	1039 55	1030 955	362 8153	49 03588	99 30706	399 61	1083 345	1521 82	3808 264	53 78125	11 21875	1062 644	1507 154	44 61237	0 788279	395 7588
W2	1431 6	-591 08	-774 7	71	1054 67	1045 929	347 8408	50 02232	101 1506	402 9	1085 415	1533 838	3806 995	53 79674	11 20326	1064 732	1519 272	44 95626	0 794254	399 0738
W2	1431 6	-591 08	-774 7	71	1069 79	1060 9	332 8703	50 99857	103 0455	405 84	1087 521	1545 933	3809 218	53 8142	11 1858	1066 862	1531 47	45 29375	0 800113	402 0432
W2	1431 6	-591 08	-774 7	71	1084 94	1075 891	317 8791	51 96837	105 0072	408 83	1089 677	1558 13	3811 194	53 83394	11 16606	1069 049	1543 775	45 6252	0 805861	405 0634
W2	1431 6	-591 08	-774 7	71	1100 05	1090 835	302 9346	52 94605	107 0089	411 9	1091 87	1570 371	3812 506	53 85451	11 14549	1071 277	1556 123	45 94933	0 811479	408 1628
W2	1431 6	-591 08	-774 7	68	1189 57	1179 215	214 5552	58 74992	120 0069	428 99	1105 794	1644 378	3833 137	54 00892	10 99108	1085 51	1630 806	47 74206	0 842462	425 4495
W2	1431 6	-591 08	-774 7	68	1204 69	1194 135	199 6349	59 62642	122 3045	432 05	1108 168	1657 038	3835 292	54 04206	10 95794	1087 963	1643 594	48 02823	0 847391	428 5447
W2	1431 6	-591 08	-774 7	68	1219 81	1209 061	184 7089	60 46517	124 5419	435 27	1110 472	1669 696	3836 001	54 07481	10 92519	1090 345	1656 378	48 31199	0 852278	431 7983
W2	1431 6	-591 08	-774 7	68	1234 93	1223 996	169 7737	61 24347	126 7391	438 14	1112 708	1682 357	3839 77	54 10874	10 89126	1092 665	1669 168	48 59341	0 857121	434 7053
W2	1431 6	-591 08	-774 7	68	1250 05	1238 94	154 83	61 97978	128 931	440 97	1114 915	1695 045	3843 901	54 14412	10 85588	1094 963	1681 988	48 87153	0 861904	437 5733
W2	1431 6	-591 08	-774 7	65	1339 54	1327 127	66 64308	67 9161	142 9581	457 7	1129 766	1771 858	3871 221	54 31681	10 68319	1110 184	1759 437	50 38565	0 887969	454 4914
W2	1431 6	-591 08	-774 7	65	1354 65	1342 003	51 7666	69 06268	145 3258	461 1	1132 359	1784 986	3871 148	54 33957	10 66043	1112 815	1772 653	50 62603	0 892114	457 9139
W2	1431 6	-591 08	-774 7	65	1369 77	1356 88	36 88962	70 19668	147 7651	464 14	1135 002	1798 178	3874 216	54 36484	10 63516	1115 505	1785 936	50 86164	0 896171	460 9801
W2	1431 6	-591 08	-774 7	65	1384 92	1371 782	21 98774	71 2965	150 2907	467 1	1137 695	1811 452	3878 081	54 39393	10 60607	1118 259	1799 308	51 09307	0 900148	463 9686
W2	1431 6	-591 08	-774 7	65	1400 04	1386 633	7 13689	72 41269	152 8635	470 03	1140 437	1824 744	3882 187	54 42359	10 57641	1121 062	1812 698	51 31895	0 904028	466 9271
W2	1431 6	-591 08	-774 7	62	1489 68	1474 822	-81 0521	78 41152	167 7507	487 8	1156 042	1903 825	3902 88	54 61104	10 38896	1137 09	1892 377	52 6112	0 926196	484 8668
W2	1431 6	-591 08	-774 7	62	1504 8	1489 712	-95 942	79 38082	170 1951	491 34	1158 596	1917 219	3902 021	54 64197	10 35803	1139 715	1905 868	52 82075	0 929789	488 4311
W2	1431 6	-591 08	-774 7	62	1519 92	1504 598	-110 828	80 431	172 046	494 95	1161 203	1930 667	3900 732	54 66969	10 33031	1142 38	1919 405	53 02608	0 933314	492 0628
W2	1431 6	-591 08	-774 7	62	1535 03	1519 456	-125 686	81 54064	175 1329	498 09	1163 873	1944 156	3903 222	54 69592	10 30408	1145 103	1932 977	53 22656	0 936757	495 2261
W2	1431 6	-591 08	-774 7	62	1550 15	1534 319	-140 549	82 65951	177 7042	501 97	1166 619	1957 715	3900 065	54 72406	10 27594	1147 906	1946 623	53 4226	0 94012	499 1257
W2	1431 6	-591 08	-774 7	58	1639 55	1622 137	-228 367	88 95448	193 1744	520 22	1182 89	2038 313	3918 174	54 90789	10 09211	1164 587	2027 746	54 5264	0 959016	517 5232
W2	1431 6	-591 08	-774 7	58	1654 67	1636 984	-243 214	89 98547	195 8401	523 76	1185 664	2052 023	3917 869	54 94118	10 05882	1167 439	2041 547	54 70389	0 962049	521 086
W2	1431 6	-591 08	-774 7	58	1669 79	1651 844	-258 074	91 16672	198 3837	527 43	1188 424	2065 757	3916 646	54 965	10 035	1170 243	2055 351	54 87954	0 965064	524 7732
W2	1431 6	-591 08	-774 7	58	1684 9	1666 718	-272 948	92 43772	200 7428	530 74	1191 086	2079 463	3918 045	54 98009	10 01991	1172 918	2069 111	55 05533	0 968094	528 0978
W2	1431 6	-591 08	-774 7	58	1700 02	1681 608	-287 838	93 64348	203 0815	534 42	1193 693	2093 172	3916 717	54 99711	10 00289	1175 548	2082 877	55 23028	0 971107	531 7916
W2	1431 6	-591 08	-774 7	54	1789 57	1769 956	-376 186	100 7839	215 7825	555 3	1208 193	2174 355	3915 641	55 06524	9 934763	1190 076	2164 341	56 2441	0 988604	552 7425
W2	1431 6	-591 08	-774 7	54	1804 69	1784 896	-391 126	101 92	217 8116	558 84	1210 507	2188 072	3915 382	55 07615	9 923846	1192 395	2178 104	56 4111	0 991487	556 2942
W2	1431 6	-591 08	-774 7	54	1819 81	1799 82	-406 05	102 9619	219 9817	563 14	1212 883	2201 828	3909 912	55 09446	9 905516	1194 803	2191 92	56 57445	0 994295	560 606
W2	1431 6	-591 08	-774 7	54	1834 93	1814 71	-420 94	103 9867	222 4137	566 04	1215 464	2215 684	3914 36	55 12047	9 879531	1197 44	2205 848	56 73084	0 996972	563 5271
W2	1431 6	-591 08	-774 7	54	1850 04	1829 577	-435 807	105 0033	224 9294	569 71	1218 11	2229 574	3913 524	55 14891	9 851092	1200 149	2219 812	56 88359	0 999583	567 2157